DISS. ETH NO. 24500

# EVOLUTION OF QUANTUM SYSTEMS

A thesis submitted to attain the degree of

DOCTOR OF SCIENCES of ETH ZURICH

(Dr. sc. ETH Zurich)

presented by

OLIVER FURTMAIER

M.Sc. Physics, ETH Zurich

born on 15.06.1989

citizen of Germany

accepted on the recommendation of

Prof. Dr. Hans Jürgen Herrmann, Examiner
Prof. Dr. Malte Henkel, Co-examiner

2017

# Kurzfassung

Die vorliegende Arbeit befasst sich zuerst mit der Entwicklung einer neuen numerischen Methode zur Simulation der Wigner Gleichung, welche zur zeitlichen Entwicklung von isolierten Quantensystem im Phasenraum, also im Orts- und Impulsraum, verwendet wird. Im Rahmen dieser Untersuchung haben wir eine semi-spektrale Simulation hergeleitet über die man den geschwindigkeitsabhängigen Teil der Wigner Funktion in eine beliebige Basis von quadratintegrablen Funktionen zerlegen und die ortsabhängigen Koeffizienten in der Zeit propagieren kann. Dabei haben wir die Dynamik unterschiedlicher Quantensysteme, wie des (an-)harmonischen Oszillators, und verschiedener Prozesse wie des quantenmechanischen Tunnelns durch eine Potentialbarriere im Phaseraum untersucht und veranschaulicht. Im zweiten Teil der Dissertation beschäftigen wir uns mit der Frage ob man den quantenmechanischen Messvorgang ausnutzen kann um Eigenzustände von hermitischen Operatoren numerisch zu approximieren. Dazu nehmen wir einen Ansatz zur Beschreibung des Messvorgangs in welchem unser System dekohärent mit einer "künstlichen" Umgebung wechselwirkt und entwickeln aus der Lindblad- eine nicht-lineare Schrödinger-Gleichung, die den Kollaps der Wellenfunktion zum wahrscheinlichsten Eigenzustand simuliert. Diese deterministische Zeitentwicklung soll keine Messung darstellen. Sie kann jedoch dazu verwendet werden, Eigenzustände von Observablen zu approximieren, welche den größtmöglichen Überlapp mit dem Anfangszustand haben. Im letzten Teil dieses Dokumentes beantworten wir die Frage ob man die elektromagnetische Kopplung zwischen Elektronen und Gitterschwingungen (Phononen) auch als eine Dynamik der Elektronen auf einer gekrümmten Riemannschen Mannigfaltigkeit auffassen kann. Die Krümmung der Mannigfaltigkeit soll dabei in Analogie zur allgemeinen Relativitätstheorie eine eigene Dynamik erhalten, die von den Phononen bestimmt wird. Wir können zeigen, dass die zwei Quantensysteme im allgemeinen nicht äquivalent sind, und daher nicht die gleichen physikalischen Beobachtungen liefern würden. Dazu haben wir eine konkrete Messgröße konstruiert, die indirekte, lokale Beobachtungen der einzelnen Komponenten des metrischen Tensors ermöglicht. Die zugrundeliegende Diskrepanz zwischen beiden Konzepten scheint durch die räumliche Ausbreitung der Wellenfunktion bedingt zu sein, die selbst lokalen Messungen Informationen über entfernte Bereiche des Raumes liefern kann. Nichtsdestotrotz gelingt es uns in zwei Dimensionen, ein Quantensystem mit einer zugehörigen Mannigfaltigkeit zu finden, die zusammen eine schwache Äquivalenz zum System aus gekoppelten Elektronen und Gitterschwingungen aufweist. Mit schwacher Äquivalenz meinen wir, dass sowohl die Messung der Energie als auch die der Metrik in Quantenzuständen mit gleicher Koordinatenrepräsentation in beiden Systemen die selben Werte liefern.

# Abstract

The thesis is concerned with three subjects. Firstly, it deals with the development of a new numerical method for the simulation of the Wigner equation, which is employed for the temporal evolution of isolated quantum systems in phase space, that is the space of position and momentum. Throughout this investigation we have derived a semi-spectral solver which enables the decompositon of the velocity-dependent part of the Wigner function into an arbitrary set of complete square-integrable basis functions and the streaming of the space-dependent coefficients to achieve a propagation in time. Thereby, we studied and visualized the dynamics of various quantum systems, such as the (an-)harmonic oscillator, and different processes like the tunneling through a potential barrier in phase space. In the second part, we have looked at the question whether the quantum mechanical measurement process can be employed to numerically calculate eigenstates of hermitian operators. To achieve this we take the ansatz of a decoherent interaction between our system and an "artificial" environment to describe a measurement and derive a non-linear Schrödinger equation from the Lindblad dynamics, which mimics the collapse of the wave function to the most probable eigenstate. Since the outcome of our simulation is deterministic. it does not represent a measurement. However, it can be used to approximate eigenstates of observables that have the largest overlap with the initial state of the dynamics. In the last part of this document we tackle the question if the quantum system of coupled electrons and lattice vibrations (phonons) can be regarded as electrons which move in a regular potential on a Riemannian manifold of non-trivial curvature. In analogy to general relativity this manifold would obtain its own dynamics that would be governed by the phonons. We can show that two systems are in general not equivalent, which means that physical observations in both systems will give different results, by constructing a concrete indirect measurement, that allows to locally determine the individual components of the metric tensor. The deeper reason behind this discrepancy seems to be the spatial spread of the wave function which gives even local measurements information about distant areas of space. Nevertheless, we are able to find two-dimensional manifolds and a respective metric tensor which show a weak equivalence to the two-dimensional system of coupled electrons and phonons. With weak equivalence we mean that the energy and curvature measurements of quantum states with equal coordinate representations give the same values in both systems.

# Declaration of originality

I hereby confirm that I am the sole author of the written work here and that I have compiled it in my own words. With my signature I confirm that

1. I have committed none of the forms of plagiarism described in the Citation etiquette [1] information sheet.

2. I have documented all methods, data and processes truthfully.

3. I have not manipulated any data.

4. I have mentioned all persons who were significant facilitators of the work.

I am aware that the work may be screened electronically for plagiarism.

**Place, date**

**Signature**

---

[1] *https://www.ethz.ch/content/dam/ethz/main/education/rechtliches-abschluesse/leistungskontrollen/plagiarism-citationetiquette.pdf*

# Acknowledgement

I would like to thank Stephan Wolfram and my dad, since without his initiative I would not have undertaken this adventure. The first special thanks goes to Miller, since he encouraged me throughout the three years of this PhD and nourished my interest in the field of numerics and computational physics. The second goes to Prof. Herrmann, because the talk in his office is the main reason I have kept the project and I am actually able to write these lines right now. Furthermore, I am very grateful for the help and support of Prof. Henkel in the last part of this thesis, who was able to bring the joy and excitement about questions in physics back on the table, and for his interest and willingness to review this work. Moreover, the financial support of the European Research Council (ERC) Advanced Grant 319968-FlowCCS is kindly acknowledged.

To my mind, this passage's primary purpose is to serve as a memory trigger such that whenever I, or anybody closely related, will read these lines again in the future, some of the amazing experience which we and I have had during these three years will start to build up in front of our eyes. Similar to the smell of an old perfume which reminds you of a long forgotten lover or friend. There would be many things to say yet very few things to write. I leave the task to my future brain to make sense out of the following keywords: Freedom, Sun, Snow, Rain, Lunch, Coop-Break, Physics, C++, MKL Library, Mathematica, Curved Space, Seminar, Movie Night, Neuchatel, Schwamen-Pub, Running with Jan, Discussions with Sergio, Party with Dominik, Finding the Balance, Rui+Schladming+Marie, 50 Shades, Back to the roots of why physics is fascinating, What is the purpose of life?!, How many nodes have remained in the PhD network?,...

# Contents

*Contents*

# 1 Introduction

## 1.1 Overview

In general the thesis deals with the evolution of non-relativistic quantum systems. Throughout this work we introduce unconventional approaches to propagate the quantum state in time or to determine the possible observations and outcomes of measurements. Firstly, we treat an isolated quantum system with an equivalent non-relativistic quantum mechanical formalism for the evolution of the quantum states, namely the Wigner formulation of quantum mechanics in phase space [189]. In this space momentum and position are treated equally which gives rise to the evolution of observables as simple functions of position and momentum which are not operators anymore. The motivation is to find an easily parallelizable numerical method based on the successful lattice Boltzmann procedure [13] which would allow the simulation of the evolution of the density operator in higher-dimensional phase-spaces. Thereby, we develop a new semi-spectral method which allows the decomposition of the density operator into an arbitrary complete set of basis functions in $L^2$ for the velocity dependence of the Wigner function that uses rotations in this function space to implement the action of the pseudo-differential operator and hence smoothed the way to a lattice Wigner simulation. The study has stipulated us to investigate the effect of a measurement on the Wigner function by taking a decoherence-based approach for the evolution of the density matrix [191]. Throughout this analysis we are able to derive a new equation for the evolution of a quantum system, which "mimics" the measurement process. Since it is a deterministic process, it cannot exactly be a measurement, but it does facilitate the convergence of the quantum state to the eigenstate with the highest probability, which can be determined using Born's law [18]. Using this method we look at a particular excited-state quantum phase transition from Ref. [22] and found that the critical exponent is not universal when changing the spectrum ratio of the quantum state whose phase transition is analyzed. The system basically describes the interaction between an atomic chain with discrete excitations and a bosonic field with a single mode of excitation. After studying such a system, we went on to increase the complexity and investigated the interaction of electrons in a periodic lattice, which have in principle also discrete excitations, and bosonic particles with multiple modes of excitation, such as phonons. The inspection of such systems has made us curious about the question, whether the interaction of electrons and phonons could be geometrically modeled by a coupling of the electron to an underlying manifold, described by a metric tensor, whose dynamics depend on the phonons. Using a non-relativistic quantum mechanical theory on a Riemannian manifold, we derive a measurement which can locally distinguish the presence of curvature, in contrast to the idea of general relativity. Therefore, the two quantum systems are not equivalent in their physical descriptions. Nevertheless, we can establish a weakly equivalent system in the case of two dimensions, which enables the coupling of electrons and phonons through a metric tensor. We determine the metric for a radial potential of type $1/|\vec{r}|$ and discuss some of the open questions which remain on the subject. In the following three sections, we shall give a more detailed overview over the three topics. The reader should note that most parts on the first two topics have been taken from Refs. [57], which has been published in the *Journal of Computational Physics*, and [56] which has been published in *Physical Review A*. The author of this thesis has contributed the most effort to the design, implementation, execution, interpretation, writing and presentation (figures) of the mathematical, numerical and computational analysis as well as the literature research for each of the two articles.

## 1.2 Wigner

The Wigner formalism, also known as quantum mechanics in phase space [189], provides an alternative but equivalent description of quantum mechanics in terms of a (quasi)-probability distribution function of the particle position and momentum. It has proven to provide a helpful supplement to operator methods in Hilbert space as well as to path integral formulations, and has offered new insights into the relation between quantum and classical physics, as it does not discriminate between coordinate and momentum space. For instance, it has given a fruitful perspective for the study of quantum chaos [72]. In addition, it offers the opportunity to systematically consider quantum corrections to the classical dynamics by expanding the *quantum Liouville equation* around $\hbar \approx 0$. Nowadays, it is also a valuable tool in the fields of quantum optics as well as nuclear, plasma and semiconductor physics to describe transport processes, for example, in open quantum systems [189]. The Wigner function, introduced by E. Wigner in Ref. [185], is the Weyl transformation of the density matrix and a quasi-probability distribution that can "intuitively" account for scattering and decoherence effects in quantum systems [71, 48]. It differs from a classical probability distributions as it can change its sign during the evolution especially in regions where quantum interference effects become important. For a physical interpretation of negative values for the Wigner distribution, the interested reader should consult Ref. [106].

The Wigner functions, is the Fourier transform of the characteristic function of two non commuting variables [156, 76] and finds its application in various fields of physics, such as quantum optics [141], information [108], chaos [73], nuclear and solid state physics [189]. In the area of quantum information and optics, the main motivation for studying the Wigner function lies in its complete information theoretical value. It contains the full quantum information of the system, no matter if it is in a mixed or pure state and importantly can be reconstructed by a measurement procedure, called quantum state tomography [102, 19, 109, 36] from an ensemble of equally prepared quantum states. As explained in Ref. [108], an experimentalist would like to determine the quantum state of a system

$$|\psi\rangle = \sum_i |a_j| e^{i\phi_j} |\psi_j\rangle \ , \tag{1.1}$$

which was prepared in a well-defined state by an unknown procedure. A single measurement on the system will destroy its quantum state and it collapses to the measured eigenstate $|\psi_j\rangle$, which means all other information that was contained, $|a_k|$ with $k \neq j$, is lost. This means its impossible to determine the full quantum information from a single state and measurement [32] and is an essential ingredient for quantum cryptography [11]. Assuming the experimentalist obtains an ensemble of equally prepared quantum states, an "ordinary" measurement still only allows him to determine the probabilities, $|a_i|$ with $j \in \mathbb{N}$, based on Born's law [18], and not the full phase information $\phi_j$. However, if he measures the probability distributions for two conjugated measurements, i.e. the marginals of the Wigner function in these two variables, such as position and momentum, he will be able to reconstruct the Wigner function and hence the complex-valued quantum state if the quantum system is in a pure state [60], i.e. extract the full quantum information. Since many quantum cryptography procedures are set up with optical systems and the reconstruction methods are very successful for photonic systems [76], the Wigner function also plays a major role in quantum optics. Furthermore, due to the popularity of coherent states in this field, since they are the states of the quantum harmonic oscillator that resemble the classical behavior the most [148], and the positivity of its Wigner functions the description of the quantum dynamics of these states with the Wigner evolution is beneficial compared to the complex-valued density operator treatment. Thanks to its strong similarities to classical mechanics scientists have looked at the boundaries between the classical and quantum realm by investigating the effects of open boundaries and measurements on the (de-)coherence of the quantum system and especially on the Wigner function [100, 36].

In the case of solid state physics, especially in the context of semi-classical simulations of semiconductors, it has been argued that the phase space approach allows for a more straightforward and quantitatively better imposition of open boundaries for transport simulations [90].

Since the Wigner equation was introduced in 1932, it has been tackled by various numerical approaches, such as finite differences [55, 97], Fourier spectral collocation [132, 4], deterministic particle [122, 187], and Monte-Carlo [151, 152], which can also handle the many-particle Wigner

problem. Here, we extend the technique described in Refs. [132, 4] to arbitrary basis functions $\phi_n(\vec{p})$ of $L^2(\mathbb{R}^d)$ in momentum-space and reveal the underlying mathematical structure of the resulting infinite-dimensional set of reaction-advection equations. By using this formulation we show that the action of the potential on the Wigner function is a unitary rotation of its coefficient vector, whereas the advection operation can be discretized by various techniques used in computational fluid dynamics, such as finite difference, finite volume or finite element, cf. Ref. [110]. In that way, one is able to construct a finite element simulation of the Wigner evolution. Employing a more general basis we assume that the higher computational costs of our method, $\mathcal{O}(N^2)$, compared to $\mathcal{O}(N \log N)$ for the spectral Fourier decomposition are outweighed by a smaller number $N$ of basis functions to obtain the same order of accuracy through focusing the computational effort to regions of interest, as for example in the case of Wigner functions that are strongly localized in momentum-space, such as particles in a periodic potential, cf. Bloch's theorem and Ref. [93]. In addition, the "artificial" periodization of the Wigner function can be avoided, which may mitigate the self-interaction of the distribution at the domain boundaries of the simulation that is present for the Fourier basis choice, cf. Ref. [154].

The chapter is organized as follows. First, we give an introduction to the Wigner formalism and present the properties of the Wigner equation, especially for the pseudo-differential operator. Second, in section 2.2 we show the details of the numerical method to handle the obtained multidimensional reaction-advection equation. Third, we validate the technique by simulating a one-dimensional (an-)harmonic oscillator, which offers the opportunity to compare with an analytical solution, cf. Ref. [70], such that we can perform a convergence analysis, and to observe quantum effects when the anharmonic potential is used. To study tunneling phenomena, we show the evolution of bounded states in the double well potential and measure the spread as well as the covariance of the Wigner function in phase space. In the last section, we shall highlight the strengths and weaknesses of the approach.

## 1.3 Decoherence

What makes eigenstates and -values of Hermitian operators interesting for physics? A postulate of the early days quantum theory says that the measurement intervention "instantaneously" causes the bound state of an isolated quantum mechanical system, which is a unit vector in a countably infinite dimensional Hilbert space, to collapse to one random eigenstate of the Hermitian operator that represents the measured observable, such that the probabilities are given by Born's rule [18, 183]. With *collapse*, one may picture the sudden reduction of the superposition of eigenstates to only one eigenstate of the observable which is then occupied by the quantum system. However, in practice one does not observe the collapse and just characterizes the measurement by the system's state before and after the measurement. Here, we take environment-induced decoherence which may offer a more fundamental explanation for this phenomenon and reconciles the deterministic, unitary, continuous time evolution of the linear Schrödinger equation with the non-deterministic, non-unitary, discontinuous reduction of the wave function in the collapse. This approach has been brought to the attention of a wider audience of scientists by *W. Zurek* in Refs. [191, 193]. Hereby, the local interaction between the measurement apparatus and the open quantum system, which together evolve according to the linear Schrödinger equation, generates entanglement that (usually irreversibly) spreads the phase information of the system into the environment, or measurement apparatus, and will finally result in a complete loss of quantum phase information, i.e. the system becomes a classical mixture of preferred states that satisfies Born's probability law [192, 144]. The selection of these states is induced by the system-environment interaction which measures certain observables of the system and hence leads to the preference of eigenstates of the corresponding Hermitian operators [125].

A popular way of modeling the process is an open quantum system with a non-unitary evolution that deflates interference, i.e. reduces the off-diagonal elements of the reduced density operator in the pointer basis [143, 48]. As indicated in Ref. [179], a master equation in Lindblad form with the dynamical semi-group property [107] can be used to achieve this effect. The reduced density operator, which is formally obtained by averaging over the environment's degrees of freedom, contains all information that is accessible via measurements on the quantum system alone [121]. There are other, more general, starting points for decoherence dynamics of the reduced density operator that explicitly ignore the environmental degrees of freedom, such as integro-differential equations which are not local in time (memory effects) [120], non-Markovian master equations

[47] or the Born-Markov master equation [20]. However, the Lindblad equation offers an intuitive and easy representation of the measurement process in the weak coupling limit [179].

Based on these insights, one can use decoherent dynamics to approximate specific eigenstates of a finite set of dimensionless commutable Hermitian operators with discrete spectra $\{\hat{O}_j\}_{j\in\mathcal{J}}$. One can imagine this as measurements on the quantum system by simultaneously and continuously monitoring the observables $O_j$. To achieve this with a reasonable computational effort, we have derived a deterministic, nonlinear Schrödinger equation, similar to the equation in Ref. [64], such that the dark states of the open quantum system are given by the eigenstates of $\{\hat{O}_j\}_{j\in\mathcal{J}}$. By *dark states* we mean the states which are unaffected by the coupling to an environment, see Ref. [43]. The equation is derived from a purely decoherent Lindblad equation for the reduced density operator, i.e. we work in the quantum-measurement limit [142]. A different approach for the problem could have been the use of quantum trajectories [63, 45], which also reduces the required computational resources compared to the master equation for the reduced density operator, but still needs the simulation of many trajectories to approximate the evolution according to the master equation with a reasonable accuracy. With our deterministic equation we sacrifice the exact compliance with Born's law for the gain of computational speed. The algorithm's computational costs scale linearly for sparse matrix representations of the involved Hermitian operators and one perturbation step. In addition, there are two simple implementations which can make use of symmetry induced subspaces. One option is to use a symmetry adapted starting vector to initialize the dynamics. The other option is to include the symmetry operator explicitly in the dynamics. Nice examples are the initialization of fermionic or bosonic wave functions, which are fully (anti-)symmetric with respect to the exchange of particles, that will result in fully (anti-)symmetric eigenstates through the dynamics if the self-adjoint operators commute with this symmetry operation, as shown in the subsection on symmetry inheritance.

There are other successful methods, [103, 10, 75, 51, 104], which allow the computation of the low-lying eigenvalue states. However, one might be interested in states that possess other characteristics such as higher energy eigenstates (orbitals) of the Kohn-Sham equations [1], states with certain localization properties, such as band edge or surface states, which are important for topological quantum system, optical properties and chemical reactions [188], inner or excited states, such as quantum states around the Fermi energy or a measured band gap that determine the electronic transport properties and also have an impact on the thermal properties of the material, as well as the influence of interactions on a certain subset of eigenstates in the spectrum or excited-state quantum phase transitions [22].

Another important application of finding the most probable eigenstate lies in the reconstruction of quantum states that were sent between experimentalists with different lab equipment [12, 123, 186]. For a concrete example on how to use it, imagine that Alice has lent Bob one of her measurement apparati, represented by the observable $\hat{O}_B$. Alice is now making a different, non commuting measurement, represented by $\hat{O}_A$, whose result is the quantum state $|\psi_a\rangle$. Bob can only decipher the communication in his eigenbasis $\{|\psi_b\rangle\}_{b\in\mathcal{B}}$, which means he has just this measurement available. Being well prepared, Alice wants to know which information Bob will most likely obtain before sending the quantum information about her state

$$|\psi_a\rangle = \sum_{b\in\mathcal{B}} c_b |\psi_b\rangle \;, \tag{1.2}$$

through a communication channel to Bob. She cannot tell with absolute certainty what Bob's measurement outcome will be, but she would like to know the probabilities. As its originally her lab equipment she knows the non-diagonal matrix representation of the observable $\hat{O}_B$ in the eigenbasis of $\hat{O}_A$. As she does not want to know the full decomposition she is satisfied by knowing all but Bob's measurement outcomes with a probability $p \leq 0.1$. In this case it is not necessary to fully diagonalize the matrix representation $O_B$ but much more efficient to perform our collapse algorithm for an initial vector $(0,\ldots,0,1_a,0,\ldots)$ and the matrix $O_B$.

By using the "folded spectrum" method [178], i.e. folding the spectrum of each operator around a given reference eigenvalue $\epsilon_j^{\mathrm{ref}}$ and using the square of the shifted self-adjoint operator $\left(\hat{O}_j - \epsilon_j^{\mathrm{ref}}\hat{\mathbb{I}}\right)^2$, the methods in Refs. [103, 10, 75, 51] would converge to the eigenstates whose eigenvalues are closest to the reference. Furthermore, as mentioned in chapter six of Ref. [75], there are extensions which facilitate the approximation of excited-states and make use of symmetries to improve the convergence. Nevertheless, all the methods mentioned so far do not allow

the computation of eigenstates based on the $L^2$ overlap with an arbitrary quantum state and mainly focus on the eigenvalue and symmetry properties as selection criteria. For example, the $L^2$ overlap of an eigenstate with a given quantum state may imply among other things certain localization characteristics, such as edge or surface states. The numerical procedure introduced in Ref. [171] allows the "targeting of specific eigenvectors using arbitrary physical properties as selection criteria". An advantage of this method is that it very well differentiates nearly degenerate states because using this procedure to target a state with a reference value $\epsilon_j^{\text{ref}}$ the respective eigenstate $|\psi_i\rangle$ with $\hat{O}_j|\psi_i\rangle = \epsilon_{j,i}|\psi_i\rangle$ has an eigenvalue $1/(\epsilon_{j,i} - \epsilon_j^{\text{ref}})$. In addition, it works with the linear instead of the quadratic operator which results in a smaller condition number and hence may reduce the numerical difficulty for solving. The disadvantage of this approach is that the employed Jacobi-Davidson method has only cubic convergence and that one needs to store the vectors in the search space, which increases the memory consumption compared to just storing a single vector that is going to approximate the desired eigenvector.

## 1.4 Electron-Phonon Coupling

Inspired by the idea of describing the interaction of an electron with phonons through the dynamics of that particle on a curved manifold, we use a formulation of non-relativistic quantum mechanics on general Riemannian manifolds from Ref. [33]. The intention is to construct a manifold whose corresponding metric tensor facilitates the interaction such that the two quantum systems are equivalent. As an intuitive picture, we imagine that the electron feels a regular lattice in curved space, where the distortions are intrinsically contained in the distance measurements of that space, i.e. in the metric tensor.

In order to understand how this work relates to the existing theories the reader should note two things. On the one hand we are not trying to unify general relativity and (quantum) electrodynamics. There have been many attempts like Weyl's conformal gravity [181], Kaluza-Klein theory [92, 99] and affine gravity, which has been developed by Eddington [24] and extended by Einstein [49] and Schrödinger [149]. For a historical review the interested reader may consult Refs. [67, 66]. Nevertheless, till today there is no generally accepted unified theory of general relativity and electrodynamics, especially not for quantum electrodynamics. Our motivation is to figure out *if* one can find a geometrical approach to model interactions of ions and electrons and not a unification. On the other hand we do not want to replace the quantum mechanical procedure for calculating electron-phonon interactions, which does have a remarkable simplicity compared to the complexity of the initial problem, which we shall show in the first sections of chapter 4. Instead the intention is to derive a coupling mechanism that makes another type of semi-classical (Born-Oppenheimer) approximation possible such that they do not require the full quantum mechanical diagonalization of the electronic subsystem for a static ionic crystal, as is often done for the Born-Oppenheimer approximation, cf. Ref. [130], but is complex enough to capture some quantum mechanical effects of the electron-phonon coupling instead of introducing a fixed scattering rate to model it [158, 170, 14]. If the resulting numerical simulation lives up to this expectation will have to be proven in practice. There are hints that a geometrical treatment is possible for the special case of graphene, as shown in Ref. [62] by *I. Giordanelli et al.*. Graphene is special, since it allows the description of the electronic flow by relativistic hydrodynamic equations, cf. Refs. [119, 127, 114, 115, 58, 15]. Such a description does not hold for every material. Their pragmatic approach is to model the interaction between the electrons and ions through temperature-scaled inertial forces in the relativistic hydrodynamic equations, that are used to model the electronic flow on the graphene sheet. The ions' momentum is changed according to the momentum change of the electrons to ensure overall momentum conservation in the system, which influences the mapping and consequently the metric tensor. We want to understand if there is a more fundamental quantum mechanical principle from which we can derive the required form of the metric tensor to model electron-phonon interactions. Moving away from this special case, there are other successful numerical methods to simulate relativistic quantum system in curved space [35] that we may be able to leverage in simulations of other materials, using the non-relativistic limit.

From a more conceptual point of view, the geometric coupling means that a different perspective on electromagnetic, non-relativistic quantum systems exists which makes use of the equivalence principle in general relativity [164]. It states that one cannot locally distinguish between the effect of curvature in space-time and a gravitational force. One may wonder if this can

be extended to other types of forces or any type of interaction between two species of particles in quantum mechanics.

During the analysis we derive a local quantum mechanical measurement which indirectly observes the effects of the metric tensor operator due to the extended nature of the wave functions and hence shows that the two quantum systems are not equivalent. This is in contrast to general relativity where one cannot locally distinguish a gravitational force from a curved space-time (*weak equivalence principle*). Nevertheless, in two dimensions we are able to derive a quantum system and manifold with an underlying spinor structure for which quantum states with equal coordinate representation approximately agree on their energy and curvature measurement in both systems. Thereby, we derive the metric tensor for the case of electron-phonon interaction, show that it fulfills the conditions of the theory, that the matrix representation of the Hamilton and metric tensor operators will be the same if the one stays in the basis of the original problem, and gave an estimate of the error for the approximation. In the end we discuss some open questions and future research opportunities based on this result.

# 2 Quantum Mechanics In Phase Space

The interest of scientists in the study of quantum mechanics in phase space is caused by its strong analogy to classical dynamics and the ability to systematically study the corrections to thermal Boltzmann averages which arise due to quantum effects, which was also Wigner's original intention when he proposed his distribution in 1932. Therefore, scientists are usually interested to study the Wigner evolution for distributions of many-particle systems in a thermodynamic ensemble and not the dynamics of single particles, which are much easier described with the Schrödinger equation for a wave function. Of special interest in this formalism is the interplay between classical and quantum mechanics for the evolution of the system, that causes the appearance of mixed states. In the original quantum theory formalism one would use the quantum Liouville or von Neumann equation [121] to describe it. Neglecting all quantum corrections in the Wigner equation one finds the Vlasov equation which is used in the field of plasma physics [26] and serves as the classical limit of the Wigner equation.

We propose a new numerical method to solve the Wigner equation in quantum systems of spinless, non-relativistic particles. The method uses a spectral decomposition into $L^2(\mathbb{R}^d)$ basis functions in momentum-space to obtain a system of first-order advection-reaction equations. The resulting equations are solved by splitting the reaction and advection steps so as to allow the combination of numerical techniques from quantum mechanics and computational fluid dynamics by identifying the skew-hermitian reaction matrix as a generator of unitary rotations. The method is validated for the case of particles subject to a one-dimensional (an-)harmonic, double-well and Morse potential using finite-differences for the advection part. Thereby, we verify the second order of convergence and observe non-classical behavior in the evolution of the Wigner function.

The goal of the research is to establish the foundations of a lattice Wigner solver, which is based on the lattice Boltzmann method [13]. The main reason for investigating this problem is to find out if it is possible to use the computational advantages of a simulation method, which has been designed or derived in the context of classical fluid dynamics, also for studying quantum systems in the phase space formulation [189] which shows very strong analogies to the Navier-Stokes or Euler equations of fluid mechanics. The most striking property of the phase space or Wigner formalism of quantum mechanics is that all the information of the system is contained in a real-valued (quasi)-probability distribution function $w$ of the phase space variables. Taking the Wigner transform of a quantum mechanical observable, one just integrates the product of these two functions over phase space to measure the expectation value of the quantum system with respect to this observable. In contrast to the case of fluid dynamics the Wigner function $w$ is not interpreted as a probability density, as it is unbounded and can have negative values, which can also be seen in the subsequent examples of this chapter. However, as was shown in Refs. [162] and [190], the quantum dynamics in phase space do reveal chaotic behavior that is similar to the case of turbulence in fluids. In classical fluid mechanics, turbulent effects are much stronger in systems of weak dissipation or scattering, i.e. very few collisions. As one broadly distinguishes through the presence of a collision operator between a quantum Boltzmann and a Wigner transport equation, cf. Ref. [111], we want to design an algorithm that is able to simulate both types of transport equations but retains the advantages of the lattice Boltzmann algorithm that is often used to simulate a quantum Boltzmann equation. This would allow a systematical analysis of the influence of collisions, i.e. semi-classical approximations ([133]), on the quantum dynamics and its turbulent behavior. From fluid mechanics we know that collisionless flow is highly unstable, which is why one often introduces dissipation mechanisms to stabilize it. In our

case, we specifically want to design a method which allows to simulate the evolution of a system without collisions, which is why the aspect of numerical stability is of major importance to us.

The chapter is organized as follows. First, we give an introduction to the Wigner formalism and the properties of the Wigner equation. Second, we develop and investigate the new numerical method. And third, we present simulations for the (an-)harmonic oscillator, the double-well as well as the Morse potential and validate the results from the previous section, such as stability and convergence. The choice of examples is made to analyze the convergence and to demonstrate on the one hand the ability of the algorithm to simulate non-classical behavior, such as the tunneling of the wave function through the potential barrier in the double-well potential. On the other hand, we want to simulate problems which have a relevance for physical systems, such as the Morse potential which is often used to model the interaction between ions in a material.

## 2.1 Wigner formalism

As an introduction into the topic of the Wigner formalism, we try to give an understanding of the underlying concepts in the formulation of quantum mechanics in phase space as well as their significance, where we mainly follow Ref. [31]. As was mentioned before, it represents one of three equivalent formulations of non-relativistic quantum mechanics and was developed from the original theory, the operator formalism on a Hilbert space [121], around the same time as the path integral approach was popularized by *R. Feynman* [53], although it has been derived much earlier ([2]) by *G. Wentzel* in Ref. [180]. The phase space formulation works in analogy to Liouville's theorem which governs the evolution of the probability density in classical mechanics [61]. The important implications are on the one hand that the quantum phase space variables $(q_1, p_1, q_2, p_2, \ldots, q_d, p_d)$ have the same meaning as their classical counterparts that are generalized position coordinates and momenta. Every point in phase space is just an element in $\mathbb{R}^{2d}$. On the other hand the object containing all the information about the dynamical (quantum) system is a real-valued (quasi)-probability distribution which evolves according to the (Wigner) Liouville equation. The two major differences between the classical and quantum dynamics in phase space are the object of the evolution and functional form of the differential or integral equation for the temporal evolution. Restricting our perspective to the evolution of pure quantum states (superpositions), the Wigner function,

$$ w : \mathbb{R} \times \mathbb{R}^d \times \mathbb{R}^d \to \left[ - \left( \frac{2}{h} \right)^d, \left( \frac{2}{h} \right)^d \right] , \tag{2.1} $$

$$ w : t, \vec{q}, \vec{p} \to w(t, \vec{q}, \vec{p}) , \tag{2.2} $$

is a bounded, real-valued quasi-probability function of $(2d + 1)$ variables unlike the classical probability density, which is unbounded and always positive. An important implication of this statement is that the Wigner function can have negative values, which prevents us from interpreting it as a "simple" probability density. However, the volume of phase space where the Wigner function is negative is in general not larger than the smallest volume of uncertainty, which is just the product of uncertainty in each physically observable position and momentum, i.e. $\left( \frac{\hbar}{2} \right)^d$. Therefore, its effect is not directly observable but can only be inferred from the measurement statistics, in the same way as Heisenberg's uncertainty principles [78]. For a more detailed discussion of negative values of the Wigner function, we refer the reader to Ref. [84]. The second difference is that the Galilei-invariant evolution of the Wigner function, the Wigner equation, is facilitated by the Moyal [118] instead of the Poisson bracket. Wigner derived its form in Ref. [185] with the intention to "calculate quantum corrections to classical thermodynamic (Boltzmann) averages" [31], which is similar to the approach that we are taking by using a Taylor expansion.

The connection to the original operator based formulation, which can be used to show the equivalence of the two approaches, is made by performing the bijective Weyl-transform of objects in the phase space formulation,

$$ \hat{A} = \int\limits_{\mathbb{R}^{3d}} d\vec{q} d\vec{p} d\vec{z} \; |\vec{q} + \vec{z}/2\rangle A(\vec{q}, \vec{p}) e^{\iota \vec{p} \cdot \vec{z}/\hbar} \langle \vec{q} - \vec{z}/2| , \tag{2.3} $$

where $|\vec{q} \pm \vec{z}/2\rangle$ is the eigenstate of the position operators $\hat{Q}_i$ that build together with $\hat{P}_j$ the generators of the Heisenberg algebra, i.e. they fulfill the canonical commutation relations, $\imath$ is the imaginary unit and $\hbar \equiv \frac{h}{2\pi}$ the reduced Planck's constant. The inverse of the Weyl map, Wigner transform

$$A(\vec{q}, \vec{p}) = \frac{1}{(2\pi\hbar)^d} \int\limits_{\mathbb{R}^d} \mathrm{d}\vec{q}' \langle \vec{q} + \vec{q}'/2 | \hat{A} | \vec{q} - \vec{q}'/2 \rangle e^{-\imath \vec{p} \cdot \vec{q}'/\hbar} \ , \tag{2.4}$$

can be used to obtain the phase space function of the operators on a Hilbert space. The structure is similar to a Fourier transform. Obviously, one could think about other transformation rules and their inverses and it should be mentioned that there exist other pairs of transformations than the Weyl- and Wigner-transform, which are based for instance on the Hussimi or Glauber transformation and are described in Ref. [80]. In analogy to the relation between Laplace and Fourier transforms one often prefers the latter since its inverse is usually easier to calculate. Using the Weyl or Wigner transform, one learns that the Wigner function is related to the density operator. Therefore, applying the Wigner transform on the quantum Liouville equation

$$\imath\hbar \partial_t \hat{\rho}(t) = \left[ \hat{H}, \hat{\rho} \right] \ , \tag{2.5}$$

one obtains the dynamical equation which governs the evolution of the Wigner function in a quantum system described by the Hamilton operator $\hat{H} = H(\hat{Q}_1, \hat{P}_1, \ldots, \hat{Q}_d, \hat{P}_d)$. Its simulation is the heart of this chapter. It may be important for the reader to understand that the phase space formulation has its own right of existence and could in principle be formulated without any reference to the operator or path integral theories. History and education are the two main forces which make our minds demand these connections.

As stated above, our aim is to simulate the time-evolution of the Wigner function $w(\tau, \vec{q}, \vec{p})$ of a $d$-dimensional system. More concretely, we are going to focus on the evolution of non-relativistic spinless particles of mass $m$ subject to the potential $U(\tau, \vec{q})$, for which the Wigner equation reads

$$0 = \partial_\tau w + \frac{\vec{p}}{m} \cdot \vec{\nabla}_q w + \Theta[U]w \ , \tag{2.6}$$

$$\Theta[U] \equiv \frac{\imath}{\hbar} \left[ U(\tau, \vec{q} + \imath\hbar\vec{\nabla}_p/2) - U(\tau, \vec{q} - \imath\hbar\vec{\nabla}_p/2) \right] \ . \tag{2.7}$$

In analogy to fluid dynamics one might picture the evolution as an advection $(\partial_\tau w + \frac{\vec{p}}{m} \cdot \vec{\nabla}_q w)$ and forcing $(\Theta[U]w)$. To understand the action of the operator $\Theta[U]$ one can use a Taylor expansion around $\hbar \approx 0$ to order $N_a$, to obtain an approximation of the Wigner equation to the order $\mathcal{O}(\hbar^{N_a+2})$ if $N_a$ is uneven or the order $\mathcal{O}(\hbar^{N_a+1})$ if $N_a$ is even. Instead of the differential representation, one can also employ the integral form, which reads

$$\Theta[U]w = \frac{\imath}{\hbar} \int\limits_{\mathbb{R}^d} \mathrm{d}\vec{\eta} \ \delta U(\tau, \vec{q}, \vec{\eta}) \tilde{w}(\tau, \vec{q}, \vec{\eta}) e^{-\imath\vec{\eta}\cdot\vec{p}} \ , \tag{2.8}$$

$$\delta U(\tau, \vec{q}, \vec{\eta}) \equiv U\left(\tau, \vec{q} + \frac{\hbar}{2}\vec{\eta}\right) - U\left(\tau, \vec{q} - \frac{\hbar}{2}\vec{\eta}\right) , \tag{2.9}$$

$$\tilde{w}(\tau, \vec{q}, \vec{\eta}) \equiv \frac{1}{(2\pi)^d} \int\limits_{\mathbb{R}^d} \mathrm{d}\vec{p}' \ w(\tau, \vec{q}, \vec{p}') e^{\imath\vec{\eta}\cdot\vec{p}'} \ . \tag{2.10}$$

The independent variables are time $\tau$, space $\vec{q}$ and momentum $\vec{p}$ respectively. Hence, the Wigner function itself has the dimension $h^{-d}$, since it fulfills

$$\int\limits_{\mathbb{R}^d} \mathrm{d}\vec{q} \int\limits_{\mathbb{R}^d} \mathrm{d}\vec{p} \ w(\tau, \vec{q}, \vec{p}) = N_p \ , \tag{2.11}$$

where $N_p$ is the number of particles in the system.

To have an easier grasp on the equation, we make it dimensionless. First of all, we measure the Wigner function with respect to $\hbar^d$, i.e. we introduce the dimensionless Wigner function

$W(\tau, \vec{q}, \vec{p}) \equiv \hbar^d w(\tau, \vec{q}, \vec{p})/N_p$, and we employ the following scaling relations

$$\vec{x} = \vec{q}/l \; , \; t = \tau/T \; , \; \vec{v} = \frac{T}{lm}\vec{p} \; , \; V(t, \vec{x}) = U(\tau, \vec{q})/\bar{U} \; , \tag{2.12}$$

described in Ref. [131] where $l$ is a length, $T$ a time and $\bar{U}$ an energy scale. Thus, we obtain the dimensionless Wigner equation

$$0 = \partial_t W + \vec{v} \cdot \vec{\nabla}_x W + \Theta[V]W \; , \tag{2.13}$$

$$\Theta[V] \equiv \frac{\imath B}{\epsilon}\left[V\left(t, \vec{x} + \frac{\imath\epsilon}{2}\vec{\nabla}_v\right) - V\left(t, \vec{x} - \frac{\imath\epsilon}{2}\vec{\nabla}_v\right)\right] \; , \tag{2.14}$$

where we have introduced the dimensionless constants

$$\epsilon \equiv \frac{\hbar T}{l^2 m} \; , \; B \equiv \frac{\bar{U}T^2}{l^2 m} \; , \tag{2.15}$$

which we call *effective* Planck's constant and potential strength, respectively. The names are not arbitrary and reflect the natural occurrence of these numbers in the dimensionless formulation of the dynamics. For instance, Eq. (2.11) directly translates into

$$\epsilon^{-d}\int_{\mathbb{R}^d}\mathrm{d}\vec{x}\int_{\mathbb{R}^d}\mathrm{d}\vec{v}\; W(t, \vec{x}, \vec{v}) = N_p \; , \tag{2.16}$$

where we have replaced Planck's constant by its scaled counterpart. The Wigner transform of a pure quantum state $\Psi$ becomes

$$W = \int_{\mathbb{R}^d}\mathrm{d}\vec{y}\; \Psi^*\left(t, \vec{x} + \frac{\vec{y}}{2}\right)\Psi\left(t, \vec{x} - \frac{\vec{y}}{2}\right)\frac{e^{\imath\vec{v}\cdot\vec{y}/\epsilon}}{(2\pi)^d} \; , \tag{2.17}$$

where $\Psi(t, \vec{x}) \equiv l^{d/2}\psi(\tau, \vec{q})$ is the dimensionless wave function in position space. Typical examples of the dimensionless Wigner functions are shown for the superposition of two one-dimensional, minimum uncertainty, Gaussian wave packets localized around the dimensionless coordinates $x = \pm a$ together with their marginal distributions,

$$\psi_a(x) = C_x\left(e^{-\frac{(x+a)^2}{2}} + e^{-\frac{(x-a)^2}{2}}\right)\bigg/\left(\pi^{1/4}\sqrt{2(1+e^{-a^2})}\right) \; , \tag{2.18}$$

$$\phi_a(v) = C_v e^{-\frac{1}{2}v(2\imath a + v)}\left(1 + e^{2\imath av}\right)\bigg/\left(\pi^{1/4}\sqrt{2(1+e^{-a^2})}\right) \; , \tag{2.19}$$

$$W_a(x, v) = e^{-(x^2+v^2)}\left[e^{-a^2}\cosh(2ax) + \cos(2av)\right]\bigg/\left[\pi\left(1 + e^{-a^2}\right)\right] \; , \tag{2.20}$$

where $C_x$, $C_v$ are only constants to scale the probabilities in the figures such that the features of the Wigner function are still well recognizable, or the states of a one-dimensional quantum harmonic oscillator in Figs. 2.1-2.9

$$\psi_n(x) = C_x\frac{1}{\sqrt{2^n n!}\pi^{1/4}}e^{-\frac{x^2}{2}}H_n(x) \; , \tag{2.21}$$

$$\phi_n(v) = C_v\frac{\imath^n}{\sqrt{2^n n!}\pi^{1/4}}e^{-\frac{v^2}{2}}H_n(v) \; , \tag{2.22}$$

$$W_n(x, v) = \frac{(-1)^n}{\pi}e^{-x^2-v^2}L_n[2(x^2+v^2)] \; , \tag{2.23}$$

where $H_n$, $L_n$ are Hermite and Laguerre polynomials [70]. Since the coordinate and momentum representation of the harmonic oscillator quantum states are identical except for a phase, their probability distributions are the same, which is why the Wigner function has the same shape in $x$- and $v$-direction. In Figs. 2.1-2.6 one observes the quantum interference structure for the superposition of two wave packets for which the distance of their localization centers are increased and the oscillation between positive and negative values of the Wigner function in that region. Especially in Figs. 2.4-2.6 the reader may observe the wave-like structure in the center of

figure that is needed to include the strong oscillations in the momentum-marginal of the Wigner distribution. In Figs. 2.7 to 2.10 one sees the appearance of more concentric rings around the center for an increase in the quantum number $n$ of the eigenstate of the one-dimensional quantum harmonic oscillator. Comparing these pictures to the classical image of a particular solution of a one-dimensional harmonic oscillator in phase space, which is just an ellipse or using a different coordinate system a circle, it seems that the underlying structure is present but smeared out and multiplied by an oscillation that causes the change between positive and negative concentric rings. Looking at the oscillations in the marginal distributions the rings justify their existence.

In the subsequent sections we shall encounter Wigner functions for other potentials and their evolution in more sophisticated environments. These Wigner functions will not be static like the ones shown here that would not change during the Wigner evolution. However, the general properties of boundedness and the oscillatory behavior for quantum mechanical interference are features which we shall observe again. The reader may have noticed that negative regions are all surrounded by positive areas such that the integral either along a line in $x$ or $v$ will yield a positive definite result. This becomes clear when looking at the expectation values of the Wigner function, the so called marginal distributions, which are given for our one-dimensional examples by

$$\int_{-\infty}^{\infty} \mathrm{d}x \ W(t,x,v) = |\psi(t,v)|^2 \geq 0 \ , \tag{2.24}$$

$$\int_{-\infty}^{\infty} \mathrm{d}v \ W(t,x,v) = |\psi(t,x)|^2 \geq 0 \ , \tag{2.25}$$

which are the obvious consequences of being a (quasi)-probability distribution in phase space.
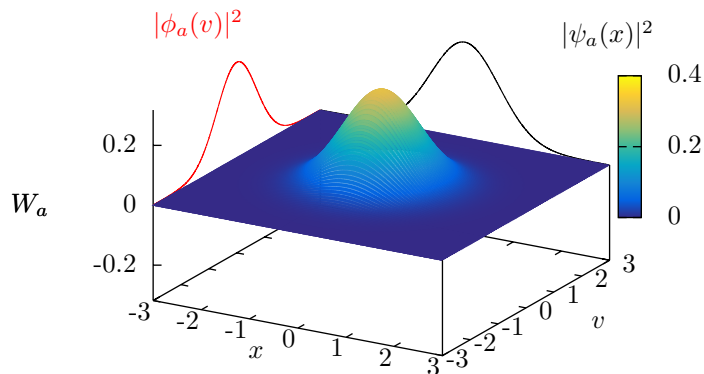


Figure 2.1: Dimensionless Wigner function and its marginals of a one-dimensional Gaussian wave packets localized around $x = 0$ with $\epsilon = B = 1$.

The dimensionless time-dependent Schrödinger equation reads

$$\imath \epsilon \partial_t \Psi = \left[ |\hat{\vec{v}}|^2/2 + B\hat{V}(t,\vec{x}) \right] \Psi \ , \tag{2.26}$$

and the canonical commutation relations in an operator based formalism of quantum mechanics [121] are written as

$$[\hat{x}_j, \hat{v}_k] = \imath \epsilon \delta_{j,k} \ . \tag{2.27}$$

The symbol $\Theta[V]$ stands for the pseudo-differential operator, whose action on $W$ can be written

Figure 2.2: Dimensionless Wigner function and its marginals of the superposition of two one-dimensional Gaussian wave packets localized around $x = \pm 1$ with $\epsilon = B = 1$.



Figure 2.3: Dimensionless Wigner function and its marginals of the superposition of two one-dimensional Gaussian wave packets localized around $x = \pm 2$ with $\epsilon = B = 1$.
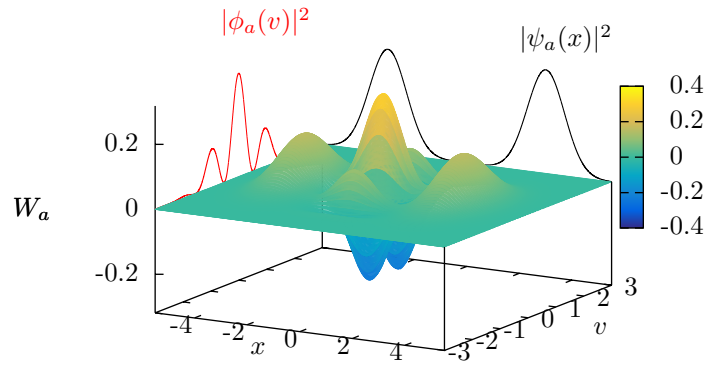
Figure 2.4: Dimensionless Wigner function and its marginals of the superposition of two one-dimensional Gaussian wave packets localized around $x = \pm 3$ with $\epsilon = B = 1$.
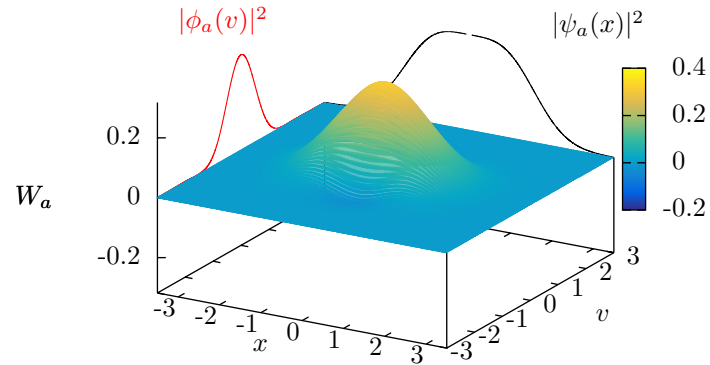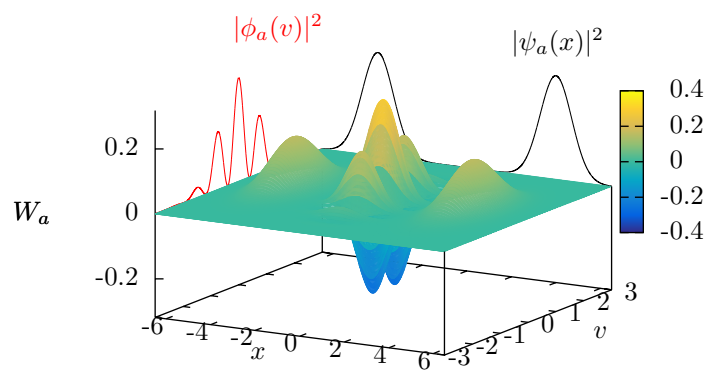


Figure 2.5: Dimensionless Wigner function and its marginals of the superposition of two one-dimensional Gaussian wave packets localized around $x = \pm 4$ with $\epsilon = B = 1$.
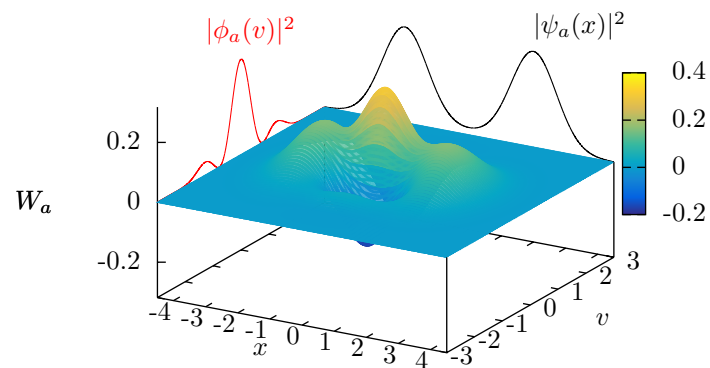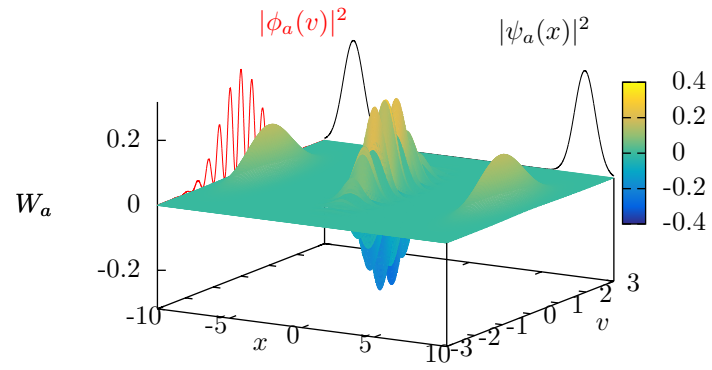
Figure 2.6: Dimensionless Wigner function and its marginals of the superposition of two one-dimensional Gaussian wave packets localized around $x = \pm 8$ with $\epsilon = B = 1$.



Figure 2.7: Dimensionless Wigner function and its marginals of the ground state ($n = 0$) of the one-dimensional quantum harmonic oscillator with $\epsilon = B = 1$.

Figure 2.8: Dimensionless Wigner function and its marginals of the first excited state $(n = 1)$ of the one-dimensional quantum harmonic oscillator with $\epsilon = B = 1$.



Figure 2.9: Dimensionless Wigner function and its marginals of the third excited state $(n = 3)$ of the one-dimensional quantum harmonic oscillator with $\epsilon = B = 1$.

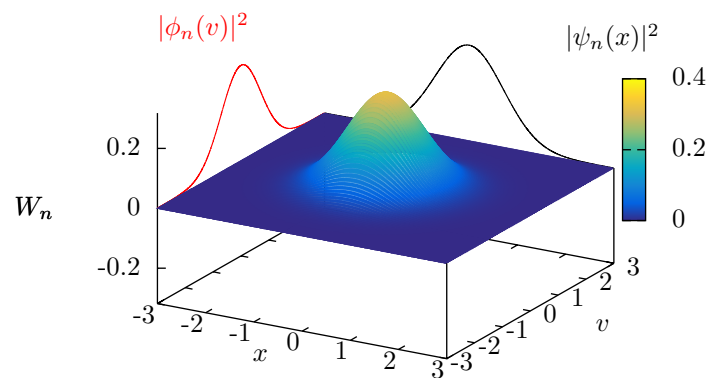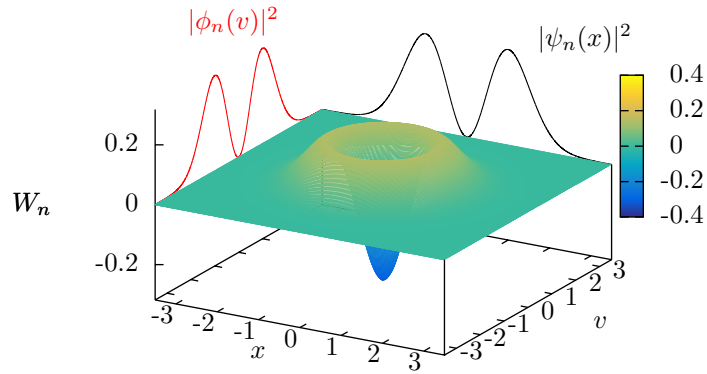Figure 2.10: Dimensionless Wigner function and its marginals of the sixth excited state ($n = 6$) of the one-dimensional quantum harmonic oscillator with $\epsilon = B = 1$.
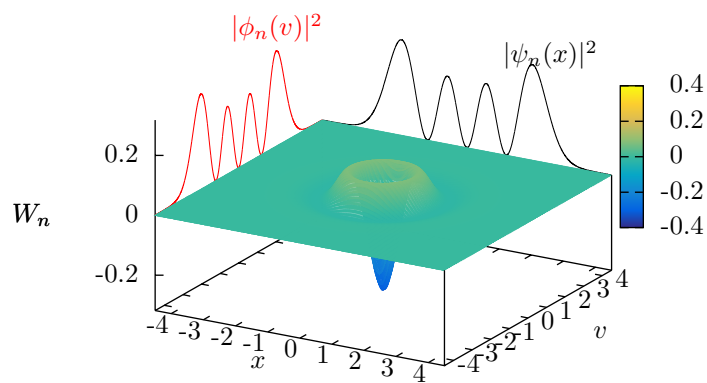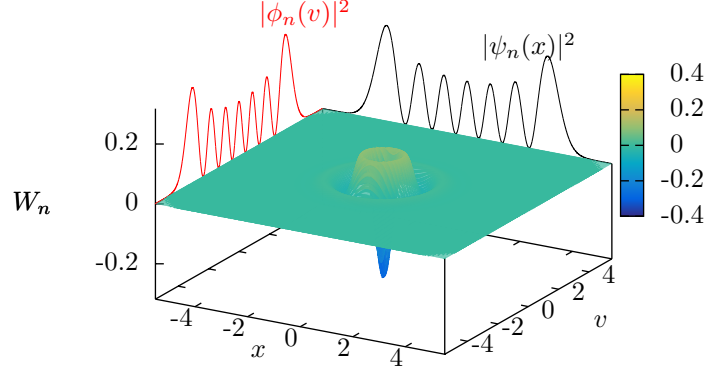
as an integral

$$\Theta[V]W = \frac{\imath B}{\epsilon} \int_{\mathbb{R}^d} \mathrm{d}\vec{\eta}\ \delta V(t,\vec{x},\vec{\eta})\tilde{W}(t,\vec{x},\vec{\eta})e^{-\imath\vec{\eta}\cdot\vec{v}} \ , \tag{2.28}$$

$$\delta V(t,\vec{x},\vec{\eta}) \equiv V\left(t,\vec{x}+\frac{\epsilon}{2}\vec{\eta}\right) - V\left(t,\vec{x}-\frac{\epsilon}{2}\vec{\eta}\right), \tag{2.29}$$

$$\tilde{W}(t,\vec{x},\vec{\eta}) \equiv \frac{1}{(2\pi)^d} \int_{\mathbb{R}^d} \mathrm{d}\vec{v}\ W(t,\vec{x},\vec{v})e^{\imath\vec{\eta}\cdot\vec{v}} \ . \tag{2.30}$$

If the potential is locally well-approximated by a Taylor series around $\epsilon \approx 0$ we can write

$$V(t,\vec{x}+\epsilon\vec{\eta}/2) \approx \sum_{|\lambda|=0}^{\infty} (\epsilon/2)^{|\lambda|} \frac{D_x^\lambda V(t,\vec{x})}{\lambda!}\vec{\eta}^\lambda \ , \tag{2.31}$$

where $\lambda$ is a multi-index of dimension $d$, i.e. $|\lambda| \equiv \sum_{i=1}^d \lambda_i$, $\lambda! = \prod_{i=1}^d \lambda_i!$, and $\vec{\eta}^\lambda \equiv \prod_{j=1}^d \eta_j^{\lambda_j}$. Therefore, the action of the pseudo-differential operator on the Wigner function reads

$$\Theta[V]W = -B \sum_{|\lambda|\in\mathbb{N}_{odd}} (\imath\epsilon/2)^{|\lambda|-1} \frac{1}{\lambda!} \left(D_x^\lambda V\right)\left(D_v^\lambda W\right) \ . \tag{2.32}$$

$\mathbb{N}_{odd}$ stands for positive odd integers, such that the sum is always real. For this treatment, the potential needs to be an *analytic function* defined on an open set $D \subset \mathbb{R} \times \mathbb{R}^d$, i.e. explicit dependence on time is possible. According to [136] this implies two important properties for us. First, the potential is locally given by a convergent power or Taylor series. Second, one can find an upper bound for all derivatives of the function $V$, since for every compact set $K \subset D$, for all $(t,\vec{x}) \in K$, and for all $|\lambda| \in \mathbb{N}_0$ there exists a constant $C$ such that

$$|D_x^\lambda V| \le C^{|\lambda|+1}\lambda! \ . \tag{2.33}$$

Hence, by choosing the right time and length scale $(T,l)$ for the problem one can find a convergent power series representation of the pseudo-differential operator. The correct choice means

$$\lim_{|\lambda|\to\infty} \left(\frac{C\epsilon}{2}\right)^{|\lambda|} = 0 \ , \tag{2.34}$$

such that the series in Eq. (2.32) converges (locally) uniformly under the assumption that $D_v^\lambda W$

is bounded.

## 2.1.1 Heisenberg's uncertainty relation

The famous uncertainty relation for position and momentum, cf. Ref. [78], can be written for a pair of canonically conjugated variables as

$$\Delta x_i \Delta v_j \geq \frac{\epsilon}{2} \delta_{ij} \ . \tag{2.35}$$

With canonically conjugated we mean that the observables which measure these quantities fulfill $[\hat{x}_i, \hat{v}_j] = \imath \epsilon \mathbb{I} \delta_{ij}$. The $\Delta$'s indicate the standard deviation in the measurement of the subsequent quantity. The deviation is measured statistically for several simultaneous measurements of position and momentum of a particle on initially identical quantum states. Here, we would like to demonstrate that this relation also holds in the phase space formulation of quantum mechanics, based on the Wigner-Weyl transform. In order to understand the problem consider the following equation

$$\langle \psi(\tau) | \hat{x}_i \hat{v}_j | \psi(\tau) \rangle \stackrel{?}{=} \int\limits_{\mathbb{R}^d \times \mathbb{R}^d} \mathrm{d}\vec{v} \mathrm{d}\vec{x} \ x_i v_j W(t, \vec{x}, \vec{v}) \ , \tag{2.36}$$

which might be obtained by just replacing the position and momentum operator through the respective phase space variables. If Eq. (2.36) were true, it would violate the uncertainty principle, as one can easily exchange position and momentum in the right hand side. Hence

$$\langle \psi(t) | \hat{x}_i \hat{v}_j | \psi(t) \rangle = \langle \psi(t) | \hat{v}_j \hat{x}_i | \psi(t) \rangle \tag{2.37}$$

such that the commutator

$$\langle \psi(t) | [\hat{x}_i, \hat{v}_j] | \psi(t) \rangle = 0 \ , \tag{2.38}$$

and one would find zero for the expression (2.35) which violates the uncertainty relation. In order to introduce a practical example for the Weyl transformation Eq. (2.3) from Ref. [182], we shall show that Eq. (2.36) is false by determining the operator, which is represented by the function $A(\vec{x}, \vec{v}) = x_j v_k$. We obtain

$$\hat{A} = \frac{1}{(2\pi)^{2d}} \int\limits_{\mathbb{R}^{4d}} \mathrm{d}\vec{x} \mathrm{d}\vec{v} \mathrm{d}\vec{a} \mathrm{d}\vec{b} \ x_j v_k e^{\imath [\vec{a} \cdot (\hat{\vec{x}} - \vec{x}) + \vec{b} \cdot (\hat{\vec{v}} - \vec{v})]} \tag{2.39}$$

$$= \frac{1}{(2\pi)^2} \int\limits_{\mathbb{R}^4} \mathrm{d}x_j \mathrm{d}v_k \mathrm{d}a_j \mathrm{d}b_k \ x_j v_k e^{\imath [a_j (\hat{x}_j - x_j) + b_k (\hat{v}_k - v_k)]} \tag{2.40}$$

$$= \frac{1}{(2\pi)^2} \int\limits_{\mathbb{R}^4} \mathrm{d}x_j \mathrm{d}v_k \mathrm{d}a_j \mathrm{d}b_k \ x_j e^{\imath a_j (\hat{x}_j - x_j)} v_k e^{\imath b_k (\hat{v}_k - v_k)} e^{-\frac{1}{2} [\imath a_j (\hat{x}_j - x_j), b_k (\hat{v}_k - v_k)]} \tag{2.41}$$

$$= \frac{1}{(2\pi)^2} \int\limits_{\mathbb{R}^4} \mathrm{d}x_j \mathrm{d}v_k \mathrm{d}a_j \mathrm{d}b_k \ x_j e^{\imath a_j (\hat{x}_j - x_j)} v_k e^{\imath b_k (\hat{v}_k - v_k)} e^{\imath \frac{\epsilon}{2} a_j b_k \delta_{jk}} \tag{2.42}$$

$$= \int\limits_{\mathbb{R}^2} \mathrm{d}a_j \mathrm{d}b_k \ e^{\imath \frac{\epsilon}{2} a_j b_k} e^{\imath a_j \hat{x}_j} e^{\imath b_k \hat{v}_k} \frac{1}{(2\pi)^2} \int\limits_{\mathbb{R}^2} \mathrm{d}x_j \mathrm{d}v_k \ x_j e^{-\imath a_j x_j} v_k e^{-\imath b_k v_k} \tag{2.43}$$

$$= -\int\limits_{\mathbb{R}^2} \mathrm{d}a_j \mathrm{d}b_k \ e^{\imath \frac{\epsilon}{2} a_j b_k} e^{\imath a_j \hat{x}_j} e^{\imath b_k \hat{v}_k} \delta'(a_j) \delta'(b_k) \tag{2.44}$$

$$= -\frac{\partial^2}{\partial a_j \partial b_k} \left[ e^{\imath \frac{\epsilon}{2} a_j b_k} e^{\imath a_j \hat{x}_j} e^{\imath b_k \hat{v}_k} \right]\Bigg|_{a_j = b_k = 0} \tag{2.45}$$

$$= -\frac{\imath \epsilon}{2} + \hat{x}_j \hat{v}_k = \frac{1}{2} \left( \hat{x}_j \hat{v}_k + \hat{v}_k \hat{x}_j \right) \ , \tag{2.46}$$

which is a symmetric operator under the exchange $\hat{x}_j \leftrightarrow \hat{v}_k$. So the next viable question would be, how does the function representation look like for the commutator? Apparently, we already calculated the functional form of the anti-commutator. So it is sufficient to determine the function for the operator $\hat{x}_j \hat{v}_j$. For this we use the Wigner map, which is the unique inverse of the Weyl

transformation to obtain

$$A(x,v) = 2 \int_{\mathbb{R}} \mathrm{d}y \ e^{-2\imath v y/\epsilon} \langle x+y|\hat{\mathrm{x}}\hat{\mathrm{v}}|x-y\rangle \tag{2.47}$$

$$= 2 \int_{\mathbb{R}} \mathrm{d}y e^{-2\imath v y/\hbar} (x+y)\langle x+y|\hat{\mathrm{v}}_k|x-y\rangle \tag{2.48}$$

$$= 2 \int_{\mathbb{R}} \mathrm{d}y e^{-2\imath v y/\hbar} (x+y)\langle x+y|\hat{\mathrm{v}}|x-y\rangle \tag{2.49}$$

$$= (xv + \imath\hbar)/2 \ , \tag{2.50}$$

such that using $\left[\hat{\mathrm{A}}, \hat{\mathrm{B}}\right] = -\{\hat{\mathrm{A}}, \hat{\mathrm{B}}\} + 2\hat{\mathrm{A}}\hat{\mathrm{B}}$ we find the obvious result $A(x_j, v_k) = \imath\hbar\delta_{jk}$ for the function that corresponds to the commutator.

## 2.1.2 General properties

Expanding the Wigner function in momentum-space into a set of orthonormal basis functions $\{\phi_k\}_{k\in\mathbb{N}}$ of $L^2(\mathbb{R}^d)$ with the inner product

$$\langle \phi_i, \phi_j \rangle_2 \equiv \int_{\mathbb{R}^d} \mathrm{d}\vec{v} \ \phi_i^*(\vec{v})\phi_j(\vec{v}) = \delta_{i,j} \ , \tag{2.51}$$

meaning that

$$W(t, \vec{x}, \vec{v}) = \sum_{k\in\mathbb{N}} a_k(t, \vec{x}) \ \phi_k(\vec{v}) \ , \tag{2.52}$$

we can rewrite the Wigner equation, Eq. (2.13), into an infinite system of linear, first-order partial differential equations (PDEs) for the coefficients $a_k(t, \vec{x}) \in \mathbb{C}$. The system can be derived by using the orthonormality property of the basis functions, Eq. (2.51). Depending on the choice of the basis we shall find different sets of PDEs. In general, all the sets can be written as a multi-dimensional *reaction-advection* equation

$$\partial_t \vec{a} + \sum_{i=1}^{d} A^{(i)} \partial_{x_i} \vec{a} + M_V(t, \vec{x})\vec{a} = \vec{0} \ , \tag{2.53}$$

where $A^{(i)}, M_V(t, \vec{x})$ are square matrices and $\vec{a} = (a_1, a_2, a_3, \dots)$ is the coefficient vector. Independent of the basis choice, the matrix $M_V(t, \vec{x})$ is *skew-hermitian* (non-hermitian), which can be demonstrated employing Eq. (2.32) or Eq. (2.28). When using formula (2.32) we have to assume that the basis functions are $C^\infty(\mathbb{R}^d)$. Under this condition we can shift the uneven derivatives, $|\lambda| \in \mathbb{N}_{odd}$, which appear as summands in the pseudo-differential operator, to show the skew-hermiticity. Demonstrating this property for a *general* set of basis functions of $L^2(\mathbb{R}^d)$, i.e. even non-differentiable, we use Eq. (2.28) to write

$$(M_V\vec{a})_k = \int_{\mathbb{R}^d} \mathrm{d}\vec{v} \ \phi_k^*(\vec{v}) \left(\Theta[V]W\right)(t, \vec{x}, \vec{v})$$

$$= \frac{\imath B}{\epsilon} \int_{\mathbb{R}^d} \mathrm{d}\vec{\eta} \ \delta V(t, \vec{x}, \vec{\eta})\hat{W}(t, \vec{x}, \vec{\eta}) \int_{\mathbb{R}^d} \mathrm{d}\vec{v} \ \phi_k^*(\vec{v})e^{-\imath\vec{v}\cdot\vec{\eta}} \ , \tag{2.54}$$

from which we conclude

$$(M_V)_{k,l} = \frac{\imath B}{(2\pi)^d \epsilon} \int_{\mathbb{R}^d} \mathrm{d}\vec{\eta} \ \delta V(t, \vec{x}, \vec{\eta}) \int_{\mathbb{R}^d \times \mathbb{R}^d} \mathrm{d}\vec{v}\mathrm{d}\vec{p} \ \phi_k^*(\vec{v})e^{-\imath\vec{v}\cdot\vec{\eta}}\phi_l(\vec{p})e^{\imath\vec{p}\cdot\vec{\eta}} \ . \tag{2.55}$$

This equation confirms the skew-hermiticity of the matrix representation of the pseudo-differential operator, which is an important property for the stability of the proposed algorithm as we shall see in the next section. An example of this matrix representation is shown in section 2.1.3. The

entries of the matrix $A^{(i)}$ are given by

$$\left(A^{(i)}\right)_{k,l} = \int\limits_{\mathbb{R}^d} \mathrm{d}\vec{v} \ \phi_k^*(\vec{v})v_i\phi_l(\vec{v}) \ , \tag{2.56}$$

which shows that it is *hermitian*.

### 2.1.3 Matrix-representation of the pseudo-differential operator

For a one-dimensional, analytical potential and a basis of *Hermite functions*, cf. section 2.3.1, the matrix-representation of the pseudo-differential operator simplifies from Eq. (2.55) to

$$M_V = \sum_{n=0}^{\infty} \left(\frac{\epsilon}{2}\right)^{2n} M_n \partial_x^{2n+1} V(t,x) \ , \tag{2.57}$$

$$(M_n)_{k,l} \equiv \imath^{k-l-1} \int\limits_{\mathbb{R}} \mathrm{d}\eta \ \frac{\eta^{2n+1}}{(2n+1)!}\phi_k(\eta)\phi_l(\eta) \ .$$

Each component of $M_n$ converges since the integrand is always a product of $e^{-\eta^2}$ with a polynomial. Looking at this result one observes how the contributions from odd higher order derivatives scale with the effective Planck constant and the change in sign. If we limit us to the set of functions $\{\phi_0,\ldots,\phi_N\}$, i.e. $N+1$ different Hermite functions it becomes clear that $M_n \in \mathbb{C}^{(N+1)\times(N+1)}$ and that matrices with larger $n$ have more non-zero entries. In the case of $N=5$, the matrix $M_V$ is already filled for $n=2$, i.e. considering the fifth derivative of the potential.

$$M_0 = \begin{pmatrix} 0 & -\frac{1}{\sqrt{2}} & 0 & 0 & 0 & 0 \\ \frac{1}{\sqrt{2}} & 0 & -1 & 0 & 0 & 0 \\ 0 & 1 & 0 & -\sqrt{\frac{3}{2}} & 0 & 0 \\ 0 & 0 & \sqrt{\frac{3}{2}} & 0 & -\sqrt{2} & 0 \\ 0 & 0 & 0 & \sqrt{2} & 0 & -\sqrt{\frac{5}{2}} \\ 0 & 0 & 0 & 0 & \sqrt{\frac{5}{2}} & 0 \end{pmatrix}$$

$$M_1 = \begin{pmatrix} 0 & -\frac{1}{4\sqrt{2}} & 0 & \frac{1}{4\sqrt{3}} & 0 & 0 \\ \frac{1}{4\sqrt{2}} & 0 & -\frac{1}{2} & 0 & \frac{1}{2\sqrt{3}} & 0 \\ 0 & \frac{1}{2} & 0 & -\frac{3\sqrt{\frac{3}{2}}}{4} & 0 & \frac{\sqrt{\frac{5}{6}}}{2} \\ -\frac{1}{4\sqrt{3}} & 0 & \frac{3\sqrt{\frac{3}{2}}}{4} & 0 & -\sqrt{2} & 0 \\ 0 & -\frac{1}{2\sqrt{3}} & 0 & \sqrt{2} & 0 & -\frac{5\sqrt{\frac{5}{2}}}{4} \\ 0 & 0 & -\frac{\sqrt{\frac{5}{6}}}{2} & 0 & \frac{5\sqrt{\frac{5}{2}}}{4} & 0 \end{pmatrix}$$

$$M_2 = \begin{pmatrix} 0 & -\frac{1}{32\sqrt{2}} & 0 & \frac{1}{16\sqrt{3}} & 0 & -\frac{1}{16\sqrt{15}} \\ \frac{1}{32\sqrt{2}} & 0 & -\frac{3}{32} & 0 & \frac{\sqrt{3}}{16} & 0 \\ 0 & \frac{3}{32} & 0 & -\frac{19}{32\sqrt{6}} & 0 & \frac{\sqrt{\frac{5}{6}}}{4} \\ -\frac{1}{16\sqrt{3}} & 0 & \frac{19}{32\sqrt{6}} & 0 & -\frac{11}{16\sqrt{2}} & 0 \\ 0 & -\frac{\sqrt{3}}{16} & 0 & \frac{11}{16\sqrt{2}} & 0 & -\frac{17\sqrt{\frac{5}{2}}}{32} \\ \frac{1}{16\sqrt{15}} & 0 & -\frac{\sqrt{\frac{5}{6}}}{4} & 0 & \frac{17\sqrt{\frac{5}{2}}}{32} & 0 \end{pmatrix}$$

## 2.2 Numerical method

For the numerical treatment, the expansion in Eq. (2.52), is cut at the index $N$, i.e. we assume all higher coefficients to be zero. The problem is hence shifted to the time-evolution of the

$N$-dimensional coefficient vector with the initial condition

$$\vec{a}(t_0, \vec{x}) = \int\limits_{\mathbb{R}^d} \mathrm{d}\vec{v} \; W(t_0, \vec{x}, \vec{v}) \vec{\phi}(\vec{v}) \;, \tag{2.58}$$

where $\vec{\phi} = (\phi_1, \phi_2, \ldots, \phi_N)$. Therefore, we work with a finite set of $N$ balance equations (PDEs) in the form of Eq. (2.53). It is important to note that, thanks to the Cauchy-Kowaleski theorem, see Ref. [85], we know that the system will *locally* have a *unique analytical* solution if the coefficient matrix $M_V$ is an analytic function. This condition is sufficient, since the matrices $A^{(i)}$ from Eq. (2.56) are constant. In addition, we would like to mention that this does not necessarily apply if $M_V$ belongs to the larger group of smooth functions, see Levy's argument in Ref. [85].

## 2.2.1 Operator-splitting

To proceed with the problem we use an operator-splitting technique ("divide-and-conquer"), i.e. we separate the action of the "streaming",

$$\mathcal{S}\vec{a} \equiv - \sum_{i=1}^{d} A^{(i)} \partial_{x_i} \vec{a} \;, \tag{2.59}$$

and "forcing",

$$\mathcal{F}_t \vec{a} \equiv -M_V(t, \vec{x})\vec{a} \;, \tag{2.60}$$

operators to apply them sequentially. First, we discretize the time interval from zero to $t$ in $N_t$ periods of duration $\delta t$. Then we can write the approximated solution to Eq. (2.53) as

$$\begin{aligned} \vec{a}(t, \vec{x}) &\approx \overleftarrow{\prod_{k=0}^{N_t-1}} \exp\left( \mathcal{S}\delta t + \int\limits_{k\delta t}^{(k+1)\delta t} \mathrm{d}t' \; \mathcal{F}_{t'} \right) \vec{a}_0(\vec{x}) \\ &\approx \overleftarrow{\prod_{k=0}^{N_t-1}} e^{\mathcal{S}\delta t} \exp\left( \int\limits_{k\delta t}^{(k+1)\delta t} \mathrm{d}t' \; \mathcal{F}_{t'} \right) \vec{a}_0(\vec{x}) \\ &\approx \overleftarrow{\prod_{k=0}^{N_t-1}} e^{\mathcal{S}\delta t} e^{\mathcal{F}_{k\delta t}\delta t} \vec{a}_0(\vec{x}) + \mathcal{O}(\delta t) \;, \end{aligned} \tag{2.61}$$

where the $\overleftarrow{\prod_{k=0}^{N_t-1}} A_k = A_{N_t-1} A_{N_t-2} \cdots A_0$. It is important to apply the operators in a time-ordered product series, which is indicated by the arrow above the product sign. During the derivation we have used a third-order accurate Fer expansion [1] in the first step, simple operator splitting in the second and the numerical integration procedure

$$\int\limits_{k\delta t}^{(k+1)\delta t} \mathrm{d}t' \; \mathcal{F}_{t'} \approx \mathcal{F}_{k\delta t}\delta t + \mathcal{O}(\delta t^2) \;, \tag{2.62}$$

in the third step. The obtained method will be first-order accurate if it is stable and the numerical procedure for each operator (streaming and forcing) is at least second-order accurate. The total error arises since the matrices $A^{(i)}\partial_{x_i}$ and $M_V$ are in general not commuting and because of the second-order accurate integration procedure. For a second-order accurate method we write

$$\vec{a}^*(t, \vec{x}) \approx \overleftarrow{\prod_{k=0}^{N_t-1}} e^{\mathcal{S}\delta t} \exp\left( \int\limits_{k\delta t}^{(k+1)\delta t} \mathrm{d}t' \; \mathcal{F}_{t'} \right) \vec{a}_0^*(\vec{x}), \tag{2.63}$$

$$\vec{a}^*(t, \vec{x}) \equiv e^{-\frac{1}{2}\mathcal{F}_t \delta t} \vec{a}(t, \vec{x}) \;, \tag{2.64}$$

---

[1] A Fer or Magnus expansion gives approximate solutions to a system of linear equations of the type $\dot{\vec{a}}(t) = M(t)\vec{a}(t)$ while preserving certain symmetry properties of the matrix $M(t)$ in the solution $\vec{a}(t)$ [87].

where we have used a second order accurate operator splitting, the Strang-splitting [163]. To achieve the demanded accuracy we have to use a third-order accurate integration formula for the forcing operation, whereas second-order accuracy in the definition of $a^*$ is sufficient, because it acts only twice during the evolution. If the potential has an explicit time-dependence one can use the midpoint rule,

$$\int\limits_{k\delta t}^{(k+1)\delta t} \mathrm{d}t' \ \mathcal{F}_{t'} \approx \mathcal{F}_{(k+\frac{1}{2})\delta t}\delta t + \mathcal{O}(\delta t^3) \ . \tag{2.65}$$

For the Wigner-Poisson problem [112] where one needs to determine the self-consistent electro-static potential, $\Delta V = e\rho(t, \vec{x})$, at every time-step, we make use of the fact that the forcing operation does not change the density and hence the electro-static potential. Taking Eq. (2.32) and integrating by parts we can show

$$\int\limits_{\mathbb{R}^d} \mathrm{d}\vec{v} \ (\partial_t W + \Theta[V]W) = \partial_t \rho = 0 \ . \tag{2.66}$$

Consequently, if the numerical procedure in this step conserves the density up to $\mathcal{O}(\delta t^3)$, it will be sufficient to re-calculate the forcing operator after each streaming, which coincides with our time-step definition in Eq. (2.63). The questions that remain to be solved are how to compute approximations of the operators' actions $e^{\mathcal{S}\delta t}\vec{a}$ ("streaming") and $e^{\mathcal{F}_k\delta t}\vec{a}$ ("forcing") such that the resulting algorithm is stable, computationally efficient, and of the desired accuracy (first- or second-order).

### 2.2.2 Forcing

As it was mentioned in section 2.1.2, the matrix $M_V$ is skew-hermitian, which means that it belongs to the Lie algebra of the group of unitary matrices [5]. Depending on the basis choice we might also find the subgroups of special unitary or special orthogonal matrices if $M_V$ is a traceless, skew-Hermitian, complex matrix or a real, skew-symmetric one. Hence, the action of the forcing operator is a *unitary rotation* of the coefficient vector, whose matrix form can in general be calculated before starting the simulation. For a skew-symmetric matrix one could use the method described in Ref. [59] or a Padé approximation [117]

$$e^{\mathcal{F}_{k\delta t}\delta t} \approx \left[\mathbf{1} + \frac{\delta t}{2}M_V(k\delta t, \vec{x})\right]^{-1} \left[\mathbf{1} - \frac{\delta t}{2}M_V(k\delta t, \vec{x})\right] \ . \tag{2.67}$$

For the case of the Wigner-Poisson problem one needs to compute the product of matrix times vector at every time-step, which for instance can be efficiently done with the "Expokit" software package [157] or using a pre-calculated explicit formula.

One might be tempted to use explicit schemes, such as Euler or Runge-Kutta, to approximate the forcing. However, these methods can become unstable for strongly changing potentials and poor temporal and spatial resolution, which we shall show for two examples in Fig. 2.11 by evaluating the amplification factor $g$ in a linear stability analysis according to [86]. Consider a time-independent one-dimensional anharmonic potential

$$V(x) = \frac{x^2}{2} + Kx^4 \ , \tag{2.68}$$

and the Euler as well as the fourth-order Runge-Kutta method (RK4) [21] as approximations of the forcing, whose amplification factors are given by

$$g_{\mathrm{Euler}} = |\mathbf{1} - \delta t M_V(x)|_2 \ , \tag{2.69}$$

$$g_{\mathrm{RK4}} = |\mathbf{1} + \sum_{j=1}^{4} \frac{[-\delta t M_V(x)]^j}{j!}|_2 \ , \tag{2.70}$$

where $|\ldots|_2$ stands for the spectral-norm [136]

$$|M|_2 \equiv \max_{|\vec{x}|=1} |M\vec{x}| \ , \tag{2.71}$$

such that Parseval's identity [136] is applicable. An amplification factor of $g = 1$ means that the method is stable, whereas an amplification factor larger than one means it is unstable. The plots for both methods are shown in Fig. 2.11. One observes the big amplification factor at the domain boundary, caused by the strong potential variation in this area, cf. Fig. 2.12, which may eventually trigger a numerical instability.
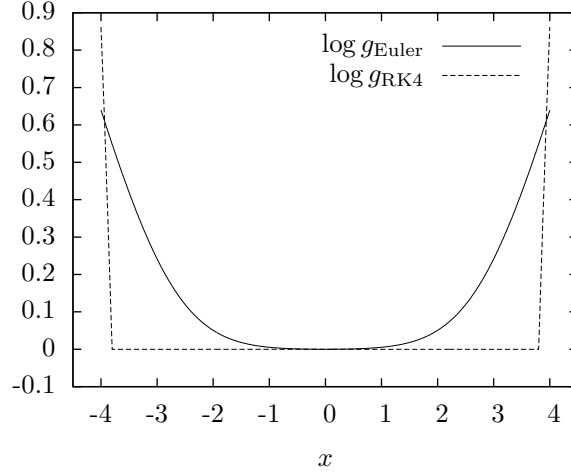


Figure 2.11: Amplification factor for an anharmonic potential ($K = 0.5$) using Euler ($1/\delta x = 100$) and RK4 ($1/\delta x = 50$) methods with $N = 10$.
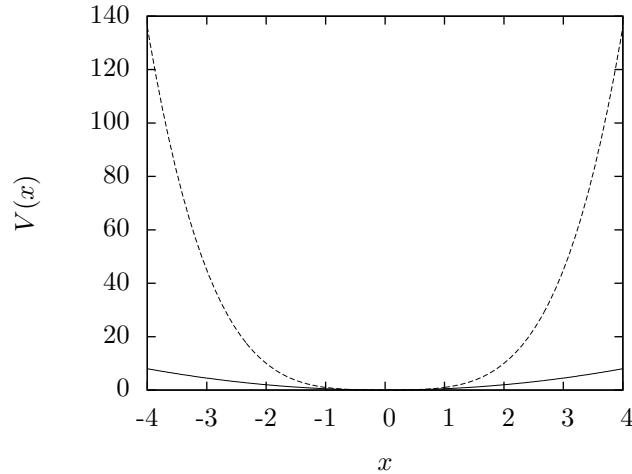


Figure 2.12: Dimensionless anharmonic potential $V(x) = \frac{x^2}{2} + Kx^4$ for $K = 0$ (solid) and $K = 0.5$ (dashed).

## 2.2.3 Streaming

The streaming can in general be achieved by methods handling (non-)linear hyperbolic systems of conservation laws, often used in computational fluid dynamics, such as finite difference, volume, elements or lattice Boltzmann [13]. Using, for example, in $d = 1$ a flux vector splitting [161], we

first diagonalize the matrix $T^{-1}A^{(1)}T = D_A$ from Eq. (2.56). Then we define the new coefficient vector $\vec{b}(t,\vec{x}) \equiv T^{-1}\vec{a}(t,\vec{x})$ and the modified forcing term $\tilde{M}_V \equiv T^{-1}M_V T$, such that the new system of partial differential equations can be written as

$$\partial_t \vec{b} + D_A \partial_x \vec{b} + \tilde{M}_V(t,\vec{x})\vec{b} = \vec{0} \ . \tag{2.72}$$

To simulate the action of the streaming operator, one can now employ the first-order accurate upwind or the second-order accurate Lax-Wendroff scheme [110], since $A^{(1)}$ only has real eigenvalues, i.e. $D_A$ is a real diagonal matrix. The drawbacks of the explicit methods are that the Courant-Friedrichs-Levy condition [28]

$$\frac{|\lambda|_{max}\delta t}{\delta x} \leq 1 \ , \tag{2.73}$$

needs to be fulfilled for a stable simulation (*conditional stability*) and that they introduce a considerable amount of dissipation, especially if structures with large gradients are streamed [110]. If we are employing Hermite functions we could - in the spirit of the lattice Boltzmann method [69, 167, 116, 169] - use an "exact" streaming operation, which will mitigate the dissipative effects. For this we perform a discrete Hermite transform in $\vec{v}$-space[105] from the coefficient vector to the Wigner function, stream, and transform back to the coefficient vector. However, a more detailed analysis and implementation can be the topic of another research project.

### 2.2.4 Stability

The proposed method for evolving the Wigner function will be stable if the operations streaming and forcing are both stable. Since the action of the forcing can be described as a unitary rotation one should make sure that the numerical technique conserves this property and hence has an amplification factor of unity. In that respect, being skew-hermitian is a sufficient but not necessary condition of the matrix representation of $\Theta[V]$ for the stability of such algorithms, which we shall demonstrate in section 2.2.5 for an asymmetric Hermite basis. This may require a very accurate result for the rotation matrix or a very different approach to implement the rotation through the use of Clifford algebras [159]. The user may choose which technique suits him better, but should be aware that we have not investigated if the use of Clifford algebras offers any computational advantage. Nevertheless, the least computationally expensive operation is the direct matrix-vector multiplication $\mathcal{O}(N^2)$, whereas the use of the algebra will need slightly more operations (although the scaling is the same). For the streaming, one can use any stable method that handles linear advection equations, such as flux vector splitting [161], Godunov, finite volume or finite element [110]. The resulting time-evolution of the Wigner function will hence be stable. There are other ways to tackle an instability problem which are for example the introduction of a collision operator, see Ref. [89], or a filtering technique, further explained in Ref. [25]. It should be stressed that these additional terms always come with other disadvantages, especially for the conservation laws.

### 2.2.5 Example for an asymmetric basis choice

Assuming we are dealing with a harmonic potential, i.e. $K = 0$ in Eq. (2.68), then the quantum corrections vanish and the Wigner and Vlasov equation are identical. Using an asymmetric Hermite basis, as described in [81], i.e.

$$W(t,x,v) = \frac{e^{-v^2}}{\pi^{1/4}} \sum_{k=0}^{N} a_k(t,x) \frac{H_k(v)}{\sqrt{2^n n!}} \ , \tag{2.74}$$

the matrix representation of $\Theta[V]$ will be lower triangular, which can be seen using formula (2.32) and integration by parts. For $N = 4$ we find

$$M_V(x) = -x \begin{pmatrix} 0 & 0 & 0 & 0 & 0 \\ \sqrt{2} & 0 & 0 & 0 & 0 \\ 0 & 2 & 0 & 0 & 0 \\ 0 & 0 & \sqrt{6} & 0 & 0 \\ 0 & 0 & 0 & 2\sqrt{2} & 0 \end{pmatrix}$$

which is not skew-hermitian or -symmetric anymore but strictly lower triangular. Examining the resulting exact forcing action, we find

$$e^{-M_V(x)\delta t} = \begin{pmatrix} 1 & 0 & 0 & 0 & 0 \\ \sqrt{2}x\delta t & 1 & 0 & 0 & 0 \\ \sqrt{2}x^2\delta t^2 & 2x\delta t & 1 & 0 & 0 \\ \frac{2x^3\delta t^3}{\sqrt{3}} & \sqrt{6}x^2\delta t^2 & \sqrt{6}x\delta t & 1 & 0 \\ \sqrt{\frac{2}{3}}x^4\delta t^4 & \frac{4x^3\delta t^3}{\sqrt{3}} & 2\sqrt{3}x^2\delta t^2 & 2\sqrt{2}x\delta t & 1 \end{pmatrix}$$

from which we conclude for the amplification factor using Eq. (2.71) for the matrix norm

$$g_{AS} = \left| e^{-M_V(x)\delta t} \right|_2 = 1 \ .$$

This means that this method can also be stable, unlike described in Ref. [150].

## 2.3 Simulation

For the validation of our numerical procedure we simulate the time-evolution of an (an-)harmonic oscillator. The advantages of these examples are that, on one hand, we can compare with the analytical Wigner function of an harmonic oscillator, which is calculated as described in Ref. [70]. On the other hand, we can observe the effects of quantum corrections to the classical dynamics for an anharmonic potential $U_{\text{anh}}(\vec{q}) = \frac{1}{2}m\omega|\vec{q}|^2 + \frac{m^2\omega^3 K}{\hbar}|\vec{q}|^4$ [185]. In the case of the double well potential $U_{\text{mh}}(\vec{q}) = cm\omega|\vec{q}|^2 + \frac{m^2\omega^3 K}{\hbar}|\vec{q}|^4$ we can observe the tunneling phenomenon in the Wigner formalism, since for certain parameter ranges $c < 0$ and $K > 0$ the system has states with eigenenergies below 0 which would not allow classical particles to travel from one potential minimum to the other. For a more physical example, we also simulate the Wigner equation for the one-dimensional Morse potential $U(q) = D_e \left(1 - e^{-\frac{q-q_e}{l}}\right)^2$. As we have described in the introduction to the Wigner formalism, see section 2.1, we use a dimensionless form of the Schrödinger and Wigner equations. For our examples, we take $l \equiv \sqrt{\frac{\hbar}{m\omega}}$, $T \equiv \frac{1}{\omega}$ and $\bar{U} \equiv \hbar\omega$ as length, time, and potential scales, respectively, to find $\epsilon = 1$ and $B = 1$. The dimensionless time-dependent Schrödinger equation reads

$$\imath\partial_t \Psi = \left( \frac{|\hat{\vec{v}}|^2}{2} + c|\hat{\vec{x}}|^2 + K|\hat{\vec{x}}|^4 \right) \Psi \ , \tag{2.75}$$

such that the eigenfunctions and -values of the dimensionless Hamilton operator at $K = 0$ and $c = 1/2$ are given by

$$\Psi_n^{|n|}(\vec{x}) = \frac{e^{-|\vec{x}|^2/2}}{\sqrt{\pi^{d/2}2^{|n|}n!}} H_n^{|n|}(\vec{x}) \ , \tag{2.76}$$

$$\mathcal{E}_n = |n| + d/2 \ , \tag{2.77}$$

where $n = (n_1, \ldots, n_d)$ is a multi-index and

$$H_n^{|n|}(\vec{x}) = (-1)^{|n|} e^{|\vec{x}|^2} \left( D^k e^{-|\vec{x}|^2} \right) \ , \tag{2.78}$$

the $d$-dimensional Hermite polynomial, according to Ref. [68]. The dimensionless Wigner equation in differential form becomes

$$\partial_t W + \vec{v} \cdot \vec{\nabla}_x W - 2(c + 2K|\vec{x}|^2)\vec{x} \cdot \vec{\nabla}_v W + \Theta_c[K]W = 0 \ , \tag{2.79}$$

where

$$\Theta_c[K]W \equiv \frac{K}{4} \sum_{|\lambda|=3} \frac{D_x^\lambda |\vec{x}|^4}{\lambda!} D_v^\lambda W \tag{2.80}$$

is the quantum correction to the "classical" dynamics of the particle.

## 2.3.1 Basis of Hermite functions

In our simulation, we choose Hermite functions as orthonormal basis set in momentum-space, i.e.

$$\phi_k^{|k|}(\vec{v}) = \frac{e^{-|\vec{v}|^2/2}}{\sqrt{\pi^{d/2}2^{|k|}k!}} H_k^{|k|}(\vec{v}) \ , \tag{2.81}$$

where $k$ is a multi-index of dimension $d$. Hence, Eq. (2.52) changes to

$$W(t,\vec{x},\vec{v}) = \sum_{|k|=0}^{N} a_k^{|k|}(t,\vec{x}) \ \phi_k^{|k|}(\vec{v}) \ . \tag{2.82}$$

The number of basis functions that is needed to simulate the evolution of a given state will in general depend on how wide the spread of the corresponding Wigner function is in momentum space. However, by scaling the Hermite functions, cf. Ref. [150], one can significantly reduce $N$ to simulate eigenstates with higher energy. One uses a velocity-scale $v_s$ (usually associated with the system temperature) to write the scaled Hermite functions as

$$\phi_k^{|k|}(\vec{v}') = \frac{1}{v_s^{d/2}}\phi_k^{|k|}\left(\frac{\vec{v}}{v_s}\right) \ , \tag{2.83}$$

which enables the Hermite functions to work around the natural velocity scale of the problem at hand and, hence reducing the number of required functions for a given accuracy. In order to find the necessary number of basis functions for a chosen accuracy one needs to take a look at the variation of the resulting Wigner function with respect to changes in $N$. In order to find the initial coefficients, $\vec{a}(t_0,\vec{x})$, we use the property of the Hermite polynomials or Hermite functions, defined by Eq. (2.81), that they are eigenfunctions of the Fourier transform operator,

$$\int_{\mathbb{R}^d}\mathrm{d}\vec{v} \ e^{\imath\vec{y}\cdot\vec{v}}\phi_k^{|k|}(\vec{v}) = (\sqrt{2\pi})^d\imath^{|k|}\phi_k^{|k|}(\vec{y}) \ . \tag{2.84}$$

The proof is given in Ref. [70]. Using the Wigner transform, defined by Eq. (2.17), we can write

$$\begin{aligned}
a_k^{|k|}(t_0,\vec{x}) &= \int_{\mathbb{R}^d}\mathrm{d}\vec{v} \ W(t_0,\vec{x},\vec{v})\phi_k^{|k|}(\vec{v}) \\
&= \frac{\epsilon^d\imath^{|k|}}{(2\pi)^{\frac{d}{2}}}\int_{\mathbb{R}^d}\mathrm{d}\vec{y} \ \Psi^*\left(t_0,\vec{x}+\frac{\epsilon\vec{y}}{2}\right)\Psi\left(t_0,\vec{x}-\frac{\epsilon\vec{y}}{2}\right)\phi_k^{|k|}(\vec{y}) \ .
\end{aligned} \tag{2.85}$$

One can see that the obtained coefficients are real due to the symmetry properties of the Hermite functions $\phi_k^{|k|}(-\vec{y}) = (-1)^{|k|}\phi_k^{|k|}(\vec{y})$. In addition, we can simplify Eq. (2.55) by using the same property to obtain

$$(M_V)_{k,l} = \frac{B}{\epsilon}\imath^{|k|-|l|-1}\int_{\mathbb{R}^d}\mathrm{d}\vec{\eta} \ \delta V(t,\vec{x},\vec{\eta})\phi_k^{|k|}(\vec{\eta})\phi_l^{|l|}(\vec{\eta}) \ . \tag{2.86}$$

Looking at this result, one can realize that $M_V$ is a real, skew-symmetric matrix. The matrices $A^{(i)}$ are real, symmetric and *sparse* for this basis choice. They are sparse, because, regardless

how the basis functions are ordered at most two entries per row or column are non-zero due to the recursion relation of the $d$-dimensional Hermite polynomials [68]. For further explanations on the conservation and convergence properties for this basis choice, we refer the reader to Ref. [150], where the authors treat the Vlasov equation, which can be considered as the classical limit, $\epsilon \to 0$, of the Wigner equation.

### 2.3.2 Harmonic oscillator

We run a simulation of a one-dimensional harmonic oscillator with the second order accurate method, using a Lax-Wendroff scheme for the streaming, a spatial resolution of $\delta x = 1/50$, and periodic boundaries at $x = \pm 3.5$. The resulting matrices for the reaction-advection system can be calculated using formula (2.57) in 2.1.3. As initial state $\Psi$ we choose a superposition between ground and first excited state $\frac{\Psi_0 + \Psi_1}{\sqrt{2}}$, whose resulting exact time-dependent Wigner function according to Ref. [31] reads

$$W_{\text{ex}}(t, x, v) = \frac{x^2 + v^2 + \sqrt{2}\left[x\cos(t) - v\sin(t)\right]}{\pi} e^{-x^2 - v^2} \tag{2.87}$$

Thus, we can observe the evolution for a system whose probability density changes in time. In Fig. 2.13, we show a comparison between the analytical spatial probability density $\rho_\Psi(t, x) \equiv |\Psi(t, x)|^2$ and the probability density calculated from the Wigner function with

$$\rho_W(t, x) \equiv \int_{\mathbb{R}} \mathrm{d}v \; W(t, x, v) = \sum_{k=0}^{N} a_k(t, x) \int_{\mathbb{R}} \mathrm{d}v \; \phi_k(v) \; .$$

The comparison shows very good agreement. However, the actual results for the Wigner function are more insightful, since they contain additional information. They are shown in Figs. 2.14-2.18 together with the contour lines at $W = 0$ and $W = \pm 0.025$. The local error is in the order of $10^{-4}$ and will be analyzed in the next section. One should observe a *rigid* rotation of the Wigner function in phase space around the negative region in the center, which is typical for the harmonic oscillator. This can be seen by using the method of characteristics [29] for solving Eq. (2.79) at $K = 0$ and $c = 0.5$ which leads to solving the Hamilton equations

$$\dot{x} = v \; , \; \dot{v} = -x \; . \tag{2.88}$$

The period for one revolution is $T = 2\pi(\mathcal{E}_1 - \mathcal{E}_0) = 2\pi$, which is also confirmed by the simulation in terms of the temporal error margin. The reader should also be able to see that the integral along any vertical or horizontal line in these Figs. gives a positive result, since the negative region is always surrounded by a compensating positive part such that the marginals, as expressed in Eq. (2.25), are probabilities. The contour line at $W = 0$ close to the boundaries shows patterns which are not present in the analytical solution. They are caused by the numerical error fluctuations, see Fig. 2.19, since the magnitude of the Wigner function in that region becomes comparable to the numerical error.

### 2.3.3 Convergence

Based on the work in Ref. [70], one can calculate the exact Wigner transform $W_{\text{ex}}$ of any wave function $\Psi(t, \vec{x})$ expanded in Hermite functions. We shall use this formula to calculate the Wigner transform for an eigenstate $\Psi_n(t, x)$ of the harmonic oscillator and compare our results for different numbers of basis functions $N$ and spatial resolutions $1/\delta x$. It is important to note that the exact Wigner function of an eigenstate for $K = 0$, $c = 0.5$ and $d = 1$ is given by Laguerre polynomials through

$$W_n(x, v) = \frac{(-1)^n}{\pi} L_n[2(x^2 + v^2)] e^{-x^2 - v^2} \; , \tag{2.89}$$

$$L_n(y) \equiv \frac{1}{n!}\left(\frac{\mathrm{d}}{\mathrm{d}x} - 1\right)^n x^n \; , \tag{2.90}$$
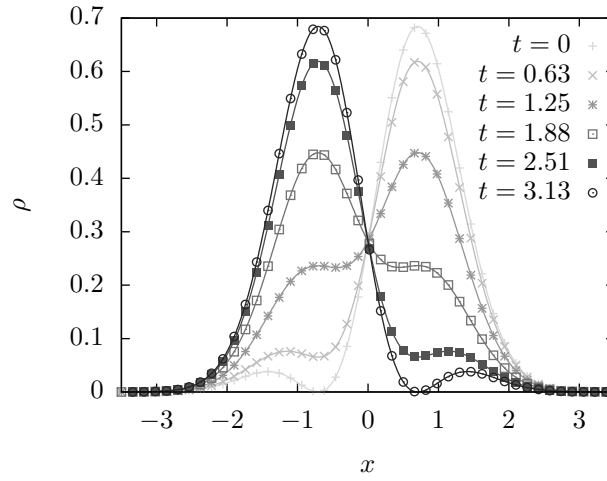
Figure 2.13: Temporal evolution of the probability density for the harmonic potential ($c = 0.5$, $K = 0$), $\rho_\Psi$ (solid lines) and $\rho_W$ (points) for $\Psi = (\Psi_0 + \Psi_1)/\sqrt{2}$ using $N = 16$ Hermite basis functions.



Figure 2.14: Wigner function for the harmonic potential ($c = 0.5$, $K = 0$) at $t = 0$ for the superposition $\Psi = (\Psi_0 + \Psi_1)/\sqrt{2}$ using $N = 16$ Hermite basis functions; contour lines at $W = 0$ (white) and $W = \pm 0.025$ (black/gray).
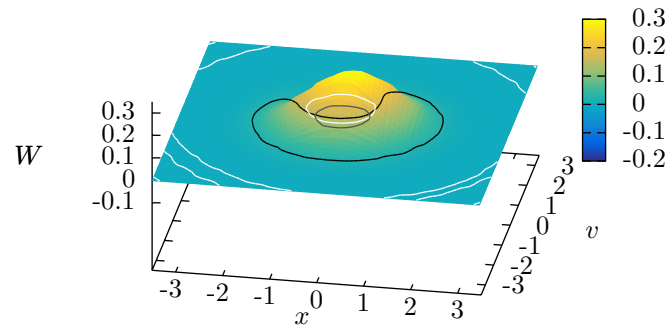
Figure 2.15: Wigner function for the harmonic potential ($c = 0.5$, $K = 0$) at $t = 1.25$ for the superposition $\Psi = (\Psi_0 + \Psi_1)/\sqrt{2}$ using $N = 16$ Hermite basis functions; contour lines at $W = 0$ (white) and $W = \pm 0.025$ (black/gray).
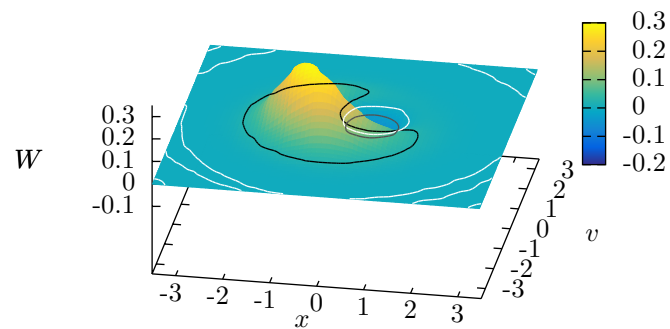


Figure 2.16: Wigner function for the harmonic potential ($c = 0.5$, $K = 0$) at $t = 2.51$ for the superposition $\Psi = (\Psi_0 + \Psi_1)/\sqrt{2}$ using $N = 16$ Hermite basis functions; contour lines at $W = 0$ (white) and $W = \pm 0.025$ (black/gray).

Figure 2.17: Wigner function for the harmonic potential ($c = 0.5$, $K = 0$) at $t = 3.76$ for the superposition $\Psi = (\Psi_0 + \Psi_1)/\sqrt{2}$ using $N = 16$ Hermite basis functions; contour lines at $W = 0$ (white) and $W = \pm 0.025$ (black/gray).



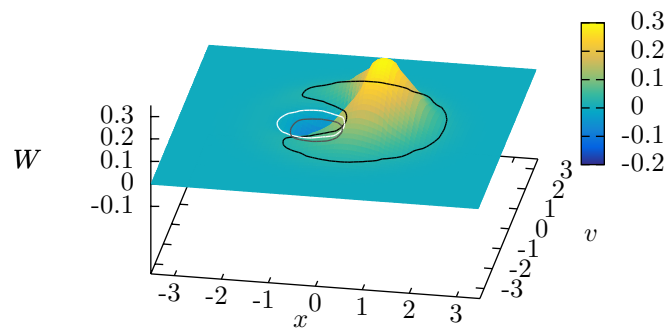Figure 2.18: Wigner function for the harmonic potential ($c = 0.5$, $K = 0$) at $t = 5.01$ for the superposition $\Psi = (\Psi_0 + \Psi_1)/\sqrt{2}$ using $N = 16$ Hermite basis functions; contour lines at $W = 0$ (white) and $W = \pm 0.025$ (black/gray).
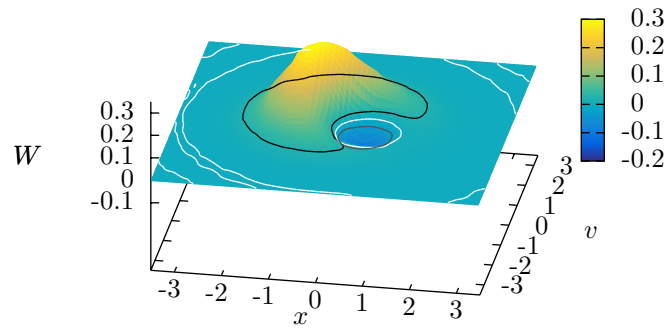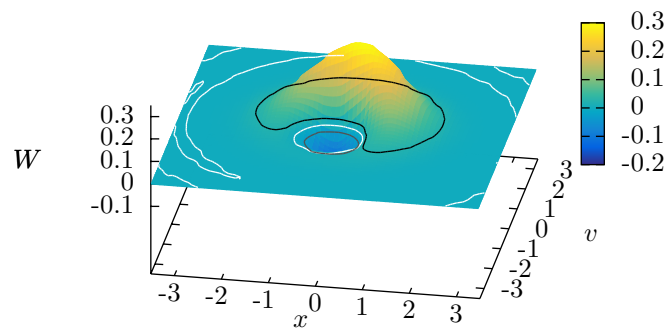
which does not give a finite expansion into Hermite functions in $v$. The deviation of our results from the analytical solution after one period is shown in Fig. 2.19. We observe that the error is of the order of $10^{-4}$ and its magnitude is rather homogeneously distributed. The three sources of it are the finite discretization $\delta x$, the limited expansion in $N$ velocity functions and the non-exact boundary condition. In practice, one expects the former to have the biggest impact on the accuracy, if the basis functions are properly chosen for the problem and the magnitude of the pure quantum states decays sufficiently fast (exponentially) for large $|x|$. It is hard to say how one makes an educated choice for the basis functions before actually trying them in a practical simulation. The Wigner functions that correspond to the decaying eigenstates will also decay exponentially for large $|v|$ or $|x|$. This means that employing periodic boundary conditions is causing an error that decreases exponentially for larger simulation domains. One should choose the size such that the magnitude of the Wigner function is below the desired error. In Fig. 2.20 we show the convergence of the second order accurate method by looking at the error

$$\Delta \equiv \sqrt{\frac{1}{N_x N_v} \sum_{i,j} |\Delta W(x_i, v_j, t)|^2} \ , \tag{2.91}$$

$$\Delta W(x_i, v_j, t) \equiv W(x_i, v_j, t) - W_{\text{ex}}(x_i, v_j, t) \ , \tag{2.92}$$

for periodic boundary conditions in real-space and a domain size $x \in [-5, 5]$. The error is evaluated by choosing the same momentum- and space-grid. The domain size is chosen such that boundary effects do not significantly influence the error in the convergence analysis, since $W(t, \pm 5, v) \sim \mathcal{O}(10^{-10})$. Looking at Fig. 2.20, we observe that the second order convergence can only be verified for sufficiently many basis functions (here: $N = 32$). This behavior is caused by a total error that is composed by the discretization of time and real-space as well as the approximation of the Wigner function with a finite number of basis functions in momentum-space. Therefore, we expect $\Delta$ to saturate for a fixed resolution and an increasing number of basis functions, or in the opposite scenario, which can be deduced from Fig. 2.20 for $N = 16$. Furthermore, in Fig. 2.21 we show the long-term error evolution during the simulation of the harmonic oscillator for two full revolutions. We observe a similar behavior for both methods with a slight advantage for the plane wave basis.



Figure 2.19: Local error of the Wigner function for the harmonic potential ($c = 0.5$, $K = 0$) at $t = 6.28$ and the superposition $\Psi = (\Psi_0 + \Psi_1)/\sqrt{2}$ with $N = 16$, $\delta x = 1/50$.

Figure 2.20: Convergence analysis of the harmonic Wigner function after $t = 2\pi$ with respect to $\delta x$ and $N \in \{8, 16, 32\}$ from top to bottom. The dotted line should serve as a visual aid for the reader to see that the convergence is indeed of second order.
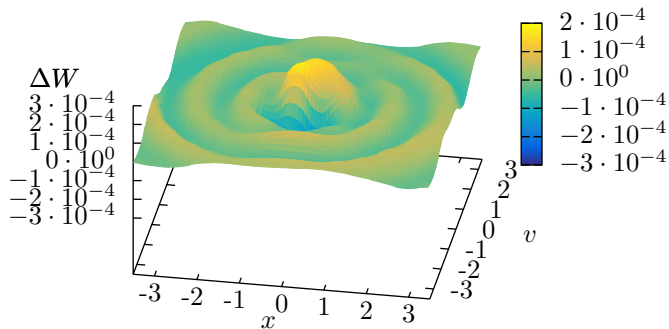


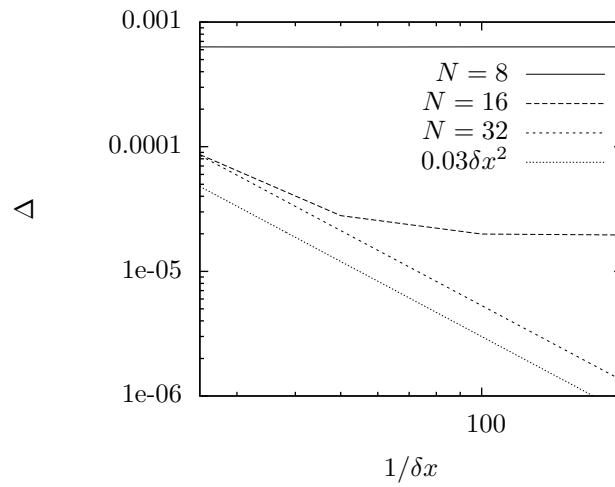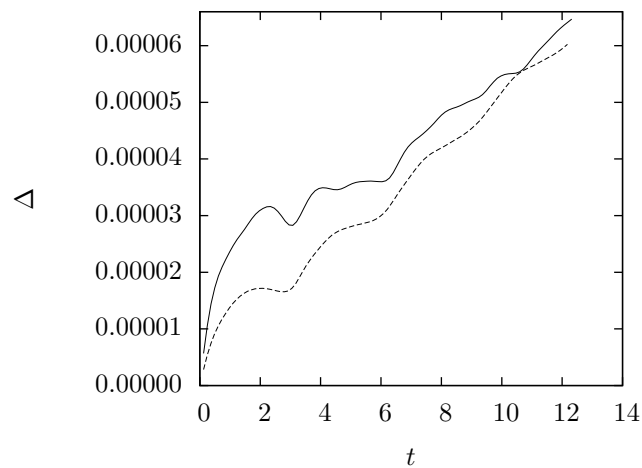Figure 2.21: Error evolution of the Wigner function for the harmonic potential ($c = 0.5$, $K = 0$) and the superposition $\Psi = (\Psi_0 + \Psi_1)/\sqrt{2}$ using $N = 16$ Hermite functions (solid) or $N = 16$ plane waves (dashed) and $\delta x = 1/50$.

## 2.3.4 Anharmonic oscillator

For an anharmonic potential $c = 0.5$ and $K > 0$ we approximate the eigenstates $\Psi_n^{(an)}$ by a superposition of $N_b$ harmonic eigenstates, i.e.

$$\Psi_n^{(an)}(t, x) \approx e^{-\imath t \mathcal{E}_n^{(an)}} \sum_{k=0}^{N_b} c_k^{(n)} \Psi_k(x) \ . \tag{2.93}$$

Then we determine the coefficient vector $\vec{c}^{(n)}$ by diagonalizing the matrix representation of the anharmonic Hamilton operator. This works very well for moderate anharmonicities, but becomes very costly for $K > 10^{-3}$, as can be seen in Figs. 2.22 and 2.23. In addition, one also observes that, as expected, the ground state converges faster than the first excited state.

The simulation is run with the second order accurate method for periodic boundary conditions at $x = \pm 3.5$ with a spatial resolution of $1/\delta x = 50$. The result for the spatial probability evolution is shown in Fig. 2.24, where we observe a good agreement with the wave function dynamics. In Figs. 2.25-2.29 we show the Wigner function evolution together with the contour lines at $W = 0$ and $W = \pm 0.025$. They depict a "rotation" with a smaller period $T_{an} = 2\pi/(\mathcal{E}_1^{(an)} - \mathcal{E}_0^{(an)}) < 2\pi$. In this case it is not a rigid rotation, since the Wigner function gets compressed in position- and broadened in momentum-space due to the larger potential and the particle number conservation. The contour line at $W = 0$ close to the boundaries shows again the numerical error fluctuations, since the magnitude of the Wigner function in that region becomes comparable to the numerical error. In Fig. 2.30 we show a comparison of the long-term error evolution of two full revolutions using our method with Hermite basis functions and the method of Ref. [4] using the plane wave basis functions. The comparison was made using the "exact" Wigner function calculated from the approximated eigenstate evolution in the Schrödinger equation. One observes a similar behavior for both methods with a slight advantage for the Hermite basis in the long-term run.
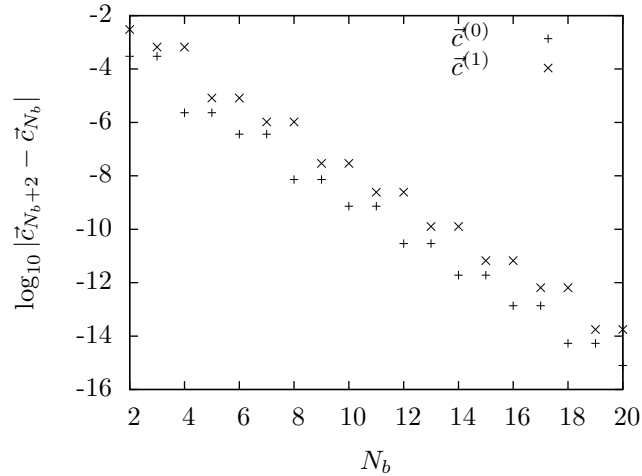


Figure 2.22: Convergence of eigenstate coefficient vector for ground and first excited states of the anharmonic potential ($c = 0.5$, $K = 0.001$) up to *double precision.*
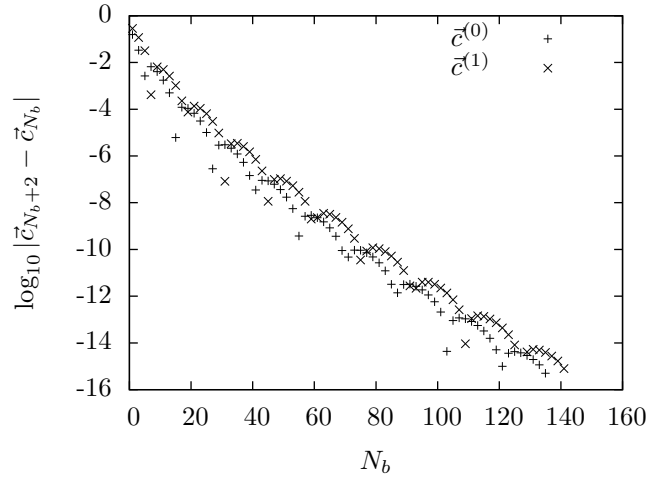
Figure 2.23: Convergence of eigenstate coefficient vector for ground and first excited states of the anharmonic potential ($c = 0.5$, $K = 0.5$) up to *double precision*.
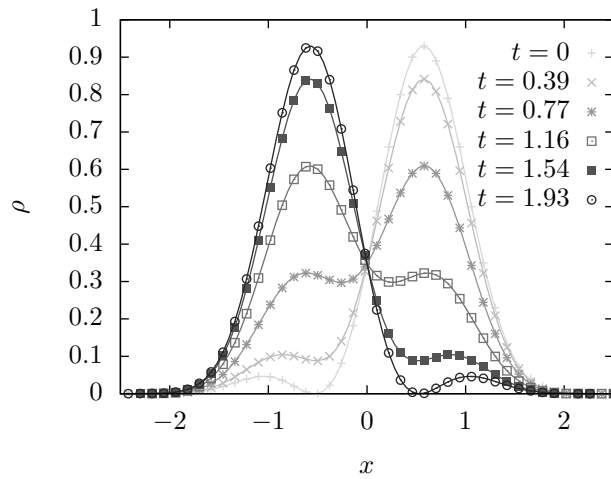


Figure 2.24: Temporal evolution of the probability density for the anharmonic potential ($c = 0.5$, $K = 0.5$), $\rho_\Psi$ (solid lines) and $\rho_W$ (points) for $\Psi = (\Psi_0^{(an)} + \Psi_1^{(an)})/\sqrt{2}$ using $N_b = 150$, and $N = 16$ Hermite basis functions.
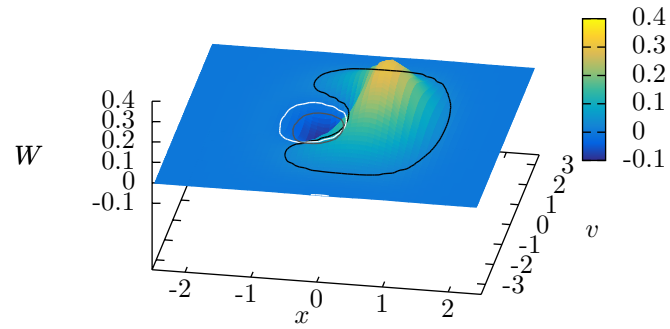
Figure 2.25: Wigner function for the anharmonic potential ($c = 0.5$, $K = 0.5$) at $t = 0$ for the superposition $\Psi = (\Psi_0^{(an)} + \Psi_1^{(an)})/\sqrt{2}$ using $N_b = 150$, and $N = 16$ Hermite basis functions; contour lines at $W = 0$ (white) and $W = \pm 0.025$ (black/gray).
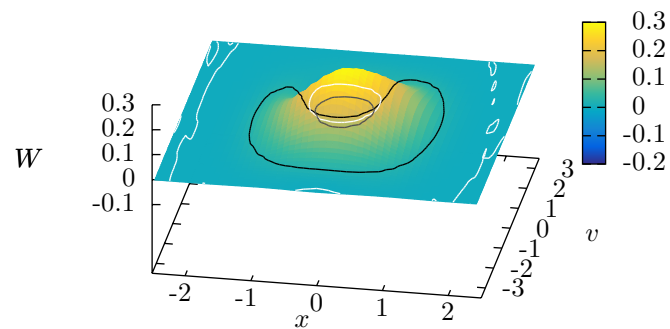


Figure 2.26: Wigner function for the anharmonic potential ($c = 0.5$, $K = 0.5$) at $t = 0.77$ for the superposition $\Psi = (\Psi_0^{(an)} + \Psi_1^{(an)})/\sqrt{2}$ using $N_b = 150$, and $N = 16$ Hermite basis functions; contour lines at $W = 0$ (white) and $W = \pm 0.025$ (black/gray).
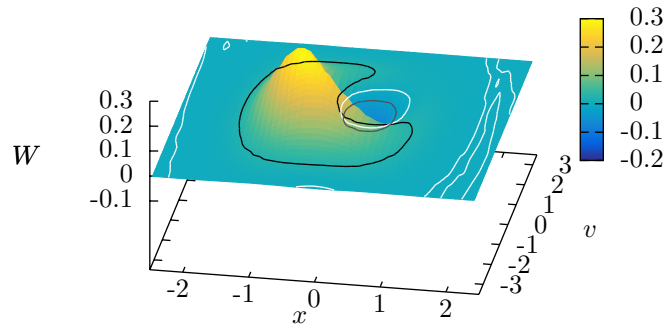
Figure 2.27: Wigner function for the anharmonic potential ($c = 0.5$, $K = 0.5$) at $t = 1.54$ for the superposition $\Psi = (\Psi_0^{(an)} + \Psi_1^{(an)})/\sqrt{2}$ using $N_b = 150$, and $N = 16$ Hermite basis functions; contour lines at $W = 0$ (white) and $W = \pm 0.025$ (black/gray).
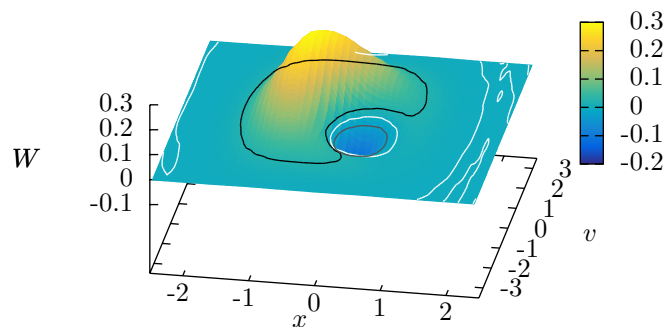


Figure 2.28: Wigner function for the anharmonic potential ($c = 0.5$, $K = 0.5$) at $t = 2.23$ for the superposition $\Psi = (\Psi_0^{(an)} + \Psi_1^{(an)})/\sqrt{2}$ using $N_b = 150$, and $N = 16$ Hermite basis functions; contour lines at $W = 0$ (white) and $W = \pm 0.025$ (black/gray).
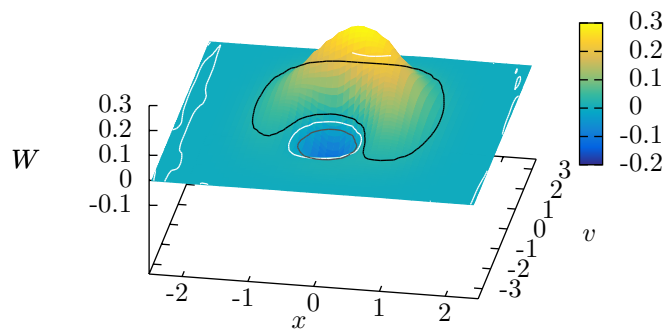
Figure 2.29: Wigner function for the anharmonic potential ($c = 0.5$, $K = 0.5$) at $t = 3.09$ for the superposition $\Psi = (\Psi_0^{(an)} + \Psi_1^{(an)})/\sqrt{2}$ using $N_b = 150$, and $N = 16$ Hermite basis functions; contour lines at $W = 0$ (white) and $W = \pm 0.025$ (black/gray).



Figure 2.30: Error evolution of the Wigner function for the anharmonic potential ($c = 0.5$, $K = 0.01$) and the superposition $\Psi = (\Psi_0 + \Psi_1)/\sqrt{2}$ using $N_b = 70$ Hermite basis functions to approximate the eigenstate, with $N = 16$ Hermite functions (solid) or $N = 16$ plane waves (dashed) and $\delta x = 1/50$.

### 2.3.5 Morse potential

For a more physical example, we simulate the time-evolution of the Wigner quasi-probability distribution for bounded states of the Morse potential

$$V(x) \equiv \left(1 - e^{-x}\right)^2 \ , \tag{2.94}$$

$$\epsilon = 1 \ , \tag{2.95}$$

$$B \equiv \frac{ml^2 D_e}{\hbar^2} \equiv \frac{\lambda^2}{2} \ , \tag{2.96}$$

$$z \equiv 2\lambda e^{-x} \ , \tag{2.97}$$

eigenfunctions

$$\psi_{\lambda,n}(t,z) = \sqrt{\frac{n!(2\lambda - 2n - 1)}{\Gamma(2\lambda - n)}} z^{\lambda - n - 1/2} e^{-z/2} \mathrm{L}_n^{2\lambda - 2n - 1}(z) e^{it\mathcal{E}_{\lambda,n}} \ , \tag{2.98}$$

and eigenenergies

$$\mathcal{E}_{\lambda,n} \equiv \frac{2\lambda(n + 1/2) - (n + 1/2)^2}{2} \ , \tag{2.99}$$

from Ref. [54], centered around the equilibrium distance $x_e = 0$ with $D_e$ as well depth, $l$ as length scale and $\mathrm{L}_n^\alpha$ as generalized Laguerre polynomial

$$L_n^\alpha(z) \equiv \frac{z^{-\alpha} e^z}{n!} \frac{\mathrm{d}^n}{\mathrm{d}z^n}\left(z^{\alpha+n} e^{-z}\right) \ . \tag{2.100}$$

We use an Hermite basis together with the second-order accurate method, periodic boundaries at $x = -2.5$ and $x = 5.5$, and a spatial resolution of $1/\delta x = 50$ to evolve the Wigner function of the superposition of ground and first excited state, $|\psi\rangle = \frac{|\psi_{\lambda,0}\rangle + |\psi_{\lambda,1}\rangle}{\sqrt{2}}$. In Fig. 2.31 the evolution of the probability density in comparison to the evolution according to the Schrödinger equation. One observes a very good agreement. In Figs. 2.32-2.36 one can see the evolution of the Wigner function together with contour lines at $W = 0$ and $W = \pm 0.025$. We observe the formation of a negative region and its shielding through the positive areas of the Wigner quasi-probability distribution. The period of one revolution $T_{morse} = \frac{2\pi}{\mathcal{E}_{\lambda,1} - \mathcal{E}_{\lambda,0}} = \frac{2\pi}{\lambda - 1}$ depends on the effective potential depth, $\lambda = 3$ in our example. The contour line at $W = 0$ highlights the expected ripples in the beginning and later shows again the numerical error fluctuations close to the boundaries, since in this region the magnitude of the Wigner function becomes comparable to the error, which is $\mathcal{O}(10^{-4})$. The error was estimated by comparing the initial and final Wigner function of one revolution.

### 2.3.6 Double well potential

To study tunneling effects, we simulate the time-evolution of the Wigner function for "bounded" states of a one-dimensional double well potential $V(x) = cx^2 + Kx^4$, cf. Fig. 2.37, with the second order accurate method, periodic boundary conditions at $x = \pm 4$ and spatial resolution $1/\delta x = 50$. We call a state bounded if its eigenenergy is smaller than zero and hence below the potential barrier around $x = 0$. Taking again the Hermite basis to approximate the ground and first excited state as in Eq. (2.93), we show in Fig. 2.38 the evolution of the probability density in comparison to the evolution according to Schrödinger's equation. The agreement is very good. In Figs. 2.39-2.43 one can see the evolution of the Wigner function for the tunneling of the state through the potential barrier together with contour lines at $W = 0$ and $W = \pm 0.025$. The error during the revolution is at most $\mathcal{O}(10^{-4})$, as can be seen in Fig. 2.44. In addition, one observes by looking at the contour line for $W = -0.025$ the appearance of ripples and valleys in the front and the back of the positive quasi-probability density during the tunneling process of the particle through the potential barrier, which indicate the non-classical behavior in the corresponding coordinate space. The contour line at $W = 0$ close to the boundaries shows again the numerical error fluctuations in regions where the magnitude of the Wigner function becomes comparable to the numerical error. The period of the revolution $T_{mh} = 2\pi/(\mathcal{E}_1^{(mh)} - \mathcal{E}_0^{(mh)}) \gg 2\pi$ is much larger than the one for a harmonic oscillator. In addition to the probability density and
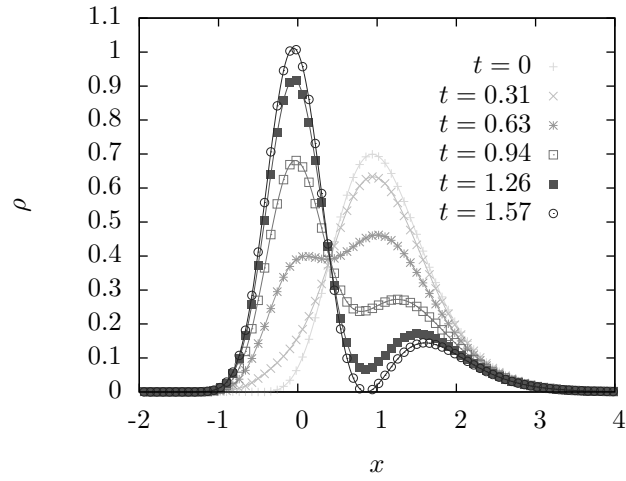
Figure 2.31: Temporal evolution of the probability density for the Morse potential ($\lambda = 3.0$), $\rho_\Psi$ (solid lines) and $\rho_W$ (points) for $\Psi = (\Psi_{\lambda,0} + \Psi_{\lambda,1})/\sqrt{2}$ using $N = 32$ Hermite basis functions.
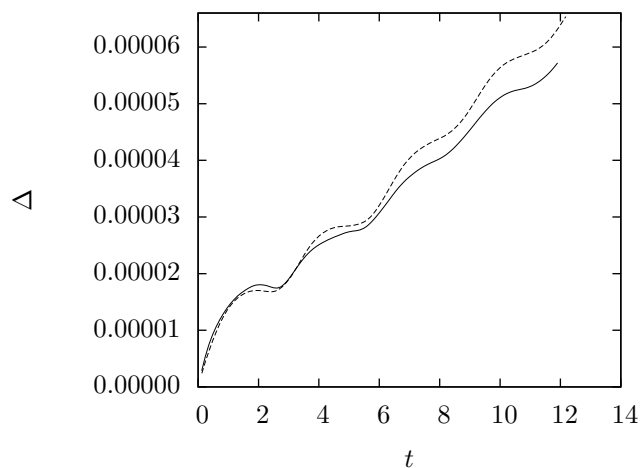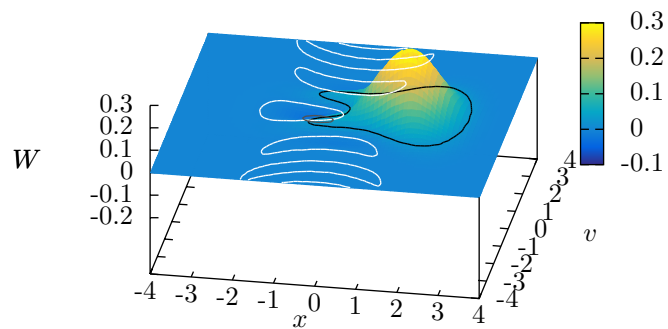


Figure 2.32: Wigner function for the Morse potential ($\lambda = 3.0$) at $t = 0$ for the superposition $\Psi = (\Psi_{\lambda,0} + \Psi_{\lambda,1})/\sqrt{2}$ using $N = 32$ Hermite basis functions; contour lines at $W = 0$ (white) and $W = \pm 0.025$ (black/gray).
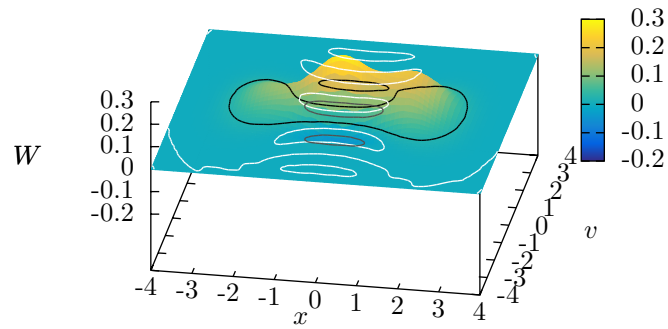
Figure 2.33: Wigner function for the Morse potential ($\lambda = 3.0$) at $t = 0.63$ for the superposition $\Psi = (\Psi_{\lambda,0} + \Psi_{\lambda,1})/\sqrt{2}$ using $N = 32$ Hermite basis functions; contour lines at $W = 0$ (white) and $W = \pm 0.025$ (black/gray).
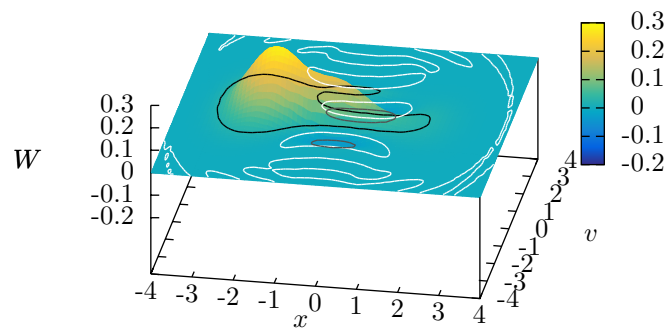


Figure 2.34: Wigner function for the Morse potential ($\lambda = 3.0$) at $t = 1.26$ for the superposition $\Psi = (\Psi_{\lambda,0} + \Psi_{\lambda,1})/\sqrt{2}$ using $N = 32$ Hermite basis functions; contour lines at $W = 0$ (white) and $W = \pm 0.025$ (black/gray).
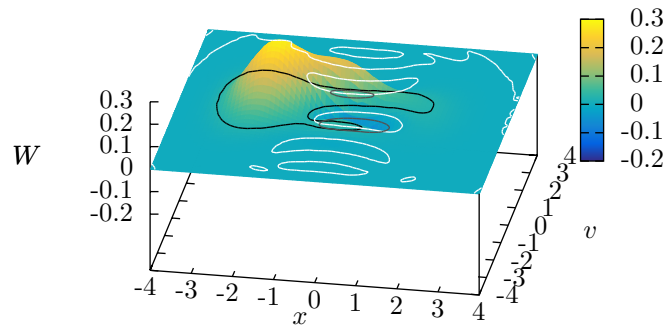
Figure 2.35: Wigner function for the Morse potential ($\lambda = 3.0$) at $t = 1.89$ for the superposition $\Psi = (\Psi_{\lambda,0} + \Psi_{\lambda,1})/\sqrt{2}$ using $N = 32$ Hermite basis functions; contour lines at $W = 0$ (white) and $W = \pm 0.025$ (black/gray).
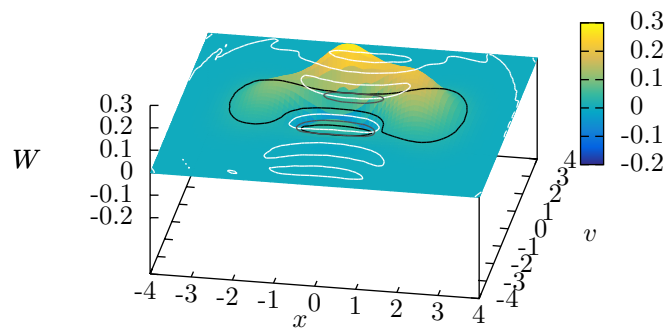


Figure 2.36: Wigner function for the Morse potential ($\lambda = 3.0$) at $t = 2.51$ for the superposition $\Psi = (\Psi_{\lambda,0} + \Psi_{\lambda,1})/\sqrt{2}$ using $N = 32$ Hermite basis functions; contour lines at $W = 0$ (white) and $W = \pm 0.025$ (black/gray).

the Wigner function, we have also analyzed the spread of the Wigner function in phase space by measuring the expectation values

$$(\Delta x^2)(\Delta v^2) \equiv \langle (\hat{x} - \langle \hat{x} \rangle)^2 \rangle \langle (\hat{v} - \langle v \rangle)^2 \rangle \tag{2.101}$$

$$= \left( \langle x^2 \rangle_W - \langle x \rangle_W^2 \right) \left( \langle v^2 \rangle_W - \langle v \rangle_W^2 \right) , \tag{2.102}$$

$$\mathrm{Cov}(x,v) \equiv \left( \frac{1}{2} \langle \hat{x}\hat{v} + \hat{v}\hat{x} \rangle - \langle \hat{x} \rangle \langle \hat{v} \rangle \right) / (\Delta x \Delta v) \tag{2.103}$$

$$= \frac{\langle xv \rangle_W - \langle x \rangle_W \langle v \rangle_W}{\sqrt{\langle x^2 \rangle_W - \langle x \rangle_W^2} \sqrt{\langle v^2 \rangle_W - \langle v \rangle_W^2}} , \tag{2.104}$$

where $\langle f(x,v) \rangle_W \equiv \int \mathrm{d}x \mathrm{d}v \; f(x,v) W$. The first quantity measures the well-known standard deviation of a quantum state in coordinate and momentum space that fulfills Heisenberg's uncertainty principle $\Delta x \Delta v \geq \frac{\epsilon}{2}$. In Fig. 2.45 we show the coordinate and momentum uncertainty in the form of rectangles, i.e. the width, height and area correspond to $\Delta x$, $\Delta v$ and $\Delta x \Delta v$, respectively. In that way, one can see that the standard deviation in position measurements mainly contributes to the uncertainty and its temporal change. The second quantity $\mathrm{Cov}(x,v)$ is the covariance between the coordinate and momentum variable in the corresponding Wigner function normalized with the standard deviations, such that $|\mathrm{Cov}(x,v)| \leq 1$. The evolution of these expectation values is shown in Fig. 2.46. One observes a periodic behavior with $T = T_{mh}/2$ and finds the maximum uncertainty $\Delta x \Delta v$ exactly when the peak of the spatial probability density tunnels through the potential barrier in the middle of the double well potential. In contrast $\mathrm{Cov}(x,v)$ behaves similar to the first temporal derivative of the uncertainty.
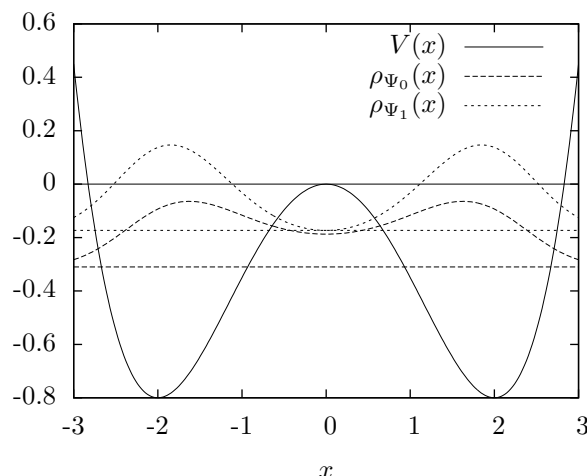


Figure 2.37: Double well potential ($c = -0.4$, $K = 0.05$) and probability density of ground and first excited states displaced from 0 by $\mathcal{E}_0^{(mh)} = -0.310$ (dashed horizontal line) and $\mathcal{E}_1^{(mh)} = -0.173$ (dotted horizontal line) for $N_b = 86$ Hermite basis functions.

## 2.4 Final remarks

With the intention to systematically study quantum corrections to

We have developed a semi-spectral simulation method for the time-evolution of the Wigner quasi-probability distribution that uses a spectral-decomposition of the distribution into arbitrary basis functions of $L^2(\mathbb{R}^d)$ in momentum-space, which transforms the original partial differential equation into an infinite-dimensional set of advection-reaction equations.

There are various other numerical approaches, such as finite differences [55, 97], Fourier spectral collocation [132, 4], deterministic particle [122, 187], and Monte-Carlo [151, 152]. The last two methods are not very accurate compared to the spectral methods but they make simulations in higher dimensional phase space feasible. The method of finite differences although the easiest to
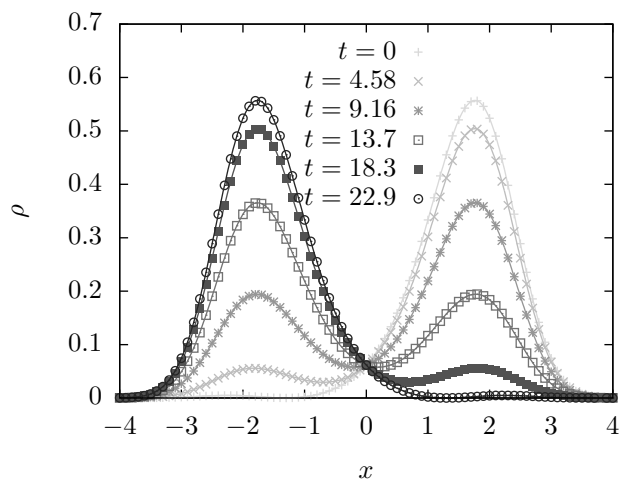
Figure 2.38: Temporal evolution of the probability density for the double well potential ($c = -0.4$, $K = 0.05$), $\rho_\Psi$ (solid lines) and $\rho_W$ (points) for the superposition $\Psi = (\Psi_0^{(mh)} + \Psi_1^{(mh)})/\sqrt{2}$ using $N_b = 86$, and $N = 32$ Hermite basis functions.
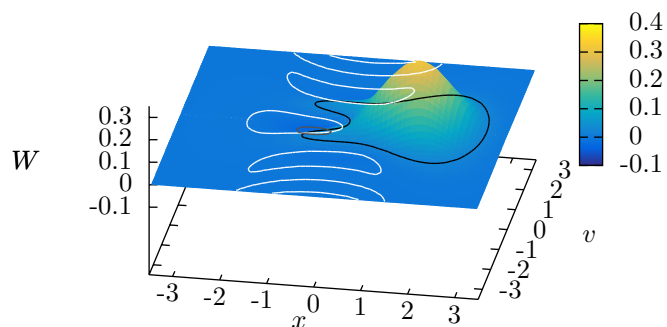


Figure 2.39: Wigner function for the double well potential ($c = -0.4$, $K = 0.05$) at $t = 0$ for the superposition $\Psi = (\Psi_0^{(mh)} + \Psi_1^{(mh)})/\sqrt{2}$ using $N_b = 86$, and $N = 32$ Hermite basis functions; contour lines at $W = 0$ (white) and $W = \pm 0.025$ (black/gray).
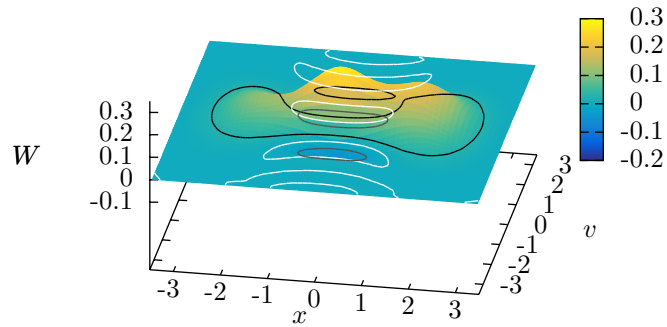
Figure 2.40: Wigner function for the double well potential ($c = -0.4$, $K = 0.05$) at $t = 9.16$ for the superposition $\Psi = (\Psi_0^{(mh)} + \Psi_1^{(mh)})/\sqrt{2}$ using $N_b = 86$, and $N = 32$ Hermite basis functions; contour lines at $W = 0$ (white) and $W = \pm 0.025$ (black/gray).
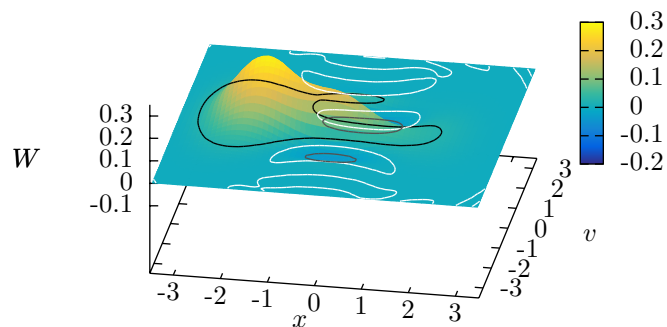


Figure 2.41: Wigner function for the double well potential ($c = -0.4$, $K = 0.05$) at $t = 18.3$ for the superposition $\Psi = (\Psi_0^{(mh)} + \Psi_1^{(mh)})/\sqrt{2}$ using $N_b = 86$, and $N = 32$ Hermite basis functions; contour lines at $W = 0$ (white) and $W = \pm 0.025$ (black/gray).
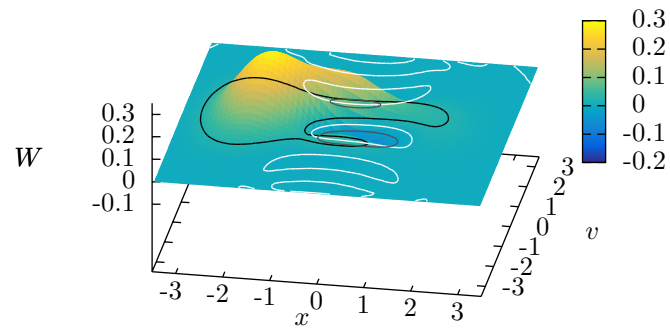
Figure 2.42: Wigner function for the double well potential ($c = -0.4$, $K = 0.05$) at $t = 27.5$ for the superposition $\Psi = (\Psi_0^{(mh)} + \Psi_1^{(mh)})/\sqrt{2}$ using $N_b = 86$, and $N = 32$ Hermite basis functions; contour lines at $W = 0$ (white) and $W = \pm 0.025$ (black/gray).
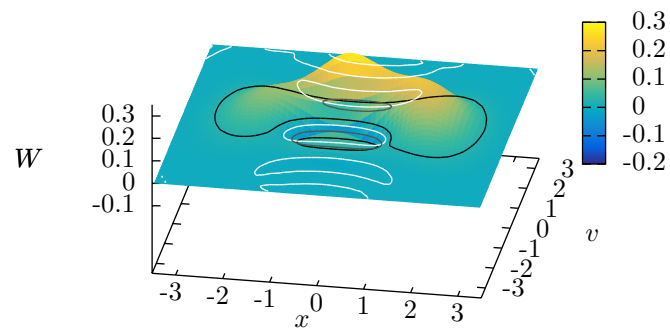


Figure 2.43: Wigner function for the double well potential ($c = -0.4$, $K = 0.05$) at $t = 36.7$ for the superposition $\Psi = (\Psi_0^{(mh)} + \Psi_1^{(mh)})/\sqrt{2}$ using $N_b = 86$, and $N = 32$ Hermite basis functions; contour lines at $W = 0$ (white) and $W = \pm 0.025$ (black/gray).
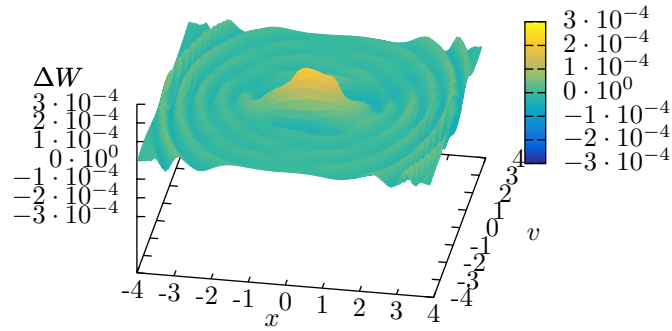
Figure 2.44: Error of the simulated Wigner function for the double well potential ($c = -0.4$, $K = 0.05$) at $t = 45.9$ for the superposition $\Psi = (\Psi_0^{(mh)} + \Psi_1^{(mh)})/\sqrt{2}$ using $N_b = 86$, and $N = 32$ Hermite basis functions.
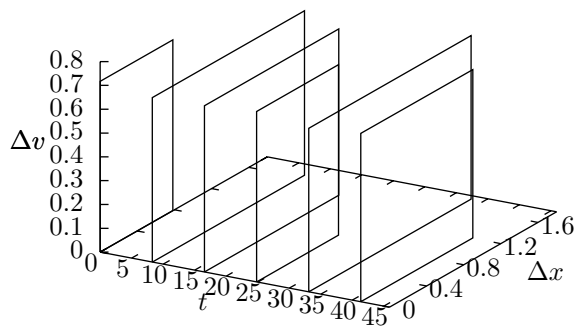


Figure 2.45: Temporal evolution of the spread in the form of rectangles (width $\equiv \Delta x$, height $\equiv \Delta v$, area $\equiv \Delta x \Delta v$) of the simulated Wigner function for the double well potential ($c = -0.4$, $K = 0.05$) for the superposition $\Psi = (\Psi_0^{(mh)} + \Psi_1^{(mh)})/\sqrt{2}$ using $N_b = 86$, and $N = 32$ Hermite basis functions.
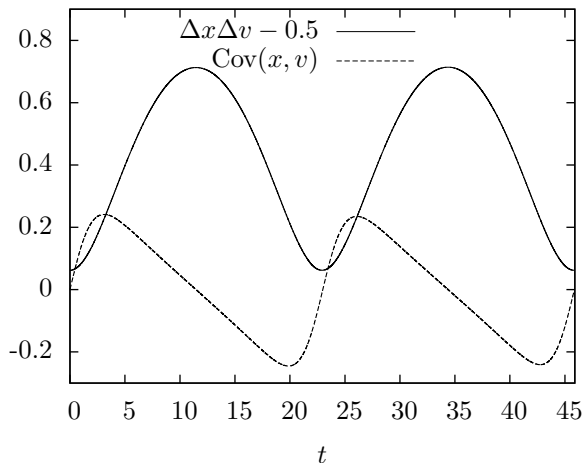
Figure 2.46: Temporal evolution of the uncertainty (solid) and covariance (dashed) of the simulated Wigner function for the double well potential ($c = -0.4$, $K = 0.05$) for the superposition $\Psi = (\Psi_0^{(mh)} + \Psi_1^{(mh)})/\sqrt{2}$ using $N_b = 86$, and $N = 32$ Hermite basis functions.

implement has the highest computational cost increase for an increase in accuracy, due to the discretization of an at least two dimensional domain. Spectral methods offer the advantage of working only with coefficients of basis functions which allows much more flexibility and depending on the basis choice less computational costs for an increase in accuracy compared to the finite difference method. However, simulations of particles in 3 dimensions are still challenging with this approach. We open the technique described in Refs. [132, 4] to arbitrary basis functions $\phi_n(\vec{p})$ of $L^2(\mathbb{R}^d)$ in momentum-space and reveal the underlying mathematical structure of the resulting infinite-dimensional set of reaction-advection equations.

The disadvantage of an arbitrary basis choice is the higher computational cost of $\mathcal{O}(N^2)$ compared to $\mathcal{O}(N \log N)$ for a Fourier basis, since the pseudo-differential operator is diagonal for this basis choice and the basis change can be performed using the fast Fourier transform, as shown in Refs. [4, 132]. However, if one only considers momentum-derivatives up to order $N_\lambda \ll N$ and an explicit scheme such as fourth order Runge-Kutta is used, the computational cost also scales like $\mathcal{O}(N)$ [150]. Employing a more general basis we assume that the higher computational costs of our method, $\mathcal{O}(N^2)$, compared to $\mathcal{O}(N \log N)$ for the spectral Fourier decomposition are outweighed by a smaller number $N$ of basis functions to obtain the same order of accuracy through focusing the computational effort to regions of interest. In addition, the artificial periodization of the Wigner distribution in momentum-space, caused by the plane wave approximation, lives in a different function space than the original Wigner function, thus giving rise to unphysical self-interactions at the domain boundaries [154]. These basis functions are also not well suited to the simulation of structures that are strongly localized in momentum-space, such as particles in periodic potentials, cf. [93], since this would require a very large number of such functions. In addition, a practical comparison has shown that for simulations of at most $N = 32$ basis functions, the direct matrix-vector multiplication is about 25% faster than using the fast Fourier transform. The CPU time for the time evolution of one revolution for the harmonic Wigner function, using the second-order accurate method with $N = 32$ Hermite basis functions and a spatial resolution $1/\delta x = 100$, i.e. 700 grid points and 4558 time-steps, is approximately 7.92 s using a single core of a 3 GHz Intel(R) Core(TM)2 Quad CPU Q9650 processor.

For the numerical treatment, we introduce a cutoff in the expansion, which makes the system finite-dimensional, and split the operators for the reaction and advection part so as to apply them sequentially to the distribution function. We demonstrate that, due to the skew-hermitian symmetry of the matrix representation of the pseudo-differential operator (Lie algebra), the action of the forcing or reaction operator (Lie group) is a unitary rotation, which stabilizes the simulation even for strongly varying potentials compared to other explicit methods, such as Euler

or RK4 [110]. The advection or streaming part can be handled by many numerical approaches from computational fluid dynamics, such as flux vector splitting [161], Godunov, finite volume or finite element [110]. Here, we have chosen a flux-vector splitting for the validation of our method by simulating a single, non-relativistic, spinless particle subject to a one-dimensional (an-)harmonic, double well or Morse potential with Hermite basis functions. Having the exact Wigner function of the harmonic oscillator, we verified the second-order convergence of the method and also demonstrated its applicability to non-classical dynamics in the case of strong anharmonicities and tunneling phenomena.

In order to simulate nanoscale semiconductors with this method one employs the standard approach, i.e. working in the mean-field approximation and reducing the Wigner evolution through symmetry considerations to effectively one or two dimensions in real- and momentum-space, see Ref. [90] for further details. For the simulation of particles with spin, one can use the technique shown in Ref. [113] to develop a spin-dependent Wigner simulation. To reduce the computational costs for these extensions one can check the stability of different numerical procedures, such as RK4, to handle the reaction part of the equation system.

As future work, one may want to study phase transitions in *open quantum systems*, the effects of scattering ("*quantum Boltzmann equation*"), for example in the case of electrons and phonons in semiconductor devices, the effects of boundary conditions, cf. Ref. [55], and stochastic perturbations. It is especially important for our simulations to tackle the dynamics of the quantum many-particle thermal distributions [17], such as Fermi-Dirac or Bose-Einstein through the Wigner evolution, since this is where the true advantage of this perspective lies compared to the wave function formalism. Furthermore, one can analyze the influence of decoherence on the topology of the Wigner function in two dimensions, cf. Ref. [162].

# 3 Open Quantum Systems

> A mind is like a parachute. It
> doesn't work if it is not open.
>
> ———————————————
>
> Frank Zappa

Open quantum systems are another newly developing field of research for which the Wigner formalism can be useful due to its symmetry between position and momentum, which often allows an easier implementation of open, macroscopic boundaries, see Ref. [91]. In addition, nowadays there is a big community of scientists who believe that the emergence of classical behavior or the collapse of the wave function is a consequence of the interaction between the described quantum system and its often macroscopic environment or the measurement apparatus [193], which represents the measurement by the operator $\hat{O}$. This interaction causes the decoherence in the quantum system, which hinders the observation of superpositions and leads to Born's rule of a probabilistic interpretation, i.e. the probability of finding a quantum state $|\psi\rangle$ in the eigenstate $|k\rangle$ and hence measuring the value $\langle k|\hat{O}|k\rangle$ is given by $1 \geq |\langle\psi|k\rangle|^2 \geq 0$. This assumes of course that the involved states are normalized. Inspired by the idea of mimicking the measurement on a quantum system through a decoherence process to target specific eigenstates based on Born's law, i.e. the hierarchy of probabilities instead of the hierarchy of eigenvalues, we transform a Lindblad equation for the reduced density operator into a non-linear Schrödinger equation to obtain a computationally feasible simulation of the decoherent dynamics in the open quantum system. This gives the opportunity to target the eigenstates which have the largest $L^2$ overlap with an initial superposition state and hence more flexibility in the selection criteria. One can use this feature for instance to approximate eigenstates with certain localization or symmetry properties. As an application of the theory we discuss *eigenstate towing*, which relies on the perturbation theory to follow the progression of an arbitrary subset of eigenstates along a sum of perturbation operators with the intention to explore for example the effect of interactions on these eigenstates. The easily parallelizable numerical method shows an exponential convergence and its computational costs scale linear for sparse matrix representations of the involved Hermitian operators.

Our initial goal is to investigate the dynamics of the Wigner function in quantum systems which are coupled to an environment and thereby study the effects of measurements on the quantum phase space evolution, see Ref. [100]. The next question is whether we can leverage this knowledge numerically to learn more about the quantum system, and more specifically about the possible outcomes (eigenvalues) and resulting quantum states (eigenstates) of a measurement represented by a certain observable. A quantum mechanical superposition is different from a statistical ensemble (perfectly mixed state), although the difference may not be observable in *one* particular measurement. In the former the system is indeed in all of the superposed quantum states at the same time, which means it is objectively impossible to determine in which, whereas in the latter the system is in one and only one state of the mixture. The observer just does not know in which. The second case is interpreted as classical uncertainty, whereas in the first case one can construct paradoxa such as the famous thought experiment of Schrödinger's cat [146], and we may call it quantum uncertainty. To arrive at a computationally feasible algorithm we derive an evolution equation which trades the higher-dimensional Wigner or density matrix formulation for a non-linear Schrödinger equation and enables the design of a simulation scheme that shows an exponential convergence to the eigenstate, which is the most probable outcome of a certain measurement on the initial quantum system.

We are proposing a decoherence based approach, modeled by a Lindblad equation, which makes use of Born's law. In section 3.3 we shall show that the only stable equilibria of the dynamics are given by the eigenstates and demonstrate the exponential convergence to one of the eigenstates contained in the input superposition, which is usually the one with the highest probability. This allows us to target eigenstates that maximize the $L^2$ overlap with a predefined function.

Furthermore, in section 3.4 an application of the dynamics, that we would describe as *eigen-state towing*, is discussed. The goal of the method is to follow the progression of an arbitrary subset of eigenstates along a perturbation strength increase. It makes use of perturbation theory [147], which ensures the collapse of the unperturbed eigenstate into the same eigenstate after an infinitesimal perturbation. This enables us to avoid any communication between the computations for different eigenstates, because each one will converge independent of the others and a parallel implementation is achievable. It should be mentioned that also other methods in quantum chemistry can approximate lower eigenstates in parallel, see Refs. [160, 65]. However, the method in Ref. [160] relies on an information exchange between the different computations to avoid the convergence to eigenstates with smaller eigenvalues. In section 3.5 we propose the (semi-)implicit Crank-Nicholson method for a specific numerical implementation, that is used in section 3.6 to analyze an example of an excited-state quantum phase transition in the Jaynes-Cummings model [88, 172, 128]. This problem also serves to compare our algorithm, in section 3.7, with one of the fastest LAPACK algorithms for determining eigenvectors and -values of tridiagonal symmetric matrices [37], the *multiple relatively robust representations* (MRRR) algorithm [41, 42].

## 3.1 Density operator

Motivated by Refs. [101, 43, 175] we have realized the potential application behind "quantum state engineering" for the extraction of desired quantum states of a given isolated quantum system. An important restriction is that these states *must be distinguishable* by at least one operator-measurement. However, this requirement is in practice irrelevant, since quantum states which cannot be discriminated by any measurement are by definition indistinguishable and hence with respect to the information content we do not need to worry about finding only a subset of them.

We assume a finite set of commuting self-adjoint operators $\{\hat{O}_j\}_{j \in \mathcal{J}}$ with discrete spectra on the Hilbert space $\mathcal{H}$. From the spectral theorem [137] we know there exists a common complete eigenbasis $\{|\psi_{\vec{a}}\rangle\}_{\vec{a} \in \mathcal{A}}$ for this set that spans the whole Hilbert space, i.e. $\forall \mathcal{I} \subseteq \mathcal{J}$

$$\left(\prod_{i \in \mathcal{I}} \hat{O}_i\right) |\psi_{\vec{a}}\rangle = \left(\prod_{i \in \mathcal{I}} a_i\right) |\psi_{\vec{a}}\rangle \ , \tag{3.1}$$

and $\forall |\psi\rangle \in \mathcal{H}$

$$|\phi\rangle = \sum_{\vec{a} \in \mathcal{A}} b_{\vec{a}} |\psi_{\vec{a}}\rangle \ , \text{ with } b_{\vec{a}} \in \mathbb{C} \ . \tag{3.2}$$

The operators form an Abelian group such that a common eigenbasis for all of them exists. The usage of more than one Hermitian operator serves the purpose of fine-tuning the targeting of a specific eigenstate in the basis by lifting potential degeneracies in the spectrum. As an example one can think of the bound eigenstates of the hydrogen atom which can be labeled by their eigenenergy measured by $\hat{H}$, the total angular momentum observable by $|\hat{\vec{J}}|^2$ and its $z$-component measurable by $\hat{J}_z$. In an attempt to model the quantum mechanical measurement process and mimic the collapse of the wave function, in analogy to the ideas expressed in Ref. [179], we employ the Lindblad equation for the density operator

$$\partial_t \hat{\rho}(t) = \sum_{j \in \mathcal{J}} \left[ [\hat{O}_j, \hat{\rho}(t)], \hat{O}_j \right] \ , \tag{3.3}$$

$$= -\sum_{j \in \mathcal{J}} \left( \hat{O}_j^2 \hat{\rho}(t) + \hat{\rho}(t) \hat{O}_j^2 - 2\hat{O}_j \hat{\rho}(t) \hat{O}_j \right) \ , \tag{3.4}$$

where we used the observables as Lindblad operators. For a comprehensive summary of the theory of the Lindblad equation the interested reader may consult Ref. [138]. One can interpret this dynamics as a continuous measurement on a quantum system which was at the beginning of the process in the pure state $\hat{\rho}(0) = |\phi\rangle\langle\phi|$ and whose expectation value does not change through

this interaction

$$\partial_t \langle \hat{O}_k \rangle (t) = \text{Tr}\left[\hat{O}_k \partial_t \hat{\rho}\right] \tag{3.5}$$

$$= 2\text{Tr}\left[\hat{O}_k^2 \hat{\rho} \hat{O}_k\right] - \text{Tr}\left[\hat{O}_k^3 \hat{\rho}\right] - \text{Tr}\left[\hat{O}_k \hat{\rho} \hat{O}_k^2\right] \tag{3.6}$$

$$= 0 \ . \tag{3.7}$$

However, we would like to point out that it is still unknown how the measurement process in quantum mechanics exactly works, giving rise to different interpretations of quantum mechanics, see Ref. [145], and that here we are using a decoherence based approach to model it. To better understand the evolution in Eq. (3.4), we look at the temporal change of the coefficients of the density operator in the eigenbasis representation of our operator set, which reads

$$\hat{\rho}(t) = \sum_{\vec{a},\vec{a}' \in \mathcal{A}} c_{\vec{a},\vec{a}'}(t) |\psi_{\vec{a}}\rangle\langle\psi_{\vec{a}'}| \ , \tag{3.8}$$

$$\partial_t c_{\vec{a},\vec{a}'} = -|\vec{a} - \vec{a}'|^2 c_{\vec{a},\vec{a}'}(t) \ , \tag{3.9}$$

$$c_{\vec{a},\vec{a}'}(0) = b_{\vec{a}} b_{\vec{a}'}^* \ . \tag{3.10}$$

The dynamics are purely decoherent, i.e. that expectation values with respect to the operators $\hat{O}_j$ are unchanged and only off-diagonal elements in the chosen representation decay exponentially which in the infinite-time limit results in a fully classical mixture

$$\hat{\rho}(t) = \sum_{\vec{a},\vec{a}' \in \mathcal{A}} e^{-|\vec{a}-\vec{a}'|^2 t} b_{\vec{a}} b_{\vec{a}'}^* |\psi_{\vec{a}}\rangle\langle\psi_{\vec{a}'}| \ , \tag{3.11}$$

$$\lim_{t \to \infty} \hat{\rho}(t) = \sum_{\vec{a} \in \mathcal{A}} |b_{\vec{a}}|^2 |\psi_{\vec{a}}\rangle\langle\psi_{\vec{a}}| \ , \tag{3.12}$$

which means that all the quantum correlations have vanished and there is only a statistical ensemble of quantum states, i.e. the system is in a mixed state with classical probabilities.

The obtained quantum state of the system is purely classical with respect to the desired set of states $\{|\psi_{\vec{a}}\rangle\}_{\vec{a} \in \mathcal{A}}$ and $|b_{\vec{a}}|^2$ represents the probability of finding the system in the state $|\psi_{\vec{a}}\rangle$ in analogy to Born's rule. Consequently, the process can be imagined as the quantum-to-classical transition, where the resulting states are prepared or chosen through the set of operators which are used for the Lindblad dynamics in Eq. (3.4). However, the probability for finding a certain state of the set is pre-determined by the initial quantum state $|\phi\rangle$.

For the extraction of a certain eigenstate $|\psi_{\vec{a}}\rangle$ we assume that we have initially chosen the state $|\phi\rangle$ such that $|b_{\vec{a}}|^2 > |b_{\vec{a}'}|^2 \ \forall \vec{a}' \neq \vec{a}$. If we have obtained the steady state density matrix, we can use the power iteration method [176] and easily extract the eigenstate with the highest probability. The $k$-th application of the iteration procedure will give

$$|\phi^k\rangle = \left(\sum_{\vec{a}' \in \mathcal{A}} |b_{\vec{a}'}|^{3k} e^{\imath\theta_{\vec{a}'}} |\psi_{\vec{a}'}\rangle\right) \Big/ \left(\sum_{\vec{a}'' \in \mathcal{A}} |b_{\vec{a}''}|^6\right)^{k/2} \ , \tag{3.13}$$

$$\approx e^{\imath\theta_{\vec{a}}} |\psi_{\vec{a}}\rangle + \sum_{\vec{a}' \neq \vec{a}} \left(\frac{|b_{\vec{a}'}|}{|b_{\vec{a}}|}\right)^{3k} e^{\imath\theta_{\vec{a}'}} |\psi_{\vec{a}'}\rangle \ . \tag{3.14}$$

Therefore, the better one prepares the initial state to find a certain eigenstate the faster will be the *cubic convergence*.

Another perspective on the problem is also that we are trying to find the eigenvector to the largest eigenvalue of the steady state density matrix, since each wave function is a vector in the Hilbert space. With this additional insight it is clear that the power iteration method is not the only possibility to find the eigenstate. One can also use more advanced algorithms, such as the Lanczos method [103].

### 3.1.1 Error analysis

A natural question, which has not been answered yet, is: How is the resulting approximation of the eigenstate affected if one only uses a numerical approximation of the steady density

matrix. To answer this question, we write the numerically approximated steady density matrix as $\hat{\tilde{\rho}} = \hat{\rho}_\infty + \delta\hat{\rho}$. Then, the eigenvalues and eigenvectors of this system are

$$|\tilde{b}_{\vec{a}}|^2 = |b_{\vec{a}}|^2 + \langle\psi_{\vec{a}}|\delta\hat{\rho}|\psi_{\vec{a}}\rangle + \mathcal{O}(\delta^2) \ , \tag{3.15}$$

$$|\tilde{\psi}_{\vec{a}}\rangle = |\psi_{\vec{a}}\rangle + \sum_{\vec{a}'\neq\vec{a}} \frac{\langle\psi_{\vec{a}'}|\delta\hat{\rho}|\psi_{\vec{a}}\rangle}{|b_{\vec{a}}|^2 - |b_{\vec{a}'}|^2}|\psi_{\vec{a}'}\rangle + \mathcal{O}(\delta^2) \ . \tag{3.16}$$

For further details on the calculation see Ref. [173]. It is important to note that a good approximation of the desired eigenstate with the initial state can significantly reduce the numerical error of the procedure.

The second source of error comes from the numerical algorithm which is used to approximate the eigenstate and eigenvalue. Hence it depends on the detailed method which is employed for this task and needs to be evaluated individually.

## 3.2 Wigner-Lindblad

Based on our findings in the previous section, we shall elaborate on the Wigner formulation of the described decoherence dynamics in Eq. (3.4). Thereby, we shall heavily make use of the formulas and definitions in chapter 2. In general, we are going to work with dimensionless operators $\hat{x}_j$ and $\hat{v}_k$ that fulfill the commutation relation

$$[\hat{x}_j, \hat{v}_k] = \imath\epsilon \ . \tag{3.17}$$

The "effective Planck's constant" $\epsilon$ measures the ratio between the quantum scale $\hbar$ and the typical momentum ($p_s$) as well as spatial ($q_s$) length scales of the system, i.e.

$$\epsilon = \frac{\hbar}{q_s p_s} \ . \tag{3.18}$$

To get a better grasp on the typical magnitude of this quantity, we take the hydrogen atom, where $q_s = a_0 = \frac{4\pi\epsilon_0\hbar^2}{m_e e^2}$ and $p_s = \sqrt{m_e|E_0|} = 2^{-1/2}\frac{m_e e^2}{4\pi\hbar\epsilon_0}$, such that we obtain $\epsilon = \sqrt{2} \sim \mathcal{O}(1)$. For these type of quantum systems it is hence not reasonable to perform a (semi-)classical approximation by neglecting higher order terms of $\epsilon$ in the expansion. Depending on the quantum mechanical problem, one might choose different canonical operators, see for example the operators for spin systems [44]. However, for demonstration purposes we stick to the operators of (scaled) real- and momentum-space.

The transformation of the Lindblad equation is done with the dimensionless operators $\{\hat{A}_i\}_{i\in\mathbb{I}}$ and undertaken to enable the application of a Wigner Monte-Carlo simulation and (semi-)classical approximations of eigenstates for the quantum mechanical problem of interest. Thereby, the commutator needs to be replaced by the Moyal bracket [118], an extension of the Poisson bracket, which can be expanded around the effective Planck's constant $\epsilon$. For the replacement of the commutator one can write

$$\frac{1}{\imath\epsilon}\left[\hat{A}, \hat{B}\right] \to \{\{A, B\}\}(\vec{x}, \vec{v}) \ , \tag{3.19}$$

where $A(\vec{x}, \vec{v})$ is the Wigner transform of the operator $\hat{A}$, based on the Wigner map introduced in the second section of the previous chapter.

The bracket can be expressed in differential and integral form. The differential form, is written as

$$\{\{A, B\}\}(\vec{x}, \vec{v}) = \frac{2}{\epsilon}A(\vec{x}, \vec{v})\sin\left[\frac{\epsilon}{2}\left(\overleftarrow{\partial}_{x_k}\overrightarrow{\partial}_{v_k} - \overleftarrow{\partial}_{v_k}\overrightarrow{\partial}_{x_k}\right)\right]B(\vec{x}, \vec{v}) \ , \tag{3.20}$$

whereas the (Fourier) integral form reads

$$\{\{A, B\}\}(\vec{x}, \vec{v}) = \frac{2}{\pi^2\epsilon}\int_{\mathbb{R}^{4d}} d\vec{v}_1 d\vec{v}_2 d\vec{x}_1 d\vec{x}_2 \ A(\vec{x} + \vec{x}_1, \vec{v} + \vec{v}_1)B(\vec{x} + \vec{x}_2, \vec{v} + \vec{v}_2)$$

$$\times \sin\left[\frac{2}{\epsilon}\left(\vec{x}_1 \cdot \vec{v}_2 - \vec{x}_2 \cdot \vec{v}_1\right)\right] \ . \tag{3.21}$$

The sinus-operator can be understood in its summation representation, i.e.

$$
\sin\left[\frac{\epsilon}{2}\left(\overleftarrow{\partial}_{x_k}\overrightarrow{\partial}_{v_k} - \overleftarrow{\partial}_{v_k}\overrightarrow{\partial}_{x_k}\right)\right] = \sum_{l=0}(-1)^l \frac{\left[\frac{\epsilon}{2}\left(\overleftarrow{\partial}_{x_k}\overrightarrow{\partial}_{v_k} - \overleftarrow{\partial}_{v_k}\overrightarrow{\partial}_{x_k}\right)\right]^{2l+1}}{(2l+1)!} \ , \tag{3.22}
$$

and by noting that the arrow above the differential operator indicates if it acts on $A$ (left) or $B$ (right). This formulation requires the Wigner maps of the operators to be differentiable. If this is not fulfilled one needs to use the integral representation. The advantage of this approach is that it enables a systematic (semi-)classical approximation of quantum mechanical eigenstates in the effective Planck's constant by making a Taylor expansion around $\epsilon \approx 0$ up to a certain order.

Consequently, the Lindblad equation in the Wigner formulation is

$$
\dot{\rho} = \sum_{i\in\mathcal{I}}\left[[\hat{A}_i, \hat{\rho}(t)], \hat{A}_i\right] \rightarrow \partial_t W = \epsilon^2 \sum_{i\in\mathcal{I}}\{\{(\{\{W, A_i\}\}), A_i\}\} \ . \tag{3.23}
$$

As mentioned in Refs. [96, 71], looking at how the negative features diminish over time is a measure of decoherence. One may hope that such a Wigner distribution is closer to a proper probability distribution and hence more accessible by traditional numerical techniques from statistical mechanics, which would include formost the Monte-Carlo method.

### 3.2.1 Hamilton operator

Assuming we are only dealing with a single measurement, namely the dimensionless Hamilton operator $\hat{H} = \frac{\hat{\vec{v}}^2}{2} + V(\hat{\vec{x}})$, then we find for the Wigner evolution subject to the Lindblad equation

$$
\partial_t W = \left(\vec{v}\cdot\vec{\nabla}_x - \Theta[V]\right)^2 W \ . \tag{3.24}
$$

The action of the operator $\Theta[V]$ can be written as differential,

$$
\Theta[V]W = -B\sum_{|\lambda|\in\mathbb{N}_{odd}} (\imath\epsilon/2)^{|\lambda|-1}\frac{1}{\lambda!}\left(D_x^\lambda V\right)\left(D_v^\lambda W\right) \ , \tag{3.25}
$$

or integral operator,

$$
\Theta[V]W = \frac{\imath B}{\epsilon}\int_{\mathbb{R}^d}\mathrm{d}\vec{\eta}\ \delta V(t,\vec{x},\vec{\eta})\tilde{W}(t,\vec{x},\vec{\eta})e^{-\imath\vec{\eta}\cdot\vec{v}} \ , \tag{3.26}
$$

$$
\delta V(t,\vec{x},\vec{\eta}) \equiv V\left(t,\vec{x}+\frac{\epsilon}{2}\vec{\eta}\right) - V\left(t,\vec{x}-\frac{\epsilon}{2}\vec{\eta}\right), \tag{3.27}
$$

$$
\tilde{W}(t,\vec{x},\vec{\eta}) \equiv \frac{1}{(2\pi)^d}\int_{\mathbb{R}^d}\mathrm{d}\vec{v}\ W(t,\vec{x},\vec{v})e^{\imath\vec{\eta}\cdot\vec{v}} \ , \tag{3.28}
$$

as described in the second section of the previous chapter. To show what this equation does in practice, we shall use again our standard example. The only operator which we employ is the dimensionless Hamilton operator

$$
\hat{H} = \frac{\hat{v}^2 + \hat{x}^2}{2} \ , \tag{3.29}
$$

with $\epsilon = 1$. The equation becomes

$$
\partial_t W = (v\partial_x - x\partial_v)^2 W = (x^2\partial_v^2 + v^2\partial_x^2 - v\partial_v - x\partial_x - 2xv\partial_x\partial_v)W \ . \tag{3.30}
$$

To demonstrate the applicability we have simulated the equation with finite differences, starting with the Wigner quasi probability distribution of the superposition of ground and first excited state $|\phi\rangle = \frac{|\psi_0\rangle + |\psi_1\rangle}{\sqrt{2}}$, which is given by

$$
W(t_0, x, v) = e^{-v^2-x^2}\frac{v^2 + x^2 + \sqrt{2}[x\cos(t_0) - v\sin(t_0)]}{\pi} \ , \tag{3.31}
$$

at $t_0 = 0$. The evolution is shown in Figs. 3.1-3.6 for periodic boundary conditions. One observes the approximation of the steady state, which is the sum of the ground and first excited state Wigner functions

$$W_{\text{st}}(x, v) \equiv e^{-v^2 - x^2} \frac{v^2 + x^2}{\pi} \ . \tag{3.32}$$

Based on Eq. (3.12), we know that in the Wigner-Lindblad dynamics the Wigner function will always evolve to a steady state, whereas in the previous chapter, we saw that in the case of the harmonic oscillator we obtain a rotation. The reason for this is that we have a quadratic action of the operator $(\vec{v} \cdot \nabla_x + \Theta[V])$ that does not allow the Wigner function to stay constant along characteristic lines of classical particle movement $(\dot{\vec{x}} = \vec{v}, \dot{\vec{v}} = -\nabla_x V)$. During this process the system performs a transition from a pure quantum state into a fully mixed state, i.e. the entropy

$$S(t) \equiv 1 - \text{Tr}[\hat{\rho}^2(t)] = 1 - 2\pi \int_{\mathbb{R} \times \mathbb{R}} \mathrm{d}x \mathrm{d}v \ W(t, x, v)^2 \ , \tag{3.33}$$

approaches its maximum, as shown in Fig. 3.7. The convergence in $L^2$-norm to the expected result,

$$\Delta W \equiv \sqrt{\sum_{i,j} [W(t, x_i, v_j) - W_{\text{st}}(x_i, v_j)]^2 \, \delta x \delta v} \ , \tag{3.34}$$

is also shown in Fig. 3.9. We find that the minimum deviation is reached after around $t \approx 10$. In Fig. 3.8 we show a potential stopping criterion, the deviation of the simulated Wigner function from one time-step to the next in $L^2$-norm,

$$\Delta W_{\delta t} \equiv \sqrt{\sum_{i,j} [W(t, x_i, v_j) - W(t + \delta t, x_i, v_j)]^2 \, \delta x \delta v} \ , \tag{3.35}$$

to determine when the simulation could be stopped. Apparently, the criterion behaves similarly as the $L^2$-convergence. However, considering this criterion one would have stopped the simulation around $t \approx 13$, which would result in a slightly bigger error than the minimum around $t \approx 10$ and a longer simulation time. Since we are performing a numerical simulation the errors in our simulation may accumulate over time such that the root mean square error, shown in Fig. 3.9, increases after reaching its minimum around $t \approx 10$.
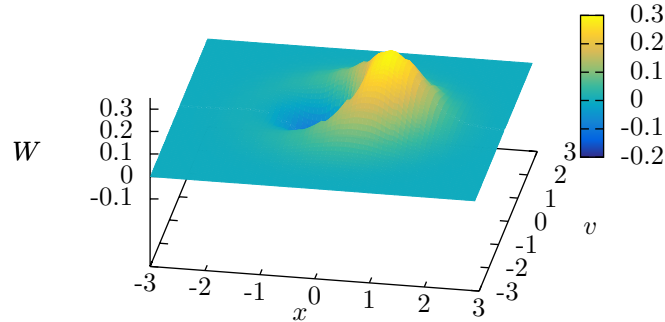


Figure 3.1: The evolution of the Wigner (quasi)-probability distribution for periodic boundary conditions at $x = \pm 4$ and $v = \pm 4$ at $t = 0$.
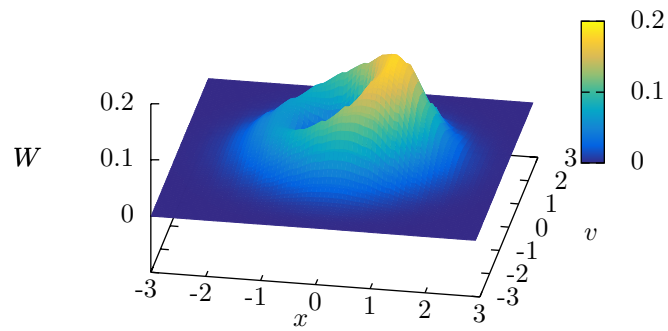
Figure 3.2: The evolution of the Wigner (quasi)-probability distribution for periodic boundary conditions at $x = \pm 4$ and $v = \pm 4$ at $t = 1$.
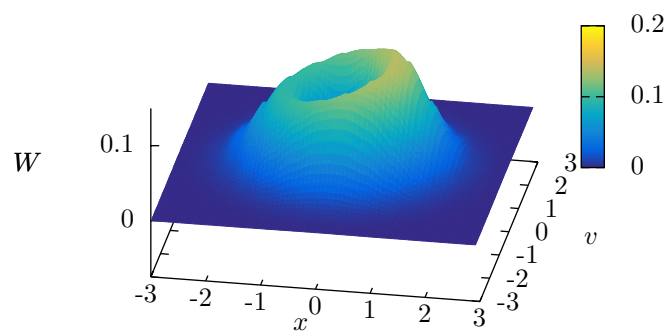


Figure 3.3: The evolution of the Wigner (quasi)-probability distribution for periodic boundary conditions at $x = \pm 4$ and $v = \pm 4$ at $t = 2$.
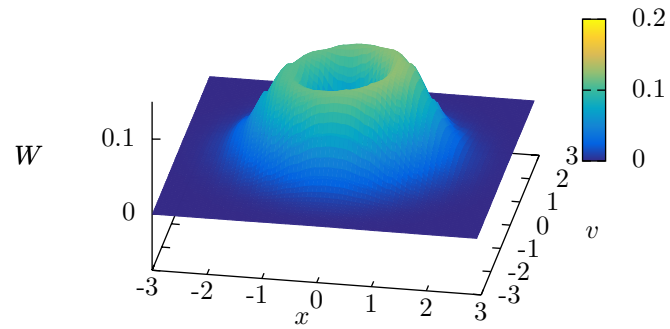
Figure 3.4: The evolution of the Wigner (quasi)-probability distribution for periodic boundary conditions at $x = \pm 4$ and $v = \pm 4$ at $t = 3$.
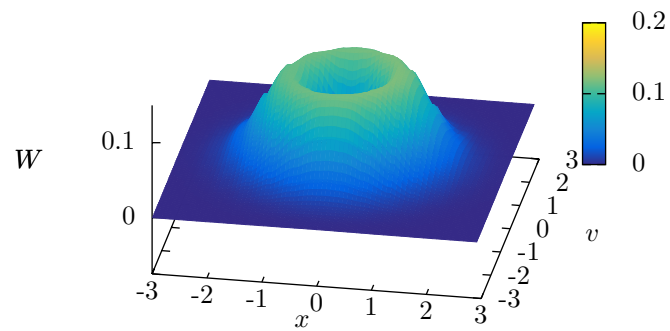


Figure 3.5: The evolution of the Wigner (quasi)-probability distribution for periodic boundary conditions at $x = \pm 4$ and $v = \pm 4$ at $t = 4$.
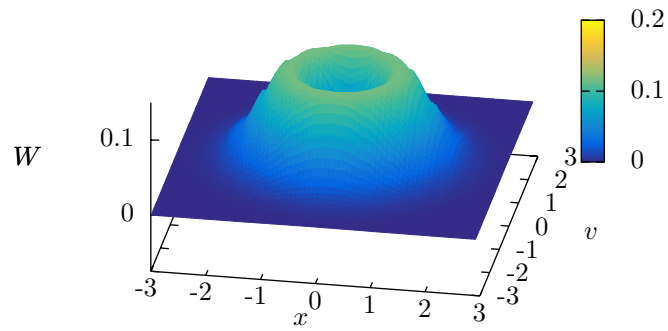
Figure 3.6: The evolution of the Wigner (quasi)-probability distribution for periodic boundary conditions at $x = \pm 4$ and $v = \pm 4$ at $t = 10$.
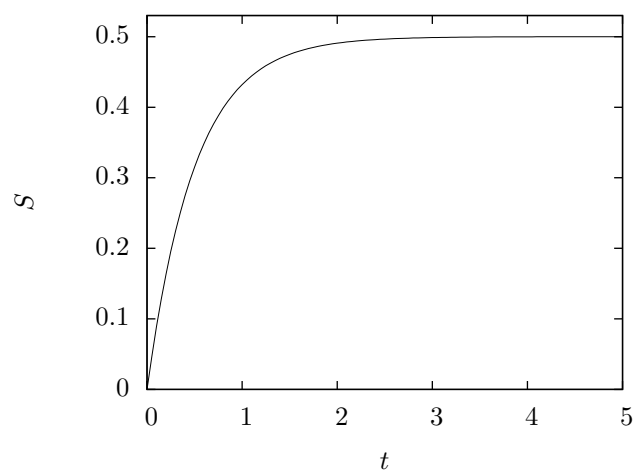


Figure 3.7: The evolution of the entropy $S$.
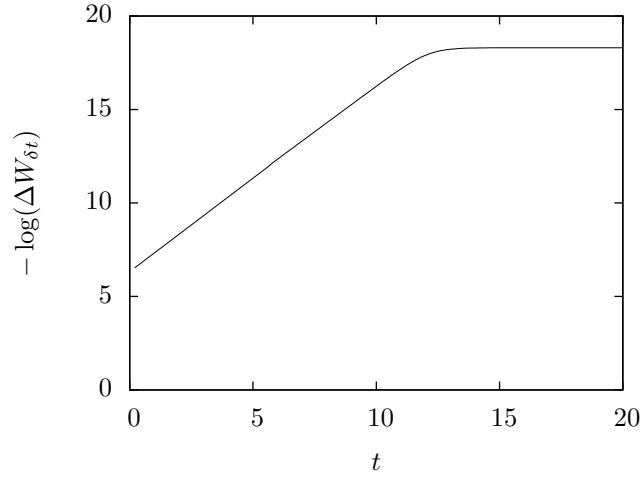
Figure 3.8: The evolution of the logarithm of the root mean square change of the Wigner function from one time-step to the next, $\Delta W_{\delta t}(t)$.
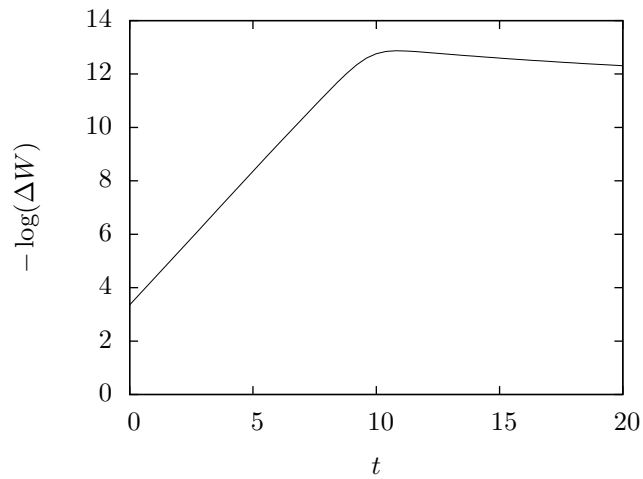


Figure 3.9: The evolution of the logarithm of the root mean square error of the Wigner function, $\Delta W(t)$.

### 3.2.2 Numerical sign problem

Now that we have established the theory, we would like to use it for a concrete and long-standing problem. We want to calculate the partition function

$$Z(\beta) \equiv \mathrm{Tr}\left[e^{-\beta\hat{\mathrm{H}}}\right] . \tag{3.36}$$

Therefore, we rewrite it as the result of a pseudo-dynamic evolution

$$Z(\beta) = \mathrm{Tr}\left[e^{-\frac{\beta}{2}\hat{\mathrm{H}}}\hat{\rho}(0)e^{-\frac{\beta}{2}\hat{\mathrm{H}}}\right] , \tag{3.37}$$

$$\hat{\rho}(0) = \mathbb{I} , \tag{3.38}$$

$$\dot{\hat{\rho}}(t) = -\{\hat{\rho}(t),\hat{\mathrm{H}}\} , \tag{3.39}$$

$$\hat{\rho}(t) = e^{-t\hat{\mathrm{H}}}\hat{\rho}(0)e^{-t\hat{\mathrm{H}}} , \tag{3.40}$$

$$Z(\beta) = \mathrm{Tr}[\hat{\rho}(\beta/2)] . \tag{3.41}$$

Now, we transform the dynamic equation into the Wigner formalism, to obtain

$$W(0,\vec{x},\vec{v}) = C , \tag{3.42}$$

$$\partial_t W(t,\vec{x},\vec{v}) = (W(t),\mathrm{H})(\vec{x},\vec{v}) , \tag{3.43}$$

$$Z(\beta) = \int\limits_{\mathbb{R}^d \times \mathbb{R}^d} \mathrm{d}\vec{x}\mathrm{d}\vec{v}\ W(\beta/2,\vec{x},\vec{v}) . \tag{3.44}$$

In Eq. (3.43) we introduced the cosine bracket, see Ref. [6], as the Wigner transform of the anti-commutator, not to be mistaken by the Moyal bracket for the commutator in the previous paragraph. It just means that in Eq. (3.20) one would replace the sin by a cos. If one would be able to develop an efficient Monte-Carlo method for the evolution of the Wigner function according to the last equation, one could try to tackle the numerical sign problem [174]. However, people are already struggling to find an efficient Monte-Carlo solver for the usual Wigner equation. Despite the claims in Ref. [153], the computational results in phase-space dimensions above $d > 2$ are not satisfactory. This information has been obtained through personal communication with the lead researcher of the article [155]. For this reason, we have not followed up on this idea. Maybe there will be somebody smarter in the future who can develop such an algorithm and make Monte-Carlo simulations of many-electron systems feasible.

The route which we take instead is to refocus our attention on the density matrix approach and try to develop a feasible numerical procedure to simulate the decoherent dynamics.

## 3.3 Non-linear Schrödinger equation

To reduce the dimensionality of the problem, similar to Refs. [46, 64], we project the density operator onto the initial quantum state of the system, i.e. $|\phi(t)\rangle \equiv \hat{\rho}(t)|\phi\rangle$ where $|\phi\rangle\langle\phi| \equiv \hat{\rho}(0)$ is the initial, normalized, pure state of the quantum system. The resulting dynamics is

$$\partial_t|\phi(t)\rangle = \dot{\hat{\rho}}(t)|\phi\rangle , \tag{3.45}$$

and the first order approximation looks like

$$|\phi(t+\delta t)\rangle \approx |\phi(t)\rangle + \delta t \sum_{j\in\mathcal{J}}\left[\left[\hat{\mathrm{O}}_j,\hat{\rho}(t)\right],\hat{\mathrm{O}}_j\right]|\phi\rangle , \tag{3.46}$$

$$= \left[\mathbb{I} - \delta t \sum_{j\in\mathcal{J}}\hat{\mathrm{O}}_j^2\right]|\phi(t)\rangle$$

$$+ \delta t \sum_{j\in\mathcal{J}}\left[2\hat{\mathrm{O}}_j\hat{\rho}(t)\hat{\mathrm{O}}_j - \hat{\rho}(t)\hat{\mathrm{O}}_j^2\right]|\phi\rangle . \tag{3.47}$$

The issue with this approach is that it requires the knowledge of the current density operator $\hat{\rho}(t)$ to evolve the wave function by an infinitesimal time $\delta t$. Nevertheless, one can advance the initial state, since $\hat{\rho}(0) = |\phi\rangle\langle\phi|$ is known from the starting condition. We find

$$\frac{|\phi(\delta t)\rangle - |\phi\rangle}{\delta t} = \sum_{j \in \mathcal{J}} \left[ \left[ \hat{O}_j, |\phi\rangle\langle\phi| \right], \hat{O}_j \right] |\phi\rangle . \tag{3.48}$$

Following this line of thought, we write down the *measurement dynamics* by making the replacements

$$\hat{\rho}(t) \rightarrow |\phi(t)\rangle\rangle\langle\phi(t)| , \tag{3.49}$$

$$|\phi\rangle \rightarrow |\phi(t)\rangle , \tag{3.50}$$

$$|\phi(0)\rangle = |\phi\rangle , \tag{3.51}$$

in the previous equation, which results in

$$\partial_t \left( |\phi(t)\rangle\langle\phi(t)|\phi(t)\rangle \right) = \sum_{j \in \mathcal{J}} \left[ [\hat{O}_j, |\phi(t)\rangle\langle\phi(t)|], \hat{O}_j \right] |\phi(t)\rangle . \tag{3.52}$$

The non-linearity in the equation follows from the replacement $\hat{\rho}(t) = |\phi(t)\rangle\langle\phi(t)|$ and the projection on $|\phi(t)\rangle$. We would like to point out that this equation does not converge to the same infinite-time limit as Eq. (3.4). Nevertheless, it allows for the reduction of the wave function to a single eigenstate in the spectrum, which will be shown subsequently and is the main purpose of it. If we rewrite the equation as

$$\partial_t |\phi(t)\rangle = \left[ \sum_{j \in \mathcal{J}} \hat{B}_j^{(\phi_t)} - \frac{\dot{n}(t)}{n(t)} \hat{\mathbb{1}} \right] |\phi(t)\rangle , \tag{3.53}$$

$$\hat{B}_j^{(\phi_t)} \equiv 2\mathbb{E}_j^{(\phi_t,1)} \hat{O}_j - \left( \hat{O}_j \right)^2 - \mathbb{E}_j^{(\phi_t,2)} \hat{\mathbb{1}} , \tag{3.54}$$

$$\mathbb{E}_j^{(\phi_t,k)} \equiv \frac{1}{n(t)} \left\langle \phi(t) \left| \left( \hat{O}_j \right)^k \right| \phi(t) \right\rangle , \tag{3.55}$$

$$n(t) \equiv \langle\phi(t)|\phi(t)\rangle , \tag{3.56}$$

where $\mathbb{E}_j^{(\phi_t,k)}$ stands for the expectation value of the observable $\left( \hat{O}_j \right)^k$ in the state $|\phi(t)\rangle$, and if we calculate the scalar product with $\langle\phi(t)|$ as well as the scalar product of $|\phi(t)\rangle$ with the complex conjugate of the previous equation we shall find

$$\dot{n}(t) + \langle\phi(t)|\dot{\phi}(t)\rangle = \sum_{j \in \mathcal{J}} \langle\phi(t)|\hat{B}_j^{(\phi_t)}|\phi(t)\rangle , \tag{3.57}$$

$$\dot{n}(t) + \langle\dot{\phi}(t)|\phi(t)\rangle = \sum_{j \in \mathcal{J}} \langle\phi(t)|\hat{B}_j^{(\phi_t)}|\phi(t)\rangle . \tag{3.58}$$

The right hand side of both equations is the same, since the operator $\hat{B}_j^{(\phi_t)}$ is hermitian. Adding both equations and using $\dot{n}(t) = \langle\dot{\phi}(t)|\phi(t)\rangle + \langle\phi(t)|\dot{\phi}(t)\rangle$ we obtain

$$\frac{\dot{n}(t)}{n(t)} = \frac{4}{3} \sum_{j \in \mathcal{J}} \left[ \left( \mathbb{E}_j^{(\phi_t,1)} \right)^2 - \mathbb{E}_j^{(\phi_t,2)} \right] \tag{3.59}$$

$$= -\frac{4}{3} \sum_{j \in \mathcal{J}} \text{Var}_j^{(\phi_t)} , \tag{3.60}$$

where $\text{Var}_j^{(\phi_t)}$ stands for the variance of the measurement $\hat{O}_j$ on the state $|\phi(t)\rangle$. This equation shows that $|\phi(t)\rangle$ is an equilibrium state of Eq. (3.52) if and only if it has zero variance in all operator measurements and hence is an eigenstate of all Hermitian operators. To simplify Eq.

(3.52) even further, we write

$$|\Phi(t)\rangle \equiv |\phi(t)\rangle\langle\phi(t)|\phi(t)\rangle \,, \tag{3.61}$$

$$\partial_t|\Phi(t)\rangle = \sum_{j\in\mathcal{J}} \hat{B}_j^{(\Phi_t)}|\Phi(t)\rangle \,, \tag{3.62}$$

and only look at the evolution of the newly defined "wave function" $|\Phi(t)\rangle$. The previously determined properties of the equation are unaffected by this change of variables. Furthermore, as shown in the next paragraph, these fixed point solutions are *asymptotically stable* and small perturbations decay exponentially with $|\vec{a} - \vec{a}'|^2$.

### 3.3.1 Stability of equilibria

Without loss of generality we write $|\Phi(t)\rangle = \sum_{\vec{a}\in\mathcal{A}} b_{\vec{a}}(t)|\psi_{\vec{a}}\rangle$ and shift the dynamics into the coefficients $b_{\vec{a}}$. Based on Eq. (3.62) we obtain the following system of coupled non-linear, first-order differential equations for the coefficients

$$\frac{\dot{b}_{\vec{a}}(t)}{b_{\vec{a}}(t)} = -\frac{\sum\limits_{\vec{a}'\in\mathcal{A}} |b_{\vec{a}'}(t)|^2 |\vec{a}' - \vec{a}|^2}{\sum\limits_{\vec{a}'\in\mathcal{A}} |b_{\vec{a}'}(t)|^2} \,. \tag{3.63}$$

The *unique asymptotically stable equilibria* for this system of differential equations are given by

$$b_{\vec{a}}(t) = \delta_{\vec{a},\vec{a}'} b_{\vec{a}'}(0) \,. \tag{3.64}$$

To prove this statement, we transform the system by using the definition $b_{\vec{a}}(t) \equiv x_{\vec{a}}(t) + \imath y_{\vec{a}}(t)$ with $(x_{\vec{a}}(t), y_{\vec{a}}(t)) \in \mathcal{B}_1^2 \subset \mathbb{R}^2$ (assuming the initial state $|\Phi\rangle$ is normalized) into an even bigger, but real system of differential equations

$$\frac{\dot{x}_{\vec{a}}}{x_{\vec{a}}} = -\frac{\sum\limits_{\vec{a}'\in\mathcal{A}} [x_{\vec{a}'}^2(t) + y_{\vec{a}'}(t)^2] |\vec{a}' - \vec{a}|^2}{\sum\limits_{\vec{a}'\in\mathcal{A}} [x_{\vec{a}'}^2(t) + y_{\vec{a}'}(t)^2]} \,, \tag{3.65}$$

$$\frac{\dot{y}_{\vec{a}}}{y_{\vec{a}}} = -\frac{\sum\limits_{\vec{a}'\in\mathcal{A}} [x_{\vec{a}'}^2(t) + y_{\vec{a}'}(t)^2] |\vec{a}' - \vec{a}|^2}{\sum\limits_{\vec{a}'\in\mathcal{A}} [x_{\vec{a}'}^2(t) + y_{\vec{a}'}(t)^2]} \,. \tag{3.66}$$

To analyze the system we define the solution vector $\vec{u}(t)$ which contains the real and imaginary function of each coefficient, i.e. it has $2 \times |\mathcal{A}|$ entries. For simplicity, we label the eigenvalues by integers, i.e. $\mathcal{A} = \{\vec{a}^{(0)}, \vec{a}^{(1)}, \vec{a}^{(2)}, \dots\}$, such that we can write

$$\vec{u}(t) = \{x_{\vec{a}^{(0)}}(t), y_{\vec{a}^{(0)}}(t), x_{\vec{a}^{(1)}}(t), y_{\vec{a}^{(1)}}(t), \dots\} \,, \tag{3.67}$$

$$\equiv \{x_0(t), y_0(t), x_1(t), y_1(t), x_2(t), y_2(t), \dots\} \,. \tag{3.68}$$

The dynamical system, Eqs. (3.65) and (3.66), can hence be summarized as

$$\dot{\vec{u}}(t) = \vec{F}(\vec{u}) \,, \tag{3.69}$$

$$F_i(\vec{u}) \equiv -\frac{u_i}{|\vec{u}|^2} \sum_j u_j^2 |\vec{a}_{\lfloor i/2\rfloor} - \vec{a}_{\lfloor j/2\rfloor}|^2 \,. \tag{3.70}$$

It is relatively easy to see that *if and only if* $\vec{u}^*$ is the equilibrium solution from Eq. (3.64) the right hand side $\vec{F}(\vec{u}^*)$ will vanish.

Let us assume without loss of generality that in Eq. (3.64) $\vec{a}' = \vec{a}^{(0)}$ then $\vec{u}^* = \{\Re[b_{\vec{a}^{(0)}}], \Im[b_{\vec{a}^{(0)}}], 0, \dots, 0\}$ and the only functions one needs to analyze are $F_0$ and $F_1$, since apparently $F_i = 0$ for $i \geq 2$. $F_0$ and $F_1$ are also zero, since they only contain summands from functions $u_i$ with $i \geq 2$ which are zero.

To determine the stability properties of the equilibrium $\vec{u}^*$, we linearize the problem with respect to small perturbations around the equilibrium solution and look at the Jacobian of the vector field $\vec{F}$ at the point $\vec{u}^*$, as described in Ref. [184]. The resulting matrix is diagonal and

its entries are

$$-\text{Diag}\left[J_{\vec{F}}(\vec{u}^*)\right] = \{0, 0, |\vec{a}^{(1)} - \vec{a}^{(0)}|^2, |\vec{a}^{(1)} - \vec{a}^{(0)}|^2,$$
$$|\vec{a}^{(2)} - \vec{a}^{(0)}|^2, |\vec{a}^{(2)} - \vec{a}^{(0)}|^2, \dots\} \ . \tag{3.71}$$

Consequently, we have shown the stability along the directions $\vec{a}^{(i)}$, $i \geq 1$ and potential instability along the direction $\vec{a}^{(0)}$. However, due to Eq. (3.60) we know that the overall norm has to decrease during the evolution. Consequently, starting with the initial condition $\sum_{\vec{a} \in \mathcal{A}} |b_{\vec{a}}(0)|^2 = 1$, we shall necessarily tend towards a final state with $\lim_{t \to \infty} |b_{\vec{a}}(t)|^2 \leq 1 \ \forall \vec{a} \in \mathcal{A}$, which must also hold for the equilibrium solutions. The small perturbation $\delta\vec{u}$ from the fixed point solution $\vec{u}^*$ decays as

$$\delta\vec{u}(t) = e^{J_{\vec{F}}(\vec{u}^*)t}\delta\vec{u}(0) \ , \tag{3.72}$$

which confirms the exponential decay rate proportional to $|\vec{a}^{(0)} - \vec{a}^{(i)}|^2$ with $i \neq 0$.

In order to conserve the symmetry of the input state for the eigenstate, the wave function is collapsing to, we can only approximate eigenstates belonging to *pairwise distinct* eigenvalues. Therefore, if the symmetry operators commute with the Hermitian operators each distinct eigenstate in the linear decomposition inherits the symmetry of the input wave function. A proof for the case of fully (anti-)symmetric many-particle wave functions is given in the next paragraph.

## 3.3.2 Symmetry inheritance

We are interested in the distinct eigenstates $\{|\psi_n\rangle\}_{n \in \mathbb{N}_0}$ of a quantum many-particle system of $N$ indistinguishable particles, such as fermions or bosons, whose dynamics is governed by the Hamilton operator $\hat{\text{H}}$. With distinct we mean that these states belong to different eigenvalues $\epsilon_n$ of $\hat{\text{H}}$, i.e.

$$\hat{\text{H}}|\psi_n\rangle = \epsilon_n|\psi_n\rangle \ . \tag{3.73}$$

They *might not* span the whole Hilbert space, i.e. we may have a degeneracy in our system. However, we assume that we can construct a complete basis with some orthogonalization procedure on each subspace $\mathcal{S}_n$ corresponding to a specific eigenvalue. Hence, we can write for all $|\phi\rangle \in \mathcal{H}$

$$|\phi\rangle = \sum_{n \in \mathbb{N}_0} \left(\sideset{}{^{\ast}}\sum_{k \in \mathcal{S}_n} b_{n,k}|\psi_{n,k}\rangle\right) \equiv \sum_n a_n|\psi_n\rangle \ , \tag{3.74}$$

where we have used the superposition principle in the definition.

In the case of bosons the eigenstates, which we desire, are fully symmetric $|\psi_n\rangle_+$ whereas for fermions they are fully anti-symmetric $|\psi_n\rangle_-$. The basis of pairwise permutations of particles $\mathcal{P}$ with $|\mathcal{P}| = \frac{n(n-1)}{2}$ elements spans the whole set of permutations and hence these (anti-)symmetric states need to fulfill

$$\langle \vec{x}_1, \dots, \vec{x}_N|\hat{P}|\psi_n\rangle_\pm = (\pm 1)\langle \vec{x}_1, \dots, \vec{x}_N|\psi_n\rangle_\pm \ , \tag{3.75}$$

for each element $\hat{P}$ in the set $\mathcal{P}$. We make the important assumption that

$$[\hat{P}, \hat{\text{H}}] = 0 \tag{3.76}$$

holds for all $\hat{P} \in \mathcal{P}$.

We choose the initial state $|\phi\rangle$ to be fully (anti-)symmetric, i.e. $|\phi\rangle = |\phi\rangle_\pm$ and

$$\hat{P}|\phi\rangle_\pm = \pm|\phi\rangle_\pm \ . \tag{3.77}$$

Hence, together with Eq. (3.76) we can conclude

$$\hat{P}\hat{\text{H}}^l|\phi\rangle_\pm = \hat{\text{H}}^l\hat{P}|\phi\rangle_\pm = \pm\hat{\text{H}}^l|\phi\rangle_\pm \ , \tag{3.78}$$

for all $l \in \mathbb{N}_0$. From Eq. (3.73) we infer that $\hat{P}|\psi_n\rangle \equiv |\psi_n^P\rangle$ is again an eigenstate to eigenvalue $\epsilon_n$. With formula (3.74) and the previous equations we can set up a system of linear equations

for all $\hat{P} \in \mathcal{P}$, which reads

$$\sum_{n \in \mathbb{N}_0} \tilde{a}_n^P \epsilon_n^l = 0 \quad (\forall l \in \mathbb{N}_0) \ , \tag{3.79}$$

$$\tilde{a}_n^P \equiv a_n(|\psi_n\rangle \mp |\psi_n^P\rangle) \ . \tag{3.80}$$

Trying to solve this system for the coefficient vector $(\tilde{a}_0^P, \tilde{a}_1^P, \dots)^T$, we write it as matrix-vector product

$$\begin{pmatrix} 1 & 1 & 1 & 1 & 1 & \dots \\ \epsilon_0 & \epsilon_1 & \epsilon_2 & \epsilon_3 & \epsilon_4 & \dots \\ \epsilon_0^2 & \epsilon_1^2 & \epsilon_2^2 & \epsilon_3^2 & \epsilon_4^2 & \dots \\ \epsilon_0^3 & \epsilon_1^3 & \epsilon_2^3 & \epsilon_3^3 & \epsilon_4^3 & \dots \\ \vdots & \vdots & \vdots & \vdots & \vdots & \dots \end{pmatrix} \begin{pmatrix} \tilde{a}_0^P \\ \tilde{a}_1^P \\ \tilde{a}_2^P \\ \tilde{a}_3^P \\ \vdots \end{pmatrix} = 0 \tag{3.81}$$

and realize that our matrix $M$ is a Vandermonde matrix [83]. Therefore, we can easily write a formula for the determinant of $M$, given by

$$\mathrm{Det}M = \prod_{0 \leq i < j \leq \infty} (\epsilon_i - \epsilon_j) \neq 0 \tag{3.82}$$

which follows since all eigenvalues are *pairwise distinct*. This implies that the matrix is invertible and only the trivial solution, $\tilde{a}_n^P = 0$ for all $n \in \mathbb{N}_0$, solves the system of equations in (3.81). Consequently, we have proven that the eigenstates, which appear with nonzero probability in the corresponding measurement of the quantum state $|\phi\rangle$ and which belong to pairwise distinct eigenvalues of the observable $\hat{\mathrm{H}}$ that commutes with all elements $\hat{P} \in \mathcal{P}$ are fully (anti)-symmetric if and only if the state $|\phi\rangle$ is fully (anti)-symmetric.

## 3.4 Eigenstate towing

By projecting the dynamics of the density operator on a wave function we have sacrificed the exact compliance with Born's law, i.e. in certain cases we may fail to converge to the most probable eigenstate of the decomposition. To exemplify this issue, let us take the problem of a one-dimensional harmonic oscillator. The only operator we use is the dimensionless Hamilton operator

$$\{\hat{\mathrm{O}}_j\}_{j \in \mathcal{J}} = \{\hat{\mathrm{H}}\} \ , \tag{3.83}$$

$$\hat{\mathrm{H}} = \frac{\hat{v}^2 + \hat{x}^2}{2} \ , \tag{3.84}$$

where

$$\hat{x} = \frac{\hat{q}}{\sqrt{\frac{\hbar}{m\omega}}} \ , \ \hat{v} = \frac{\hat{p}}{\sqrt{\hbar m \omega}} \ , \tag{3.85}$$

are the dimensionless position and momentum operator. For the representation, we choose the well-known eigenfunctions

$$\psi_n(x) = \frac{\pi^{-\frac{1}{4}}}{\sqrt{2^n n!}} e^{-x^2/2} H_n(x) \tag{3.86}$$

as a basis such that

$$\hat{\mathrm{H}}|\psi_n\rangle = (n + 1/2)|\psi_n\rangle \ . \tag{3.87}$$

As an initial state we pick

$$|\Psi(0)\rangle = b_0|\psi_0\rangle + b_1|\psi_1\rangle + b_2|\psi_2\rangle \ , \tag{3.88}$$

with $b_0, b_1, b_2 \in \mathbb{C}$ and $|b_0|^2 + |b_1|^2 + |b_2|^2 \equiv p_0 + p_1 + p_2 = 1$. The dynamics of the coefficients are easily simulated with Eqs. (3.65) and (3.66). In Figs. 3.10-3.12 we show three important examples. In the first example, see Fig. 3.10, there are only two nonzero coefficients. One coefficient is chosen slightly bigger than the other, such that the coefficient simulation converges to one of them. In practice, numerical noise together with a renormalization of the wave function

will trigger the collapse to one of the eigenstates. In the second example, see Fig. 3.11, the three lowest eigenstates participate in the competition with $p_0 > p_1 > p_2$. Due to the stronger influence of state $n = 0$ on $n = 2$ and vice versa the first state $n = 1$ survives the competition, although the ground state is initially the most probable one. In the third example, see Fig. 3.12, we show that the system will tend again to the most probable state if $p_0$ is increased from 13/30 to 14/30 while reducing $p_2$ from 7/30 to 6/30. It should be stressed that the trends of survival which are shown in the Figs. 3.10-3.12 remain valid for longer simulation times, i.e. the eigenstate with the highest probability will remain whereas the others are exponentially supressed. In conclusion, the dynamics tend to favor eigenstates in the center of the spectrum of all states $|\psi_{\vec{a}}\rangle$ contained in the linear combination of the input state, i.e. $\{\vec{a} \in \mathcal{A} \text{ with } |b_{\vec{a}}|^2 > 0\}$. This is caused by the overall damping rate $\gamma_{\vec{a}}$ for the eigenstate with eigenvalue $\vec{a}$

$$\gamma_{\vec{a}} = - \sum_{\vec{a}' \in \mathcal{A}} |\vec{a} - \vec{a}'|^2 |b_{\vec{a}'}|^2 \ . \tag{3.89}$$

that is stronger for eigenstates at the boundary than for states in the center of the spectrum.
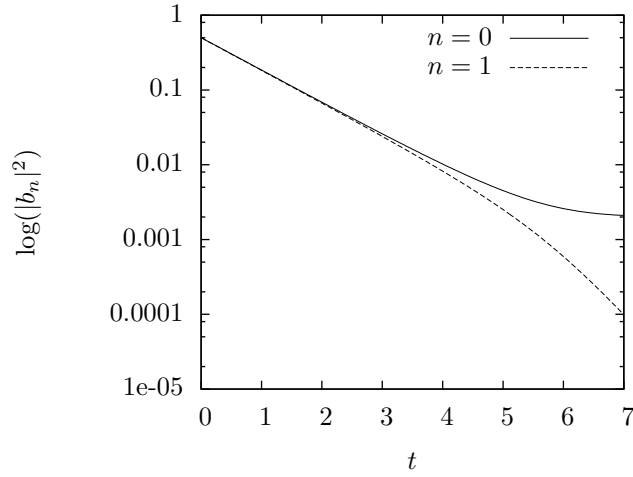


Figure 3.10: Evolution of the probabilities $p_0(t)$ (solid) and $p_1(t)$ (dashed) for $p_0(0) = \frac{501}{1000}$, $p_1(0) = \frac{499}{1000}$ and $p_2(0) = 0$.
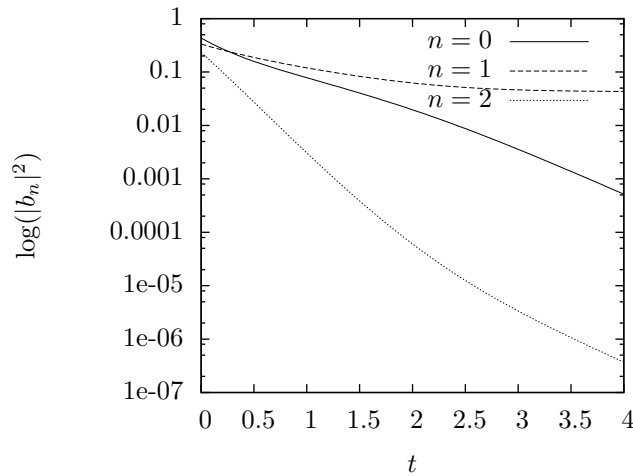


Figure 3.11: Evolution of the probabilities $p_0(t)$ (solid), $p_1(t)$ (dashed) and $p_2(t)$ (dotted) for $p_0(0) = \frac{13}{30}$, $p_1(0) = \frac{10}{30}$ and $p_2(0) = \frac{7}{30}$.
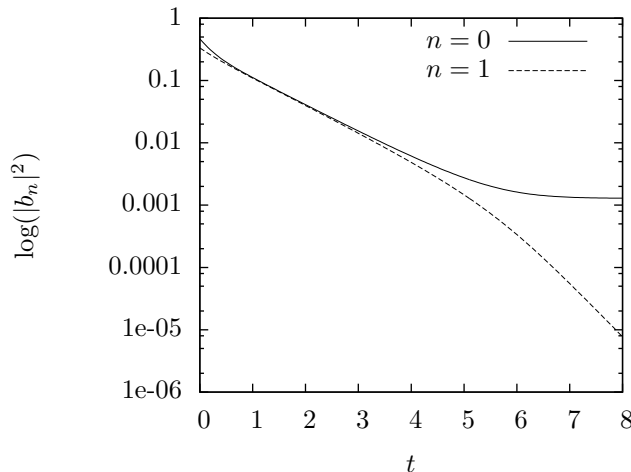
Figure 3.12: Evolution of the probabilities $p_0(t)$ (solid) and $p_1(t)$ (dashed) for $p_0(0) = \frac{14}{30}$, $p_1(0) = \frac{10}{30}$ and $p_2(0) = \frac{6}{30}$.

In order to overcome this difficulty, we now propose the method of *eigenstate towing* (ET), based on the theoretical model described in the previous section, in the following way. One starts with a set of operators $\{\hat{O}_j^{(0)}\}_{j \in \mathcal{J}}$ that have a well-known eigenbasis $\{|\psi_{\vec{a}_0}\rangle\}_{\vec{a}_0 \in \mathcal{A}_0}$ and gradually perturbs the set with the operators $\{\hat{\delta}_j^{(i)}\}_{j \in \mathcal{J}}$ for $i \in \{0, 1, \dots, M\} \subset \mathbb{N}_0$ to reach the desired problem $\{\hat{O}_j^{(M)}\}_{j \in \mathcal{J}}$ with corresponding eigenstates $\{|\psi_{\vec{a}_M}\rangle\}_{\vec{a}_M \in \mathcal{A}_M}$, i.e.

$$\hat{O}_j^{(i)} \equiv \hat{O}_j^{(0)} + \sum_{k=0}^{i-1} \hat{\delta}_j^{(k)} \ . \tag{3.90}$$

It is important to note that the choice of perturbation operators is not limited by

$$\hat{\delta}_j^{(i)} = \frac{\hat{O}_j^{(M)} - \hat{O}_j^{(0)}}{M} \ , \tag{3.91}$$

but can have any form that fulfills Eq. (3.90) for $i = M$. As an example, one can imagine the helium atom in the discrete hyper-spherical harmonics' basis such that the matrix representation of the Hamilton operator becomes sparse [3] and the off-diagonal elements can be treated as perturbations; or one thinks of the quantum phase transition from the $U(5)$- to the $SU(3)$-symmetry group in the interacting boson model at $\kappa = \kappa_c$ [50]. The quantum states, whose progression along the perturbations we would like to follow, are the finite subset of eigenstates $\{|\psi_{\vec{a}_0}\rangle\}_{\vec{a}_0 \in \mathcal{B}_0}$ with $\mathcal{B}_0 \subset \mathcal{A}_0$. One can imagine the procedure as towing the eigenstates along the line of perturbations. The choice of the subset $\mathcal{B}_0$ is theoretically arbitrary. The reason is that from time-independent perturbation theory we know that for infinitesimal perturbations the eigenstates change very little, which implies that for perturbations of the form (3.91) and in the limit of large $M$ the overlap between the unperturbed $|\psi_{\vec{a}_i}\rangle$ and perturbed eigenstate $|\psi_{\vec{a}_{i+1}}\rangle$ satisfies

$$|\langle \psi_{\vec{a}_i} | \psi_{\vec{a}_{i+1}} \rangle|^2 \lesssim 1 \ , \tag{3.92}$$

with $i \in \{0, 1, \dots, M-1\}$. This ensures that the input wave function $|\psi_{\vec{a}_i}\rangle$ will converge to the eigenstate $|\psi_{\vec{a}_{i+1}}\rangle$ using the operators $\{\hat{O}_j^{(i+1)}\}_{j \in \mathcal{J}}$ for the dynamics in Eq. (3.62). However, depending on the (un-)perturbed operators, excited states are often more affected by perturbations and hence subject to bigger changes. Therefore, it may be necessary to adjust the set of perturbation operators to every state which is going to be simulated $\{\hat{\delta}_j^{(i_{\vec{a}})}\}_{j \in \mathcal{J}}$ with $i_{\vec{a}} \in \{0, 1, \dots, M_{\vec{a}}\}$ and $\vec{a} \in \mathcal{B}$ to establish the reported convergence. In practice, the adjustments may only require a larger number $M_{\vec{a}}$ whereas the functional form of the operator stays unchanged, which leads to a higher computational effort to simulate the behavior of these states. In general, it is difficult

to determine $M$, $M_{\vec{a}}$ or the total set $\{\hat{\delta}_j^{(i_{\vec{a}})}\}_{j \in \mathcal{J}}$ for a given state and problem in advance. Therefore, one should check the convergence to the correct eigenstate by decreasing the perturbation increment and comparing the results to the larger perturbation increment. However, since the ET simulation does not require the results from the other computations, each single one can be performed independently and in parallel, which can represent a significant advantage if the required resources for the calculations are available. A natural stopping criterion for the convergence in the $i_{\vec{a}}$-th perturbation step of Eq. (3.62) is the $L^2$-norm of the temporal derivative of the wave function, whose exponential convergence will be shown for a concrete example in section 3.6.

## 3.5 Numerical implementation

With the intention to show a practical application of the proposed algorithm from the previous section we use the (semi-)implicit Crank-Nicolson method for the numerical implementation, which is based on the trapezoidal rule and reads in our case

$$\frac{\vec{\Phi}_{t+\delta t} - \vec{\Phi}_t}{\delta t} = \sum_{j \in \mathcal{J}} \frac{1}{2} \left[ \mathrm{B}_j^{(\Phi_{t+\delta t})} \vec{\Phi}_{t+\delta t} + \mathrm{B}_j^{(\Phi_t)} \vec{\Phi}_t \right] \ , \tag{3.93}$$

where $\mathrm{B}_j^{(\Phi_t)}$ is the matrix representation of the Hermitian operator $\hat{\mathrm{B}}_j^{(\Phi_t)}$ of Eq. (3.54). The issue with this procedure is that we do not know the expectation values $\mathbb{E}_j^{(\Phi_{t+\delta t}, i)}$ and hence would need to approximate them to first order, such that we preserve the second order accuracy, i.e.

$$\mathbb{E}_j^{(\Phi_{t+\delta t}, i)} \approx \mathbb{E}_j^{(\Phi_t, i)} + 2\delta t \sum_{j' \in \mathcal{J}} \vec{\Phi}_t^T \left( \mathrm{O}_j \right)^i \mathrm{B}_{j'}^{(\Phi_t)} \vec{\Phi}_t \ . \tag{3.94}$$

However, practical numerical examples have revealed that a zeroth order approximation

$$\mathrm{B}_j^{(\Phi_{t+\delta t})} \approx \mathrm{B}_j^{(\Phi_t)} \ , \tag{3.95}$$

is more stable, such that a significantly larger time-step can be used and a faster convergence is obtained. To solve the system of algebraic equations we use a Cholesky decomposition of our real symmetric, positive-definite matrix

$$\mathrm{M}^{(\Phi_{t+\delta t})} \equiv \mathbb{I} + \frac{\delta t}{2} \sum_{j \in \mathcal{J}} \mathrm{B}_j^{(\Phi_t)} \ . \tag{3.96}$$

The matrix is positive-definite, since for any eigenvector $\vec{\Psi}_{\vec{a}}$ of the set of matrices $\{\mathrm{O}_j\}_{j \in \mathcal{J}}$ we know

$$\mathrm{B}_j^{(\Psi_{\vec{a}})} \Psi_{\vec{a}} = \vec{0} \ , \tag{3.97}$$

$$\mathrm{M}^{(\Psi_{\vec{a}})} \vec{\Psi}_{\vec{a}} = \vec{\Psi}_{\vec{a}} \ , \tag{3.98}$$

i.e. $M^{(\Psi)}$ only has the positive eigenvalue $+1$. For a sparse matrix representation of the observables, the Crank-Nicolson method offers the advantage of higher stability, and hence larger time-steps compared to an explicit method, whereas the computational costs for each step are compatible due to the Cholesky decomposition. In section 3.7 we further analyze the convergence and scaling properties of our algorithm compared to the MRRR method [41] for eigenvector computations of tridiagonal matrices, which arise in the example of an excited-state quantum phase transition that will be discussed in the next section.

## 3.6 Application to quantum phase transitions

As a practical example we consider the excited-state quantum phase transition (see Refs. [22, 129]) in the Jaynes-Cummings model, further explained in Refs. [88, 172, 128]. The quantum optical model depicts the behavior of $N$ identical two-level molecules coupled to a single-mode

radiation field. The model is simple but still covers the main features of the class of problems we are interested in. The Hamilton operator can be written as

$$\hat{H}_\kappa = \omega_0 \hat{J}_z + \omega \hat{b}^\dagger \hat{b} + \frac{\kappa}{\sqrt{4j}} \left[ \hat{b} \hat{J}_+ + \hat{b}^\dagger \hat{J}_- \right] \ , \tag{3.99}$$

where $2j$ equals the number of molecules $N$ and $\kappa$ determines the interaction strength between the radiation field and the molecules. In the limit $j \to \infty$ it becomes dual to a bosonic spin model [177]. The operators fulfill the usual bosonic and $SU(2)$ commutation relations

$$\left[ \hat{J}_z, \hat{J}_\pm \right] = \pm \hat{J}_\pm \ , \tag{3.100}$$

$$\left[ \hat{J}_+, \hat{J}_- \right] = 2 \hat{J}_z \ , \tag{3.101}$$

$$\left[ \hat{b}, \hat{b}^\dagger \right] = 1 \ . \tag{3.102}$$

For $\omega \to 0$ one can make a Bethe ansatz to find an eigenbasis of the Hamilton operator, as described in Ref. [9]. In the case $\omega \neq 0$ we choose the states $|n\rangle|j,m\rangle$ which are eigenstates of the non-interacting system as a basis, such that

$$\hat{H}_0 \left( |n\rangle|j,m\rangle \right) = \left( \omega_0 m + \omega n \right) \left( |n\rangle|j,m\rangle \right) \ , \tag{3.103}$$

and at the same time eigenstates of the operator $\hat{J}^2$ with

$$\hat{J}^2 \equiv \hat{J}_z^2 + (\hat{J}_+ \hat{J}_- + \hat{J}_- \hat{J}_+)/2 \ , \tag{3.104}$$

$$\hat{J}^2 \left( |n\rangle|j,m\rangle \right) = j(j+1) \left( |n\rangle|j,m\rangle \right) \ , \tag{3.105}$$

in analogy to the angular momentum formalism. Another important observation is that both $\hat{b}^\dagger \hat{b} + \hat{J}_z$ and $\hat{J}^2$ commute with $\hat{H}_\kappa$. Hence we choose the energy eigenstates $|j,c,\epsilon\rangle$ to be eigenstates of these two operators as well, i.e.

$$\hat{J}^2 |j,c,\epsilon\rangle = j(j+1)|j,c,\epsilon\rangle \ , \tag{3.106}$$

$$\left( \hat{b}^\dagger \hat{b} + \hat{J}_z \right) |j,c,\epsilon\rangle = c|j,c,\epsilon\rangle \ , \tag{3.107}$$

$$\hat{H}_\kappa |j,c,\epsilon\rangle = \epsilon|j,c,\epsilon\rangle \ . \tag{3.108}$$

Therefore we write the eigenstate as

$$|j,c,\epsilon\rangle = \sum_{n=c-j}^{c+j} A_n^{(j,c,\epsilon)} |n\rangle|j,c-n\rangle \ , \tag{3.109}$$

where the sum can only run along $n \in \mathbb{N}_0$ number of bosons. The eigenvector problem hence transforms into determining the coefficient vector $A_n^{(j,c,\epsilon)}$, and the matrix representation of $\hat{H}_\kappa$ becomes tridiagonal in this basis. The reason is that the interaction term can only alter the parameter $n$ by $\pm 1$, which leads to a system of equations

$$\frac{\kappa}{\sqrt{4j}} \left[ \sqrt{n} C_{j,c-n} A_{n-1}^{(j,c,\epsilon)} + \sqrt{n+1} C_{j,c-n-1} A_{n+1}^{(j,c,\epsilon)} \right]$$
$$+ \left[ (c-n)\omega_0 + n\omega - \epsilon \right] A_n^{(j,c,\epsilon)} = 0 \ , \tag{3.110}$$

where $C_{j,c-n} \equiv \sqrt{j(j+1) - (c-n)(c-n+1)}$. In summary, this means that we choose

$$\hat{O}^{l_k} \equiv \hat{H}_{\frac{l}{M_k}\kappa} \tag{3.111}$$

$$l \in \{1, 2, \ldots, M_k\} \,, \tag{3.112}$$

$$\{|\psi\rangle_{a_0}\}_{a_0 \in \mathcal{A}_0} \equiv \{|n\rangle|j, c-n\rangle\}_{n \in \{c-j,\ldots,c+j\}} \,, \tag{3.113}$$

$$\hat{O}_{(0)}|n\rangle|j, c-n\rangle = [(c-n)\omega_0 + n\omega]\,|n\rangle|j, c-n\rangle \,, \tag{3.114}$$

$$\hat{\delta}^{(l_k)} \equiv \frac{l}{M_k}\frac{\kappa}{\sqrt{4j}}\left[\hat{b}\hat{J}_+ + \hat{b}^\dagger\hat{J}_-\right] \,, \tag{3.115}$$

$$k \in \{c-j, c-j+1, \ldots, c+j\} \,, \tag{3.116}$$

For the numerical implementation this choice of basis functions implies that we pick an initial vector $\vec{\Phi}_0$ from the set of standard basis vectors $\{\hat{e}_0, \hat{e}_2, \ldots, \hat{e}_{2j}\}$ which span the space $\mathbb{R}^{2j+1}$, for instance $\vec{\Phi}_0 \equiv \vec{\Phi}_{k,0} = \hat{e}_k$, and apply the first $(l = 1)$ measurement dynamical evolution, defined in section 3.3, with the matrix

$$\left(H_{\frac{1}{M_k}\kappa}\right)_{ii'} = [(j-i)\omega_0 + (c-j+i)\omega]\,\delta_{i,i'}$$
$$+ \frac{1}{M_k}\frac{\kappa}{\sqrt{4j}}\left[\sqrt{c-j+i}\,C_{j,j-i}\delta_{i,i'-1}\right.$$
$$\left.+\sqrt{c-j+i+1}\,C_{j,j-i-1}\delta_{i,i'+1}\right] \,. \tag{3.117}$$

The matrix representation of the time evolution operator, defined in Eq. (3.54), that is applied in the first operation of the algorithm looks like

$$B^{(\phi_{k,0})} = 2\mathbb{E}^{(\phi_{k,0},1)}H_{\frac{1}{M_k}\kappa} - H^2_{\frac{1}{M_k}\kappa} - \mathbb{E}^{(\phi_{k,0},2)}\mathbb{I} \,, \tag{3.118}$$

$$\mathbb{E}^{(\phi_{k,0},1)} = (\hat{e}_k)^T H_{\frac{1}{M_k}\kappa}\hat{e}_k = (j-k)\omega_0 + (c-j+k)\omega \,, \tag{3.119}$$

$$\mathbb{E}^{(\phi_{k,0},2)} = (\hat{e}_k)^T H^2_{\frac{1}{M_k}\kappa}\hat{e}_k = \sum_{i=0}^{2j}\left(H_{\frac{1}{M_k}\kappa}\right)_{ki}\left(H_{\frac{1}{M_k}\kappa}\right)_{ik} \,. \tag{3.120}$$

The only part that is going to change when making the next time-step of the algorithm are the expectations values, which hence changes the matrix $B$, which is used for the next time-step. This procedure will be iterated until the desired convergence, based on the criterion exemplified in Fig. 3.13, is reached. The resulting vector $\vec{\Phi}_{t_{\text{conv}}}$ is then called $\vec{\Phi}_0$ again and the next measurement dynamics $(l = 2)$ with the matrix $H_{\frac{2}{M_k}\kappa}$ is started. This process is repeated until $l = M_k$.

In the case of an excited-state as opposed to a usual quantum phase transition one observes the transition and hence the critical scaling behavior with respect to an increase in the interaction strength $\kappa$ not only in the ground state but also for eigenstates belonging to larger energy eigenvalues, cf. Ref. [22]. Therefore, we analyze the scaling behavior of the atomic inversion $\langle\hat{J}_z\rangle$ not just as a function of the number of identical two-level molecules $N = 2j$ in the ground state, where it serves as an order parameter, but also as a function of the spectrum ratio $q \equiv k/N$. $k$ is the level of the excited-state eigenvector $\vec{\Phi}_k$ in the vector space $\mathbb{R}^{N+1}$. The scaled atomic inversion,

$$\langle\hat{J}_z\rangle_q/j = 1 - \frac{1}{j}\sum_{i=0}^{N}\Phi_{k,i}^2 i \,, \tag{3.121}$$

shown in Fig. 3.14, decreases from one above the theoretical transition point $\kappa_c = \sqrt{\frac{(\omega-\omega_0)^2}{2}}$ [128] for the ground state $(q = 0)$, similar to the magnetization in an Ising model that increases from zero for the phase transition. In addition, we observe the finite size effects for different numbers of molecules [23, 79]. In the case of an excited state, the atomic inversion also shows critical scaling as a function of the interaction strength or the scaled energy $\varepsilon \equiv \epsilon/j$, as demonstrated in Ref. [128]. Although it does not serve as an order parameter to distinguish the two phases,

see Fig. 3.15, one can for instance still analyze its finite size scaling

$$\langle \hat{J}_z \rangle_q = N^{\beta_q/\nu_q} \mathcal{F}_{J_z,q} \left[ (\varepsilon - \varepsilon_c) N^{1/\nu_q} \right] \, , \tag{3.122}$$

where $\varepsilon_c$ is the critical scaled energy. To measure the critical exponent $\beta_q/\nu_q$ as a function of the spectrum ratio $q \equiv k/N$, we measure the slope of the linear model fit of the maximum atomic inversion plotted against the number of molecules, as shown in Fig. 3.16. The results are shown in Fig. 3.17 and demonstrate a general trend for an increase of $\beta_q/\nu_q$ with an increasing spectrum ratio $q$, which means that the critical exponents are not independent of the spectrum ratio. The errors depict the 95% confidence interval for the slope parameter of the fitted linear regression model. Note that the error bars and the small relative change of 2.5% may suggest that the critical exponent ratio would be universal. However, we have refocused our simulation efforts around the critical points $\kappa_c(q)$ to reduce the main source of error, which is to underestimate the maximum value due to the discrete scanning of $\kappa$ values, and the general trend as well as the measured slopes are unchanged. Furthermore, we changed $\omega$ and found that, as expected, the critical exponent ratios do not change. Based on our findings a quantum state of this system does have fundamentally different properties depending on its ratio in the total spectrum. This is in accordance with the physical intuition, since for instance the correspondance principle [16] tells us that a quantum state with a large quantum number behaves classically and hence fundamentally different from a low quantum number state. The opposite behavior would have been a surprise.
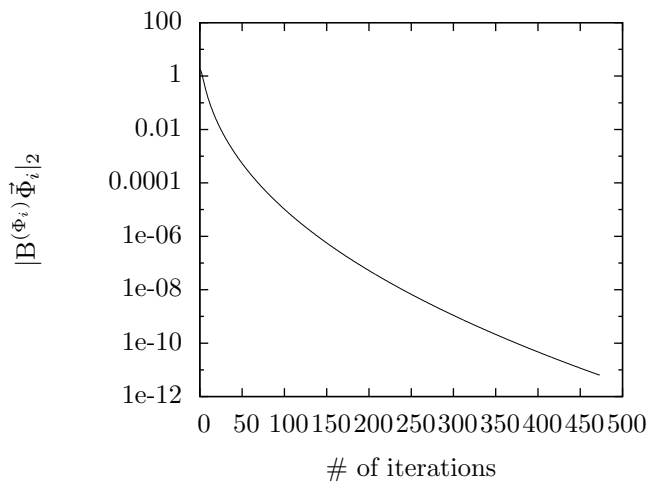


Figure 3.13: Evolution of the stopping criterion for the collapse algorithm using $\delta t = 1.1$, $N = 80$ molecules targeting the 8-th eigenvector for $c = j$, $\kappa = 0.1$, $\omega_0 = 1$ and $\omega = 2$.

## 3.7 Benchmarking

In order to compare our method to other state-of-the-art eigensolvers on the problem of excited-state quantum phase transitions in the Jaynes-Cummings model, described in the previous section, which essentially boils down to the diagonalization of a tridiagonal matrix, we choose one of the fastest, but still accurate algorithms, the MRRR algorithm [41, 42], in the publicly available *Linear Algebra PACKage* (LAPACK) via the *INTEL Math Kernel Library* version 11.0.3. [37]. In Fig. 3.18 we show the convergence of a higher-order eigenvector to the result computed by the MRRR algorithm, implemented in the LAPACK library [42]. First of all, one observes that the convergence is not exponential throughout the whole dynamics. Nevertheless, from Eq. (3.72) we infer that the exponential convergence only holds close to the exact result, which can be confirmed by looking at the graph between 300 and 400 iterations. In addition, the renormalization which is performed every time-step affects the dynamics and hence also the convergence properties, especially in the beginning where the variance and consequently the change in the norm of the vector, see Eq. (3.60), are quite large. Second, due to the accumulation of numer-
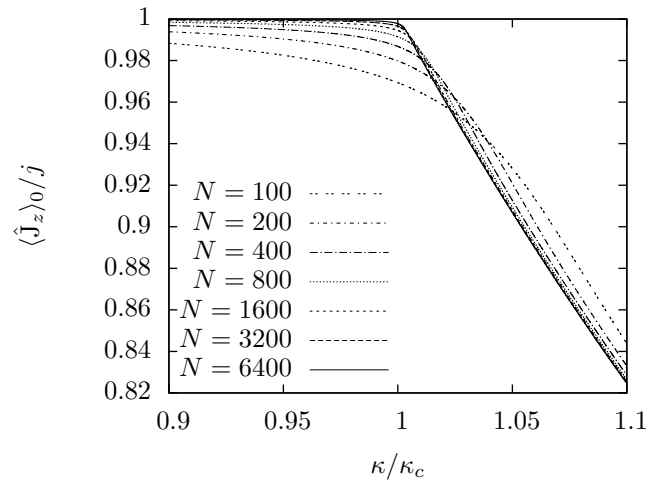
Figure 3.14: Scaled atomic inversion as a function of the interaction strength for the ground state eigenvector using different numbers of molecules $N$, $c = j$, $\omega_0 = 1$ and $\omega = 2$.
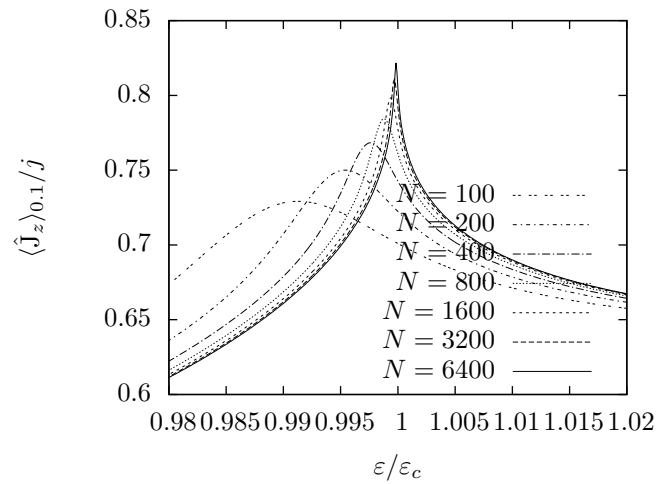


Figure 3.15: Atomic inversion as a function of the scaled energy for the spectrum ratio $q = 0.1$ using different numbers of molecules $N$, $c = j$, $\omega_0 = 1$ and $\omega = 2$.
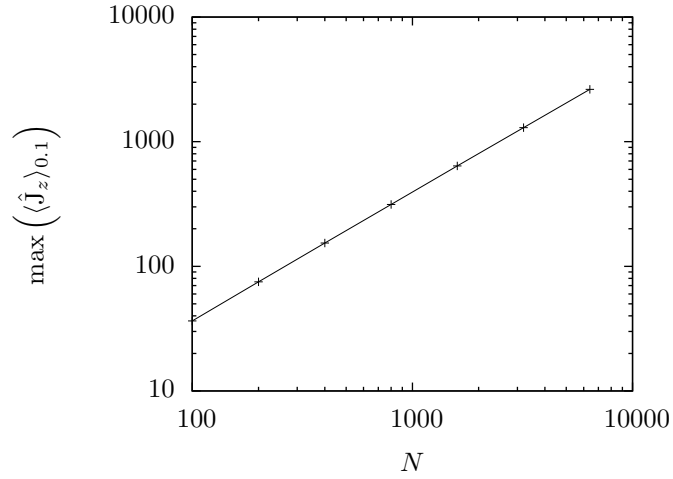
Figure 3.16: Maximum atomic inversion as a function of the number of molecules for the spectrum ratio $q = 0.1$, $c = j$, $\omega_0 = 1$ and $\omega = 2$, measuring a slope $\beta_q/\nu_q \approx 1.03$.
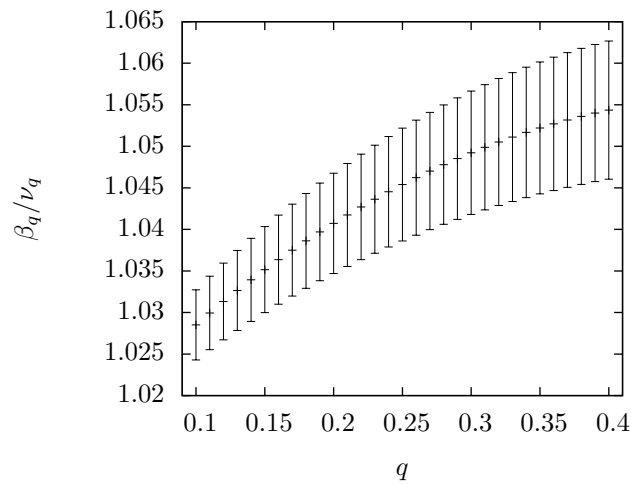


Figure 3.17: Change in the critical exponent ratio $\beta_q/\nu_q$ of the atomic inversion as function of the spectrum ratio $q = k/N$ with $c = j$, $\omega_0 = 1$ and $\omega = 2$, and errors showing the 95% confidence interval of the linear regression model.

ical noise, we find that the eigenvectors do not converge with machine precision to the MRRR result, but instead observe a precision loss with an increased number of entries in the matrix representation. The reason is the higher number of floating point operations in the matrix-vector multiplications. This also causes the tremor at the end of the line in Fig. 3.18. One can reduce the noise by decreasing the time step after the preliminary convergence and re-running the convergence algorithm. As mentioned at the end of section 3.4, Fig. 3.13 shows the evolution of the approximated temporal derivative that is used as a stopping criterion for the algorithm. The behavior is similar to the convergence of the eigenvector in the previous figure. As before, one observes the exponential decay at the end of the evolution, between 300 and 450 iterations. In Fig. 3.19 we compare the scaling behavior of our ET algorithm with the MRRR algorithm that computes all and only one specific eigenvector. Using our method to sequentially calculate all eigenvectors and -values mainly means that the computation times are multiplied by $N$, the number of eigenvectors in the problem, which is why we did not include it in this figure. In general, we find the expected linear scaling behavior for the single-eigenvector LAPACK MRRR algorithm. For the LAPACK algorithm that computes all eigenvectors, we found a slope of 1.6 although in theory we would expect 2.0. We attribute the difference to parallelization, which has probably affected the computation times more significantly for larger matrix sizes. For our algorithm we observe a scaling with a slope of 1.3 that lies in the middle between the LAPACK algorithms. The scaling behavior of the ET algorithm is mainly caused by the increased number of perturbation steps, which are required to ensure convergence to the correct eigenvector in the spectrum. In addition, we demonstrate the parallelization of the ET algorithm in Fig. 3.20 for different matrix sizes and different numbers of computed excited-state eigenvectors. The reason the curves for a given $N$ are not perfectly horizontal is the OpenMP maximally-parallelized "parallel direct solver" (PARDISO) [140, 139, 95], which slows down if less processors per eigenvector computation are available. We have tested other solving modes of PARDISO, but did not find another scaling behavior.
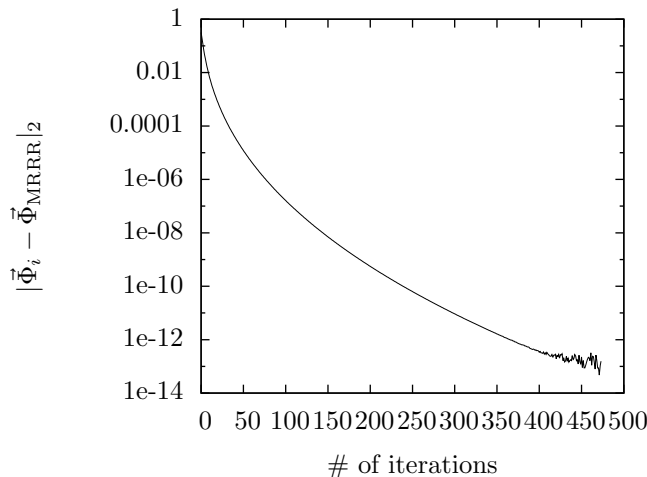


Figure 3.18: Convergence of ET algorithm using $\delta t = 1.1$ for $N = 80$ molecules towards the 8-th eigenvector calculated by LAPACK MRRR algorithm [41, 42] for $c = j$, $\kappa = 0.1$, $\omega_0 = 1$ and $\omega = 2$.

## 3.8 Final remarks

Starting from a physically motivated perspective on the problem of finding eigenstates of a set of Hermitian operator with discrete spectra, we developed a non-linear Schrödinger equation for an isolated quantum mechanical system by projecting the decoherent collapse dynamics of the Lindblad equation onto a wave function. The measurements favor the collapse to eigenstates based on Born's law instead of the hierarchy of eigenvalues, which is the case in most of the other eigensolvers [103, 10, 75, 51, 104]. The method, discussed in Ref. [171], gives the possibility to target
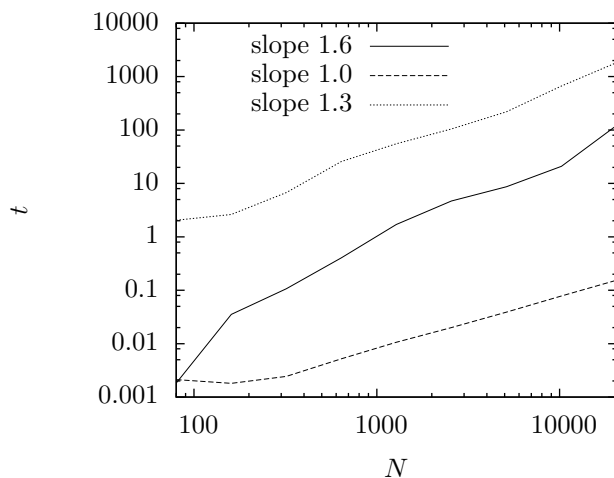
Figure 3.19: Scaling behavior of CPU time for LAPACK MRRR algorithm [41, 42] targeting only the $N/10$-th eigenvector (dashed), all eigenvectors (solid) and first-order ET algorithm targeting only the $N/10$-th eigenvector using $\delta t = 1.1$ (dotted) with $c = j$, $\kappa = 0.1$, $\omega_0 = 1$ and $\omega = 2$ on 6 Intel(R) Xeon(R) CPUs E5-1650 v3 3.50GHz with 15.36 MB cache and 12 processors.
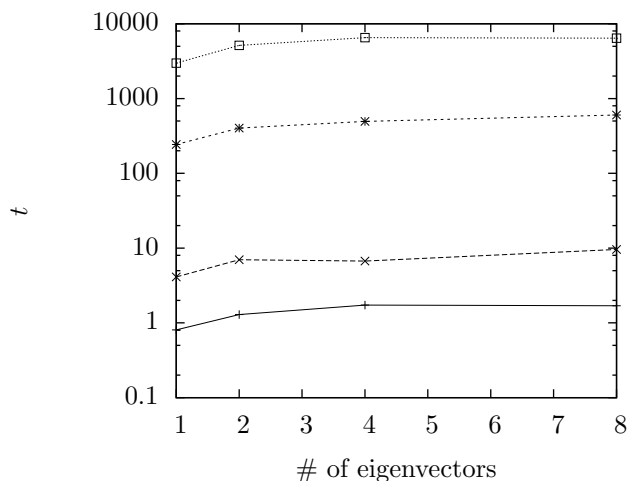


Figure 3.20: Parallel first-order ET algorithm targeting $n$ eigenvectors ($\{N/10, N/10 - 1, \ldots, N/10 - (n-1)\}$) with $N = 80$ (solid), 640 (long dashed), 5120 (short dashed), 20480 (dotted) using $\delta t = 1.1$ with $c = j$, $\kappa = 0.1$, $\omega_0 = 1$, $\omega = 2$ and the OpenMP maximally parallelized PARDISO [140, 139, 95] for the implicit time-step on 6 Intel(R) Xeon(R) CPUs E5-1650 v3 3.50GHz with 15.36 MB cache and 12 processors.

eigenstates with other (arbitrary) selection criteria, which would include Born's law. However, it has only cubic convergence, whereas our non-linear Schrödinger equation offers exponential convergence to the eigenstate. We showed that the unique stable equilibria of the obtained equation are given by the eigenstates of the observables and discussed the eigenstate towing as an application to approximate these states. Thereby, one makes use of the time-independent perturbation theory to follow the progression of an arbitrary subset of eigenstates along a line of perturbations. On the one hand, it gives the possibility to see the effect of stronger interactions on excited eigenstates or states with certain localization properties, such as edge or surface states, which is important for excited-state quantum phase transitions [22] and was demonstrated in paragraph 3.6 for the Jaynes-Cummings model system [88, 172, 128]. On the other hand, one is able to track the progression of each eigenstate individually and in parallel without the exchange of information between the different computations, which allows an efficient calculation on multi-processor clusters, as seen in paragraph 3.7 using the (semi-)implicit Crank-Nicolson method as a specific numerical implementation, discussed in section 3.5. For a scaling of the computational costs with $\mathcal{O}\left[N^{1.3}\right]$, as seen in Fig. 3.19, we need a sparse but not necessarily a tridiagonal matrix structure. In the case of a dense matrix, there are two issues which we face. First, if we use a semi-implicit method we need to invert a dense matrix which costs about $\mathcal{O}[N^3]$ and is hence not desirable. Second, if we use an explicit method we have to deal with a high condition number which requires us to use a very small time step and hence many iterations till we converge. Both approaches are undesirable which is why the method should not be used in this case. Similar to other methods, such as Ref. [75], a simple implementation of symmetries, either directly in the input state or explicitly through the usage of the corresponding symmetry operator in the dynamics, is feasible. This can help to further increase the convergence rate, since the distance between the eigenvalues of states contained in the decomposition of the input state may increase or is enhanced by the explicit symmetry operator usage.

As future work, one may want to examine other decoherent evolution equations with stronger coupling between the quantum system and the measurement apparatus as well as stochastic numerical simulation techniques to make higher-dimensional computations feasible.

# 4 Electron-Phonon Coupling

> Mathematics, rightly viewed,
> possesses not only truth, but
> supreme beauty - ...
>
> —————————————————
>
> Betrand Russell

    In this chapter we want to analyze if one can replace the interaction of electrons and phonons through the dynamics of the particles on a curved, Riemannian manifold with a metric tensor that depends in some way on the phonons. The idea is that the metric tensor takes care of the displacements which are created by the phonons and changes the length measurements on the manifold accordingly. The resulting quantum system should then be able to work with a lattice potential that appears regular in the coordinates of the manifold.

    First, we shall give an introduction to the standard approach of treating electron-phonon coupling. Second, we review the concept of non-relativistic quantum mechanics on Riemannian manifolds. There, we shall discuss the differences and challenges which arise when we try to match the respective theories, and also derive a measurement that shows the nonequivalence of the two quantum systems, i.e. we shall demonstrate that the outcomes of measurements in both systems will not always agree. Nevertheless, we are going to construct a weakly equivalent system in the special case of two dimensions, for which the energy measurements will return the same value for a quantum state whose coordinate representation is the same in both systems. A more detailed explanation of the notion of weak equivalence will be given in the second last section. Throughout these calculations we derive the form of the metric tensor operator that is related to the potential which facilitates the electron-phonon interaction.

## 4.1 Standard approach

As a starting point, we are concerned with the description of the dynamics of (valence) electrons and ions in a (macroscopic) crystal in the Euclidean space $\mathbb{R}^d$ with $d = 1, 2$ or $3$. We assume that the system is stable and is not losing energy through radiation, which is why we are treating the electro-static problem,

$$\hat{H} \equiv \hat{H}_{el} + \hat{H}_{ion} + \hat{V}_{el\text{-}ion} \; , \tag{4.1}$$

$$\hat{H}_{el} = \hat{T}_{el} + \hat{V}_{el\text{-}el} \; , \tag{4.2}$$

$$\hat{T}_{el} = \sum_{i=1}^{N_{el}} \frac{\left| \hat{\vec{p}}_i \right|^2}{2m} \; , \tag{4.3}$$

$$\hat{V}_{el\text{-}el} = \sum_{i<j} V_{el\text{-}el} \left( \hat{\vec{r}}_i - \hat{\vec{r}}_j \right) \; , \tag{4.4}$$

$$\hat{H}_{ion} = \hat{T}_{ion} + \hat{V}_{ion\text{-}ion} \; , \tag{4.5}$$

$$\hat{T}_{ion} = \sum_{i=1}^{N_{ion}} \frac{\left| \hat{\vec{P}}_i \right|^2}{2M} \; , \tag{4.6}$$

$$\hat{V}_{ion\text{-}ion} = \sum_{i<j} V_{ion\text{-}ion} \left( \hat{\vec{R}}_i - \hat{\vec{R}}_j \right) \; , \tag{4.7}$$

$$\hat{V}_{el\text{-}ion} = \sum_{i=1}^{N_{el}} \sum_{j=1}^{N_{ion}} V_{el\text{-}ion} \left( \hat{\vec{r}}_i - \hat{\vec{R}}_j \right) \; . \tag{4.8}$$

The reader should be aware that the system still allows for a dynamical evolution of the configuration of electrons and ions. However, at each point in time the system is not subject to any incoming or outgoing radiation. In $d = 3$ dimensions, the potentials are the usual Coulomb potential

$$V_{\text{el-el}}\left(\hat{\vec{r}}_i - \hat{\vec{r}}_j\right) = \frac{e_0^2}{\left|\hat{\vec{r}}_i - \hat{\vec{r}}_j\right|} \ , \tag{4.9}$$

$$V_{\text{ion-ion}}\left(\hat{\vec{R}}_i - \hat{\vec{R}}_j\right) = \frac{Z^2 e_0^2}{\left|\hat{\vec{R}}_i - \hat{\vec{R}}_j\right|} \ , \tag{4.10}$$

$$V_{\text{el-ion}}\left(\hat{\vec{r}}_i - \hat{\vec{R}}_j\right) = -\frac{Z e_0^2}{\left|\hat{\vec{r}}_i - \hat{\vec{R}}_j\right|} \ . \tag{4.11}$$

In dimensions $d = 1$ or $2$ the potentials are adapted to reflect the effective potentials which act on the electrons and are usually not Coulomb potentials anymore. People often employ projections of the three-dimensional Coulomb potential by setting the irrelevant coordinates to zero, i.e. the symmetry with respect to $i \leftrightarrow j$ are conserved. And furthermore, any potential which only depends on the relative distance between ions and electrons does conserve the total momentum of the system, i.e. for all $k \in \{1, \ldots, d\}$ it holds

$$\left[\sum_{i=1}^{N_{\text{el}}} \hat{p}_{i,k} + \sum_{j=1}^{N_{\text{ion}}} \hat{P}_{j,k}, \hat{H}\right] = 0 \ . \tag{4.12}$$

This can be checked using the property of the commutator of an operator function $f(\hat{\vec{r}}_1, \ldots, \hat{\vec{r}}_d)$ with the momentum operator, which reads

$$\left[\hat{f}, \hat{p}_{i,k}\right] = \imath\hbar \left.\frac{\partial f}{\partial r_{i,k}}\right|_{\hat{\vec{r}}_1, \ldots, \hat{\vec{r}}_d} \ , \tag{4.13}$$

which can be derived using the multi-dimensional Taylor expansion of the operator $\hat{f}$ with respect to the position operators.

We are concerned with the evolution of the quantum state $|\Psi(t)\rangle \in \mathcal{H}_{\text{el}} \bigotimes \mathcal{H}_{\text{ion}}$ whose dynamics can be described by the Schrödinger equation

$$\imath\hbar\partial_t|\psi(t)\rangle = \left(\hat{T}_{\text{el}} + \hat{V}_{\text{el-el}} + \hat{T}_{\text{ion}} + \hat{V}_{\text{ion-ion}} + \hat{V}_{\text{el-ion}}\right)|\psi(t)\rangle \ . \tag{4.14}$$

$\mathcal{H}_{\text{el}}$ is the Hilbert space of $N_{\text{el}}$ electrons with the complete fully antisymmetric basis $\{|\phi\rangle\}$ and $\mathcal{H}_{\text{ion}}$ the Hilbert space of $N_{\text{ion}}$ ions with the fully (anti-)symmetric basis $\{|\theta\rangle\}$. Whether the Hilbert space of ions requires a fully antisymmetric or symmetric basis depends, according to the spin-statistics theorem [124], on whether the spin is an integer or not. A quantum state of the system can be expressed as

$$|\Psi(t)\rangle = \sum_{|\Phi\rangle, |\Theta\rangle} C_{|\Phi\rangle, |\Theta\rangle}(t)|\Phi\rangle \bigotimes |\Theta\rangle \ . \tag{4.15}$$

If the ions and electrons do not interact with each other, the quantum state could be written as

$$|\Psi(t)\rangle = |\psi_{\text{el}}\rangle \bigotimes |\psi_{\text{ion}}\rangle \ . \tag{4.16}$$

Interactions between the two types of particles lead to a superposition of these product states. If one uses a single particle basis $|\phi\rangle$ we can write an electronic basis state $|\Phi\rangle$ as

$$\langle\vec{r}_{\text{el}}| \equiv \langle\vec{r}_1, \vec{r}_2, \ldots, \vec{r}_{N_{\text{el}}}| \ , \tag{4.17}$$

$$\langle\vec{r}_{\text{el}}|\Phi\rangle = \frac{1}{\sqrt{N_{\text{el}}!}} \sum_{\pi \in \mathcal{S}_{N_{\text{el}}}} \text{sign}(\pi) \left[\sum_{\phi_1, \ldots, \phi_{N_{\text{el}}}} A_{\phi_1, \ldots, \phi_{N_{\text{el}}}} \prod_{i=1}^{N_{\text{el}}} \langle\vec{r}_{\pi(i)}|\phi_i\rangle\right] \ . \tag{4.18}$$

A symmetric version would be given by ignoring the sign of the permutation. The reader may have noticed already that the spin does not have any direct influence on the dynamics of the system since it is not entering the Hamilton operator but only has an influence on the statistics. Since we are concerned with the modeling of the Hamilton operator through another system of the same type of particles we shall not consider the spin quantum number in the subsequent discussion as it is irrelevant for our actual problem. (Anti-)Symmetrization with respect to additional quantum numbers should always be possible afterwards. To tackle the problem, we restrict the probability distribution of ions to localized point particles at positions $\vec{R}_i^{(\mathrm{loc})}$, i.e. demanding

$$|\langle \vec{R}_{\mathrm{ion}}|\psi_{\mathrm{ion}}\rangle|^2 = \sum_{i=1}^{N_{\mathrm{ion}}} \delta(\vec{R}_i - \vec{R}_i^{(\mathrm{loc})}) \ . \tag{4.19}$$

This is a big reduction of the ionic Hilbert space $\mathcal{H}_{\mathrm{ion}}$, and not always justified, especially for rather extended ionic wave functions. There are other approaches such as introducing a homogeneous positive charge background and seeing phonons as elementary excitations in this "vacuum" in the same way as photons fill the vacuum in a black body chamber. Nevertheless, one usually introduces some sort of restriction on the ionic wave function depending on the physical system one tries to describe. We call the resulting Hilbert space $\mathcal{H}_{\mathrm{ph}}$, where ph stands for phonons.

## 4.2 Phonons

If we write the $i$-th ions position as $\vec{R}_i = \vec{R}_i^{(0)} + \vec{u}_i$, where $\vec{u}_i$ is a displacement around the ions equilibrium positions $\vec{R}_i^{(0)}$, we shall make a simple basis change from $\hat{\mathrm{R}}_{i,j}$ to $R_{i,j}^{(0)} + \hat{\mathrm{u}}_{i,j}$. Assuming small displacements, we make a Taylor expansion of the ionic potential in the coordinate space representation

$$V_{\mathrm{ion\text{-}ion}}(\vec{R}_i - \vec{R}_j) \approx V_{\mathrm{ion\text{-}ion}}(\vec{R}_i^{(0)} - \vec{R}_j^{(0)})$$
$$+ \sum_{l,m=1}^{d} \frac{1}{2} \left.\frac{\mathrm{d}^2 V_{\mathrm{ion\text{-}ion}}}{\mathrm{d}R_l \mathrm{d}R_m}\right|_{\vec{R}_i^{(0)} - \vec{R}_j^{(0)}} (\vec{u}_i - \vec{u}_j)_l \, (\vec{u}_i - \vec{u}_j)_m \ , \tag{4.20}$$

$$V_{\mathrm{ion\text{-}ion}} = C + \frac{1}{2} \sum_{i,j=1}^{N_{\mathrm{ion}}} \sum_{l,m=1}^{d} D_{lm}(\vec{R}_i^{(0)} - \vec{R}_j^{(0)}) u_{i,l} u_{j,m} \ , \tag{4.21}$$

$$C \equiv \sum_{i<j} V_{\mathrm{ion\text{-}ion}}(\vec{R}_i^{(0)} - \vec{R}_j^{(0)}) \ , \tag{4.22}$$

$$D_{lm}(\vec{R}_i^{(0)} - \vec{R}_j^{(0)}) \equiv - \left.\frac{\mathrm{d}^2 V_{\mathrm{ion\text{-}ion}}}{\mathrm{d}R_l \mathrm{d}R_m}\right|_{\vec{R}_i^{(0)} - \vec{R}_j^{(0)}} + \delta_{ij} \sum_{k=1}^{N_{\mathrm{ion}}} \left.\frac{\mathrm{d}^2 V_{\mathrm{ion\text{-}ion}}}{\mathrm{d}R_l \mathrm{d}R_m}\right|_{\vec{R}_i^{(0)} - \vec{R}_k^{(0)}} \ , \tag{4.23}$$

where $C$ is just a constant, i.e. irrelevant for the dynamics, and $D_{lm}$ a positive-definite matrix, since $\vec{R}_i^{(0)}$ is the equilibrium solution. The reader should note that this approximation of the potential does not violate the conservation of the total ion momentum, i.e.

$$\left[\sum_{i=1}^{N_{\mathrm{ion}}} \hat{\mathrm{P}}_{i,k}, \hat{\mathrm{V}}_{\mathrm{ion\text{-}ion}}\right] = -\frac{\imath\hbar}{2} \sum_{i,j=1}^{N_{\mathrm{ion}}} \left[D_{kl}(\vec{R}_i^{(0)} - \vec{R}_j^{(0)}) + D_{lk}(\vec{R}_j^{(0)} - \vec{R}_i^{(0)})\right] \hat{\mathrm{u}}_{j,l} = 0 \ . \tag{4.24}$$

This can be seen by using Eq. (4.23). If the crystal has $N_u \equiv \prod_{i=1}^{d} N_i$ unit cells as well as $n_a$ ions per unit cell, i.e. $N_{\mathrm{ion}} = n_a N_u$, it is more instructive to write the potential as

$$V_{\mathrm{ion\text{-}ion}} = \frac{1}{2} \sum_{i_1,j_1=1}^{N_1} \cdots \sum_{i_d,j_d=1}^{N_d} \sum_{k,k'=1}^{n_a} D_{lm}(\vec{R}_{\vec{i}_k}^{(0)} - \vec{R}_{\vec{j}_{k'}}^{(0)}) u_{\vec{i}_k,l} u_{\vec{j}_{k'},m} \tag{4.25}$$

$$\equiv \frac{1}{2} \sum_{\vec{i},\vec{j}} \sum_{k,k'=1}^{n_a} D_{lm}(\vec{R}_{\vec{i}_k}^{(0)} - \vec{R}_{\vec{j}_{k'}}^{(0)}) u_{\vec{i}_k,l} u_{\vec{j}_{k'},m} \ . \tag{4.26}$$

To arrive at an harmonic oscillator Hamilton operator with eigenfrequency $\omega_{\vec{q},s}$, one needs to impose periodic boundary conditions (Born-von-Karman) at the ends of the crystal and make the transformation to the operators

$$\hat{\mathrm{u}}_{j,k} = \frac{1}{\sqrt{N_{\mathrm{ion}}}} \sum_{\vec{q},s} \hat{\mathrm{Q}}_{\vec{q},s} e^{\imath \vec{q} \cdot \vec{R}_j^{(0)}} \left(e_{\vec{q},s}\right)_k \ , \tag{4.27}$$

$$\hat{\mathrm{p}}_{j,k} = \frac{1}{\sqrt{N_{\mathrm{ion}}}} \sum_{\vec{q},s} \hat{\mathrm{P}}_{\vec{q},s} e^{-\imath \vec{q} \cdot \vec{R}_j^{(0)}} \left(e_{\vec{q},s}\right)_k \ . \tag{4.28}$$

The inverse transformations are given by

$$\hat{\mathrm{Q}}_{\vec{q},s} = \frac{1}{\sqrt{N_{\mathrm{ion}}}} \sum_{j=1}^{N_{\mathrm{ion}}} \sum_{k=1}^{d} e^{-\imath \vec{R}_j^{(0)} \cdot \vec{q}} \hat{\mathrm{u}}_{j,k} \left(e_{\vec{q},s}\right)_k \ , \tag{4.29}$$

$$\hat{\mathrm{P}}_{\vec{q},s} = \frac{1}{\sqrt{N_{\mathrm{ion}}}} \sum_{j=1}^{N_{\mathrm{ion}}} \sum_{k=1}^{d} e^{\imath \vec{R}_j^{(0)} \cdot \vec{q}} \hat{\mathrm{p}}_{j,k} \left(e_{\vec{q},s}\right)_k \ . \tag{4.30}$$

First of all, the allowed wave vectors $\vec{q}$ are constrained by the overall periodic boundary conditions. Second, wave vectors which differ by a reciprocal lattice vector $\vec{K}_i$ pointing to the $i$th Brillouin zone (BZ) lead to the same displacement and momentum operators, since $\vec{K}_i \cdot \vec{R}_j = 2\pi\delta_{ij}$. Therefore, we regard phonons with wave vectors in another BZ as equivalent to their respective counterpart in the first BZ. For an introduction to the concept of the reciprocal lattice as well as BZ we refer the reader to Ref. [98]. The wave vectors in the first BZ of the reciprocal lattice read in the case of a mono-atomic chain ($d = 1$) with lattice constant $a$

$$q = 2\pi k/(N_{\mathrm{ion}}a) \ , \tag{4.31}$$

with $k \in \{0, \pm 1, \pm 2, \ldots, \pm\frac{1}{2}N_{\mathrm{ion}}-1, \frac{N_{\mathrm{ion}}}{2}\}$. The polarization counts the different phonon branches for a given wave vector, which arise due to the dimensionality of the crystal (longitudinal and transversal modes) and due to the internal structure of the unit cell (optical branches). If there are two atoms per unit cell in a three dimensional crystal one expects six different phonon branches, one set of acoustical modes and another set of optical modes, which can each time be grouped into one longitudinal and two transversal branches. In general, a $d$-dimensional crystal with $N_u$ unit cells and $n_a$ ions per unit cell has in total $N_{\mathrm{ac}} = dN_u - d_f^{(\mathrm{trans})} - d_f^{(\mathrm{rot})}$ acoustical phonon modes and $N_{\mathrm{op}} = dN_u(n_a - 1)$ optical modes. $d_f^{(\mathrm{trans})} = d$ and $d_f^{(\mathrm{rot})}$ are the number of degrees of freedom for a global translation and rotation of the crystal. The degrees of freedom for rotations are zero in one dimension, 1 in two dimensions and 3 in three dimensions. In addition, since $\hat{\mathrm{u}}_{j,k}$ and $\hat{\mathrm{p}}_{j,k}$ are hermitian, we impose

$$\hat{\mathrm{Q}}_{\vec{q},s}^{\dagger} = \hat{\mathrm{Q}}_{-\vec{q},s} \ , \tag{4.32}$$

$$\hat{\mathrm{P}}_{\vec{q},s}^{\dagger} = \hat{\mathrm{P}}_{-\vec{q},s} \ . \tag{4.33}$$

Throughout the following calculations, it will become clear why that is sufficient. If we introduce these operators into the ionic potential we shall find

$$\frac{1}{2} \sum_{\vec{q},\vec{q}',s,s'} \hat{Q}_{\vec{q},s} \hat{Q}_{\vec{q}',s'} \frac{1}{N_{\text{ion}}} \sum_{\vec{i},\vec{j}} \sum_{k,k'=1}^{n_a} \vec{e}_{\vec{q},s}^{T} D(\vec{R}_{\vec{i}_k}^{(0)} - \vec{R}_{\vec{j}_{k'}}^{(0)}) \vec{e}_{\vec{q}',s'} e^{\imath \left( \vec{q} \cdot \vec{R}_{\vec{i}_k}^{(0)} + \vec{q}' \cdot \vec{R}_{\vec{j}_k}^{(0)} \right)} \tag{4.34}$$

$$= \frac{1}{2} \sum_{\vec{q},\vec{q}',s,s'} \hat{Q}_{\vec{q},s} \hat{Q}_{\vec{q}',s'} \frac{1}{n_a} \sum_{k,k'} \frac{1}{N_u} \sum_{\vec{i}} e^{\imath \vec{R}_{\vec{i}_k}^{(0)} \cdot (\vec{q} - \vec{q}')}$$

$$\times \sum_{\vec{j}} \vec{e}_{\vec{q},s}^{T} D(\vec{R}_{\vec{i}_k}^{(0)} - \vec{R}_{\vec{j}_{k'}}^{(0)}) \vec{e}_{\vec{q}',s'} e^{-\imath \vec{q}' \cdot (\vec{R}_{\vec{i}_k}^{(0)} - \vec{R}_{\vec{j}_{k'}}^{(0)})} \tag{4.35}$$

$$= \frac{1}{2} \sum_{\vec{q},\vec{q}',s,s'} \hat{Q}_{\vec{q},s} \hat{Q}_{\vec{q}',s'} \delta_{\vec{q},-\vec{q}'} \frac{1}{n_a} \sum_{k,k'} \vec{e}_{\vec{q},s}^{T} \tilde{D}(-\vec{q}',k,k') \vec{e}_{\vec{q}',s'} \tag{4.36}$$

$$= \frac{1}{2} \sum_{\vec{q},s,s'} \hat{Q}_{\vec{q},s} \hat{Q}_{-\vec{q},s'} \frac{1}{n_a} \sum_{k,k'} \vec{e}_{\vec{q},s}^{T} \tilde{D}(\vec{q},k,k') \vec{e}_{-\vec{q},s'} \;, \tag{4.37}$$

where we have used that the last term in the second equation does not depend on the cell index $\vec{i}$. The term $\delta_{\vec{q},-\vec{q}}$ arises through the sum over the lattice vectors which connect one lattice cell with the other. Usually, one would demand that $\vec{q} - \vec{q} = \vec{K}$, where $\vec{K}$ is an arbitrary reciprocal lattice vector. However, since the quantum state of a phonon whose wave vector is shifted by a reciprocal lattice vector is equivalent and $\vec{q}, \vec{q}'$ are vectors from the first BZ, the sum just reduces to $\delta_{\vec{q},-\vec{q}}$. The polarization vectors $\vec{e}_{\vec{q},s}$ are chosen to diagonalize the set of $n_a$ matrices $\tilde{D}(\vec{q},k,k)$. Such a set of eigenvectors can always be found for a real symmetric matrix and constitutes are complete orthonormal basis set. The eigenvalues can be labeled $M\omega_{\vec{q},s}^2$, since the matrix is positive-definite and hence possess only positive eigenvalues. Since the matrix $\tilde{D}(\vec{q},k,k')$ is symmetric with respect to the operation $\vec{q} \to -\vec{q}$ due to the symmetry in the Coulomb potential and the boundary conditions, the eigenvectors and eigenvalues are also symmetric. Although some textbooks suggest that a restriction to nearest-neighbor interaction between the ions is necessary that is not correct. The existence of phonons with a well-defined energy-momentum relation is not limited to this case, as we have seen above. However, it may in practice become very hard to evaluate the matrix entries $\tilde{D}(\vec{q},k,k)$ and hence find the eigenvectors and -values for long-range interactions between the ions. Nevertheless, the final result hence reads

$$V_{\text{ion-ion}} = \frac{M}{2} \sum_{\vec{q},s} \omega_{\vec{q},s}^2 \hat{Q}_{\vec{q},s} \hat{Q}_{-\vec{q},s} \;. \tag{4.38}$$

The calculation for the kinetic energy of the ions is more straightforward and leads to

$$\hat{T}_{\text{ion}} = \frac{1}{2M} \sum_{\vec{q},s} \hat{P}_{\vec{q},s} \hat{P}_{-\vec{q},s} \;. \tag{4.39}$$

Making a basis transformation to the operators

$$\hat{b}_{\vec{q},s}^{\dagger} \equiv \frac{1}{\sqrt{2\hbar}} \left[ \sqrt{M\omega_{\vec{q},s}} \hat{Q}_{-\vec{q},s} - \imath \frac{\hat{P}_{\vec{q},s}}{\sqrt{M\omega_{\vec{q},s}}} \right] \;, \tag{4.40}$$

$$\hat{b}_{\vec{q},s} \equiv \frac{1}{\sqrt{2\hbar}} \left[ \sqrt{M\omega_{\vec{q},s}} \hat{Q}_{\vec{q},s} + \imath \frac{\hat{P}_{-\vec{q},s}}{\sqrt{M\omega_{\vec{q},s}}} \right] \;, \tag{4.41}$$

one realizes that they are ladder operators, i.e. fulfill the commutation relations

$$\left[ \hat{b}_{\vec{q},s}, \hat{b}_{\vec{q}',s'}^{\dagger} \right] = \delta_{\vec{q},\vec{q}'} \delta_{s,s'} \;, \tag{4.42}$$

$$\left[ \hat{b}_{\vec{q},s}, \hat{b}_{\vec{q}',s'} \right] = 0 \;, \tag{4.43}$$

$$\left[ \hat{b}_{\vec{q},s}^{\dagger}, \hat{b}_{\vec{q}',s'}^{\dagger} \right] = 0 \;. \tag{4.44}$$

One can show these relations by explicit calculations using the definitions from Eqs. (4.29) and (4.30), as well as $[\hat{u}_{j,k}, \hat{p}_{l,m}] = \imath\hbar\delta_{j,l}\delta_{k,m}$. The inverse transformations are

$$\hat{Q}_{\vec{q},s} = \sqrt{\frac{\hbar}{2M\omega_{\vec{q},s}}}(\hat{b}^{\dagger}_{-\vec{q},s} + \hat{b}_{\vec{q},s}) \ , \tag{4.45}$$

$$\hat{P}_{\vec{q},s} = \imath\sqrt{\frac{\hbar M\omega_{\vec{q},s}}{2}}(\hat{b}^{\dagger}_{\vec{q},s} - \hat{b}_{-\vec{q},s}) \ , \tag{4.46}$$

such that the actual hermitian displacement operator is given by

$$\hat{u}_{j,k} = \sqrt{\frac{\hbar}{2MN_{\text{ion}}}} \sum_{\vec{q},s} \frac{e^{\imath\vec{q}\cdot\vec{R}^{(0)}_j}(e_{\vec{q},s})_k}{\sqrt{\omega_{\vec{q},s}}} \left(\hat{b}^{\dagger}_{-\vec{q},s} + \hat{b}_{\vec{q},s}\right) \ . \tag{4.47}$$

Looking at the hermitian operator

$$\hbar\omega_{\vec{q},s}(\hat{b}^{\dagger}_{\vec{q},s}\hat{b}_{\vec{q},s} + 1/2) = \hbar\omega_{\vec{q},s}/2(2\hat{b}^{\dagger}_{\vec{q},s}\hat{b}_{\vec{q},s} + 1) \tag{4.48}$$

$$= \hbar\omega_{\vec{q},s}/2(\hat{b}^{\dagger}_{\vec{q},s}\hat{b}_{\vec{q},s} + \hat{b}_{\vec{q},s}\hat{b}^{\dagger}_{\vec{q},s} + 1 - \left[\hat{b}_{\vec{q},s}, \hat{b}^{\dagger}_{\vec{q},s}\right]) \tag{4.49}$$

$$= \hbar\omega_{\vec{q},s}/2(\hat{b}^{\dagger}_{\vec{q},s}\hat{b}_{\vec{q},s} + \hat{b}^{\dagger}_{-\vec{q},s}\hat{b}_{-\vec{q},s}) \tag{4.50}$$

we see that the original Hamilton operator is recovered, and consequently

$$\hat{H}_{\text{ph}} \equiv \sum_{\vec{q},s} \hbar\omega_{\vec{q},s}(\hat{b}^{\dagger}_{\vec{q},s}\hat{b}_{\vec{q},s} + 1/2) \ . \tag{4.51}$$

This means that we are dealing with independent harmonic oscillators of different eigenfrequencies. If we regard the operators $\hat{b}^{\dagger}_{\vec{q},s}$ and $\hat{b}_{\vec{q},s}$ as bosonic creation and annihilation operators for a phonon from the second quantization formalism perspective, one will say that we create or add a phonon with wave vector $\vec{q}$, polarization $s$ and energy $\hbar\omega_{\vec{q},s}$ to the system of $n$ phonons of wave vector $\vec{q}$ and polarization $s$ by exciting the harmonic oscillator with eigenfrequency $\omega_{\vec{q},s}$ from the $n$-th to the $(n+1)$-th eigenstate. A useful basis for the space is the occupation number basis, where one just specifies the number of phonons in a given mode

$$|n_1, \ldots, n_{N_{\text{modes}}}\rangle = |n_1, \vec{q}_1, s_1\rangle|n_2, \vec{q}_2, s_2\rangle \ldots |n_{N_{\text{modes}}}, \vec{q}_{N_{\text{modes}}}, s_{N_{\text{modes}}}\rangle \tag{4.52}$$

$$= \prod_{i=1}^{N_{\text{modes}}} \frac{\left(\hat{b}^{\dagger}_{\vec{q}_i,s_i}\right)^{n_i}}{\sqrt{n_i!}}|0\rangle \ , \tag{4.53}$$

and $|0\rangle$ is the vacuum phonon state and $N_{\text{ph}} = N_{\text{ac}} + N_{\text{op}} = N_{\text{ion}} - d_f^{(\text{trans})} - d_f^{(\text{rot})}$ is the total number of phonon modes in the first BZ, which means the ones leading to different ionic displacements. The term $1/2$ in the phononic Hamilton operator is irrelevant for the dynamics and can be dropped for the following calculations. From a physical point of view, it means that there are always fluctuations in the system and that the ions are never perfectly localized on their positions.

Which kind of displacements do these state produce and how does the wave function look like in the displacement basis $|\vec{u}_1, \ldots, \vec{u}_{N_{\text{ion}}}\rangle$? As we have mentioned before, the crystal basically gets filled with $N_{\text{ph}}$ independent harmonic oscillators of different frequency and excitation. The vacuum state, which is defined by $\hat{b}_{\vec{q},s}|0\rangle = 0$ for all $\vec{q}, s$, is the product of all these ground states, i.e.

$$0 = \langle\vec{u}_1, \ldots, \vec{u}_{N_{\text{ion}}}|\hat{b}_{\vec{q},s}|0\rangle \tag{4.54}$$

$$= \sqrt{\frac{M\omega_{\vec{q},s}}{2\hbar}}\frac{1}{\sqrt{N_{\text{ion}}}}\sum_{j=1}^{N_{\text{ion}}}e^{-\imath\vec{q}\cdot\vec{R}^{(0)}_j}\sum_{k=1}^{d}(e_{\vec{q},s})_k\left(u_{j,k} + \frac{\hbar}{M\omega_{\vec{q},s}}\frac{\partial}{\partial u_{j,k}}\right)\psi_0(\vec{u}_1, \ldots, \vec{u}_{N_{\text{ion}}}) \ , \tag{4.55}$$

from which we conclude

$$\langle \vec{u}_1, \ldots, \vec{u}_{N_{\text{ion}}} | 0 \rangle = \prod_{i=1}^{N_{\text{ph}}} \psi_{0, \vec{q}_i, s_i}(\vec{u}_1, \ldots, \vec{u}_{N_{\text{ion}}}) , \tag{4.56}$$

$$\psi_{0, \vec{q}, s}(\vec{u}_1, \ldots, \vec{u}_{N_{\text{ion}}}) = \prod_{j=1}^{dN_{\text{ion}}} \phi_{0, \vec{q}, s}(u_j) , \tag{4.57}$$

$$\phi_{0, \vec{q}, s}(u) \equiv \left( \frac{M \omega_{\vec{q}, s}}{\pi \hbar} \right)^{1/4} e^{-\frac{M \omega_{\vec{q}, s}}{2\hbar} u^2} , \tag{4.58}$$

such that for instance a state with one phonon is given by

$$\langle \vec{u}_1, \ldots, \vec{u}_{N_{\text{ion}}} | 0_1, \ldots, 0_{i-1}, 1_i, 0_{i+1}, \ldots, 0_{N_{\text{ph}}} \rangle = \langle \vec{u}_1, \ldots, \vec{u}_{N_{\text{ion}}} | \hat{\mathrm{b}}^{\dagger}_{\vec{q}_i, s_i} | 0 \rangle , \tag{4.59}$$

$$= \sqrt{\frac{M \omega_{\vec{q}_i, s_i}}{2\hbar N_{\text{ion}}}} \left[ \sum_{j=1}^{N_{\text{ion}}} e^{-\imath \vec{q}_i \cdot \vec{R}_j^{(0)}} \sum_{k=1}^{d} (e_{\vec{q}_i, s_i})_k \left( u_{j,k} - \frac{\hbar}{M \omega_{\vec{q}_i, s_i}} \frac{\partial}{\partial u_{j,k}} \right) \right] \langle \vec{u}_1, \ldots, \vec{u}_{N_{\text{ion}}} | 0 \rangle , \tag{4.60}$$

$$= \psi_{1, \vec{q}_i, s_i}(\vec{u}_1, \ldots, \vec{u}_{N_{\text{ion}}}) \prod_{j \neq i} \psi_{0, \vec{q}_j, s_j}(\vec{u}_1, \ldots, \vec{u}_{N_{\text{ion}}}) , \tag{4.61}$$

$$\psi_{1, \vec{q}, s}(\vec{u}_1, \ldots, \vec{u}_{N_{\text{ion}}}) = \frac{1}{\sqrt{N_{\text{ion}}}} \sum_{j=1}^{N_{\text{ion}}} \left[ e^{\imath \vec{q} \cdot \vec{R}_j^{(0)}} \sum_{k=1}^{d} (e_{\vec{q}, s})_k \, \phi_{1, \vec{q}, s}(u_{j,k}) \right.$$

$$\left. \prod_{(j', k') \neq (j,k)} \phi_{0, \vec{q}, s}(u_{j', k'}) \right] , \tag{4.62}$$

$$\phi_{1, \vec{q}, s}(u) = \frac{1}{\sqrt{2}} \left( \frac{M \omega_{\vec{q}, s}}{\pi \hbar} \right)^{1/4} e^{-\frac{M \omega_{\vec{q}, s}}{2\hbar} u^2} H_1 \left( \sqrt{\frac{M \omega_{\vec{q}, s}}{\hbar}} u \right) , \tag{4.63}$$

where $H_1$ is the known hermite polynomial from chapter 2. The generalization to a state $|n_1, n_2, \ldots, n_{N_{\text{ph}}}\rangle$ is straightforward.

It is worth to mention that if one includes a third-order term in the Taylor expansion of Eq. (4.20) one obtains interacting phonons and the problem becomes much more involved. Since we are dealing with the possible representation of the electron-phonon interaction through curvature, we shall not consider the problem of interacting phonons here. It should be stressed, however, that in principle it would be possible to include this effect in the resulting dynamics in curved space in the same way as the total energy of the phononic state could be added.

## 4.3 Bloch state

This section is crucial for understanding the central issue of this chapter, since it concerns everything that we are trying to replace through the dynamics of electrons in a curved space. This is the reason, we shall try to give more complete and lengthy explanations here. In the presentation of the subject we mainly follow the ideas from Ref. [98].

The restriction of the ionic Hilbert space to $\mathcal{H}_{\text{ph}}$ also influences the electron-ion interaction. Assuming small displacements in the coordinate space representation, the interaction is written as a Taylor series around $\vec{u}_i \approx 0$ up to first order

$$\sum_{j=1}^{N_{\text{ion}}} V_{\text{el-ion}}(\vec{r} - \vec{R}_j) \approx V_{\text{lat}}(\vec{r}) + V_{\text{el-ph}}(\vec{r}) , \tag{4.64}$$

$$V_{\text{lat}}(\vec{r}) \equiv \sum_{j=1}^{N_{\text{ion}}} V_{\text{el-ion}}(\vec{r} - \vec{R}_j^{(0)}) , \tag{4.65}$$

$$V_{\text{el-ph}}(\vec{r}) \equiv - \sum_{j=1}^{N_{\text{ion}}} \vec{u}_j \cdot \vec{\nabla} V_{\text{el-ion}}(\vec{r} - \vec{R}_j^{(0)}) . \tag{4.66}$$

One imposes the same periodic boundary conditions (Born-von-Karman) as for the ions on the electrons. Therefore, each electron is subject to the same static crystal lattice potential $V_{\text{latt}}$ as well as the same electron-phonon potential $V_{\text{el-ph}}$. This means that every single electron feels the same potential landscape. Furthermore, the lattice potential is invariant with respect to translations of the electron's coordinate by an arbitrary lattice vector, $\vec{r} \to \vec{r} + \vec{R}_i^{(0)}$, whereas the potential $V_{\text{el-ph}}$ is *not invariant* with respect to such a transformation since the displacement vector $\vec{u}_j$ will in general be different at every lattice site $j$. Furthermore, the reader should know that this approximated potential does not conserve the total momentum anymore, which we shall demonstrate in the following. Looking at the commutator, it is obvious from the calculations in section 4.1 that we only need to check the commutator between the total momentum of the electrons and the first-order correction in the electron-ion potential, since the rest necessarily sums to zero. One finds

$$-\sum_{i,j=1}^{N_{\text{el}}} \sum_{l=1}^{N_{\text{ion}}} \sum_{m=1}^{d} \hat{\text{u}}_{l,m} \left[ \hat{\text{p}}_{i,k}, \left. \frac{\partial V_{\text{el-ion}}}{\partial r_{j,m}} \right|_{\hat{\vec{r}}_j - \vec{R}_l^{(0)}} \right] = \imath\hbar \sum_{i=1}^{N_{\text{el}}} \sum_{j=1}^{N_{\text{ion}}} \sum_{l=1}^{d} \hat{\text{u}}_{j,l} \left. \frac{\partial^2 V_{\text{el-ion}}}{\partial r_{i,k} \partial r_{i,l}} \right|_{\hat{\vec{r}}_i - \vec{R}_j^{(0)}} \tag{4.67}$$

$$= -\imath\hbar Z e_0^2 \sum_{i=1}^{N_{\text{el}}} \sum_{j=1}^{N_{\text{ion}}} \frac{\sum_{l=1}^{d} 3\hat{\text{u}}_{j,l} \left( \hat{\text{r}}_{i,l} - R_{j,l}^{(0)} \right) \left( \hat{\text{r}}_{i,k} - R_{j,k}^{(0)} \right) - |\hat{\vec{r}}_i - \vec{R}_j^{(0)}|^2 \hat{\text{u}}_{j,k}}{|\hat{\vec{r}}_i - \vec{R}_j^{(0)}|^5} \neq 0 , \tag{4.68}$$

which is not always equal to zero, such that the total momentum is in general not conserved in this approach. It should be mentioned that higher order terms in the expansion above will lead to more sophisticated interactions between one electron and the phonons than just absorption or emission of one phonon, such as scattering (absorption plus emission), emission or absorption of two phonons for the second order correction. The dynamics of all electrons is hence described by the Hamilton operator

$$\hat{\text{H}} = \sum_{i=1}^{N_{\text{el}}} \hat{\text{H}}_i^{(\text{el})} + \hat{\text{V}}_{\text{el-el}} , \tag{4.69}$$

$$\hat{\text{H}}_i^{(\text{el})} \equiv \sum_{j=1}^{d} \frac{\hat{\text{p}}_{i,j}^2}{2m} + V_{\text{latt}}(\hat{\text{r}}_{i,1}, \ldots, \hat{\text{r}}_{i,d}) + V_{\text{el-ph}}(\hat{\text{r}}_{i,1}, \ldots, \hat{\text{r}}_{i,d}) . \tag{4.70}$$

Ignoring the interaction between electrons for a moment, we shall analyze the second Hamilton operator. Since the electron obeys the periodic boundary conditions

$$\psi(x_1, \ldots, x_{d-1}, 0) = \psi(x_1, \ldots, x_{d-1}, L_d) , \tag{4.71}$$

$$(\partial_d \psi)(x_1, \ldots, x_{d-1}, 0) = (\partial_d \psi)(x_1, \ldots, x_{d-1}, L_d) , \tag{4.72}$$

$$\psi(x_1, \ldots, x_{d-2}, 0, x_d) = \psi(x_1, \ldots, x_{d-2}, L_{d-1}, x_d) , \tag{4.73}$$

$$(\partial_{d-1} \psi)(x_1, \ldots, x_{d-2}, 0, x_d) = (\partial_{d-1} \psi)(x_1, \ldots, x_{d-2}, L_{d-1}, x_d) , \tag{4.74}$$

$$\vdots$$

$$\psi(0, x_2, \ldots, x_d) = \psi(L_1, x_2, \ldots, x_d) , \tag{4.75}$$

$$(\partial_1 \psi)(0, x_2, \ldots, x_d) = (\partial_1 \psi)(L_1, x_2, \ldots, x_d) , \tag{4.76}$$

for a crystal of length $L_i$ in direction $\vec{e}_i$, the eigenstates of the free Hamiltonian $\hat{\text{T}}_{\text{kin}} \equiv \sum_{i=1}^{d} \frac{\hat{\text{p}}_i^2}{2m}$, which we call kinetic energy since no potentials are present, are given by

$$\sum_{i=1}^{d} \frac{\hat{\text{p}}_i^2}{2m} |\psi_{\vec{n}}\rangle = \frac{\hbar |\vec{k}_{\vec{n}}|^2}{2m} |\psi_{\vec{n}}\rangle , \tag{4.77}$$

and can be labeled by the discrete quantum number(s) $n_1, \ldots, n_d \in \mathbb{Z}$ through

$$\vec{k}_{\vec{n}} = 2\pi \left( \frac{n_1}{L_1}, \ldots, \frac{n_d}{L_d} \right) \tag{4.78}$$

where $\hbar\vec{k}$ is the momentum of this state. The quantization condition comes directly from the

periodic boundary conditions. The eigenvalues are necessarily positive since the operator is positive-definite. Their coordinate representation is given by

$$\langle \vec{x} | \psi_{\vec{n}} \rangle = \psi_{\vec{n}}(\vec{x}) = \frac{1}{\sqrt{\text{vol}(V)}} e^{i \vec{k}_{\vec{n}} \cdot \vec{x}} \; , \qquad (4.79)$$

and with the crystal volume $\text{vol}(V) \equiv \prod_{i=1}^{d} L_i$ they build a complete orthonormal basis set on the one electron Hilbert space. Orthogonality follows immediately for states which belong to different quantum numbers, since the lengths $L_i$ can be varied independently. Choosing for instance $1/L_i$ as different irrational numbers for all $i = \{1, \ldots, d\}$, every state can belong to a different eigenvalue of the momentum operator. To show completeness, we need to demonstrate

$$\sum_{\vec{n} \in \mathbb{Z}^d} |\psi_{\vec{n}}\rangle \langle \psi_{\vec{n}}| = \mathbb{I} \; , \qquad (4.80)$$

$$\langle \vec{x}' | \left( \sum_{\vec{n} \in \mathbb{Z}^d} |\psi_{\vec{n}}\rangle \langle \psi_{\vec{n}}| \right) |\vec{x}\rangle = \delta(\vec{x}' - \vec{x}) \; . \qquad (4.81)$$

First of all, we want to represent the sum $\sum_{\vec{n} \in \mathbb{Z}^d}$ by an integral over momentum space. Therefore, we define a piece-wise constant function and divide the resulting integral by the momentum volume in $\mathbb{R}^d$ which is occupied by each state. The volume is $\prod_{i=1}^{d} \frac{2\pi\hbar}{L_i}$ for each cell in momentum space. In the limit $L_1, L_2, \ldots, L_d \to \infty$, we find the expression

$$\frac{1}{(2\pi\hbar)^d} \int_{\mathbb{R}^d} d\vec{p} \; e^{\frac{\vec{p} \cdot (\vec{x} - \vec{x}')}{\hbar}} = \delta(\vec{x} - \vec{x}') \; , \qquad (4.82)$$

which proves the completeness in the limit of infinite crystal size. In practice the crystal usually has a much bigger scale than the electron, which is why such an approach would be justified. In addition, we know that our crystal belongs to a certain space group (symmetry group), which has a point and translation group as its basis. For an introduction to space groups and symmetry operators in quantum mechanics we refer the reader to Ref. [74] and Ref. [137]. Since the kinetic energy does not require a special underlying geometry in the Euclidean space, we know that the Hamilton operator $\hat{H}_{\text{Bl}} = \hat{T}_{\text{kin}} + V_{\text{latt}}(\hat{r}_1, \ldots, \hat{r}_d)$ is invariant, i.e. commutes, with the (unitary) symmetry operators of the space group, especially with the group of translations. Consequently, there exists a common eigenbasis of the symmetry operators and the Hamilton operator. We call an eigenstate of the operator $\hat{H}_{\text{Bl}}$ a *Bloch state* to the eigenvalue $\epsilon_{n,\vec{k}}$ if it is also an eigenstate for every operator in the translation group. According to Bloch's theorem, such a state can be labeled by the quantum numbers $n$ and $\vec{k}$, where $n \in \mathbb{N}$ is the band index and $\vec{k}$ is the crystal or (quasi-)momentum in the first BZ. Two Bloch states with the same band index and two wave vectors which differ by a reciprocal lattice vector are equivalent, i.e. $|\psi_{n,\vec{k}+\vec{K}}\rangle = |\psi_{n,\vec{k}}\rangle$. For a more detailed discussion of the band structures in solids, we refer the reader to Ref. [98]. The state's coordinate representation is written as

$$\psi_{n,\vec{k}}(\vec{x}) = \frac{1}{\sqrt{\text{vol}(V)}} e^{i \vec{k} \cdot \vec{x}} U_{n,\vec{k}}(\vec{x}) \; . \qquad (4.83)$$

The function $U_{n,\vec{k}}$ has the same translational symmetry as the crystal, i.e. $U_{n,\vec{k}}(\vec{x} + \vec{R}_i) = U_{n,\vec{k}}(\vec{x})$ for an arbitrary lattice vector and fulfills the orthogonality relation

$$\frac{1}{\text{vol}(\Omega_i)} \int_{\Omega_i} d\vec{x} \; U_{n,\vec{k}}^*(\vec{x}) U_{n',\vec{k}}(\vec{x}) = \delta_{n,n'} \qquad (4.84)$$

on an arbitrary Wigner-Seitz cell $\Omega_i \in \{\Omega_1, \ldots, \Omega_{N_u}\}$ and $\Omega_i \subset \mathbb{R}^d$ with the volume $\text{vol}(\Omega_i)$. Due to its periodicity, the function $U_{n,\vec{k}}$ can be written as a discrete Fourier series over the reciprocal lattice vectors, i.e.

$$U_{n,\vec{k}}(\vec{x}) = \sum_{\vec{K}} U_{n,\vec{k}}(\vec{K}) e^{i \vec{K} \cdot \vec{x}} \; , \qquad (4.85)$$

such that

$$\psi_{n,\vec{k}}(\vec{x}) = \frac{1}{\sqrt{\mathrm{vol}(V)}} \sum_{\vec{K}} U_{n,\vec{k}}(\vec{K}) e^{\imath(\vec{K}+\vec{k})\cdot\vec{x}} \ . \tag{4.86}$$

However, this state needs to obey the periodic boundary conditions as well and hence for every combination $\vec{k} + \vec{K}$ exists an $\vec{m} \in \mathbb{Z}^d$ with $\vec{k}_{\vec{m}} = \vec{k} + \vec{K}$, such that a Bloch state is just a specific linear combination of plane waves. In contrast to the free particle, the numbers $\vec{k}$ in the first BZ are in general not equal to the momentum. Theoretically, we define them as the phase factor of the eigenvalue of this state $|\psi_{n,\vec{k}}\rangle$ with the translation operator $\hat{T}_i$, which is $e^{-\imath\vec{k}\cdot\vec{R}_i}$. In order to get a better idea on how these functions behave the reader should take a look at the exactly-solvable one-dimensional Kronig-Penney model in Ref. [98]. In order to show that the states build a complete orthonormal basis we can use the same trick as for the completeness relation of the discrete plane wave basis. So far, we have been a little sloppy with our formalism for integration, since everything has happened in Euclidean space $\mathbb{R}^d$ up to this point. Now, while things are still relatively easy to grasp, we would like to introduce our formalism for integrations on oriented manifolds while showing the orthonormality of the Bloch states. For an introduction to the subject of integration on manifolds or more generally differential geometry, we refer the reader to [165]. We look at the integral over the complex $d$-form

$$\int_V \omega_{n,\vec{k},n',\vec{k}'} = \int_{\phi(V)} (\phi^{-1})^* \omega_{n,\vec{k},n',\vec{k}'} = \int_{\phi(V)} \mathrm{d}\vec{x}\ \psi^*_{n,\vec{k}}(\vec{x}) \psi_{n',\vec{k}'}(\vec{x}) \ , \tag{4.87}$$

$$\langle \psi_{n,\vec{k}} | \psi_{n',\vec{k}'} \rangle = \int_V \omega_{n,\vec{k},n',\vec{k}'} = \sum_{i=1}^{N_u} \int_{\Omega_i} \omega_{n,\vec{k},n',\vec{k}'} = \sum_{i=1}^{N_u} \int_{f_i(\Omega_1)} \omega_{n,\vec{k},n',\vec{k}'} \tag{4.88}$$

$$= \sum_{i=1}^{N_u} \int_{\Omega_1} f_i^* \omega_{n,\vec{k},n',\vec{k}'} = \sum_{i=1}^{N_u} \int_{\theta(\Omega_1)} (\theta^{-1})^* f_i^* \omega_{n,\vec{k},n',\vec{k}'} \tag{4.89}$$

$$= \sum_{i=1}^{N_u} \int_{\theta(\Omega_1)} \mathrm{d}\vec{y}\ |J[\phi \circ f_i \circ \theta^{-1}(\vec{y})]| \psi^*_{n,\vec{k}}[\phi \circ f_i \circ \theta^{-1}(\vec{y})] \psi_{n',\vec{k}'}[\phi \circ f_i \circ \theta^{-1}(\vec{y})] \tag{4.90}$$

$$= \sum_{i=1}^{N_u} \int_{\theta(\Omega_1)} \mathrm{d}\vec{y}\ \psi^*_{n,\vec{k}}(\vec{y}+\vec{R}_i) \psi_{n',\vec{k}'}(\vec{y}+\vec{R}_i) \tag{4.91}$$

$$= \sum_{i=1}^{N_u} e^{\vec{R}_i\cdot(\vec{k}'-\vec{k})} \int_{\theta(\Omega_1)} \mathrm{d}\vec{y}\ \psi^*_{n,\vec{k}}(\vec{y}) \psi_{n',\vec{k}'}(\vec{y}) \tag{4.92}$$

$$= \delta_{\vec{k},\vec{k}'} \frac{1}{\mathrm{vol}(\Omega_1)} \int_{\theta(\Omega_1)} \mathrm{d}\vec{y}\ U^*_{n,\vec{k}}(\vec{y}) U_{n',\vec{k}}(\vec{y}) \tag{4.93}$$

$$= \delta_{\vec{k},\vec{k}'} \delta_{n,n'} \tag{4.94}$$

where $\Omega_i$ is the $i$-th Wigner-Seitz cell around the lattice vector $\vec{R}_i$, i.e. $V = \cup_{i=1}^{N_u} \Omega_i$ and the overlap $\Omega_i \cap \Omega_j$ is of measure zero for $i \neq j$. In this case the positively oriented charts $(V, \phi)$, $(\Omega_1, \theta)$ are given by the identity maps

$$\phi : V \to \mathbb{R}^d \tag{4.95}$$
$$\phi(\vec{x}) = \vec{x} \ , \tag{4.96}$$
$$\theta : \Omega_1 \to \mathbb{R}^d \tag{4.97}$$
$$\theta(\vec{y}) = \vec{y} \ , \tag{4.98}$$

and $f_i$ is an orientation preserving diffeomorphism

$$f_i : \Omega_1 \to \Omega_i \ , \tag{4.99}$$

$$\phi \circ f_i \circ \theta^{-1} : \theta(\Omega_1) \subset \mathbb{R}^d \to \phi(V) \subset \mathbb{R}^d \tag{4.100}$$

$$\phi \circ f_i \circ \theta^{-1}(\vec{y}) \equiv \vec{x} = \vec{y} + \vec{R}_i \tag{4.101}$$

from the first to the $i$-th Wigner-Seitz cell whose Jacobian $J = \frac{\partial x_i}{\partial y_j}$ has determinant 1. In the third last step, we used the translation property of the Bloch states.

In the language of second quantization, we define the operators $\hat{a}^\dagger_{n,\vec{k}}$ and $\hat{a}_{n,\vec{k}}$ for the creation and annihilation of an electron in the Bloch state $|\psi_{n,\vec{k}}\rangle$. Since the electrons are fermions and not bosons, these operators fulfill the anti-commutation rules

$$\left\{ \hat{a}_{n,\vec{k}}, \hat{a}^\dagger_{n',\vec{k}'} \right\} = \delta_{n,n'}\delta_{\vec{k},\vec{k}'} \ , \tag{4.102}$$

$$\left\{ \hat{a}_{n,\vec{k}}, \hat{a}_{n',\vec{k}'} \right\} = 0 \ , \tag{4.103}$$

$$\left\{ \hat{a}^\dagger_{n,\vec{k}}, \hat{a}^\dagger_{n',\vec{k}'} \right\} = 0 \ . \tag{4.104}$$

This means that we can express a fully antisymmetric state of $N_{\text{el}}$ electrons through

$$|\psi_{\text{el}}\rangle = \sum_{\pi \in \mathcal{S}_{N_{\text{el}}}} \left( \prod_{i=1}^{N_{\text{el}}} \hat{a}^\dagger_{n_{\pi(i)},\vec{k}_{\pi(i)}} \right) |0\rangle \ , \tag{4.105}$$

where $|0\rangle$ is the vacuum state without any electrons. Now that we have found a basis which diagonalizes the first part of $\hat{H}_{\text{el}}$ as well as a basis which diagonalizes the ionic Hamilton operator, we should analyze the matrix elements of the interaction operator $\hat{V}_{\text{el-ph}}(\hat{r}_{i,1}, \ldots, \hat{r}_{i,d})$ in this basis, i.e.

$$-\sum_{j=1}^{N_{\text{ion}}} \hat{u}_{j,i}\langle \psi_{n,\vec{k}}|(\partial_i V_{\text{el-ion}})(\hat{r}_1 - R_{j,1}, \ldots, \hat{r}_d - R_{j,d})|\psi_{n',\vec{k}'}\rangle = \tag{4.106}$$

$$-\sum_{j=1}^{} \hat{u}_{j,i}e^{\imath \vec{R}_j \cdot (\vec{k}'-\vec{k})}\langle \psi_{n,\vec{k}}|(\partial_i V_{\text{el-ion}})(\hat{r}_1, \ldots, \hat{r}_d)|\psi_{n',\vec{k}'}\rangle = \tag{4.107}$$

$$\sum_{\vec{q},s}(\hat{b}^\dagger_{-\vec{q},s} + \hat{b}_{\vec{q},s})C_{n,n',s}(\vec{k}, \vec{k}', \vec{q}) \sum_{j=1}^{} e^{\imath \vec{R}_j \cdot (\vec{k}'-\vec{k}+\vec{q})} = \tag{4.108}$$

$$\sum_{\vec{K}} \delta_{\vec{k}'-\vec{k}+\vec{q},\vec{K}} \sum_{\vec{q},s}(\hat{b}^\dagger_{-\vec{q},s} + \hat{b}_{\vec{q},s})C_{n,n',s}(\vec{k}, \vec{k}', \vec{q}) \ . \tag{4.109}$$

where $\vec{K}$ is a reciprocal lattice vector. The sum over the lattice vectors is necessary since the wave vector $\vec{k}' = \vec{k} - \vec{q}$ can lie outside the first BZ, such that an addition or subtraction with a reciprocal lattice vector shifts it back to its uniquely determined wave vector in the first BZ. One calls phonon absorptions or emissions with $\vec{K} \neq 0$ *Umklapp* processes, since the electron's wave vector enters the first BZ from the opposite side. We have also defined our specific coupling constant

$$C_{n,n',s}(\vec{k}, \vec{k}', |\vec{q}|) \equiv -\sqrt{\frac{\hbar N_{\text{ion}}}{2M\omega_{|\vec{q}|,s}}} \left(e_{|\vec{q}|,s}\right)_i \langle \psi_{n,\vec{k}}|(\partial_i V_{\text{el-ion}})(\hat{r}_1, \ldots, \hat{r}_d)|\psi_{n',\vec{k}'}\rangle \ , \tag{4.110}$$

with $C \in \mathbb{C}$ and

$$C^*_{n,n',s}(\vec{k}, \vec{k}', \vec{q}) = C_{n',n,s}(\vec{k}', \vec{k}, \vec{q}) \ . \tag{4.111}$$

It determines the probability of the emission or absorption of a single phonon by a single electron. The probability can be calculated using Fermi's golden rule and is well explained in Ref. [98]. The reader should be aware that the specific formula for the coupling is in practice not really relevant, since one does not know how the electron-ion potential which couples valence electrons and ions looks like in a certain material. It can be through a Coulomb potential of type (4.11) but might also work differently due to screening effects of other core electrons. Therefore, it is more useful

to actually measure the coupling constant through Raman spectroscopy, angle-resolved photon emission spectroscopy (ARPES), inelastic neutron-scattering and others, and find a numerical fit for the coupling constant from the data. The interested reader should consult Refs. [52, 30, 126]. Rewriting the result in the operator formalism of second quantization, we obtain the hermitian operator

$$\hat{V}_{\text{el-ph}} = \sum_{n,n',\vec{k}} \sum_{\vec{K}} \sum_{\vec{q},s} C_{n,n',s}(\vec{k} + \vec{q} + \vec{K}, \vec{k}, \vec{q}) \hat{a}^\dagger_{n,\vec{k}+\vec{q}+\vec{K}} \hat{a}_{n',\vec{k}} (\hat{b}^\dagger_{-\vec{q},s} + \hat{b}_{\vec{q},s}) \ . \tag{4.112}$$

It is important to note that the eigenvalues of this operator are real.

## 4.3.1 Polaron

The particle whose quantum state is an eigenstate of the Hamilton operator

$$\hat{H}_{\text{pol}} \equiv \sum_{n,\vec{k}} \epsilon_{n,\vec{k}} \hat{a}^\dagger_{n,\vec{k}} \hat{a}_{n,\vec{k}} + \sum_{\vec{q},s} \hbar\omega_{\vec{q},s} \hat{b}^\dagger_{\vec{q},s} \hat{b}_{\vec{q},s}$$
$$+ \sum_{n,n',\vec{k}} \sum_{\vec{K}} \sum_{\vec{q},s} C_{n,n',s}(\vec{k} + \vec{q} + \vec{K}, \vec{k}, \vec{q}) \hat{a}^\dagger_{n,\vec{k}+\vec{q}+\vec{K}} \hat{a}_{n',\vec{k}} (\hat{b}^\dagger_{-\vec{q},s} + \hat{b}_{\vec{q},s}) \ , \tag{4.113}$$

is called polaron [38]. It is an electron which lives together with the polarizations, that it introduces to the surrounding ionic lattice, in perfect harmony. One can introduce several simplifications of this Hamiltonian such as forbidding inter-band transitions in the interaction ($n' = n$), Umklapp processes ($\vec{K} = 0$), and explicit formulas for the electron's $\epsilon_{n,\vec{k}}$ and phonon's dispersion relation $\hbar\omega_{\vec{q},s}$. If one chooses a quadratic dispersion relation for the electron with a modified electron mass, $\epsilon_{n,\vec{k}} = \frac{\hbar|\vec{k}|^2}{2m_n^*}$, which amounts to an approximation of a weak lattice potential or a very extended electronic wave function, one calls the resulting particle large polaron. If one approximates the electron's dispersion in a tight binding model, i.e. the assumption of a strong lattice potential, one talks about the small polaron. Furthermore, one can introduce the dimensionless Fröhlich coupling constant $\alpha$ which measures the strength of the interaction between electrons and phonons [38]. In general, we define our coupling constant as the ratio between the electron's energy and the coupling energy, which means it depends on the band and wave vector of the electron as well as the wave vector and polarization of the phonon. For specific approximations one can write down explicit formulas for the coupling, which we shall do in the next subsection. The coupling strengths for longitudinal phonons, which is much stronger than for transversal phonons, are on the order of $10^{-2}$ till $10^0$ [40]. Unfortunately, the exact solutions to the eigenstates of these particles have not been found so far. Depending on the coupling strength one can obtain approximate results in the weak or strong coupling regimes, as described in Refs. [38] and [39].

## 4.3.2 Hermitian transition

The effective operator acting on an electron is not necessarily hermitian for every phonon transition. Calculating the fundamental matrix elements for the absorption of one phonon we find the *non-hermitian* operator

$$\hat{V}_{\text{ab}}(n_{\text{ph}}, \vec{q}, s) \equiv \langle n_{\text{ph}} - 1, \vec{q}, s | \hat{V}_{\text{el-ph}} | n_{\text{ph}}, \vec{q}, s \rangle \tag{4.114}$$

$$= \sqrt{n_{\text{ph}}} \sum_{n,n',\vec{k},\vec{K}} C_{n,n',s}(\vec{k} + \vec{q} + \vec{K}, \vec{k}, \vec{q}) \hat{a}^\dagger_{n,\vec{k}+\vec{q}+\vec{K}} \hat{a}_{n',\vec{k}} \ , \tag{4.115}$$

$$\left[ \hat{V}_{\text{ab}}(n_{\text{ph}}, \vec{q}, s) \right]^\dagger = \sqrt{n_{\text{ph}}} \sum_{n,n',\vec{k},\vec{K}} C_{n,n',s}(\vec{k} - \vec{q} + \vec{K}, \vec{k}, \vec{q}) \hat{a}^\dagger_{n,\vec{k}-\vec{q}+\vec{K}} \hat{a}_{n',\vec{k}} \ , \tag{4.116}$$

and for the emission we also find a non-hermitian operator

$$\hat{V}_{em}(n_{ph}, \vec{q}, s) \equiv \langle n_{ph}, \vec{q}, s | \hat{V}_{el\text{-}ph} | n_{ph} - 1, \vec{q}, s \rangle \tag{4.117}$$

$$= \sqrt{n_{ph}} \sum_{n,n',\vec{k},\vec{K}} C_{n,n',s}(\vec{k} - \vec{q} + \vec{K}, \vec{k}, \vec{q}) \hat{a}^\dagger_{n,\vec{k}-\vec{q}+\vec{K}} \hat{a}_{n',\vec{k}} \; , \tag{4.118}$$

$$\left[ \hat{V}_{em}(n_{ph}, \vec{q}, s) \right]^\dagger = \sqrt{n_{ph}} \sum_{n,n',\vec{k},\vec{K}} C_{n,n',s}(\vec{k} + \vec{q} + \vec{K}, \vec{k}, \vec{q}) \hat{a}^\dagger_{n,\vec{k}+\vec{q}+\vec{K}} \hat{a}_{n',\vec{k}} \; . \tag{4.119}$$

However, one observes that $\left[ \hat{V}_{ab}(n_{ph}, \vec{q}, s) \right]^\dagger = \hat{V}_{em}(n_{ph}, \vec{q}, s)$. This will become important in the next section.

To learn some more about this interaction, in a first approach, we ignore the static lattice potential, which means we set $\hat{V}_{latt} = 0$, and try to find a solution for the simpler problem. Therefore, we define operators

$$\hat{H}_{free} \equiv \sum_{\vec{k}} \frac{\hbar^2 |\vec{k}|^2}{2m} \hat{a}^\dagger_{\vec{k}} \hat{a}_{\vec{k}} = \sum_{i=1}^d \frac{\hat{p}_i^2}{2m} \; , \tag{4.120}$$

$$\hat{H}_{IA} \equiv \sum_{\vec{k},\vec{K},\vec{q},s} C'_s(\vec{k} + \vec{q} + \vec{K}, \vec{k}, \vec{q}) \hat{a}^\dagger_{\vec{k}+\vec{q}+\vec{K}} \hat{a}_{\vec{k}} (\hat{b}^\dagger_{-\vec{q},s} + \hat{b}_{\vec{q},s}) \; , \tag{4.121}$$

where $\hat{a}^\dagger_{\vec{k}}$ creates an electron in the state $|\psi_{\vec{k}}\rangle$ with momentum $\hbar\vec{k}$ and $\vec{k}, \vec{q}, \vec{K} \in \{\vec{k}_{\vec{n}} | \vec{n} \in \mathbb{Z}^d\}$. Using Eq. (4.110) the new coupling constant becomes

$$C'_s(\vec{k} + \vec{q} + \vec{K}, \vec{k}, \vec{q}) = -\imath \sqrt{n_{ph} N_{ion} \frac{\hbar}{2M\omega_{\vec{q},s}}} \vec{e}_{\vec{q},s} \cdot (\vec{q} + \vec{K}) \mathcal{F}[V_{el\text{-}ion}](\vec{q} + \vec{K}) \tag{4.122}$$

$$= E_{el\text{-}ph}(n_{ph}, |\vec{q}|, s) \vec{e}_{|\vec{q}|,s} \cdot \vec{F}(\vec{n}_{\vec{q}} + \vec{m}_{\vec{K}}) \; , \tag{4.123}$$

$$E_{el\text{-}ph}(n_{ph}, |\vec{q}|, s) \equiv \frac{(2\pi)^2 Z e_0^2}{L} \sqrt{N_{ion} n_{ph} \frac{\hbar^2}{2ML^2}} / \left( \hbar\omega_{|\vec{q}|,s} \right) \in \mathbb{R} \; , \tag{4.124}$$

$$\vec{F}(\vec{n}_{\vec{q}} + \vec{m}_{\vec{K}}) \equiv \imath(\vec{n}_{\vec{q}} + \vec{m}_{\vec{K}}) \int\limits_{-\pi}^{\pi} dy_1 \cdots \int\limits_{-\pi}^{\pi} dy_d \; \frac{e^{-\imath \vec{y} \cdot (\vec{n}_{\vec{q}} + \vec{m}_{\vec{K}})}}{|\vec{y}|} \in \mathbb{C}^d / \mathbb{R}^d \tag{4.125}$$

$$= \imath(\vec{n}_{\vec{q}} + \vec{m}_{\vec{K}}) 2^d \int\limits_{0}^{\pi} dy_1 \cdots \int\limits_{0}^{\pi} dy_d \; \frac{\cos[\vec{y} \cdot (\vec{n}_{\vec{q}} + \vec{m}_{\vec{K}})]}{|\vec{y}|} \; , \tag{4.126}$$

$$\vec{F}(-\vec{n}_{\vec{q}} - \vec{m}_{\vec{K}}) = [\vec{F}(\vec{n}_{\vec{q}} + \vec{m}_{\vec{K}})]^* = -\vec{F}(\vec{n}_{\vec{q}} + \vec{m}_{\vec{K}}) \; , \tag{4.127}$$

where we have assumed $L_i = L$. The result is independent of the electron's wave vector. Calculating the simplified effective emission and absorption operators we find

$$\hat{V}_{em}(n_{ph}, \vec{q}, s) \equiv \langle n_{ph}, \vec{q}, s | \hat{H}_{IA} | n_{ph} - 1, \vec{q}, s \rangle \tag{4.128}$$

$$= E_{el\text{-}ph}(n_{ph}, |\vec{q}|, s) \vec{e}_{|\vec{q}|,s} \cdot \left[ \sum_{\vec{k},\vec{K}} \vec{F}^*_{\vec{n}_{\vec{q}} + \vec{m}_{\vec{K}}} \hat{a}^\dagger_{\vec{k}-\vec{q}-\vec{K}} \hat{a}_{\vec{k}} \right] \; , \tag{4.129}$$

$$\left[ \hat{V}_{em}(n_{ph}, \vec{q}, s) \right]^\dagger = \hat{V}_{ab}(n_{ph}, \vec{q}, s) \tag{4.130}$$

$$= E_{el\text{-}ph}(n_{ph}, |\vec{q}|, s) \vec{e}_{|\vec{q}|,s} \cdot \left[ \sum_{\vec{k},\vec{K}} \vec{F}_{\vec{n}_{\vec{q}} + \vec{m}_{\vec{K}}} \hat{a}^\dagger_{\vec{k}+\vec{q}+\vec{K}} \hat{a}_{\vec{k}} \right] \; . \tag{4.131}$$

The reciprocal lattice vector $\vec{K}$ is not necessary in this formulation, since the electron's wave vector is not limited to the first BZ. However, in order to have a better analogy to the case of Bloch states, we keep the reciprocal lattice vector for the Umklapp processes and state that wave vectors are equivalent if they differ by a reciprocal lattice vector, i.e. they carry the same physical

information. As we are interested to study the effect of the electron-phonon coupling on a more fundamental level, we want to look at its effect on a set of eigenstates and -vectors. However, the operators $\hat{V}_{\text{em}}(n_{\text{ph}}, \vec{q}, s)$ and $\hat{V}_{\text{ab}}(n_{\text{ph}}, \vec{q}, s)$ are non-hermitian. That is why we analyze the hermitian operator $\hat{V}_{\text{IA}} \equiv [\hat{V}_{\text{em}}(n_{\text{ph}}, \vec{q}, s) + \hat{V}_{\text{ab}}(n_{\text{ph}}, \vec{q}, s)]/2$. This amounts to taking the matrix element of $\hat{H}_{\text{free}} + \hat{H}_{\text{IA}}$ with the product state $\mathbb{I} \bigotimes (|n_{\text{ph}} - 1, \vec{q}, s\rangle + |n_{\text{ph}}, \vec{q}, s\rangle)/\sqrt{2}$ which results in the effective hermitian operator

$$\hat{H}_{\text{eff}} \equiv \sum_{\vec{k}} \frac{\hbar^2 |\vec{k}|^2}{2m} \hat{a}_{\vec{k}}^\dagger \hat{a}_{\vec{k}} + [\hat{V}_{\text{em}}(n_{\text{ph}}, \vec{q}, s) + \hat{V}_{\text{ab}}(n_{\text{ph}}, \vec{q}, s)]/2 . \tag{4.132}$$

It is also interesting to see what happens to the actual displacement field from Eq. (4.47) for the transition, which is

$$|\psi_{\text{ph}}\rangle \equiv (|n_{\text{ph}} - 1, \vec{q}, s\rangle + |n_{\text{ph}}, \vec{q}, s\rangle)/\sqrt{2} , \tag{4.133}$$

$$\langle \psi_{\text{ph}} | \hat{u}_{j,k} | \psi_{\text{ph}} \rangle = \sqrt{\frac{\hbar n_{\text{ph}}}{2 M N_{\text{ion}} \omega_{|\vec{q}|,s}}} \left( e_{|\vec{q}|,s} \right)_k \cos(\vec{q} \cdot \vec{R}_j) . \tag{4.134}$$

The first statement, which can be made about the operator $\hat{H}_{\text{eff}}$, is about its trace

$$\text{Tr}\left[\hat{H}_{\text{eff}}\right] = \sum_{\vec{k}} \frac{\hbar^2 |\vec{k}|^2}{2m} \text{Tr}[\hat{a}_{\vec{k}}^\dagger \hat{a}_{\vec{k}}] = \sum_{\vec{n} \in \mathbb{Z}^d} \frac{\hbar^2 |\vec{k}_{\vec{n}}|^2}{2m} , \tag{4.135}$$

$$\text{Tr}[\hat{V}_{\text{em}}(n_{\text{ph}}, \vec{q}, s) + \hat{V}_{\text{ab}}(n_{\text{ph}}, \vec{q}, s)] = \sum_{i=1}^{\infty} \lambda_i^{\text{em+ab}} = 0 , \tag{4.136}$$

which tells us that the interaction operator is indefinite with positive and negative real eigenvalues. Let us try to diagonalize the operator $\hat{H}_{\text{eff}}$ in the plane wave basis for which the first part is diagonal. The off-diagonal matrix elements which arise due to the electron-phonon coupling are

$$\langle \vec{k}' | [\hat{V}_{\text{em}}(n_{\text{ph}}, \vec{q}, s) + \hat{V}_{\text{ab}}(n_{\text{ph}}, \vec{q}, s)] | \vec{k} \rangle = E_{\text{el-ph}}(n_{\text{ph}}, |\vec{q}|, s)$$

$$\vec{e}_{|\vec{q}|,s} \cdot \left[ \sum_{\vec{K}} \vec{F}_{\vec{n}_{\vec{q}} + \vec{m}_{\vec{K}}} \left( \delta_{\vec{k}', \vec{k} + \vec{q} + \vec{K}} - \delta_{\vec{k}', \vec{k} - \vec{q} - \vec{K}} \right) \right] . \tag{4.137}$$

The resulting matrix does have one set of off-diagonal entries above and below the diagonal, which are complex conjugates of each other. The relation between the constants

$$\alpha(n_{\text{ph}}, |\vec{q}|, s) \equiv 2 E_{\text{el-ph}}(n_{\text{ph}}, |\vec{q}|, s) / \frac{h^2}{2mL^2} \in \mathbb{R}_0^+ , \tag{4.138}$$

determines the coupling strength between the electron and phonons. If we assume a weak coupling, $\alpha(n_{\text{ph}}, |\vec{q}|, s) \ll 1$, one would hope that the $\vec{n}$-th eigenstate and -value of $\hat{H}_{\text{eff}}$ are only slightly perturbed from the plane wave quantum state $|\psi_{\vec{n}}\rangle$ and the value $\frac{\hbar^2 |\vec{k}_{\vec{n}}|^2}{2m}$. First of all, it is important to realize the following. Given an arbitrary phonon with wave vector $\vec{q} = \frac{2\pi}{L} \vec{n}_{\vec{q}}$ from the first Brillioun zone it can only couple quantum states along its own wave vector. What does this tell us? It means that the interaction which is facilitated between the quantum states of different wave vectors is effectively a one-dimensional chain of nearest-neighbor interactions. If we choose a wave vector $\vec{k}$, only the basis states out of the complete set of $N^d$ plane waves whose wave vector $\vec{k}' = \vec{k} + n\vec{q}$ with $n \in \mathbb{N}$ are going to interact with each other and hence form a block matrix within the total interaction matrix. The size of the block depends on the wave vector $\vec{q}$ through its integer components $\vec{n}_{\vec{q}}$ in the following way. If $N$ is the number of independent atoms in each individual direction then there exist a minimal $s \in \{2, \ldots, N\}$ and a minimal $\vec{r} \in \mathbb{N}^d$ with $r_i \in \{1, 2, \ldots, (n_{\vec{q}})_i\}$ such that

$$s \vec{n}_{\vec{q}} = N \vec{r} , \tag{4.139}$$

which means that adding the wave vector $\vec{q}$ *exactly* $s$ times to an arbitrary wave vector $\vec{k}$ leads

*for the first time* to

$$\vec{k}' \equiv \vec{k} + s\vec{q} = \vec{k} + \vec{K} \ , \tag{4.140}$$

where $\vec{K}$ is a reciprocal lattice vector and consequently $\vec{k}'$ equivalent to $\vec{k}$. The value $s = 1$ would imply that the atom gets coupled to itself due to the periodic boundary conditions, which would be equivalent to a phonon with wave vector $\vec{q} = 0$. This interaction is not of interest to us, since there will be no energy transfer between the electron and phonons in this case. The values $r_i$ specify the number of Umklapp processes which will be required per direction throughout the summation to stay in the first BZ. The block matrix which describes this influence of the phonon on the quantum state $\vec{k}$ has size $s \times s$ with $s \geq 2$ and $s \leq N$ and has necessarily an almost tridiagonal shape. There will only be one entry at the edges of the block where the last state in the row couples to the first due to another Umklapp process. One can achieve this by starting the block with a state at the Brillioun zone boundary. If we choose another wave vector $\vec{k}'' \neq \vec{k} + n\vec{q}$, this quantum state belongs to a different tridiagonal block matrix of the same size $s \times s$. Overall we can conclude that any matrix of this type can be written in block-diagonal form, where each block has size $s \times s$, and there are $N/s$ number of blocks along this direction. Since there are $d - 1$ other directions, one ends up with $N^{d-1} \times N/s$ blocks. This statement holds in any dimension, and significantly reduces the complexity of the matrix diagonalization. One just needs to define the blocks for a given wave vector $\vec{q}$. Since they are of size $s \times s$ and tridiagonal, the complexity of diagonalizing the $N^d \times N^d$ matrix representation of $\hat{H}_{\text{eff}}$ requires only about $N^{d-1} \times (N/s) \times s = N^d$ steps, which means it scales linearly in the number of atoms, despite the quadratic scaling of the matrix representation. In our simplified case, the off-diagonal matrix elements only depend on the phonons and are hence the same for every block. The reader should note that due to the Umklapp processes they may not all be the same within one block. However, the only thing which changes from one block to another are the diagonal elements. Hence if one is able to find the eigenvalues and -vectors for arbitrary diagonal elements one has solved the problem for any number of atoms.

For a concrete example, consider a two-dimensional square lattice ($d = 2$). The band structure becomes a paraboloidal surface, see Fig. 4.1 and the Fourier transform exists even for $m = 0$ (no screening). If the phonon wave vector is $\vec{q} = \vec{e}_1$ one can obtain blocks of tridiagonal matrices for choosing to order the basis states according to

$$\begin{aligned}
\{ &|\psi_{-N/2+1,-N/2+1}\rangle, |\psi_{-N/2+2,-N/2+1}\rangle, \dots, |\psi_{N/2,-N/2+1}\rangle; \\
&|\psi_{-N/2+1,-N/2+2}\rangle, |\psi_{-N/2+2,-N/2+2}\rangle, \dots, |\psi_{N/2,-N/2+2}\rangle; \\
&\qquad\qquad\qquad\qquad\qquad\qquad\vdots \\
&|\psi_{-N/2+1,N/2}\rangle, |\psi_{-N/2+2,N/2}\rangle, \dots, |\psi_{N/2,N/2}\rangle \} \ ,
\end{aligned} \tag{4.141}$$

such that the independent blocks of size $N \times N$ are indicated by the semicolons. Solving each of those blocks is as demanding as the one-dimensional problem, which means that the complexity scales linearly with the number of atoms $N^2$, despite the quadratic matrix size increase.

### 4.3.3 Example: 1D atomic chain

We choose the longitudinal phonon excitation of the one-dimensional periodic mono-atomic chain with a linear dispersion relation for the phonon $\omega_{|q|} = c_s|q|$, where $c_s$ is the sound velocity in the material. Since the Fourier transform of $1/|\vec{y}|$ does not exist for $d = 1$, we introduce a screening to obtain the Yukawa potential $V = \frac{e^{-\gamma|y|}}{|y|}$ and analyze the behavior for small $\gamma$, such that the Fourier transform converges. Furthermore, we assume $\alpha(n_{\text{ph}}, n_q = 1, s) \sim \mathcal{O}(10^{-1})$, which is a relatively strong coupling. The spectrum and a comparison of the resulting eigenvalues with the non-interacting system are shown in Figs. 4.2 and 4.3. One observes the opening of a band gap at the phonon wave vector $\pm q/2$, which is the reason for the famous Peierls' instability of an atomic chain [98]. If one imagines the band to be filled up to the Fermi wave vector $k_F$ then the system will be unstable with respect to phonon excitations around the wave vector $q = 2k_F$, since the electronic system can lower its energy. The effect will also appear for a non-zero lattice potential and using Bloch states instead of plane waves.

In summary, throughout this and the previous section we have performed a second quantization of the harmonic approximation of the small lattice vibrations around the ions' equilibrium
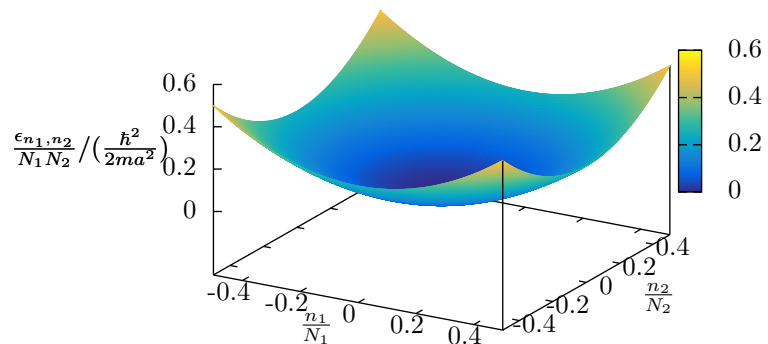
Figure 4.1: Continuum approximation of eigenspectrum for non-interacting electron of a two-dimensional square lattice with vanishing lattice potential.
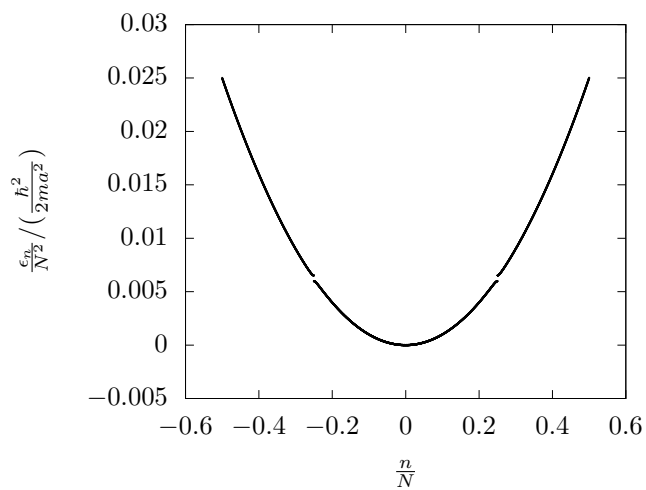


Figure 4.2: Normalized eigenspectrum for coupled electron-phonon system of a mono-atomic chain of $N = 5000$ atoms, $q = N/2$, $\alpha = 1/5$, $\gamma = 10^{-3}$.

Figure 4.3: Comparison of (non-)interacting electron for coupled electron-phonon system of a mono-atomic chain of $N = 5000$ atoms, $q = N/2$, $\alpha = 1/5$, $\gamma = 10^{-3}$.

positions. The central assumption are well-localized ionic wave functions and small displacements from their equilibrium position. This lead to an ionic energy which is just a sum of independent harmonic oscillators, and a linear interaction term between electrons and phonons.

### 4.3.4 Electron-Electron interaction

Now, we can turn our attention back to the interaction between electrons. Using the creation and annihilation operators of single Bloch electrons, one can express the interaction again as an operator in second quantization

$$\hat{V}_{\text{el-el}} = \sum_{\vec{K}} \sum_{n_1,n_2,n_3,n_4} \sum_{\vec{k}_2,\vec{k}_3,\vec{k}_4} C_{n_1,n_2,n_3,n_4}(\vec{k}_3 + \vec{k}_4 - \vec{k}_2 + \vec{K}, \vec{k}_2, \vec{k}_3, \vec{k}_4)$$

$$\hat{a}^\dagger_{n_1,\vec{k}_3+\vec{k}_4-\vec{k}_2+\vec{K}} \hat{a}^\dagger_{n_2,\vec{k}_2} \hat{a}_{n_3,\vec{k}_3} \hat{a}_{n_4,\vec{k}_4} \, , \tag{4.142}$$

$$C_{n_1,n_2,n_3,n_4}(\vec{k}_1, \vec{k}_2, \vec{k}_3, \vec{k}_4) \equiv \int\limits_{\phi(V)\times\phi(V)} \mathrm{d}\vec{x}\mathrm{d}\vec{y} \; \psi^*_{n_1,\vec{k}_1}(\vec{x})\psi^*_{n_2,\vec{k}_2}(\vec{y}) V_{\text{el-el}}(\vec{x} - \vec{y})$$

$$\psi_{n_3,\vec{k}_3}(\vec{y})\psi_{n_4,\vec{k}_4}(\vec{x}) \, , \tag{4.143}$$

where $C \in \mathbb{C}$ is the respective coupling constant. However, we shall not deal with the problem of interacting of electrons in the remaining part of this chapter, since we first want to find a curved space approach which describes the simplified electron-phonon coupling. One usually incorporates this interaction by only altering the dispersion relation for electrons subject to a static lattice potential if one assumes a weak electron-electron interaction in the material such that the quasi-particle picture, see Ref. [77], still holds. The idea behind the quasi-particle picture sounds very similar to the approach in curved space, where one only changes the metric of the underlying manifold. In the subsequent discussion, we shall not consider these interactions, since we are focusing on the feasibility in the simpler case.

## 4.4 Curved space approach

After the preliminary discussion, we can state the intention of the *curved space approach* a little more precisely. We want to model the single electron Hamilton operator

$$\hat{H}_{el} = \sum_{i=1}^{d} \frac{\hat{p}_i^2}{2m} + V_{latt}(\hat{r}_1, \ldots, \hat{r}_d) + \hat{V}_{el-ph}(\hat{r}_1, \ldots, \hat{r}_d) \tag{4.144}$$

$$= \sum_{i=1}^{d} \frac{\hat{p}_i^2}{2m} + \sum_{j=1}^{N_{ion}} \left[ V_{el-ion}(\hat{r}_1 - R_{j,1}^{(0)}, \ldots, \hat{r}_d - R_{j,d}^{(0)}) \right.$$

$$\left. + \hat{u}_{j,i} \left( \partial_i V_{el-ion} \right) (\hat{r}_1 - R_{j,1}^{(0)}, \ldots, \hat{r}_d - R_{j,d}^{(0)}) \right] , \tag{4.145}$$

or expressed in second quantization

$$\hat{H}_{el} = \sum_{n,\vec{k}} \left[ \epsilon_{n,\vec{k}} \hat{a}_{n,\vec{k}}^\dagger \hat{a}_{n,\vec{k}} + \sum_{n',\vec{K},\vec{q},s} \tilde{C}_{n,n',s}(\vec{K},\vec{k},\vec{q}) \hat{a}_{n,\vec{k}+\vec{q}+\vec{K}}^\dagger \hat{a}_{n',\vec{k}} (\hat{b}_{-\vec{q},s}^\dagger + \hat{b}_{\vec{q},s}) \right] \tag{4.146}$$

through an electron which moves on a connected, $d$-dimensional, Riemannian manifold $M$ with metric tensor $g$. The idea is that the positions of ions appear regular in this space, whereas the metric reflects the displacements of ions from their equilibrium positions. If the displacements are small the presence of phonons may manifest itself through small deviations of our manifold from the Euclidean space $\mathbb{R}^d$ with the metric tensor $g_{ij} = \delta_{ij}$, i.e. $g_{ij} = \delta_{ij} + \delta g_{ij}$. By regular, we mean that the coordinates of the points on $M$, where the electron feels the minima of the lattice potential, build a crystal lattice structure. More formally, at the points $\{m_1, \ldots, m_{N_{ion}}\} \in M$, which have the coordinates $\vec{q}_{m_i} = \vec{R}_i$ in $\mathbb{R}^d$, the electron feels the potential's minima. As a consequence, the manifold should depend on the quantum state of the phonons, as they change the ions' positions.

For a description of this non-relativistic quantum mechanical problem we use the approach developed in Ref. [33]. There are other approaches to deal with non-relativistic quantum mechanics in curved spaces, such as Ref. [27]. We have chosen the approach from Ref. [33] as it represents an intrinsic method which does not rely on an embedding of our manifold into a larger Euclidean space. Furthermore, the issues which we have encountered here in formulating such a theory would have shown up in the exact same way in the other approach, since they are intrinsic to the operator algebra, which we shall demonstrate later in this section.

We are working on an infinite-dimensional, separable Hilbert space $\mathcal{H}_M$ of complex-valued functions, which are square-integrable over the manifold $M$, and we employ the Schrödinger picture, where the state vector $|\psi(t)\rangle \in \mathcal{H}_M$ carries the time-dependence, while the operators are time-independent. On this Hilbert space, there is a set of *generalized* position and *conjugated* momentum operators $\{\hat{q}_1, \ldots, \hat{q}_d\}$, $\{\hat{P}_1, \ldots, \hat{P}_d\}$ which are unbounded, hermitian and fulfill the canonical commutation relations

$$\left[ \hat{q}_j, \hat{P}_k \right] = i\hbar \delta_{jk} \mathbb{I} , \tag{4.147}$$

$$[\hat{q}_j, \hat{q}_k] = 0 , \tag{4.148}$$

$$\left[ \hat{P}_j, \hat{P}_k \right] = 0 . \tag{4.149}$$

All other operators on $\mathcal{H}_M$ are only (non-)linear functions of operators from this basic set. We do not consider the spin of the particle here, since in the original problem except for the statistics it was irrelevant. The reader should notice the symmetry between position and momentum in the relations above, which would make it an almost trivial task to exchange the meaning of them while replacing $i \to -i$. Since complex numbers are an artificial concept, nature will not notice the difference [135].

### 4.4.1 Generalized coordinates and momenta

In Ref. [34] and chapter 5 of Ref. [33], the author derives the coordinate representation of the quantum dynamics on the manifold. Since, the terminology as well as the right interpretation

are essential for the following parts, we shall present the most important results of the two Refs. here. Furthermore, in case that there is no confusion, we shall suppress the term *generalized* as an adjective for the operators from now on.

Using the spectral theorem, one finds a complete eigenbasis of the position operators, which we define as $\{|\vec{q}\rangle\}_{\vec{q}\in\mathbb{R}^d}$. It has the property $\hat{q}_i|\vec{q}\rangle = q_i|\vec{q}\rangle$ for all $i = 1,\ldots,d$, where $q_i \in \mathbb{R}$ is the generalized $i$-th coordinate of the state $|\vec{q}\rangle$. Furthermore, the $q_i$ are the *coordinates* in the Riemannian manifold $M$ with the metric tensor $g_{ij}$, such that a quantum state $|\psi(t)\rangle \in \mathcal{H}_M$ can be expressed as

$$|\psi(t)\rangle \equiv \int_{\mathbb{R}^d} d\omega \ |\vec{q}\rangle\langle\vec{q}|\psi(t)\rangle \ , \tag{4.150}$$

where $d\omega$ is the volume element of the manifold and $\langle\vec{q}|\psi(t)\rangle \equiv \psi(\vec{q},t)$ is the wave function with

$$\psi : \mathbb{R}^d \times \mathbb{R} \to \mathbb{C} \ , \tag{4.151}$$

such that $|\psi(\vec{q},t)|^2 d\omega$ is interpreted as the probability of finding the particle in the volume $d\omega$ around $\vec{q}$ at time $t$ and

$$\int_{\mathbb{R}^d} d\omega \ |\psi(\vec{q},t)|^2 d\omega = 1 \ . \tag{4.152}$$

The reader should note that if $\vec{q} \in \mathbb{R}^d$ does not represent the coordinates of a point on the manifold, the volume element will just be zero and hence has no contribution to the measurable physical quantities, i.e. the expectation values. In addition, one requires the normalization condition of the position eigenstates through

$$\langle\vec{q}|\vec{q}'\rangle = \delta(\vec{q},\vec{q}') \ , \tag{4.153}$$

$$\delta(\vec{q},\vec{q}') \equiv 0 \ \forall \vec{q} \neq \vec{q}' \ , \tag{4.154}$$

$$\int_{\mathbb{R}^d} d\omega_{q'} \ \delta(\vec{q},\vec{q}')f(\vec{q}') \equiv f(\vec{q}) \ , \tag{4.155}$$

where one uses a *generalized* delta distribution. It is important to stress that the previous equation should be valid for any choice of coordinate system. On a Riemannian manifold, we can express the volume element as $d\omega_q = d\vec{q}\sqrt{g(\vec{q})}$. $g$ is the determinant of the metric tensor $g_{ij}$ and the generalized delta distribution becomes

$$\delta(\vec{q},\vec{q}') = g^{-1/2}(\vec{q})\delta(\vec{q}-\vec{q}') = g^{-1/2}(\vec{q}')\delta(\vec{q}-\vec{q}') \ , \tag{4.156}$$

for which $\delta(\vec{q}-\vec{q}') = \prod_{i=1}^d \delta(q_i - q_i')$ is the normal $d$-dimensional delta distribution. The name generalized coordinates for the real eigenvalues $q_i$ of the hermitian operators $\hat{q}_i$ are supposed to stress the analogy to classical Hamilton mechanics. The reader should notice that the eigenvalues of this operator do not need to have the unit length and should be aware that the Stone-von Neumann theorem [135] which would fix the representation of the position or momentum operators in the eigenbasis of the other ones to simple partial derivatives, cannot be applied in our case, since we are operating on a general Riemannian manifold, potentially different from Euclidean space. Using the canonical commutation relations together with the hermiticity of the momentum operator, one can derive its coordinate representation

$$\langle\vec{q}|\hat{P}_j|\vec{q}'\rangle = -\imath\hbar \left[\frac{\partial}{\partial q_i} + \frac{1}{2}\Gamma_{ji}^j(\vec{q})\right] \delta(\vec{q},\vec{q}') \tag{4.157}$$

$$= \imath\hbar \left[\frac{\partial}{\partial q_i'} + \frac{1}{2}\Gamma_{ji}^j(\vec{q}')\right] \delta(\vec{q},\vec{q}') \ , \tag{4.158}$$

$$\Gamma_{ji}^j(\vec{q}') = \frac{1}{2} \left.\frac{\partial \log g}{\partial q_i'}\right|_{\vec{q}'} \ , \tag{4.159}$$

where $\Gamma_{ji}^j$ is the contracted Christoffel symbol.

As a side note, we would like to mention that the reader may have noticed that the additional term in the coordinate representation of the momentum operator in Eq. (4.157) could be

described by a vector potential

$$A_i(\vec{x}) = \frac{\imath\hbar}{4} \partial_i \log g(\vec{x}) \ , \tag{4.160}$$

and therefore may wonder if the impact of the metric on the dynamics could be modeled by an interaction with an electromagnetic field. However, if one looks at the resulting kinetic energy operator using minimal coupling

$$\hat{H}_{el} = \sum_{i=1}^{D_{el}} \frac{(\hat{p}_i + e\hat{A}_i)(\hat{p}_i + e\hat{A}_i)}{2m} = \frac{1}{2m} \sum_{i=1}^{D_{el}} \hat{p}_i\hat{p}_i + e^2 \hat{A}_i\hat{A}_i + \left\{ \hat{p}_i, \hat{A}_i \right\} \ , \tag{4.161}$$

and the definition of the Hamilton operator in curved space, which will be given in the next section, one will realize the fundamental difference in the term that is quadratic in the momentum operators. This already hints at a possible problem when thinking about the potential equivalence of the two quantum systems and we shall give more details on this issue in the section on equivalence.

In the same way, there also exists a complete eigenbasis of the momentum operators, which we define as $|\vec{P}\rangle$, such that $\hat{P}_i|\vec{P}\rangle = P_i|\vec{P}\rangle$ for all $i = 1, \ldots, d$. The coordinate representation of these can be calculated using the previously mentioned representation of the momentum operator, such that one obtains

$$\hat{P}_i|\vec{P}\rangle = P_i|\vec{P}\rangle \ , \tag{4.162}$$

$$\langle \vec{q}|\hat{P}_i|\vec{P}\rangle = P_i\langle \vec{q}|\vec{P}\rangle \equiv P_i f_{\vec{P}}(\vec{q}) \ , \tag{4.163}$$

$$\int\limits_{\mathbb{R}^d} \mathrm{d}\omega_{q'} \ \langle \vec{q}|\hat{P}_i|\vec{q}'\rangle\langle \vec{q}'|\vec{P}\rangle = -\imath\hbar \left\{ \partial_i + \frac{1}{4} \left[ \partial_i \log g(\vec{q}) \right] \right\} f_{\vec{P}}(\vec{q}) \ , \tag{4.164}$$

$$P_i f_{\vec{P}}(\vec{q}) = -\imath\hbar \left\{ \partial_i + \frac{1}{4} \left[ \partial_i \log g(\vec{q}) \right] \right\} f_{\vec{P}}(\vec{q}) \ , \tag{4.165}$$

$$\langle \vec{q}|\vec{P}\rangle = f_{\vec{P}}(\vec{q}) = h(\vec{P}) \frac{e^{\imath \frac{\vec{P}\cdot\vec{q}}{\hbar}}}{g^{\frac{1}{4}}(\vec{q})} \ , \tag{4.166}$$

where $f_{\vec{P}}(\vec{q})$ is the coordinate representation of the momentum eigenstate with eigenvalue $\vec{P}$. The function $h(\vec{P})$ can be chosen arbitrarily and does not change any of the dynamics. The orthogonality relation now depends on this function through

$$\langle \vec{P}|\vec{P}'\rangle = \int\limits_{\mathbb{R}^d} \mathrm{d}\omega_q \ \langle \vec{P}|\vec{q}\rangle\langle \vec{q}|\vec{P}'\rangle \tag{4.167}$$

$$= \int\limits_{\mathbb{R}^d} \mathrm{d}\omega_q \ h^*(\vec{P})h(\vec{P}')g^{-\frac{1}{2}}(\vec{q})e^{\imath \frac{\vec{q}\cdot(\vec{P}'-\vec{P})}{\hbar}} \tag{4.168}$$

$$= h^*(\vec{P})h(\vec{P}') \int\limits_{\mathbb{R}^d} \mathrm{d}\vec{x} \ e^{\imath \frac{\vec{q}\cdot(\vec{P}'-\vec{P})}{\hbar}} \tag{4.169}$$

$$= |h|^2(\vec{P})(2\pi\hbar)^d \delta(\vec{P}'-\vec{P}) \equiv \delta(\vec{P}, \vec{P}') \ . \tag{4.170}$$

The integration over momentum space needs to be adapted with

$$\int\limits_{\mathbb{R}^d} \mathrm{d}\omega_p \ \langle \vec{q}|\vec{P}\rangle\langle \vec{P}|\vec{q}'\rangle = \int\limits_{\mathbb{R}^d} \mathrm{d}\omega_p \ |h|^2(\vec{P})g^{-\frac{1}{4}}(\vec{q})g^{-\frac{1}{4}}(\vec{q}')e^{\imath \frac{\vec{P}\cdot(\vec{q}-\vec{q}')}{\hbar}} \tag{4.171}$$

$$= g^{-\frac{1}{4}}(\vec{q})g^{-\frac{1}{4}}(\vec{q}') \frac{1}{(2\pi\hbar)^d} \int\limits_{\mathbb{R}^d} \mathrm{d}\vec{P} \ e^{\imath \frac{\vec{P}\cdot(\vec{q}-\vec{q}')}{\hbar}} = \delta(\vec{q}, \vec{q}') \ , \tag{4.172}$$

which would mean that $\mathrm{d}\omega_p |h|^2(\vec{P}) = \frac{1}{(2\pi\hbar)^d}$. One can formulate the respective momentum representation of the position operator in the same way as before, where $g \to \frac{1}{(2\pi\hbar)^{d/2}|h|^4}$. However, this does not really offer any new insights into the problem, which is why we set $h(\vec{P}) = 1$.

## 4.4.2 Dynamics

On our Hilbert space $\mathcal{H}_M$, we have a matrix of operators $\hat{\mathrm{G}}$, which we call metric tensor operator, since its coordinate representation is equal or at least proportional to the metric tensor $g_{ij}$ of our manifold, see Ref. [34]. This means that the components for $i, j \in \{1, \ldots, d\}$ fulfill

$$\hat{\mathrm{G}}_{ij} = G_{ij}(\hat{\mathrm{q}}_1, \ldots, \hat{\mathrm{q}}_d) \ , \tag{4.173}$$

$$\hat{\mathrm{G}}_{ij} = \hat{\mathrm{G}}_{ji} \ , \tag{4.174}$$

$$\langle \psi | \hat{\mathrm{G}} | \psi \rangle \equiv G \ , \tag{4.175}$$

where $G$ is a real, symmetric, *positive-definite* matrix for $|\psi\rangle \in \mathcal{H}_M$. The dynamics of the particle on the $d$-dimensional manifold is given by the Schrödinger equation

$$\hat{\mathrm{H}}_c |\psi(t)\rangle = \imath \hbar \partial_t |\psi(t)\rangle \ , \tag{4.176}$$

with the Hamilton operator

$$\hat{\mathrm{H}}_c \equiv \hat{\mathrm{T}}_{\mathrm{kin}} + \hat{\mathrm{V}}_{\mathrm{geo}} + \hat{\mathrm{V}}_{\mathrm{latt}} \ . \tag{4.177}$$

The operator $\hat{\mathrm{V}}_{\mathrm{latt}}$ is a static lattice potential felt by the electron,

$$\hat{\mathrm{V}}_{\mathrm{latt}} \equiv V_{\mathrm{latt}}(\hat{\mathrm{q}}_1, \ldots, \hat{\mathrm{q}}_d) \ , \tag{4.178}$$

which does not need to be the same as the lattice potential in the previous section. The operator $\hat{\mathrm{V}}_{\mathrm{geo}}$ is a geometric potential which gets introduced due to the non-Euclidean geometry,

$$\hat{\mathrm{V}}_{\mathrm{geo}} \equiv \xi \hbar^2 \hat{\mathrm{R}} \ , \tag{4.179}$$

$$\hat{\mathrm{R}} = R(\hat{\mathrm{G}}) = R(\hat{\mathrm{q}}_1, \ldots, \hat{\mathrm{q}}_d) \ , \tag{4.180}$$

where $\xi$ is a real number and $R$ is the Ricci scalar of the curved manifold described by the metric tensor $\hat{\mathrm{G}}$. It is necessary to ensure the compatibility of the theory with the correspondence principle [16], i.e. the system should behave classically in the limit of large quantum numbers. Depending on the different procedures for taking the limit of large quantum numbers one finds different values of $\xi$, while at the same time different values of $\xi$ lead to the same classical limit

$$H_c = \frac{1}{2m} \sum_{j,k=1}^{d} G^{jk} P_j P_k + V_{\mathrm{latt}}(\vec{q}) \ . \tag{4.181}$$

This tells us that $\xi$ cannot be determined from the classical theory. There have been several attempts, see Ref. [94], to find a universal value for $\xi$, which have unfortunately been unsuccessful so far. This could imply that there is something missing or wrong in the formulation of a (non-)relativistic quantum system on non-trivial geometries, which would allow to study limiting cases of quantum gravitational systems. However, in our case we want to set up a consistent non-relativistic quantum mechanical theory in curved space, and then try to describe the interaction of an electron with phonons by using the metric for the effective coupling. In addition, we are mainly concerned with quantum mechanical transport properties of the resulting electron-phonon system, which means the behavior around the Fermi energy, i.e. the highest energy level which is occupied by an electron in a system of zero temperature, [98]. Therefore, changes of the electronic energy levels around this energy should be reproduced adequately and there is a priori no need for a specific value of $\xi$, which is why we shall treat it as a free parameter.

The operator $\hat{\mathrm{T}}_{\mathrm{kin}}$ can be seen as a kinetic energy of the particle in curved space,

$$\hat{\mathrm{T}}_{\mathrm{kin}} \equiv \sum_{j,k=1}^{d} \frac{1}{2m} \hat{\mathrm{g}}^{-\frac{1}{4}} \hat{\mathrm{P}}_j \hat{\mathrm{g}}^{\frac{1}{2}} \hat{\mathrm{G}}^{jk} \hat{\mathrm{P}}_k \hat{\mathrm{g}}^{-\frac{1}{4}} \ , \tag{4.182}$$

since it is the only operator that contains the momentum operators. $\hat{\mathrm{G}}^{jk}$ is the $j, k$-th component of the inverse of the metric tensor operator, i.e. $\hat{\mathrm{G}}^{jk} \equiv \hat{\mathrm{G}}_{jk}^{-1}$, $\hat{\mathrm{g}}$ is the determinant of the metric tensor operator $\hat{\mathrm{G}}$. Since the hermitian operator $\hat{\mathrm{H}}_c$ still measures the energy, the operators $\hat{\mathrm{G}}^{ij}$ and $V_{\mathrm{latt}}$ must carry the required units to transform eigenvalues of $P_i, q_j$ to energies.

In order to better understand the underlying group structure and the similarity to Bargmann's superselection rules, the interested reader may consult the work on the relativistic wave equation in Ref. [8].

### 4.4.3 Galilean invariance

For a general introduction to the Galilei group in quantum mechanics we refer the interested reader to Ref. [7]. With the word *consistent* quantum theory on $M$, we mean a Schrödinger equation which is form invariant under general, i.e. also time dependent, point transformations in the coordinate space, which implies Galilean invariance. To see the form-invariance of the theory, one should look at the coordinate representation of the Hamilton operator, which reads

$$\langle \vec{q}|\hat{\mathrm{H}}_c|\psi(t)\rangle = -\frac{\hbar^2}{2m} g^{-1/2}(\vec{q})\partial_i \left[ g^{1/2}(\vec{q})G^{ij}(\vec{q})\partial_j\psi(\vec{q},t)\right] + [V_{\mathrm{geo}}(\vec{q}) + V_{\mathrm{latt}}(\vec{q})]\psi(\vec{q},t) \qquad (4.183)$$

and look at how the metric tensor and lattice potential transform under coordinate transformations $\vec{q}' = \vec{q}'(\vec{q},t)$,

$$g_{ij} = \frac{\partial q'_k}{\partial q_i}\frac{\partial q'_l}{\partial q_j}g'_{kl} \;, \qquad (4.184)$$

$$g = |J(\vec{q},t)|^2 g' \;, \qquad (4.185)$$

$$V_{\mathrm{latt}} = V'_{\mathrm{latt}} - \frac{1}{2}g'_{ij}\frac{\partial q'_i}{\partial t}\frac{\partial q'_j}{\partial t} \;, \qquad (4.186)$$

where $J_{ik}(\vec{q}) \equiv \frac{\partial q_i}{\partial q'_k}$ is the Jacobian. For all types of Galilei transformations, such as translations, rotations, boosts and time translations we know $|J(\vec{q})| = 1$. The Ricci scalar is invariant under coordinate transformations. The proof for time-dependent transformations is done in Ref. [33]. One may be interested to know the generators of infinitesimal coordinate transformations. They can be calculated very easily, since these transformations are represented as unitary operators by

$$\hat{\mathrm{U}} = \mathbb{I} - \frac{\imath}{2\hbar}\left\{\hat{\mathrm{P}}_j, \delta\hat{\mathrm{q}}_j\right\} \;, \qquad (4.187)$$

$$\hat{\mathrm{q}}'_j = \hat{\mathrm{U}}\hat{\mathrm{q}}_j\hat{\mathrm{U}}^{-1} = \hat{\mathrm{q}}_j - \delta\hat{\mathrm{q}}_j \;, \qquad (4.188)$$

$$\hat{\mathrm{P}}'_j = \hat{\mathrm{U}}\hat{\mathrm{P}}_j\hat{\mathrm{U}}^{-1} = \hat{\mathrm{P}}_j + \frac{1}{2}\left\{\hat{\mathrm{P}}_k, \partial_j\delta\hat{\mathrm{q}}_k\right\} \;, \qquad (4.189)$$

where $\delta q_i = \delta q'_i(\vec{q})$ is the transformation rule. An immediate consequence is that infinitesimal translations in the $j$-th coordinate direction are generated by the operator $\hat{\mathrm{P}}_j$. The three different rotations in three dimensions are generated by the angular momentum operator $\hat{\mathrm{J}}_k = \epsilon_{klm}\hat{\mathrm{q}}_l\hat{\mathrm{P}}_l$. In two dimensions, the single type of rotation, where one just fixes the $z$-axis, is generated by $\hat{\mathrm{J}}_3$. For boosts it is important to understand what the velocity operator $\hat{v}_i$ or also just the velocity of the partice looks like in this particular case. It does not hold $\hat{v}_i = \hat{\mathrm{P}}_i/m$. Using the ideas in Ref. [7] one can look at the meaning of velocity as a change of a particle's coordinate in time, one finds

$$\hat{v}_j = \imath[\hat{\mathrm{H}}_c, \hat{\mathrm{q}}_j] = \frac{\hbar}{2m}\{\hat{\mathrm{G}}^{jk}, \hat{\mathrm{P}}_k\} \;. \qquad (4.190)$$

The generator for boosts are given by

$$\hat{\mathrm{K}}_i = \delta v_i t\hat{\mathrm{P}}_i + \hat{\mathrm{F}}_{ij}\delta v_j \;. \qquad (4.191)$$

Using the definition for $\hat{\mathrm{U}}_i = \mathbb{I} - \frac{\imath}{\hbar}\hat{\mathrm{K}}_i$, one finds

$$\hat{\mathrm{q}}'_j = \hat{\mathrm{q}}_j + \frac{\imath}{\hbar}\delta v_k t\left[\hat{\mathrm{q}}_j, \hat{\mathrm{P}}_k\right] = \hat{\mathrm{q}}_j - \delta v_j t \;, \qquad (4.192)$$

$$\hat{v}'_j = \hat{v}_j + \frac{\imath}{2\hbar}\delta v_l\left(\hat{\mathrm{G}}^{jk}\left[\hat{\mathrm{P}}_k, \hat{\mathrm{F}}_{jl}\right] + \left[\hat{\mathrm{P}}_k, \hat{\mathrm{F}}_{jl}\right]\hat{\mathrm{G}}^{kj}\right) \qquad (4.193)$$

$$= \hat{v}_j - \frac{\delta v_l}{2}\left[\hat{\mathrm{G}}^{jk}\partial_k\hat{\mathrm{F}}_{jl} + \left(\partial_k\hat{\mathrm{F}}_{jl}\right)\hat{\mathrm{G}}^{jk}\right] = \hat{v}_j - \delta v_j \;, \qquad (4.194)$$

if we choose $\partial_k \hat{F}_{jl} = \hat{G}_{jk}\delta_{kl}$. As mentioned in Ref. [33] the unitary operator for finite transformations $q'_i = \Lambda_i(\vec{q}, t)$ is given by

$$\hat{U} = e^{-\frac{i}{2\hbar}\{\hat{P}_j, \hat{\Lambda}_j\}} \ . \tag{4.195}$$

Looking at the Schrödinger equation for the dynamics of the particle it is obvious that translations in time are generated by the Hamilton operator. Another problem, which we have not adressed so far is that the operators $\hat{U}$ are not normalized in the new coordinate system, i.e.

$$\hat{U}|\vec{q}\rangle = C^{1/2}|\vec{q} + \delta\vec{q}\rangle \ , \tag{4.196}$$

where $C \in \mathbb{C}$ needs to be determined, since we are transforming in a non-Euclidean space, where the volume element is changing as well. As it turns out by looking at the infinitesimal change for $\langle\vec{q}|\hat{U}^{-1}|\psi\rangle = \left(C^{1/2}\right)^* \langle\vec{q} + \delta\vec{q}|\psi\rangle$ one finds

$$C = 1 + \sum_{i=1}^{d} \left[ \frac{\partial\delta q_i}{\partial q_i} + \frac{1}{2} \left.\frac{\partial\log g}{\partial q_i}\right|_{\vec{q}} \delta q_i \right] \ . \tag{4.197}$$

It is instructive to see what happens for a concrete simple example, such as a translation.

**Translation**

The action of the translation operator is defined through

$$\hat{T}_{\vec{a}}|\vec{q}\rangle \equiv C^{1/2}(\vec{q}, \vec{a})|\vec{q} + \vec{a}\rangle \ , \tag{4.198}$$

$$\langle\vec{q}'|\hat{T}_{\vec{a}}|\vec{q}\rangle = C^{1/2}(\vec{q}, \vec{a})\langle\vec{q}'|\vec{q} + \vec{a}\rangle = C^{1/2}(\vec{q}, \vec{a})\delta(\vec{q}', \vec{q} + \vec{a}) \ , \tag{4.199}$$

with $C^{1/2}(\vec{q}, \vec{a}) \in \mathbb{C}$ and $\vec{a} \in \mathbb{R}^d$ a translation vector. We demand that the translation operators commute and that they are unitary. From the second property, it follows for the parameter $C$

$$\langle\vec{q}_1|\hat{T}_{\vec{a}}\hat{T}_{\vec{a}}^\dagger|\vec{q}_2\rangle = \langle\vec{q}_1|\mathbb{I}|\vec{q}_2\rangle = \delta(\vec{q}_1, \vec{q}_2) \tag{4.200}$$

$$= \int_{\mathbb{R}^d} d\omega_q \ \langle\vec{q}_1|\hat{T}_{\vec{a}}|\vec{q}\rangle\langle\vec{q}|\hat{T}_{\vec{a}}^\dagger|\vec{q}_2\rangle \tag{4.201}$$

$$= \int_{\mathbb{R}^d} d\omega_q \ C^{1/2}(\vec{q}, \vec{a})\langle\vec{q}_1|\vec{q} + \vec{a}\rangle \left(\langle\vec{q}_2|\hat{T}_{\vec{a}}|\vec{q}\rangle\right)^\dagger \tag{4.202}$$

$$= \int_{\mathbb{R}^d} d\omega_q \ C^{1/2}(\vec{q}, \vec{a})\delta(\vec{q}_1, \vec{q} + \vec{a}) \left(C^{1/2}(\vec{q}, \vec{a})\langle\vec{q}_2|\vec{q} + \vec{a}\rangle\right)^\dagger \tag{4.203}$$

$$= \int_{\mathbb{R}^d} d\omega_q \ |C(\vec{q}, \vec{a})|\delta(\vec{q}_1, \vec{q} + \vec{a})\delta(\vec{q}_2, \vec{q} + \vec{a}) \tag{4.204}$$

$$= \int_{\mathbb{R}^d} d\omega_{q'} \ \sqrt{\frac{g(\vec{q}' - \vec{a})}{g(\vec{q}')}} \ |C(\vec{q}' - \vec{a}, \vec{a})|\delta(\vec{q}_1, \vec{q}')\delta(\vec{q}_2, \vec{q}') \tag{4.205}$$

$$= \sqrt{\frac{g(\vec{y} - \vec{a})}{g(\vec{y})}}|C(\vec{y} - \vec{a}, \vec{a})|\delta(\vec{q}_2, \vec{q}_1) \ , \tag{4.206}$$

$$|C^{1/2}(\vec{q}, \vec{a})| = \left(\frac{g(\vec{q} + \vec{a})}{g(\vec{q})}\right)^{1/4} \ . \tag{4.207}$$

Therefore, we make the definition

$$\hat{T}_{\vec{a}}|\vec{q}\rangle \equiv \left(\frac{g(\vec{q} + \vec{a})}{g(\vec{q})}\right)^{1/4} |\vec{q} + \vec{a}\rangle \ . \tag{4.208}$$

The reader should observe again, that if the translation maps the coordinates $\vec{q}$ to new coordinates $\vec{q} + \vec{a}$ which are outside of the domains of the atlas of the respective manifold, the state will become zero and hence does not contribute to the expectation values. From this definition and property

(*a*) we obtain

$$\hat{T}_{\vec{a}'}\hat{T}_{\vec{a}}|\vec{q}\rangle = C^{1/2}(\vec{q},\vec{a})C^{1/2}(\vec{q}+\vec{a},\vec{a}')|\vec{q}+\vec{a}+\vec{a}'\rangle \ , \tag{4.209}$$

$$C^{1/2}(\vec{q},\vec{a})C^{1/2}(\vec{q}+\vec{a},\vec{a}') = \left(\frac{g(\vec{q}+\vec{a})}{g(\vec{q})}\frac{g(\vec{q}+\vec{a}+\vec{a}')}{g(\vec{q}+\vec{a})}\right)^{1/4} \ , \tag{4.210}$$

$$\hat{T}_{\vec{a}}\hat{T}_{\vec{a}'}|\vec{q}\rangle = C^{1/2}(\vec{q},\vec{a}')C^{1/2}(\vec{q}+\vec{a}',\vec{a})|\vec{q}+\vec{a}'+\vec{a}\rangle \ , \tag{4.211}$$

$$C^{1/2}(\vec{q},\vec{a}')C^{1/2}(\vec{q}+\vec{a}',\vec{a}) = \left(\frac{g(\vec{q}+\vec{a}')}{g(\vec{q})}\frac{g(\vec{q}+\vec{a}'+\vec{a})}{g(\vec{q}+\vec{a}')}\right)^{1/4} \ , \tag{4.212}$$

$$\hat{T}_{\vec{a}+\vec{a}'}|\vec{q}\rangle = C^{1/2}(\vec{q},\vec{a}+\vec{a}')|\vec{q}+\vec{a}+\vec{a}'\rangle \ , \tag{4.213}$$

$$C^{1/2}(\vec{q},\vec{a}+\vec{a}') = \left(\frac{g(\vec{q}+\vec{a}+\vec{a}')}{g(\vec{q})}\right)^{1/4} \ , \tag{4.214}$$

$$C^{1/2}(\vec{q},\vec{a})C^{1/2}(\vec{q}+\vec{a},\vec{a}') = C^{1/2}(\vec{q},\vec{a}')C^{1/2}(\vec{q}+\vec{a}',\vec{a}) = C^{1/2}(\vec{q},\vec{a}+\vec{a}') \ , \tag{4.215}$$

for all vectors $\vec{a}$ and $\vec{a}'$. From there, we conclude

$$\hat{T}_{\vec{0}} = \mathbb{I} \ , \tag{4.216}$$

$$\hat{T}_{\vec{a}}^{-1} = \hat{T}_{-\vec{a}} \ , \tag{4.217}$$

$$\langle\vec{q}|\hat{T}_{\vec{a}} = \left(\hat{T}_{\vec{a}}^{\dagger}|\vec{q}\rangle\right)^{\dagger} = \left(\hat{T}_{-\vec{a}}|\vec{q}\rangle\right)^{\dagger} = \langle\vec{q}-\vec{a}|\left(\frac{g(\vec{q}-\vec{a})}{g(\vec{q})}\right)^{1/4} \ . \tag{4.218}$$

**Rotation**

The action of the rotation operator in $d=3,2$-dimensional curved space is defined through

$$\hat{R}_{\vec{\alpha}}|\vec{q}\rangle \equiv C^{1/2}(\vec{\alpha},\vec{q})|R_{\vec{\alpha}}\vec{q}\rangle \ , \tag{4.219}$$

where $\vec{\alpha}$ uniquely characterizes the rotation in $d=2$ or 3 and $R_{\vec{\alpha}}$ is the orthogonal rotation matrix. In $d=2$ $\alpha$ has only one component, whereas in $d=3$ it has three components, where one could for instance identify the direction $\vec{\alpha}/|\vec{\alpha}|$ with the rotation axis and the length $|\vec{\alpha}|$ with the angle of the counterclockwise rotation around that axis. For further explanation of this concept see Ref. [134]. Another important difference is that for $d=2$ rotations commute, whereas in 3 dimensions they only commute if they are performed around the same axis. To determine the constant $C^{1/2}$ we use that the symmetry operator is unitary, i.e.

$$\langle\vec{q}_1|\hat{R}_{\vec{\alpha}}\hat{R}_{\vec{\alpha}}^{\dagger}|\vec{q}_2\rangle = \langle\vec{q}_1|\mathbb{I}|\vec{q}_2\rangle = \delta(\vec{q}_1,\vec{q}_2) \tag{4.220}$$

$$= \int_{\mathbb{R}^d}\mathrm{d}\omega_q \ \langle\vec{q}_1|\hat{R}_{\vec{\alpha}}|\vec{q}\rangle\langle\vec{q}|\hat{R}_{\vec{\alpha}}^{\dagger}|\vec{q}_2\rangle \tag{4.221}$$

$$= \int_{\mathbb{R}^d}\mathrm{d}\omega_q \ C^{1/2}(\vec{q},\vec{\alpha})\langle\vec{q}_1|R_{\vec{\alpha}}\vec{q}\rangle\left(\langle\vec{q}_2|\hat{R}_{\vec{\alpha}}|\vec{q}\rangle\right)^{\dagger} \tag{4.222}$$

$$= \int_{\mathbb{R}^d}\mathrm{d}\omega_q \ |C(\vec{q},\vec{\alpha})|\delta(\vec{q}_1,R_{\vec{\alpha}}\vec{q})\delta(\vec{q}_2,R_{\vec{\alpha}}\vec{q}) \tag{4.223}$$

$$= \int_{\mathbb{R}^d}\mathrm{d}\vec{q} \ \sqrt{g(R_{\vec{\alpha}}^{-1}\vec{q})}|C(R_{\vec{\alpha}}^{-1}\vec{q},\vec{\alpha})|\delta(\vec{q}_1,\vec{q})\delta(\vec{q}_2,\vec{q}) \tag{4.224}$$

$$= \sqrt{\frac{g(R_{\vec{\alpha}}^{-1}\vec{q}_1)}{g(\vec{q}_1)}}|C(R_{\vec{\alpha}}^{-1}\vec{q}_1,\vec{\alpha})|\delta(\vec{q}_1,\vec{q}_2) \ . \tag{4.225}$$

Therefore, we define the rotation operator by the action

$$\hat{R}_{\vec{\alpha}}|\vec{q}\rangle \equiv \left(\frac{g(R_{\vec{\alpha}}\vec{q})}{g(\vec{q})}\right)^{1/4}|R_{\vec{\alpha}}\vec{q}\rangle \ . \tag{4.226}$$

Using this definition, we find the action of two consecutive rotations

$$\hat{R}_{\vec{\alpha}}\hat{R}_{\vec{\alpha}'}|\vec{q}\rangle = \left(\frac{g(R_{\vec{\alpha}'}\vec{q})}{g(\vec{q})}\right)^{1/4} \hat{R}_{\vec{\alpha}}|R_{\vec{\alpha}'}\vec{q}\rangle \tag{4.227}$$

$$= \left(\frac{g(R_{\vec{\alpha}'}\vec{q})}{g(\vec{q})}\right)^{1/4} \left(\frac{g(R_{\vec{\alpha}}R_{\vec{\alpha}'}\vec{q})}{g(R_{\vec{\alpha}'}\vec{q})}\right)^{1/4} |R_{\vec{\alpha}}R_{\vec{\alpha}'}\vec{q}\rangle \tag{4.228}$$

$$= \left(\frac{g(R_{\vec{\alpha}}R_{\vec{\alpha}'}\vec{q})}{g(\vec{q})}\right)^{1/4} |R_{\vec{\alpha}}R_{\vec{\alpha}'}\vec{q}\rangle \ . \tag{4.229}$$

This tells us that the operators $\hat{R}_{\vec{\alpha}}$ and $\hat{R}_{\vec{\alpha}'}$ commute if the underlying rotations commute.

### 4.4.4 Electronic Bloch states in curved space

The reader might wonder, how the Bloch states, which we have introduced in section 4.3, look like for an electron on a generalized manifold and if the same ideas apply as in the Euclidean space. In the original problem the commutation of the kinetic energy as well as the commutation of the static lattice potential with translations by a lattice vector, showed us that it is possible to construct common eigenbasis of the discrete translation operator and the non-interacting single-electron Hamilton operator. Therefore, it seems to be a good start to determine what happens to an operator $\hat{V} = V(\hat{\vec{q}}_1, \ldots, \hat{q}_d)$ for a translation in the coordinate space of the manifold. The commutator becomes

$$\langle\vec{q}|\left[\hat{T}_{\vec{n}}, \hat{V}\right]|\psi\rangle = \int_\Omega dV_{x'} \ \langle\vec{q}|\left[\hat{T}_{\vec{n}}, \hat{V}\right]|\vec{q}'\rangle\langle\vec{q}'|\psi\rangle \tag{4.230}$$

$$= \int_{\mathbb{R}^d} d\omega_{q'} \ \left[\left(\frac{g(\vec{q}-\vec{a})}{g(\vec{q})}\right)^{\frac{1}{4}} V(\vec{q}')\langle\vec{q}-\vec{a}|\vec{q}'\rangle\right.$$

$$\left. - \left(\frac{g(\vec{q}'+\vec{a})}{g(\vec{q}')}\right)^{\frac{1}{4}} V(\vec{q})\langle\vec{q}|\vec{q}'+\vec{a}\rangle\right] \psi(\vec{q}') \tag{4.231}$$

$$= \left(\frac{g(\vec{q}-\vec{a})}{g(\vec{q})}\right)^{\frac{1}{4}} V(\vec{q}-\vec{a})\psi(\vec{q}-\vec{a})$$

$$- \int_{\mathbb{R}^d} d\omega_{q'} \ \left(\frac{g(\vec{q}'-\vec{a})}{g(\vec{q}')}\right)^{\frac{1}{4}} V(\vec{q})\langle\vec{q}|\vec{q}'\rangle\psi(\vec{q}'-\vec{a}) \tag{4.232}$$

$$= \left(\frac{g(\vec{q}-\vec{a})}{g(\vec{q})}\right)^{\frac{1}{4}} \psi(\vec{q}-\vec{a})\left[V(\vec{q}-\vec{a}) - V(\vec{q})\right] \ . \tag{4.233}$$

If the coordinate-space representation $V(\vec{q})$ is symmetric under a simple translation from $\vec{q} \to \vec{q} + \vec{a}$ then the operator will commute with the translation operator. The other important commutator is

$$\left[\hat{T}_{\vec{n}}, \hat{P}_i\hat{G}^{ij}\hat{P}_j\right] = \left[\hat{T}_{\vec{n}}, \hat{P}_i\right] \hat{G}^{ij}\hat{P}_j + \hat{P}_i \left[\hat{T}_{\vec{n}}, \hat{G}^{ij}\right] \hat{P}_j + \hat{P}_i\hat{G}^{ij} \left[\hat{T}_{\vec{n}}, \hat{P}_j\right] \ . \tag{4.234}$$

To calculate the commutator with the momentum operator defined by Eq. (4.157), we work in the momentum basis and find

$$\langle \vec{P}' | \left[ \hat{T}_{\vec{a}}, \hat{P}_i \right] | \psi \rangle = \int\limits_{\mathbb{R}^d} \mathrm{d}\omega_P \ (P_i - P_i') \langle \vec{P}' | \hat{T}_{\vec{a}} | \vec{P} \rangle \langle \vec{P} | \psi \rangle \ , \tag{4.235}$$

$$\langle \vec{P}' | \hat{T}_{\vec{a}} | \vec{P} \rangle = \int\limits_{\mathbb{R}^d} \mathrm{d}\omega_x \ \langle \vec{P}' | \hat{T}_{\vec{a}} | \vec{q} \rangle \langle \vec{q} | \vec{P} \rangle \ , \tag{4.236}$$

$$= \int\limits_{\mathbb{R}^d} \mathrm{d}\vec{q} \ g^{\frac{1}{4}}(\vec{q} + \vec{a}) g^{\frac{1}{4}}(\vec{q}) \langle \vec{P} | \vec{q} + \vec{a} \rangle \langle \vec{q} | \vec{P}' \rangle \ , \tag{4.237}$$

$$= e^{-i \frac{\vec{P}' \cdot \vec{a}}{\hbar}} \delta(\vec{p}, \vec{p}') \ , \tag{4.238}$$

where we have used Eqs. (4.166) and (4.208). The action on a state $|\psi\rangle$ can be written as

$$\int\limits_{\mathbb{R}^d} \mathrm{d}\omega_P \ (P_i - P_i') \delta(\vec{P}, \vec{P}') e^{-i \frac{\vec{P}' \cdot \vec{a}}{\hbar}} \psi(\vec{P}) = 0 \ , \tag{4.239}$$

and hence shows $\left[ \hat{T}_{\vec{a}}, \hat{P}_i \right] = 0$. Consequently, the ability of the kinetic energy operator to commute with a translation operator depends solely on the metric tensor operator. The issue is that we do not know the operator yet, and we need to assume that it does not commute in the same way as the static lattice potential. Furthermore, although we have defined a kinetic energy operator it is not clear which parts belong to a physical definition of a kinetic energy. From the point of the construction of the Hamilton operator in Ref. [33], the operator $\hat{T}_{\mathrm{kin}} + \hat{V}_{\mathrm{geo}}$ would measure the free particle energy and hence should be seen as a kinetic energy, which makes the computation of a Bloch state even more cumbersome.

For a minimum viable example, let us consider the case of $d = 1$, a general metric $G(q)$ and periodic boundary conditions at the end of the domain $[0, L] \subset \mathbb{R}$. In this case, we can write down the eigenstates of this free-particle operator, which read

$$\psi_n(q) = C e^{\sqrt{G(q)}/2} e^{i \int\limits_0^q \mathrm{d}q' \ \sqrt{k_n^2 + \frac{1}{2} G''(q') - \frac{1}{4} [G'(q')]^2}} \ , \tag{4.240}$$

and each eigenvalue fulfills the equation

$$\int\limits_0^L \mathrm{d}q' \ \sqrt{k_n^2 + \frac{1}{2} G''(q') - \frac{1}{4} [G'(q')]^2} = 2\pi n \ , \tag{4.241}$$

with $n \in \mathbb{N}$. The negative values can be obtained when looking at the momentum of these states. For a sensible approach, we needed to impose the periodic boundary conditions to $G$ as well. In higher dimensions, we could not find general solutions for arbitrary metric tensors. However, in the case of a diagonal metric tensor with the form $G_{ii} = f(q_i)$ one can use the separation of variables technique to find independent one-dimensional waves, which allows to tackle the problem. The solution is a simple product of $d$ waves of the same form as shown in the previous equation. Independent of this discussion, there is a much deeper problem for the relation between the curved space approach and the usual electron-phonon interaction, which we shall elaborate on in the next section.

## 4.5 Nonequivalence theorem

For a quick overview, reminder and anticipation of what we are going to show, we give an overview about the relation between the Euclidean and Riemannian non-relativistic quantum systems in table 4.5.

| property | **Flat** | **Curved** |
|---|---|---|
| geometry | Euclidean $(\mathbb{R}^d, E)$ | Riemannian $(M, g)$ |
| metric | $\hat{G}_{ij} = \mathbb{I}\delta_{ij}$ | $\hat{G}_{ij} = \mathbb{I}\delta_{ij} + \delta\hat{G}_{ij}$ |
| algebra | $[\hat{r}_j, \hat{p}_k] = \imath\hbar\mathbb{I}\delta_{jk}$ | $\left[\hat{x}_j, \hat{P}_k\right] = \imath\hbar\mathbb{I}\delta_{jk}$ |
| coordinates | $\hat{r}_i|\vec{r}\rangle = r_i|\vec{r}\rangle$ w/ $r_i \in \mathbb{R}$ | $\hat{x}_i|\vec{x}\rangle = x_i|\vec{x}\rangle$ w/ $x_i \in \mathbb{R}$ |
| probability | $|\psi(\vec{r})|^2 \mathrm{d}\vec{r}$ | $\sqrt{g(\vec{x})}|\psi(\vec{x})|^2 \mathrm{d}\vec{x}$ |
| function $|\psi\rangle$ | $L^2(\mathbb{R}^d)$ | $L^2(M)$ |
| free particle | $\frac{\hat{p}_i\hat{p}_i}{2m}$ | $\frac{1}{2m}\frac{1}{\hat{g}^{\frac{1}{4}}}\hat{P}_j\hat{g}^{\frac{1}{2}}\hat{G}^{jk}\hat{P}_k\frac{1}{\hat{g}^{\frac{1}{4}}} + \hat{V}_{\text{geo}}$ |
| Galilei | invariant | invariant |
| potential | $\hat{V}_{\text{latt}}$ | $\hat{V}_{\text{latt}}$ |
| $\sigma_{v_j}\sigma_{x_k} \geq$ | $\frac{\hbar}{m}\delta_{jk}$ | $\frac{\hbar}{m}|\langle\psi_c|\hat{G}^{jk}|\psi_c\rangle|$ |

The goal of this section is to prove that the "flat" quantum system $S_1$ described by the Hilbert space $\mathcal{H}_{\text{el}}$ of complex-valued square-integrable functions over the $d$-dimensional volume $V = [0, L] \times \cdots \times [0, L] \subset \mathbb{R}^d$, the set of operators $\{\hat{x}_1, \hat{p}_1, \hat{x}_2, \hat{p}_2, \ldots, \hat{x}_d, \hat{p}_d\}$ with their usual canonical commutation relations and the Hamilton operator $\hat{H}_1 \equiv \hat{H}_{\text{el}}$ from Eq. (4.70), *and* the "curved" quantum system $S_2$ described by the Hilbert space $\mathcal{H}_M$ of complex-valued square-integrable functions over the $d$-dimensional Riemannian manifold $M$ with metric $g_{ij}$, the set of operators $\{\hat{q}_1, \hat{P}_1, \ldots, \hat{q}_d, \hat{P}_d\}$, which fulfill the usual canonical commutation relations, and the Hamilton operator $\hat{H}_2 \equiv \hat{H}_c$ from Eq. (4.177) cannot be equivalent. With equivalent, we mean that they describe the same physical system.

The proof goes along the following lines: If they describe the same physical system, all the observations in $S_1$ and $S_2$ must be the same. More precisely, it means that for any measurable observables $\hat{O}_1$ in $S_1$ and $\hat{O}_2$ in $S_2$, that have the same meaning, one finds the same eigenvalues. Consequently, there exists a unitary transformation $\hat{U}$ from system $S_2$ to $S_1$ which transforms the set of basic operators from $\{\hat{q}_1, \hat{P}_1, \hat{q}_2, \hat{P}_2, \ldots, \hat{q}_d, \hat{P}_d\}$ to the set $\{\hat{x}_1, \hat{p}_1, \ldots, \hat{x}_d, \hat{p}_d\} = \{\hat{U}\hat{q}_1\hat{U}^{-1}, \hat{U}\hat{P}_1\hat{U}^{-1}, \ldots, \hat{U}\hat{q}_d\hat{U}^{-1}, \hat{U}\hat{P}_d\hat{U}^{-1}\}$. Our measurable observable $\hat{O}_1$ hence transforms like $\hat{O}_1 = \hat{U}\hat{O}_2\hat{U}^{-1}$. In order to analyze the equivalence claim we make the comparison of the observables $\hat{A}_{jk}^{(1)} \equiv \left[\left[\hat{H}_1, \hat{x}_j\right], \hat{x}_k\right]$ in $S_1$ and $\hat{A}_{jk}^{(2)} \equiv \left[\left[\hat{H}_2, \hat{q}_j\right], \hat{q}_k\right]$ in $S_2$. The first thing, we need to prove is that both operators are indeed observables, i.e. hermitian operators. Looking at $\hat{A}_{jk}^{(1)}$ we find

$$\left(\hat{A}_{jk}^{(1)}\right)^\dagger = -\left[\left(\left[\hat{H}_1, \hat{x}_j\right]\right)^\dagger, \hat{x}_k\right] = \left[\left[\hat{H}_1, \hat{x}_j\right], \hat{x}_k\right] = \hat{A}_{jk}^{(1)} , \tag{4.242}$$

where we have used

$$\left(\left[\hat{B}_1, \hat{B}_2\right]\right)^\dagger = \left(\hat{B}_1\hat{B}_2\right)^\dagger - \left(\hat{B}_2\hat{B}_1\right)^\dagger = \hat{B}_2\hat{B}_1 - \hat{B}_1\hat{B}_2 = -\left[\hat{B}_1, \hat{B}_2\right] , \tag{4.243}$$

assuming $\hat{B}_{1,2}$ are hermitian. Of course, the same calculation holds for $\hat{A}_{jk}^{(2)}$. Second, we analyze their expression in form of the position and momentum operators. Looking at Eq. (4.132) for $\hat{H}_1$, we find

$$\hat{A}_{jk}^{(1)} = \sum_{l=1}^{d} \frac{1}{2m}\left[[\hat{p}_l\hat{p}_l, \hat{x}_j], \hat{x}_k\right] = -\frac{\imath\hbar}{m}[\hat{p}_j, \hat{x}_k] = -\frac{\hbar^2}{m}\delta_{jk}\mathbb{I} . \tag{4.244}$$

To determine the form of $\hat{A}_{jk}^{(2)}$ we want to show some important derivations for the operator $\hat{H}_2$.

Looking at $\hat{T}_{\text{kin}}$ we can write

$$\hat{T}_{\text{kin}} = \frac{1}{2m} \sum_{j,k=1}^{d} \hat{g}^{-\frac{1}{4}} \hat{P}_j \hat{g}^{\frac{1}{2}} \hat{G}^{jk} \hat{P}_k \hat{g}^{-\frac{1}{4}} \tag{4.245}$$

$$= \frac{1}{2m} \sum_{j,k=1}^{d} \left( \left[ \hat{g}^{-\frac{1}{4}}, \hat{P}_j \right] + \hat{P}_j \hat{g}^{-\frac{1}{4}} \right) \hat{g}^{\frac{1}{2}} \hat{G}^{jk} \left( \left[ \hat{P}_k, \hat{g}^{-\frac{1}{4}} \right] + \hat{g}^{-\frac{1}{4}} \hat{P}_k \right) \tag{4.246}$$

$$= \frac{1}{2m} \sum_{j,k=1}^{d} \left( \hat{P}_j \hat{G}^{jk} \hat{P}_k + \left[ \hat{g}^{-\frac{1}{4}}, \hat{P}_j \right] \hat{g}^{\frac{1}{4}} \hat{G}^{jk} \hat{P}_k - \hat{P}_j \hat{g}^{\frac{1}{4}} \hat{G}^{jk} \left[ \hat{g}^{-\frac{1}{4}}, \hat{P}_k \right] \right.$$
$$\left. - \left[ \hat{g}^{-\frac{1}{4}}, \hat{P}_j \right] \hat{g}^{\frac{1}{2}} \hat{G}^{jk} \left[ \hat{g}^{-\frac{1}{4}}, \hat{P}_k \right] \right) \tag{4.247}$$

$$= \frac{1}{2m} \sum_{j,k=1}^{d} \left( \hat{P}_j \hat{G}^{jk} \hat{P}_k + \left[ \left[ \hat{g}^{-\frac{1}{4}}, \hat{P}_j \right] \hat{g}^{\frac{1}{4}} \hat{G}^{jk}, \hat{P}_k \right] - \left[ \hat{g}^{-\frac{1}{4}}, \hat{P}_j \right] \hat{g}^{\frac{1}{2}} \hat{G}^{jk} \left[ \hat{g}^{-\frac{1}{4}}, \hat{P}_k \right] \right) \tag{4.248}$$

$$= \frac{1}{2m} \sum_{j,k=1}^{d} \left[ \hat{P}_j \hat{G}^{jk} \hat{P}_k + \frac{\hbar^2}{16} \left( 4 \frac{\partial^2 \hat{g}}{\partial \hat{q}_j \partial \hat{q}_k} \hat{G}^{jk} + 4 \frac{\partial \hat{g}}{\partial \hat{q}_j} \frac{\partial \hat{G}^{jk}}{\partial \hat{q}_k} + \frac{\partial \hat{g}}{\partial \hat{q}_j} \hat{G}^{jk} \frac{\partial \hat{g}}{\partial \hat{q}_k} \right) \right] \tag{4.249}$$

where we have used that the commutator of a function of position operators with the momentum operator acts like a derivative, i.e.

$$\left[ \hat{g}^{-\frac{1}{4}}, \hat{P}_j \right] = -\frac{\imath \hbar}{4} \frac{\partial \hat{g}}{\partial \hat{q}_j} \hat{g}^{-1/4} \ , \tag{4.250}$$

$$\left[ \left[ \hat{g}^{-\frac{1}{4}}, \hat{P}_j \right] \hat{g}^{\frac{1}{4}} \hat{G}^{jk}, \hat{P}_k \right] = -\frac{\imath \hbar}{4} \left[ \frac{\partial \hat{g}}{\partial \hat{q}_j} \hat{G}^{jk}, \hat{P}_k \right] = \frac{\hbar^2}{4} \left( \frac{\partial^2 \hat{g}}{\partial \hat{q}_j \partial \hat{q}_k} \hat{G}^{jk} + \frac{\partial \hat{g}}{\partial \hat{q}_j} \frac{\partial \hat{G}^{jk}}{\partial \hat{q}_k} \right) \tag{4.251}$$

is only a function of position operators and hence commutes with $\hat{G}^{jk}$, as well as $\hat{G}^{jk} = \hat{G}^{kj}$. The underlying reason, that the commutator with $\hat{P}_k$ acts like the $k$-th derivative, is the canonical commutation between position and momentum. The derivatives of an operator function are understood with respect to the multi-dimensional Taylor series of this operator, i.e. one sets

$$\hat{g} = \sum_{|\alpha|=0}^{\infty} \frac{\partial^\alpha g(\vec{0})}{\alpha!} \hat{q}_1^{\alpha_1} \cdots \hat{q}_d^{\alpha_d} \ , \tag{4.252}$$

with the multi-index $\alpha$. Consequently, the operator $\hat{H}_2$ can be written as

$$\hat{H}_2 = \frac{1}{2m} \sum_{j,k=1}^{d} \hat{P}_j \hat{G}^{jk} \hat{P}_k + V(\hat{q}_1, \ldots, \hat{q}_d) \ , \tag{4.253}$$

which makes the calculation for the observable $\hat{A}_{jk}^{(2)}$ particularly simple and we get

$$\hat{A}_{jk}^{(2)} = \frac{1}{2m} \sum_{l,m=1}^{d} \left[ \left[ \hat{P}_l \hat{G}^{lm} \hat{P}_m, \hat{q}_j \right], \hat{q}_k \right] = -\frac{\hbar^2}{m} \hat{G}^{jk} \ . \tag{4.254}$$

This tells us that the components of the metric tensor operator are measurable observables and it hence needs to be a hermitian operator. This restriction has already been made at the beginning of this section. Furthermore, we come to the central conclusion of this section, which is that if the two quantum systems were equivalent, it would have to hold

$$\hat{A}_{jk}^{(2)} = \hat{U} \hat{A}_{ij}^{(1)} \hat{U}^\dagger \ , \tag{4.255}$$

see Ref. [137]. And therefore we would find

$$\hat{G}^{jk} \propto \delta_{jk} \hat{U} \mathbb{I} \hat{U}^\dagger = \delta_{jk} \mathbb{I} \ , \tag{4.256}$$

which means that the manifold needs to be flat, since the metric is proportional to $\delta_{jk}$. However, if $\hat{G}_{ij} = \delta_{ij}$ all the remaining terms in the operator $\hat{H}_2$ which contain operator derivatives of $\hat{G}_{ij}$ with respect to the generalized position operators will vanish, which would imply no interaction between electrons and phonons in the curved space approach, and is an obvious contradiction to the demand that the two system describe the same physical system. Consequently, the two quantum systems $S_1$ and $S_2$ are not equivalent, *since we do not obtain the same physical observations.* This concludes the proof.

It holds in general for any Hamilton operator of the type $\sum_{i=1}^{d} \hat{p}_i \hat{p}_i + V(\hat{x}_1, \hat{p}_1, \ldots, \hat{x}_d, \hat{p}_d)$ if $V$ depends only linearly on $\hat{p}_i$ for all $i \in \{1, \ldots, d\}$. Therefore, we make the following statement: The non-relativistic quantum system of $N$ particles in Euclidean space $\mathbb{R}^{Nd}$ that interact with an external electromagnetic field, is **not equivalent** to another non-relativistic quantum system of particles moving on an $Nd$-dimensional Riemannian manifold with a non-trivial metric, since the components of the metric tensor operator are observables. What is the meaning of the quantities $\hat{A}_{ij}^{(1,2)}$? According to subsection 4.4.3, the generalized velocity is measured by the operator

$$\hat{V}_j = \frac{\iota}{\hbar} \left[ \hat{H}_2, \hat{q}_j \right] \ , \tag{4.257}$$

and hence the operators $\hat{A}_{ij}^{(1,2)}$ tell us the uncertainty relation between the (generalized) velocity $\hat{V}_j$ and the (generalized) position measurement $\hat{q}_k$ similar to the famous Heisenberg uncertainty relation ([137]), which are

$$\sigma_{v_j} \sigma_{x_k} = \sqrt{\langle \hat{v}_j^2 \rangle - \langle \hat{v}_j \rangle^2} \sqrt{\langle \hat{x}_k^2 \rangle - \langle \hat{x}_k \rangle^2} \geq \frac{1}{2} |\langle [\hat{v}_j, \hat{x}_k] \rangle| = \frac{\hbar}{2m} \delta_{jk} \ , \tag{4.258}$$

$$\sigma_{V_j} \sigma_{q_k} = \sqrt{\langle \hat{V}_j^2 \rangle - \langle \hat{V}_j \rangle^2} \sqrt{\langle \hat{q}_k^2 \rangle - \langle \hat{q}_k \rangle^2} \geq \frac{1}{2} \left| \left\langle \left[ \hat{V}_j, \hat{q}_k \right] \right\rangle \right| = \frac{\hbar}{2m} |\langle \hat{G}^{jk} \rangle| \ . \tag{4.259}$$

If we prepare quantum states $|\psi_1\rangle \in \mathcal{H}_{el}$, $|\psi_2\rangle \in \mathcal{H}_M$ and measure the standard deviation of simultaneous position and velocity measurements we shall find a state-independent lower bound in $S_1$, whereas in $S_2$ the bound depends on $|\langle \psi_2 | \hat{G}^{jk} | \psi_2 \rangle|$, the absolute value of the expectation value of the component of the metric tensor. The deeper reason behind this discrepancy seems to be the spatial spread of the wave function which gives even local measurements information about distant areas of space and hence makes the effects of curvature locally observable in contrast to the principle of general relativity.

Nevertheless, we can also take a more pragmatic approach to the problem by demanding that only the energy measurements agree for a limited set of states. In the next section, we shall explore how far this idea can bring us.

## 4.6 Weak equivalence theorem

Despite the shortcomings, which we have mentioned in the previous section, we want to see if we can establish a weak equivalence.

With weak equivalence we mean that the matrix representation of the Hamilton operator $\hat{H}_2$ in the eigenbasis of $\hat{H}_1$ is identitcal to the diagonal representation of $\hat{H}_1$.

For the proof, we are further developing an idea from Ref. [94]. It goes along the following lines. First, we work in the Hilbert space $\mathcal{H}$ with the usual set of position and momentum operators $\{\hat{x}_1, \hat{p}_1, \ldots, \hat{x}_d, \hat{p}_d\}$ in the Euclidean space $\mathbb{R}^d$ and the *Hamilton* operator

$$\hat{H}' \equiv \frac{1}{2m} \sum_{i=1}^{d} \hat{p}_i \hat{p}_i + V(\hat{x}_1, \ldots, \hat{x}_d) - E \ . \tag{4.260}$$

We assume that this operator has a countable complete orthonormal eigenbasis $\{|\psi_n\rangle\}_{n \in \mathbb{N}}$, i.e.

$$\langle \vec{x} | \hat{H}' | \psi_n \rangle = \left[ -\frac{1}{2m} \sum_{i=1}^{d} \frac{\partial^2}{\partial x_i^2} + V(\vec{x}) - E \right] \psi_n(\vec{x}) = (E_n - E) \psi_n(\vec{x}) \equiv \delta E_n \psi_n(\vec{x}) \ . \tag{4.261}$$

Second, we work in two Hilbert spaces $\mathcal{H}_{\pm}$. On each of these spaces we define a set of (generalized) position and momentum operators $\{\hat{q}_{\pm,1}, \hat{P}_{\pm,1}, \ldots, \hat{q}_{\pm,d}, \hat{P}_{\pm,d}\}$ which measure the coordinates

and momenta on the $d$-dimensional Riemannian manifolds $M_\pm \equiv \{\vec{q} \in \mathbb{R}^d | \pm [V(\vec{q}) - E] > 0\} \subset \mathbb{R}^d$, which are open sets in $\mathbb{R}^d$ with the metric tensor operators

$$\hat{G}^{(\pm)}_{jk} \equiv |V(\hat{q}_{\pm,1}, \ldots, \hat{q}_{\pm,d}) - E|\delta_{jk} , \qquad (4.262)$$

and the Hamilton operators

$$\hat{H}'_{c,\pm} \equiv \frac{1}{2m} \sum_{j,k=1}^{d} \hat{g}_\pm^{-\frac{1}{4}} \hat{P}_{\pm,j} \hat{g}_\pm^{\frac{1}{2}} \hat{G}_\pm^{jk} \hat{P}_{\pm,k} \hat{g}_\pm^{-\frac{1}{4}} + \xi\hbar^2 \hat{R}_\pm \pm 1 . \qquad (4.263)$$

The chart for each manifold is just the identity map from $\mathbb{R}^d$ to $\mathbb{R}^d$ and each is just a conformal map of the ordinary Euclidean space, $\delta_{ij} \to e^{2\phi_\pm}\delta_{ij}$, with

$$\phi_\pm(\vec{q}) \equiv \frac{1}{2}\log\{\pm[V(\vec{q}) - E]\} , \qquad (4.264)$$

such that angles are preserved. The Ricci scalar on these manifolds becomes

$$R_\pm(\vec{q}) = \frac{1}{\pm(V(\vec{q}) - E)} \left\{ 2(d-1)\sum_{i=1}^{d} \left.\frac{\partial^2\phi_\pm}{\partial q_i^2}\right|_{\vec{q}} - (d-2)(d-1)\left[\sum_{i=1}^{d}\left(\frac{\partial\phi_\pm}{\partial q_i}\right)^2\right] \right\} \qquad (4.265)$$

$$= \pm(1-d)\left[ \frac{\sum_{i=1}^{d}\partial_i^2 V}{[V(\vec{q}) - E]^2} + \frac{6-d}{4}\frac{\sum_{i=1}^{d}(\partial_i V)^2}{[V(\vec{q}) - E]^3} \right] . \qquad (4.266)$$

We assume that $|\psi_n\rangle \in \mathcal{H}$ is square-integrable over each of the manifolds, i.e. $|\psi_n\rangle \in \mathcal{H}_\pm$ for all $n \in \mathbb{N}$. This requirement would be easily fulfilled if $|V(\vec{q}) - E|$ was bounded, i.e. $|V(\vec{q}) - E| \leq C$ for all $\vec{q} \in M_\pm$, since in this case we could conclude

$$\int\limits_{M_\pm} d\vec{q} \, |V(\vec{q}) - E|^{d/2}|\psi_n|^2(\vec{q}) \leq C^{d/2}\int\limits_{\mathbb{R}^d} d\vec{q} \, |\psi_n|^2(\vec{q}) = C^{d/2} , \qquad (4.267)$$

Furthermore, we define $|\psi_n^{(\pm)}\rangle \equiv |\psi_n\rangle \in \mathcal{H}_\pm$.

For $d = 2$ dimensions and $\xi(d = 2) = 0$, i.e. no contribution by the Gaussian curvature, we obtain

$$\langle\vec{q}|\hat{H}'_{c,\pm}|\psi_n^{(\pm)}\rangle = -\frac{1}{2m|V(\vec{q}) - E|}\sum_{i=1}^{2}\left.\frac{\partial^2\psi_n^{(\pm)}}{\partial q_i^2}\right|_{\vec{q}} \pm \psi^{(\pm)}(\vec{q}) = \frac{\delta E_n}{|V(\vec{q}) - E|}\psi_n^{(\pm)}(\vec{q}) , \qquad (4.268)$$

which is different from the result in Eq. (4.261). To see that it is correct, please consult the coordinate space representation of the Hamilton operator from Eq. (4.183) for $V_{\text{geo}} = V_{\text{latt}} = 0$, and use the metric from Eq. (4.262). It should be stressed that this construction will not work in this way if the other potentials contribute.

The result tells us that $|\psi_n^{(\pm)}\rangle$ is not an eigenstate of $\hat{H}'_{c,\pm}$. However, if we define a "manifold spinor" $|\Psi\rangle \equiv (|\psi_+\rangle, |\psi_-\rangle)$, similar to idea for spin in quantum mechanics, then the diagonal matrix valued operator will be

$$\hat{H}'_c \equiv \begin{pmatrix} \hat{H}'_{c,+} & 0 \\ 0 & \hat{H}'_{c,-} \end{pmatrix} , \qquad (4.269)$$

such that we obtain for the matrix element in this "spinor" space

$$\langle\Psi_m|\hat{\mathrm{H}}'_c|\Psi_n\rangle = \langle\psi_m^{(+)}|\hat{\mathrm{H}}'_{c,+}|\psi_n^{(+)}\rangle + \langle\psi_m^{(-)}|\hat{\mathrm{H}}'_{c,-}|\psi_n^{(-)}\rangle \tag{4.270}$$

$$= \delta E_n \left[\langle\psi_m^{(+)}|\left(|V(\hat{\mathsf{q}}_{+,1},\hat{\mathsf{q}}_{+,2}) - E|^{-1}\right)|\psi_n^{(+)}\rangle\right.$$
$$\left. + \langle\psi_m^{(-)}|\left(|V(\hat{\mathsf{q}}_{-,1},\hat{\mathsf{q}}_{-,2}) - E|^{-1}\right)|\psi_n^{(-)}\rangle\right] \tag{4.271}$$

$$= \delta E_n \left[\int_{M_+}\mathrm{d}\vec{q}\,\frac{|V(\vec{q}) - E|}{|V(\vec{q}) - E|}\psi_m^*(\vec{q})\psi_n(\vec{q}) + \int_{M_-}\mathrm{d}\vec{q}\,\frac{|V(\vec{q}) - E|}{|V(\vec{q}) - E|}\psi_m^*(\vec{q})\psi_n(\vec{q})\right] \tag{4.272}$$

$$= \delta E_n \int_{M_+\cup M_-}\mathrm{d}\vec{q}\,\psi_m^*(\vec{q})\psi_n(\vec{q}) \tag{4.273}$$

$$= \delta E_n \int_{\mathbb{R}^2}\mathrm{d}\vec{q}\,\psi_m^*(\vec{q})\psi_n(\vec{q}) \tag{4.274}$$

$$= \delta E_n\delta_{mn} , \tag{4.275}$$

where we assumed in the second last step that $V(\vec{q})$ is injective, defined on the complete space $\mathbb{R}^2$ and that the set $M_0 \equiv \{\vec{q}\in\mathbb{R}^2|V(\vec{q}) = E\}$ has measure zero on our integration domain. This concludes the proof.

Consequently, the matrix representation of the Hamilton operator $\hat{\mathrm{H}}'_c$ on the Hilbert space $\mathcal{H}_{\mathrm{sub}} \equiv \mathrm{span}\{|\Psi_1\rangle,|\Psi_2\rangle,\dots\}$ is the same as for the operator $\hat{\mathrm{H}}'$ in the Hilbert space $\mathcal{H}$. However, the reader should be aware that the quantum states $|\Psi_n\rangle \in \mathcal{H}_c$ are not orthonormal and that they do not build a complete basis, i.e. $\mathcal{H}_{\mathrm{sub}}$ is a true subset of the complete Hilbert space $\mathcal{H}_c \equiv \mathcal{H}_+ \bigoplus \mathcal{H}_-$. It is obvious that the evolution is not influenced by adding or subtracting constants to the Hamilton operator, which is why one can choose $E = 0$.

The problem in other dimensions ($d = 1, 3$) is that one obtains a first-order derivative, which can in general not be compensated by any choice of the metric, that is non-constant, and hence would require either an ansatz where the metric depends on the employed set of quantum states which is used or the introduction of a vector potential through minimal coupling. Both of which are not desirable considering the initial motivation of the problem. One can see this very easily when looking at the change of the Laplace operator under conformal transformations, which reads in our case

$$\Delta_\pm\psi = e^{-2\phi_\pm}\left[\Delta - (d - 2)\left(\partial_i\phi_\pm\right)\left(\partial_i\psi\right)\right] . \tag{4.276}$$

Since we have mentioned the nonequivalence of the two quantum systems, let us take a look at what we would measure for the lower bound of the uncertainty relation between velocity and position for the set of quantum states in $\mathcal{H}_{\mathrm{sub}}$. According to Eq. 4.259 we need to calculate

$$\langle\psi_n^{(+)}|\hat{\mathrm{G}}^{ij}|\psi_n^{(+)}\rangle + \langle\psi_n^{(-)}|\hat{\mathrm{G}}^{ij}|\psi_n^{(-)}\rangle = \delta_{ij}\int_{\mathbb{R}^2}\mathrm{d}\vec{q}|\psi_n|^2(\vec{q}) = \delta_{ij} , \tag{4.277}$$

which tells us that also this observation agrees on this space. Now that we have seen a potential solution for an arbitrary scalar hermitian potential in $d = 2$, we want to see if the necessary and sufficient conditions of this theory are valid in the case of the electron-phonon interaction.

## 4.7 Electron-Phonon Coupling

Taking these results, we would like to describe the interaction facilitated with the operator $\hat{\mathrm{H}}_{\mathrm{eff}}$ from (4.132) for $d = 2$. The potential is given by

$$V_{n_{\mathrm{ph}},|\vec{q}|,s}(\vec{x}) \equiv -\sqrt{\frac{\hbar n_{\mathrm{ph}}}{2M\omega_{|\vec{q}|,s}}}\sum_{k=1}^{2}(e_{|\vec{q}|,s})_k\frac{1}{\sqrt{N_{\mathrm{ion}}}}\sum_{j=1}^{N_{\mathrm{ion}}}\cos(\vec{q}\cdot\vec{R}_j)\left.\frac{\partial V_{\mathrm{el\text{-}ion}}}{\partial x_k}\right|_{\vec{x}-\vec{R}_j} \in \mathbb{R} , \tag{4.278}$$

where we used Eqs. (4.66) and (4.134). Now, we shall finally take the limit of infinite lattice size $L_i \to \infty$ with $a_i \to 0$, while keeping $L_ia_i = 2\pi a^2$ fixed. $a$ is a natural length scale which gets

introduced. The resulting potential simplifies to

$$V_{n_{\text{ph}},|\vec{q}|,s}(\vec{x}) = (-1)^4 \sqrt{\frac{\hbar n_{\text{ph}}}{2M\omega_{|\vec{q}|,s}}} \sin(\vec{q} \cdot \vec{x}) \vec{e}_{|\vec{q}|,s} \cdot \vec{q} \frac{1}{2\pi a^2} \int\limits_{\mathbb{R}^2} \mathrm{d}\vec{R} \; e^{i\vec{q}\cdot\vec{R}} V_{\text{el-ion}}(\vec{R}) \;, \tag{4.279}$$

We can simplify the result even further by performing the Fourier transform, assuming we are dealing with a reduced Coulomb potential

$$\frac{1}{2\pi} \int\limits_{\mathbb{R}^2} \mathrm{d}\vec{R} \; e^{i\vec{q}\cdot\vec{R}} V_{\text{el-ion}}(\vec{R}) = -\frac{Ze_0^2}{2\pi} \int\limits_0^\infty \mathrm{d}r \int\limits_0^{2\pi} \mathrm{d}\phi \; \cos[|\vec{q}|r\sin(\phi)] \tag{4.280}$$

$$= -\frac{Ze_0^2}{|\vec{q}|} \int\limits_0^\infty \mathrm{d}r \; J_0(r) = -\frac{Ze_0^2}{|\vec{q}|} \;, \tag{4.281}$$

such that we obtain the form

$$V_{n_{\text{ph}},|\vec{q}|,s}(\vec{x}) = -\sqrt{n_{\text{ph}}} \frac{Ze_0^2}{a} \sqrt{\frac{\hbar^2 a^{-2}}{2M}/(\hbar\omega_{|\vec{q}|,s})} \sin(\vec{q} \cdot \vec{x}) \vec{e}_{|\vec{q}|,s} \cdot \left(\frac{\vec{q}}{|\vec{q}|}\right) \;. \tag{4.282}$$

This shows us that the resulting potential is injective, defined for all $\vec{x} \in \mathbb{R}^2$, bounded and that the set $M_0$ has measure zero in $\mathbb{R}^2$, which means that all conditions of the previous theory are fulfilled. In Fig. 4.4 we show a plot of the potential for a specific wave and polarization vector.

Then we would choose the manifold $\mathbb{R}^2$ with the metric tensor operator $\hat{G}_{ij}^{(\pm)} = |V_{n_{\text{ph}},\vec{q},s}(\hat{r}_{\pm,1},\hat{r}_{\pm,2})|\delta_{ij}$ that depends on the phonon number $n_{\text{ph}}$, wave vector $\vec{q}$, polarization $s$ and the electron's coordinates $\vec{r}_\pm$ in $M_\pm$. Using Eq. (4.266) the Ricci scalars are given by

$$R_\pm = \pm \frac{1}{\sqrt{n_{\text{ph}}} \frac{Ze_0^2}{a} \sqrt{\frac{\hbar^2 a^{-2}}{2M}/(\hbar\omega_{|\vec{q}|,s})} \vec{e}_{|\vec{q}|,s} \cdot \left(\frac{\vec{q}}{|\vec{q}|}\right)} \frac{|\vec{q}|^2 \cos(2\vec{q}\cdot\vec{r}_\pm)}{\sin^3(\vec{q}\cdot\vec{r}_\pm)} \;, \tag{4.283}$$

which shows a strong singularity around $\vec{q}\cdot\vec{r}_\pm \approx 0$. The integral of the Ricci scalar over the total manifold diverges. However, since we neglected its contribution to the dynamics, we do not have to deal with this issue.
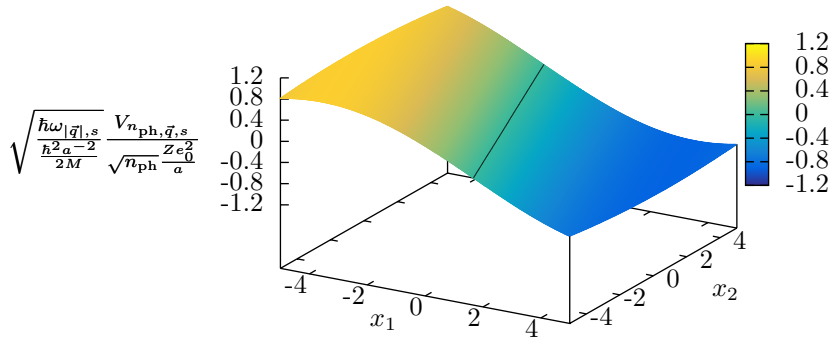


Figure 4.4: Plot of the positive and negative parts of the potential for polarization vector $\vec{e}_{|\vec{q}|,s} = (1,1)/\sqrt{2}$ and phonon wave vector $\vec{q} = (0.3,0.1)$, where the black line shows the division between the two parts.

The first important question that remains to be answered is whether this concept can be generalized to single phonon transitions, such as single emission $|n_{\text{ph}}-1,\vec{q},s\rangle \to |n_{\text{ph}},\vec{q},s\rangle$ or absorp-

tion $|n_{\mathrm{ph}}, \vec{q}, s\rangle \to |n_{\mathrm{ph}} - 1, \vec{q}, s\rangle$ processes, where the operators $\hat{\mathrm{V}}_{\mathrm{em}}(n_{\mathrm{ph}}, \vec{q}, s)$ and $\hat{\mathrm{V}}_{\mathrm{ab}}(n_{\mathrm{ph}}, \vec{q}, s)$ are non-hermitian. This cannot be done because the phase of the operator will depend on the electron's coordinate, which in principle means that we need to keep a contribution which does depend on the phonons as well as the electron, and cannot be described by such a metric. This is not in agreement with the initial idea behind the coupling.

However, if we define the metric tensor operators by

$$\left(\hat{\mathrm{G}}_\pm\right)_{i,j} = \pm f_{\vec{u}_1, \dots, \vec{u}_{N_{\mathrm{ion}}}}\left(\hat{\vec{q}}_\pm\right) \delta_{ij} \ , \tag{4.284}$$

$$f_{\vec{u}_1, \dots, \vec{u}_{N_{\mathrm{ion}}}}\left(\hat{\vec{q}}_\pm\right) = \frac{E_{\mathrm{ph}} + V_{\mathrm{latt}}(\hat{\vec{q}}_\pm) - \sum_{i=1}^{N_{\mathrm{ion}}} \sum_{j=1}^{2} u_{i,j} \partial_j V_{\mathrm{el\text{-}ion}}\left(\hat{\vec{q}}_\pm - \vec{R}_i^{(0)}\right)}{E_{\mathrm{ph}} + V_{\mathrm{latt}}\left(\hat{\vec{q}}_\pm\right)} \ , \tag{4.285}$$

$$V_{\mathrm{latt}}(\hat{\vec{q}}_\pm) \equiv \sum_{i=1}^{N_{\mathrm{ion}}} V_{\mathrm{el\text{-}ion}}\left(\hat{\vec{q}}_\pm - \vec{R}_i^{(0)}\right) \ , \tag{4.286}$$

which means they depend on the set of real parameters $\{\vec{u}_1, \dots, \vec{u}_{N_{\mathrm{ion}}}\}$ with $\vec{u}_i \in \mathbb{R}^2$, we shall see that they are hermitian, positive-definite and depend only on the electron's position operators assuming we define the two parameter-dependent manifolds as

$$M_\pm \equiv \left\{ \vec{q} \in V \,\middle|\, \pm f_{\vec{u}_1, \dots, \vec{u}_{N_{\mathrm{ion}}}}(\vec{q}) > 0 \right\} \ , \tag{4.287}$$

where $V \subset \mathbb{R}^2$ is the volume of the crystal with periodic boundary conditions. In Fig. 4.5 we have visualized the function $f$ and the manifolds for a square lattice of four atoms and specific displacement vectors. The black contour line at $f(\vec{q}) = 0$ separates the manifolds. It is already clear that the area of the negative manifold will shrink if the displacements decrease. If one deals with a "large" total energy of the phonons then the area of the negative valued manifold will shrink even more, as can be seen in Figs. 4.6 to 4.8. Since the total energy of the phonons is a macroscopic quantity, it scales proportional to the volume of the crystal. If we use the average internal energy of a phonon system in a canonical ensemble of temperature $T = 300$ K of a monoatomic crystal surface, and a speed of sound $c_s = c \approx 10^3$ m/s together with the formula

$$\langle E_{\mathrm{ph}} \rangle \frac{a}{Ze_0^2} = \frac{(k_B T)^3 N_{\mathrm{ion}} a^3}{\hbar^2 \pi c_s^2 Z e_0^2} \int\limits_0^{\frac{\hbar \omega_D}{k_B T}} \mathrm{d}x \ \frac{x^2}{e^x - 1} \approx 10^{-3} N_{\mathrm{ion}} \ , \tag{4.288}$$

where we have used $a \approx 10^{-10}$ m for the lattice constant and $\omega_D = \sqrt{2\pi} \frac{c_s}{a}$ for the Debye frequency. It tells us that we need about 1000 atoms to reach a similar magnitude between the phonon energy and lattice potential scale. In practice, one would deal with crystals of a very large number of atoms. In this case, one does not need to consider the negative manifold $M_-$ since its integral value becomes very small in two dimensions.

Now, we would need to check if the eigenstates of the flat Hamilton operator are still square-integrable over the manifold. Since we do not know the eigenstates, we shall make an estimate
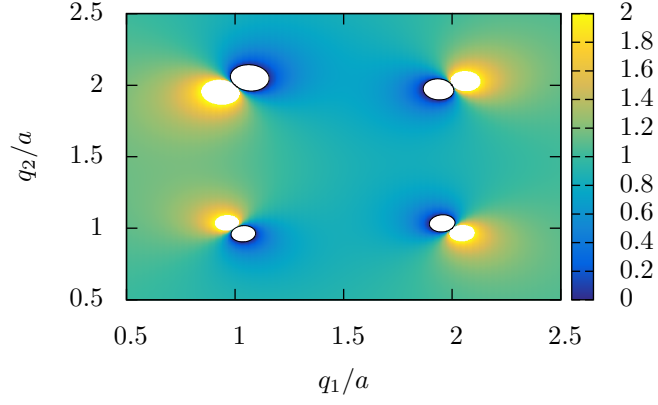
Figure 4.5: Plot of the metric function $f$ using 4 atoms, $E_{\text{ph}} = 0$, displacements $\vec{u}_{1,1} = (0.1, -0.1)a$, $\vec{u}_{1,2} = (0.2, 0.15)a$, $\vec{u}_{2,1} = (-0.12, 0.09)a$, $\vec{u}_{2,2} = (-0.17, -0.08)a$ and the black contour lines at $f = 0$ and the white area for $f > 2$, which are symmetric around the lattice sites.
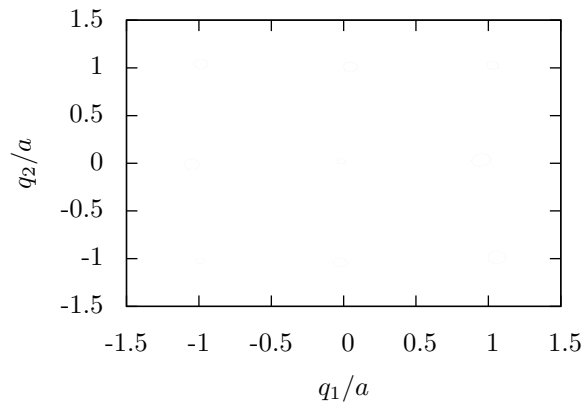


Figure 4.6: Plot of the contour showing the different manifolds using 9 atoms, $E_{\text{ph}} = 0$, displacements $\vec{u}_{-1,-1} = (0.02, -0.07)a$, $\vec{u}_{-1,0} = (-0.16, -0.04)a$, $\vec{u}_{-1,1} = (0.04, 0.13)a$, $\vec{u}_{0,-1} = (-0.07, -0.12)a$, $\vec{u}_{0,0} = (-0.04, 0.06)a$, $\vec{u}_{0,1} = (0.15, 0.03)a$, $\vec{u}_{1,-1} = (0.19, 0.05)a$, $\vec{u}_{1,0} = (-0.18, 0.12)a$, $\vec{u}_{1,1} = (0.08, 0.07)a$.
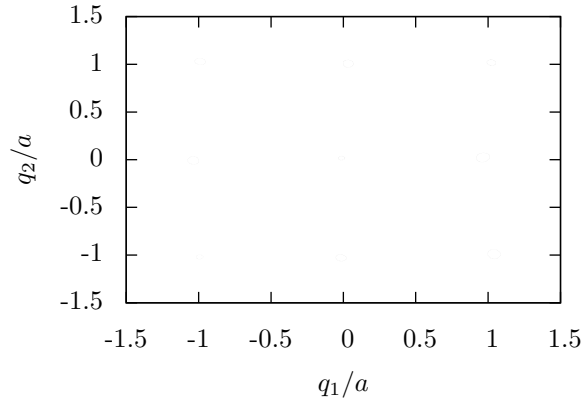
Figure 4.7: Plot of the contour showing the different manifolds using 9 atoms, $E_{\mathrm{ph}} = 10Ze_0^2/a$, displacements $\vec{u}_{-1,-1} = (0.02, -0.07)a$, $\vec{u}_{-1,0} = (-0.16, -0.04)a$, $\vec{u}_{-1,1} = (0.04, 0.13)a$, $\vec{u}_{0,-1} = (-0.07, -0.12)a$, $\vec{u}_{0,0} = (-0.04, 0.06)a$, $\vec{u}_{0,1} = (0.15, 0.03)a$, $\vec{u}_{1,-1} = (0.19, 0.05)a$, $\vec{u}_{1,0} = (-0.18, 0.12)a$, $\vec{u}_{1,1} = (0.08, 0.07)a$.



Figure 4.8: Plot of the contour showing the different manifolds using 9 atoms, $E_{\mathrm{ph}} = 100Ze_0^2/a$, displacements $\vec{u}_{-1,-1} = (0.02, -0.07)a$, $\vec{u}_{-1,0} = (-0.16, -0.04)a$, $\vec{u}_{-1,1} = (0.04, 0.13)a$, $\vec{u}_{0,-1} = (-0.07, -0.12)a$, $\vec{u}_{0,0} = (-0.04, 0.06)a$, $\vec{u}_{0,1} = (0.15, 0.03)a$, $\vec{u}_{1,-1} = (0.19, 0.05)a$, $\vec{u}_{1,0} = (-0.18, 0.12)a$, $\vec{u}_{1,1} = (0.08, 0.07)a$.
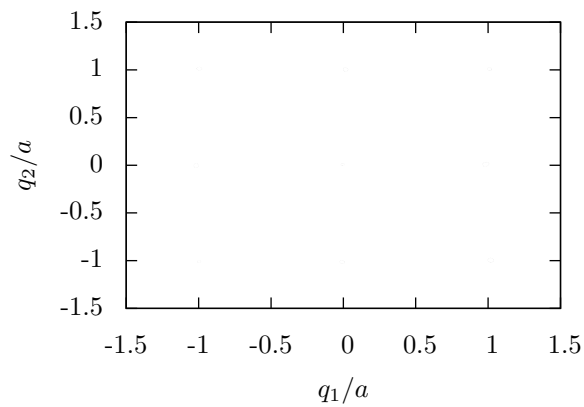
based on two "plane" waves,

$$
|h_{\vec{k},\vec{k}'}| \equiv \left| \frac{1}{V} \int\limits_{M_+ \cup M_-} d\vec{q} \; e^{\imath \vec{q} \cdot (\vec{k} - \vec{k}')} |f_{\vec{u}_1, \dots, \vec{u}_{N_{\mathrm{ion}}}}(\vec{q})| \right| \tag{4.289}
$$

$$
= \left| \frac{1}{V} \int\limits_V d\vec{q} \; e^{\imath \vec{q} \cdot (\vec{k} - \vec{k}')} |f_{\vec{u}_1, \dots, \vec{u}_{N_{\mathrm{ion}}}}(\vec{q})| \right| \tag{4.290}
$$

$$
\leq \frac{1}{V} \int\limits_V d\vec{q} \; |f_{\vec{u}_1, \dots, \vec{u}_{N_{\mathrm{ion}}}}(\vec{q})| \tag{4.291}
$$

$$
\leq 1 + \frac{1}{V} \int\limits_V d\vec{q} \; \left| \frac{\delta V_{\vec{u}_1, \dots, \vec{u}_{N_{\mathrm{ion}}}}(\vec{q})}{V_{\mathrm{latt}}(\vec{q})} \right| \tag{4.292}
$$

$$
\leq 1 + \frac{1}{V} \sum_{i=1}^{N_{\mathrm{ion}}} \sum_{j=1}^{2} |u_{i,j}| \int\limits_V d\vec{q} \; \left| \partial_j \log V_{\mathrm{el\text{-}ion}} \left( \vec{q} - \vec{R}_i^{(0)} \right) \right| \tag{4.293}
$$

$$
\leq 1 + \frac{1}{V} \sum_{i=1}^{N_{\mathrm{ion}}} \sum_{j=1}^{2} |u_{i,j}| \int\limits_V d\vec{q} \; \left| \partial_j \log V_{\mathrm{el\text{-}ion}} (\vec{q}) \right| \tag{4.294}
$$

$$
\leq 1 + \frac{1}{V} \sum_{i=1}^{N_{\mathrm{ion}}} \sum_{j=1}^{2} |u_{i,j}| \int\limits_0^{2\pi} d\phi \; \left[ |\cos(\phi)\delta_{j,1}| + |\sin(\phi)\delta_{j,2}| \right] \int\limits_0^R dr \; |r\partial_r \log r| \tag{4.295}
$$

$$
\leq 1 + \frac{2\pi R}{V} \sum_{i=1}^{N_{\mathrm{ion}}} \sum_{j=1}^{2} |u_{i,j}| \; , \tag{4.296}
$$

which shows that the matrix elements are always finite. For the derivation we took a disk with $V \subset [0, 2\pi] \times [0, R]$.

For the Hamilton operators we choose

$$
\hat{H}_{c,\pm} \equiv \frac{1}{2m} \sum_{j,k=1}^{2} \hat{g}_\pm^{-\frac{1}{4}} \hat{P}_{\pm,j} \hat{g}_\pm^{\frac{1}{2}} \hat{G}_\pm^{jk} \hat{P}_{\pm,k} \hat{g}_\pm^{-\frac{1}{4}} \pm \left[ E_{\mathrm{ph}} + V_{\mathrm{latt}} \left( \hat{\vec{q}}_\pm \right) \right] \; . \tag{4.297}
$$

Calculating the resulting matrix element between two electronic manifold spinors $|\Psi_1\rangle$ and $|\Psi_2\rangle$ we find the integral

$$
\langle \Psi_1 | \hat{H}_c | \Psi_2 \rangle = \langle \psi'_{1,+} | \hat{H}_{c,+} | \psi_{2,+} \rangle + \langle \psi'_{1,-} | \hat{H}_{c,-} | \psi_{2,-} \rangle \tag{4.298}
$$

$$
= \int\limits_{M_+} dV_q \; \psi_{1,+}^*(\vec{q}) \left[ -\frac{1}{G_+(\vec{q})} \frac{\hbar^2}{2m} \sum_{i=1}^{2} \frac{\partial^2}{\partial q_i^2} + V_{\mathrm{latt}}(\vec{q}) + E_{\mathrm{ph}} \right] \psi_{2,+}(\vec{q})
$$

$$
+ \int\limits_{M_-} dV_q \; \psi_{1,-}^*(\vec{q}) \left[ -\frac{1}{G_-(\vec{q})} \frac{\hbar^2}{2m} \sum_{i=1}^{2} \frac{\partial^2}{\partial q_i^2} - V_{\mathrm{latt}}(\vec{q}) - E_{\mathrm{ph}} \right] \psi_{2,-}(\vec{q}) \tag{4.299}
$$

$$
= \int\limits_V d\vec{q} \; \psi_1^*(\vec{q}) \left[ -\frac{\hbar^2}{2m} \sum_{i=1}^{2} \frac{\partial^2}{\partial q_i^2} + V_{\mathrm{latt}}(\vec{q}) - \sum_{i=1}^{N_{\mathrm{ion}}} \sum_{j=1}^{2} u_{i,j} \partial_j V_{\mathrm{el\text{-}ion}} \left( \vec{q} - \vec{R}_i^{(0)} \right) + E_{\mathrm{ph}} \right] \psi_2(\vec{q}) \; . \tag{4.300}
$$

Therefore, we state that the matrix representation of this operator in a basis of quantum states from the original Hilbert space $\mathcal{H}$ is the same, which is why we regard the two approaches as weakly equivalent approximations of the electron-phonon coupling. The dynamics are given by

the Schrödinger equation

$$\imath\hbar\partial_t|\Psi(t)\rangle = \hat{H}_c|\Psi(t)\rangle \tag{4.301}$$

$$\imath\hbar\begin{pmatrix}\partial_t|\psi_+(t)\rangle \\ \partial_t|\psi_-(t)\rangle\end{pmatrix} = \begin{pmatrix}\hat{H}_+ & 0 \\ 0 & \hat{H}_-\end{pmatrix}\begin{pmatrix}|\psi_+(t)\rangle \\ |\psi_-(t)\rangle\end{pmatrix} , \tag{4.302}$$

$$\hat{H}_\pm = \frac{1}{2m}\sum_{j,k=1}^{2}\hat{g}_\pm^{-\frac{1}{4}}\hat{P}_{\pm,j}\hat{g}_\pm^{\frac{1}{2}}\hat{G}_\pm^{jk}\hat{P}_{\pm,k}\hat{g}_\pm^{-\frac{1}{4}} \pm \left[\sum_{\vec{q},s}\hbar\omega_{\vec{q},s}\hat{b}_{\vec{q},s}^\dagger\hat{b}_{\vec{q},s} + V_{\text{latt}}\left(\hat{\vec{x}}_\pm\right)\right] , \tag{4.303}$$

$$\left(\hat{G}_\pm\right)_{ij} \equiv \pm\left[\frac{\hat{H}_{\text{ph}} + V_{\text{latt}}(\hat{\vec{x}}_\pm) - \sum_{i=1}^{N_{\text{ion}}}\sum_{j=1}^{2}\hat{u}_{i,j}\partial_j V_{\text{el-ion}}\left(\hat{\vec{x}}_\pm - \vec{R}_i^{(0)}\right)}{\hat{H}_{\text{ph}} + V_{\text{latt}}\left(\hat{\vec{x}}_\pm\right)}\right]\delta_{ij} , \tag{4.304}$$

where $\hat{x}_i$ is the position operator of the electron and $\vec{q}$ the phonon's wave vector. If one imagines the crystal to be in contact with a large heat reservoir, such that it behaves according to the canonical ensemble, the metric tensor operator will also be temperature dependent due to its dependence on the phonon energy and displacement vectors.

In practice one could evolve the wave function in the coordinate representation of electron and phonons, i.e. looking at

$$\psi(t, \vec{x}, \vec{u}_1, \ldots, \vec{u}_{N_{\text{ion}}}) = \left(\langle\vec{x}|\bigotimes\langle\vec{u}_1, \ldots, \vec{u}_{N_{\text{ion}}}|\right)|\Psi(t)\rangle . \tag{4.305}$$

The disadvantage is the high-dimensional space of the wave function, which is why one may try to obtain the continuum or infinite lattice limit, similar to the idea which was used in the beginning of this section. However, comparing this result with the standard approach Hamilton operator, it looks much more sophisticated and difficult to diagonalize. It does not seem to a promising endeavor and hence calls for another way of utilizing this result, which we shall discuss in the next paragraph.

Another question one may have is if one attempted a simulation with the dynamics described by the Hamilton operator from Eq. (4.269), how stable would such a simulation be, considering that the construction only works on the subspace $\mathcal{H}_{\text{sub}}$. One could try to introduce a constraint through a Lagrange parameter that ensures the compatibility with the observation, expressed in Eq. (4.259). However, it is not clear whether this will be sufficient to stabilize it in the Hilbert space of the curved system.

In a concrete simulation, one may simulate the dynamics of the ions through molecular dynamics in a thermostat ([82]) and extract the total energy of the ionic manifold ($E_{\text{ph}}$) as well as the ions displacement from the equilibrium position. The dynamics of the electrons can then be obtained by running a curved space quantum lattice Boltzmann simulation till it reaches a steady state, given the static metric tensor $G_\pm$ and external potentials $V_{\text{ext}} = \pm(E_{\text{ph}} + V_{\text{latt}})$. This assumes that the time scale of the electrons is much smaller than for the ions, such that they reach the equilibrium for a given "static" lattice configuration before the ions move again. For the simulation one uses an extended version of the lattice Boltzmann algorithm for quantum mechanics, whose original form has been derived in Ref. [168], and whose applications as well as relativistic extension are discussed in Ref. [166]. In our case we do not need a relativistic treatment of the electron flow. Therefore, it seems reasonable to merge the concepts from Refs. [168] and [114] to create a curved space non-relativistic quantum lattice Boltzmann simulation technique. In summary, it means that we perceive the electrons as non-relativistic quantum fluid of manifold spinors which flow on a curved manifold, whose metric is given by Eq. (4.304). The advantages of such an approach compared to the usual Born-Oppenheimer approximation still need to be shown and discussed in practice. Using a simplified metric, a concrete numerical simulation has been done in Ref. [62].

## 4.8 Final remarks

The physically most important result is that in contrast to the weak equivalence principle in general relativity [164] the effect of curvature would be even locally observable by determining

the lower bound on the uncertainty relation between simultaneous velocity and position measurements in the same or different directions. From there, we can show the nonequivalence of a quantum system in Euclidean space that interacts with an electromagnetic field and a "free" quantum system on a Riemannian manifold with a non-trivial metric. The reason for this discrepancy is the spread of the wave function which makes it even for local measurements possible to acquire information from distant areas in space and hence measure the effect of curvature.

Despite this problem, we managed to construct a spinor-type Hilbert space with a Hamilton operator matrix whose representation in the "restricted" spinor set is within the same as for the two-dimensional Hamilton operator of an electron interacting with phonons causing only small ion displacements. The restrictive validity is not a problem since the subset of quantum states, on which the matrix representations coincide, covers the complete Hilbert space of the original problem. Therefore, if we take an arbitrary quantum state, such as a simple plane wave from Euclidean space its evolution will be the same in both systems. Within this approach we have determined the manifolds and the required metric tensor operator as a function of the phonon number, wave vector and polarization. Its deviation from the Euclidean metric is governed by the ratio between the electron-phonon interaction and the lattice potential plus the total energy of the phonons. In the case of a hermitian transition, we have calculated the infinite lattice limit and visualized the form of the potential.

Future research on this subject should first analyze the effect of this coupling on a semi-classical approximation [130] and find out how the scattering approach is influenced. Especially, if one obtains simplifications compared to the full scattering integral or improvements with respect to the single scattering rate ansatz [158, 170, 14]. Furthermore, one should try to determine the numerical stability of this approach, due its restricted validity within the Hilbert spaces on the curved manifolds. The general ideas could also be applied when using the Dirac equation instead of a non-relativistic approach and one could analyze how far the equivalence can be pushed there. In addition, one might want to figure out if such a weak equivalence can be constructed in other dimensions or for other types of interactions.

# 5 Conclusion

<div align="right">
There is no real ending. It is just
the place where you stop the story.

Frank Herbert
</div>

In this work we have presented a new numerical method for the simulation of the Wigner equation, which is oriented on the lattice Boltzmann method, usually used in fluid dynamics. We discussed its novelty, shortcomings as well as advantages compared to other numerical techniques for the evolution of the density operator in phase space. A main advantage is the more flexible basis choice for the spectral decomposition of the velocity-dependent part of the Wigner function, which allows the user to pick functions which are better suited for his or her application. Furthermore, we presented the dynamics of various isolated quantum systems and phenomena in phase space and validated the convergence and stability of the algorithm in practice. There are still relevant questions which can be explored, such as the effect of stochastic perturbations on the Wigner function or the studying of phase transitions in phase space. It would especially be necessary to simulate thermal distributions, such as Fermi-Dirac or Bose-Einstein to leverage the full potential of the Wigner formalism and our simulation technique.

Second, we opened the quantum system to interactions with an artificial environment to mimic the decoherence-based measurement process and use it to approximate the most probable eigenstates of observables, whose main intention stems from a simplified quantum state reconstruction. Its application lies mainly in the field of quantum communication to give good measurement predictions for experimentalists that perform non-commuting measurements on the same quantum state without needing to fully diagonalize both observables. We developed an advanced parallelizable numerical procedure which allows the towing of eigenstates along a perturbation and hence gave us the possibility to study excited-state quantum phase transitions. We could show that the phase transition in the Jaynes-Cummings model is not universal with respect to a change in spectrum ratio and validated our simulation technique. The comparison between our method and $MRRR$ eigensolver from the $LAPACK$ library revealed a competitive efficiency, especially in the ability to parallelize the simulation of several eigenstates. Future research could examine other decoherent evolution equations with stronger coupling between the quantum system and the measurement apparatus as well as stochastic numerical simulation techniques to make higher-dimensional computations feasible.

In the last project, we answered the question whether a non-relativistic quantum system of electromagnetically interacting electrons and ions is equivalent to a quantum system of electrons which move on a Riemannian manifold whose metric depends on the dynamics of the ions. We could construct a measurement that indirectly enables the local observation of the components of the metric tensor and would allow one to distinguish locally between a Euclidean and non-Euclidean metric, in contrast to the principle of general relativity. Despite the general nonequivalence, we have found a two-dimensional quantum system with corresponding manifolds for which quantum states with equal coordinate representation in both systems give the same energy measurement and hence follow the same dynamical evolution. We explicitly derived the metric tensor and his dependence on the phonon potential. We also calculated the continuum limit for a specific hermitian transition of the phonon system. Concerning our initial motivation, we have derived the concrete mathematical form of the metric tensor operator that could be used in curved space lattice Boltzmann simulations and would reduce the number of fitting parameters that were necessary in the electron-phonon coupling simulation in graphene from Ref. [62]. The introduction of a temperature dependent coupling constant would not be necessary then, since the temperature dependence is implicitly contained in the ionic displacements (phonons). All other principles should stay the same. However, as we have seen in the last paragraph, the metric becomes very small and diverges close to the ions' positions. This will present a major challenge in the curved space simulation and needs to be analyzed. An advantage is that the areas for which the metric becomes very small or large shrink if one simulates more ions, as this

increases the average phonon energy which decreases the metric perturbation. Further research on this subject should analyze the stability of this evolution, since the limited equivalence only holds in the Hilbert space of the original problem, and analyze the implications of this result to semi-classical (Born-Oppenheimer) approximations of systems of electrons and ions.

# Bibliography

[1] M. Aichinger and E. Krotscheck. "A fast configuration space method for solving local Kohn-Sham equations". In: *Computational Materials Science* 34.2 (Sept. 2005), 188–212.

[2] Salvatore Antoci and Dierck-E Liebscher. "Wentzel's Path Integrals". In: *International journal of theoretical physics* 37.1 (1998), 531–535.

[3] V. Aquilanti and S. Cavalli. "Discrete analogs of hyperspherical harmonics and their use for the quantum mechanical three body problem". In: *Few Body Systems* 6 (1992), 573–580.

[4] A. Arnold and C. Ringhofer. "Operator splitting methods applied to spectral discretizations of quantum transport equations". In: *SIAM Journal of Numerical Analysis* 32.6 (Dec. 1995), 1876–1894.

[5] Vladimir Igorevich Arnol'd. *Mathematical methods of classical mechanics*. Vol. 60. Springer Science & Business Media, 2013.

[6] George A. Baker. "Formulation of Quantum Mechanics Based on the Quasi-Probability Distribution Induced on Phase Space". In: *Phys. Rev.* 109 (6 Mar. 1958), 2198–2206. DOI: 10.1103/PhysRev.109.2198. URL: https://link.aps.org/doi/10.1103/PhysRev.109.2198.

[7] L. E. Ballentine. *Quantum Mechanics: A modern development*. World Scientific, 2000.

[8] Valentine Bargmann and Eugene P Wigner. "Group theoretical discussion of relativistic wave equations". In: *Proceedings of the National Academy of Sciences* 34.5 (1948), 211–223.

[9] Peter Barmettler, Davide Fioretto, and Vladimir Gritsev. "Non-equilibrium dynamics of Gaudin models". In: *EPL (Europhysics Letters)* 104.1 (2013), p. 10004. URL: http://stacks.iop.org/0295-5075/104/i=1/a=10004.

[10] K. J. Bathe and E. L. Wilson. *Numerical Methods in Finite Element Analysis*. Englewood Cliffs, N.J.: Prentice-Hall, 1976.

[11] Charles H Bennett and Gilles Brassard. "An Update on Quantum Cryptography." In: *Crypto*. Vol. 84. Springer. 1984, 475–480.

[12] Charles H. Bennett and Peter W. Shor. "Quantum information theory". In: *IEEE transactions on information theory* 44.6 (1998), 2724–2742.

[13] R. Benzi, S. Succi, and M. Vergassola. "The lattice Boltzmann equation: theory and applications". In: *Physics Reports* 222.3 (1992), 145–197. ISSN: 0370-1573. DOI: 10.1016/0370-1573(92)90090-M. URL: http://www.sciencedirect.com/science/article/pii/037015739290090M.

[14] R. Bistritzer and A. H. MacDonald. "Hydrodynamic theory of transport in doped graphene". In: *Phys. Rev. B* 80 (8 2009), p. 085109. DOI: 10.1103/PhysRevB.80.085109. URL: https://link.aps.org/doi/10.1103/PhysRevB.80.085109.

[15] R. Bistritzer and A. H. MacDonald. "Hydrodynamic theory of transport in doped graphene". In: *Phys. Rev. B* 80 (8 2009), p. 085109. DOI: 10.1103/PhysRevB.80.085109. URL: https://link.aps.org/doi/10.1103/PhysRevB.80.085109.

[16] N. Bohr. "Über die Serienspektra der Elemente". In: *Zeitschrift für Physik* 2.5 (1920), 423–469. ISSN: 0044-3328. DOI: 10.1007/BF01329978. URL: http://dx.doi.org/10.1007/BF01329978.

[17] Denys I. Bondar et al. "Efficient computations of quantum canonical Gibbs state in phase space". In: *Phys. Rev. E* 93 (6 2016), p. 063304. DOI: 10.1103/PhysRevE.93.063304. URL: https://link.aps.org/doi/10.1103/PhysRevE.93.063304.

[18] M. Born. "Zur Quantenmechanik der Stossvorgänge". In: *Zeitschrift für Physik* 37.12 (Dec. 1926), 863–867.

[19] G Breigenbach, S Schiller, and J Mlynek. "Measurement of the quantum states of squeezed light". In: *Nature* 387.6632 (1997), p. 471.

[20] H.-P. Breuer and F. Petruccione. *The theory of open quantum systems.* New York: Oxford University Press, 2002.

[21] J. C. Butcher. *Numerical Methods for Ordinary Differential Equations.* New York: John Wiley & Sons Ltd., 2008.

[22] M. A. Caprio, P. Cejnar, and F. Iachello. "Excited state quantum phase transitions in many-body systems". In: *Annals of Physics* 323.5 (May 2008), 1106–1135.

[23] John Cardy. *Finite-size scaling.* Vol. 2. Elsevier, 2012.

[24] RD Carmichael et al. "AS Eddington, The Mathematical Theory of Relativity". In: *Bulletin of the American Mathematical Society* 31.9-10 (1925), 563–563.

[25] Cheng and Knorr. "The integration of the Vlasov Equation in Configuration Space". In: *Journal of Computational Physics* 22 (1976), 330–351.

[26] Gianpiero Colonna and Antonio D'Angola. *Plasma Modeling.* 2053-2563. IOP Publishing, 2016. ISBN: 978-0-7503-1200-4. DOI: `10.1088/978-0-7503-1200-4`. URL: `http://dx.doi.org/10.1088/978-0-7503-1200-4`.

[27] R. C. T. da Costa. "Quantum mechanics of a constrained particle". In: *Phys. Rev. A* 23 (4 Apr. 1981), 1982–1987. DOI: `10.1103/PhysRevA.23.1982`. URL: `https://link.aps.org/doi/10.1103/PhysRevA.23.1982`.

[28] R. Courant, K. Friedrichs, and H. Lewy. "Über die partiellen Differenzengleichungen der mathematischen Physik". In: *Mathematische Annalen* 100.1 (1928), 32–74. ISSN: 1432-1807. DOI: `10.1007/BF01448839`. URL: `http://dx.doi.org/10.1007/BF01448839`.

[29] Richard Courant and David Hilbert. *Methods of mathematical physics.* Vol. 1. CUP Archive, 1966.

[30] T. Cuk et al. "A review of electron–phonon coupling seen in the high-Tc superconductors by angle-resolved photoemission studies (ARPES)". In: *physica status solidi (b)* 242.1 (2005), 11–29. ISSN: 1521-3951. DOI: `10.1002/pssb.200404959`. URL: `http://dx.doi.org/10.1002/pssb.200404959`.

[31] T. L. Curtright, D. B. Fairlie, and C. K. Zachos. *A concise treatise on quantum mechanics in phase space.* Singapore: World Scientific, 2013.

[32] G Mauro D'Ariano and HP Yuen. "Impossibility of measuring the wave function of a single quantum system". In: *Physical review letters* 76.16 (1996), p. 2832.

[33] B. S. DeWitt. "Dynamical Theory in Curved Spaces. I. A Review of the Classical and Quantum Action Principles". In: *Reviews of Modern Physics* 29.3 (July 1957), 377–397.

[34] B. S. DeWitt. "Point Transformations in Quantum Mechanics". In: *Physical Revew* 85.4 (Feb. 1952).

[35] J.-D. Debus. "Flows in curved spaces". PhD thesis. ETH Zurich, 2016. URL: `https://doi.org/10.3929/ethz-a-010795142`.

[36] Samuel Deleglise et al. "Reconstruction of non-classical cavity field states with snapshots of their decoherence". In: *Nature* 455.7212 (2008), 510–514.

[37] J. W. Demmel et al. "Performance and accuracy of LAPACK's symmetric tridiagonal eigensolvers". In: *SIAM Journal on Scientific Computing* 30.3 (2008), 1508–1526.

[38] J. T. Devreese. "Fröhlich Polarons. Lecture course including detailed theoretical derivations". In: (Nov. 2016).

[39] J T Devreese. "Fröhlich polarons from 0D to 3D: concepts and recent developments". In: *Journal of Physics: Condensed Matter* 19.25 (2007), p. 255201. URL: `http://stacks.iop.org/0953-8984/19/i=25/a=255201`.

[40] Jozef T Devreese and Alexandre S Alexandrov. "Fröhlich polaron and bipolaron: recent developments". In: *Reports on Progress in Physics* 72.6 (2009), p. 066501. URL: `http://stacks.iop.org/0034-4885/72/i=6/a=066501`.

[41]    I. S. Dhillon. "A new $O(n^2)$ Algorithm for the Symmetric Tridiagonal Eigenvalue/Eigenvector Problem". PhD thesis. University of California, Berkeley, 1997.

[42]    I. S. Dhillon, B. N. Parlett, and C. Vömel. "The Design and Implementation of the MRRR Algorithm". In: *ACM Trans. Math. Softw.* 32.4 (Dec. 2006), 533–560.

[43]    S. Diehl et al. "Quantum states and phases in driven open quantum systems with cold atoms". In: *Nature Physics* 4 (Nov. 2008), p. 878.

[44]    "Discrete Wigner function and quantum-state tomography". In: (5).

[45]    L. Diósi. "Quantum stochastic processes as models for state vector reduction". In: *Journal Physics A* 21 (1988), 2885–2898.

[46]    L. Diósi. "Stochastic pure state representation for open quantum systems". In: *Physics Letters A* 114.8-9 (Mar. 1986), 451–454.

[47]    M. Dubé and P. C. E. Stamp. "Mechanisms of decoherence at low temperatures". In: *Chem. Phys.* 268 (2001), 257–272.

[48]    B. Duplantier, J.-M. Raimond, and V. Rivasseau, eds. *Quantum Decoherence Poincáre Seminar 2005*. Vol. 48. Progress in Mathematical Physics. Basel: Birkhäuser, 2005.

[49]    Albert Einstein. "A generalized theory of gravitation". In: *Reviews of Modern Physics* 20.1 (1948), p. 35.

[50]    D. H. Feng, R. Gilmore, and S. R. Deans. "Phase transitions and the geometric properties of the interacting boson model". In: *Physical Review C* 23.3 (Mar. 1981), 1254–1258.

[51]    Y. T. Feng and D. R. J. Owen. "Conjugate Gradient Methods For Solving The Smallest Eigenpair Of Large Symmetric Eigenvalue Problems". In: *International Journal for Numerical Methods in Engineering* 39 (1996), 2209–2229.

[52]    A. Ferrari. "Raman spectroscopy of graphene and graphite: Disorder, electron-phonon coupling, doping and nonadiabatic effects". In: *Solid State Communications* 143.1-2 (July 2007), 47–57.

[53]    R. P. Feynman. "Space-Time Approach to Non-Relativistic Quantum Mechanics". In: *Rev. Mod. Phys.* 20 (2 1948), 367–387. DOI: `10.1103/RevModPhys.20.367`. URL: `https://link.aps.org/doi/10.1103/RevModPhys.20.367`.

[54]    Alejandro Frank, Ana Leonor Rivera, and Kurt Bernardo Wolf. "Wigner function of Morse potential eigenstates". In: *Phys. Rev. A* 61 (5 2000), p. 054102. DOI: `10.1103/PhysRevA.61.054102`. URL: `https://link.aps.org/doi/10.1103/PhysRevA.61.054102`.

[55]    W. R. Frensley. "Boundary conditions for open quantum systems driven far from equilibrium". In: *Review of Modern Physics* 62.745 (July 1990).

[56]    O. Furtmaier and M. Mendoza. "Targeting eigenstates using a decoherence-based nonlinear Schrödinger equation". In: *Phys. Rev. A* 96 (2 2017), p. 022134. DOI: `10.1103/PhysRevA.96.022134`. URL: `https://link.aps.org/doi/10.1103/PhysRevA.96.022134`.

[57]    O. Furtmaier, S. Succi, and M. Mendoza. "Semi-spectral method for the Wigner equation". In: *Journal of Computational Physics* 305 (2016), 1015–1036. ISSN: 0021-9991. DOI: `10.1016/j.jcp.2015.11.023`. URL: `http://www.sciencedirect.com/science/article/pii/S0021999115007639`.

[58]    O. Furtmaier et al. "Rayleigh-Bénard Instability in Graphene". In: *Physical Review B* 91.085401 (Feb. 2015).

[59]    J. Gallier and D. Xu. "Computing exponentials of skew-symmetric matrices and logarithms of orthogonal matrices". In: *International Journal of Robotics and Automation* 17.4 (2002).

[60]    Ralph W Gerchberg. "A practical algorithm for the determination of the phase from image and diffraction plane pictures". In: *Optik* 35 (1972), 237–246.

[61]    J Willard Gibbs. *Elementary principles in statistical mechanics*. Courier Corporation, 2014.

[62] I. Giordanelli, M. Mendoza, and H. J. Herrmann. "Modelling electron-phonon interactions in graphene with curved space hydrodynamics". arXiv:1702.04156 [cond-mat.mtrl-sci]. 2017.

[63] N. Gisin. "Quantum measurement and stochastic processes". In: *Physical Review Letters* 52 (1984), 1657–1660.

[64] N. Gisin and M. Rigo. "Relevant and irrelevant nonlinear Schrödinger equations". In: *Journal Physics A: Mathematical Generalizations* 28 (1995), 7375–7390.

[65] S. Goedecker. "Linear scaling electronic structure methods". In: *Reviews of Modern Physics* 71.4 (July 1999), 1085–1123.

[66] Hubert FM Goenner. "" On the History of Unified Field Theories. Part II.(ca. 1930–ca. 1965)". In: *Living Rev. Relativity* 17.5 (2014).

[67] Hubert FM Goenner. "On the history of unified field theories". In: *Living reviews in relativity* 7.2 (2004), 1830–1923.

[68] H. Grad. "Note on N-Dimensional Hermite Polynomials". In: *Communications on Pure and Applied Mathematics* 2.4 (Dec. 1949), 325–330.

[69] H. Grad. "On the kinetic theory of rarefied gases". In: *Communications on Pure and Applied Mathematics* 2.4 (Dec. 1949), 331–407.

[70] H.J. Groenewold. "On the principles of elementary quantum mechanics". In: *Physica* 12.7 (1946), 405–460.

[71] D. Guilini et al. *Decoherence and the Appearance of a Classical World in Quantum Theory.* Berlin: Springer, 1996.

[72] F. Haake. *Quantum signatures of chaos.* Berlin: Springer, 2001.

[73] Salman Habib, Kosuke Shizume, and Wojciech Hubert Zurek. "Decoherence, chaos, and the correspondence principle". In: *Physical review letters* 80.20 (1998), p. 4361.

[74] T. Hahn. *International Tables for Crystallography, Volume A: Space Group Symmetry.* 5th. Berlin: Springer, 2002.

[75] B. L. Hammond, W. A. Lester Jr., and P. J. Reynolds. *Monte Carlo Methods in Ab Initio Quantum Chemistry.* Singapore: World Scientific, 1994.

[76] Hermann A Haus. *Electromagnetic noise and quantum optical measurements.* Springer Science & Business Media, 2012.

[77] Lars Hedin and Stig Lundqvist. "Effects of Electron-Electron and Electron-Phonon Interactions on the One-Electron States of Solids". In: *Solid State Physics* 23 (1970), 1–181. ISSN: 0081-1947. DOI: 10.1016/S0081-1947(08)60615-3. URL: http://www.sciencedirect.com/science/article/pii/S0081194708606153.

[78] W. Heisenberg. "Über den anschaulichen Inhalt der quantentheoretischen Kinematik und Mechanik". In: *Zeitschrift für Physik* 43.3 (1927), 172–198. ISSN: 0044-3328. DOI: 10.1007/BF01397280. URL: http://dx.doi.org/10.1007/BF01397280.

[79] Malte Henkel et al. *Non-equilibrium phase transitions.* Vol. 1. Springer, 2008.

[80] H. Hillery et al. "Distribution functions in physics: fundamentals". In: *Physics Reports* 106.3 (1984), 121–167.

[81] J. P. Holloway. "Spectral velocity discretizations for the Vlasov-Maxwell equations". In: *Transport Theory and Statistical Physics* 25.1 (1996), 1–32.

[82] William G. Hoover. "Canonical dynamics: Equilibrium phase-space distributions". In: *Phys. Rev. A* 31 (3 1985), 1695–1697. DOI: 10.1103/PhysRevA.31.1695. URL: https://link.aps.org/doi/10.1103/PhysRevA.31.1695.

[83] R. A. Horn and C. R. Johnson. *Topics in matrix analysis.* Cambridge University Press, 1991.

[84] Robin L Hudson. "When is the Wigner quasi-probability density non-negative?" In: *Reports on Mathematical Physics* 6.2 (1974), 249–252.

[85] L. Hörmander. *The analysis of linear partial differential operators I.* Vol. 256. Grundlagen Mathematische Wissenschaften. Springer, 1983. ISBN: 3-540-121-4-8.

[86]  E. Isaacson and H. B. Keller. *Analysis of numerical methods*. New York: Dover Publications, 1994. ISBN: 0-486-68029-0.

[87]  A. Iserles et al. "Lie-group methods". In: *Acta Numerica* 8 (Mar. 1999), 1–199.

[88]  E. T. Jaynes and F. W. Cummings. "Comparison of quantum and semiclassical radiation theories with application to the beam maser". In: *Proceedings of the IEEE* 51.1 (Jan. 1963), 89–109.

[89]  G. Joyce, G. Knorr, and H. K. Meier. "Numerical Integration Methods of the Vlasov Equation". In: *Journal of Computational Physics* 8 (1971), 53–63.

[90]  A. Jüngel. *Transport Equations for Semiconductors*. Berlin: Springer, 2009.

[91]  Ansgar Jüngel and Josipa-Pina Milišić. "Quantum Navier–Stokes equations". In: *Progress in Industrial Mathematics at ECMI 2010*. Springer, 2012, 427–439.

[92]  Theodor Kaluza. "Zum unitätsproblem der physik". In: *Sitzungsber. Preuss. Akad. Wiss. Berlin.(Math. Phys.)* 1921.966972 (1921), p. 45.

[93]  B.S. Kandemir. "Wigner functions of an electron moving in a one-dimensional periodic potential". In: *Physics Letters A* 245 (1998), 209–219.

[94]  A. Karamatskou and H. Kleinert. "Geometrization of the Schrödinger equation: Application of the Maupertius Principle to quantum mechanics". In: *International Journal of Geometric Methods in Physics* 11 (2014).

[95]  G. Karypis and V. Kumar. "A fast and high quality multilevel scheme for partitioning irregular graphs". In: *SIAM Journal on Scientific Computing* 20.1 (1998), 359–392.

[96]  C Kiefer et al. "Quantum Future". In: (1998).

[97]  K.-Y. Kim and B. Lee. "On the high order numerical calculation schemes for the Wigner transport equation". In: *Solid-State Electronics* 43 (1999), 2243–2245.

[98]  C. Kittel. *Introduction to Solid State Physics*. 8th. New York: Wiley.

[99]  Oskar Klein. "Quantum theory and five-dimensional relativity theory". In: *The Oskar Klein Memorial Lectures: 1988–1999* (2014), p. 69.

[100]  Andrey R. Kolovsky. "Quantum coherence, evolution of the Wigner function, and transition from quantum to classical dynamics for a chaotic system". In: *Chaos: An Interdisciplinary Journal of Nonlinear Science* 6.4 (1996), 534–542. DOI: 10.1063/1.166201. eprint: http://dx.doi.org/10.1063/1.166201. URL: http://dx.doi.org/10.1063/1.166201.

[101]  B. Kraus et al. "Preparation of entangled states by quantum Markov processes". In: *Physical Review A* 78.042307 (2008).

[102]  Ch Kurtsiefer, T Pfau, and J Mlynek. "Measurement of the Wigner function of an ensemble of helium atoms". In: *Nature* 386.6621 (1997), p. 150.

[103]  C. Lanczos. "An Iteration Method for the Solution of the Eigenvalue Problem of Linear Differential and Integral Operators". In: *Journal of Research of the National Bureau of Standards* 45.4 (Oct. 1950), p. 255.

[104]  L. Lehtovaara, J. Toivanen, and J. Eloranta. "Solution of time-independent Schrödinger equation by the imaginary time propagation method". In: *Journal of Computational Physics* 221 (2007), 148–157.

[105]  G. Leibon et al. "A fast Hermite transform". In: *Theoretical Computer Science* 409 (2008), 211–228.

[106]  D. Liebfried, T. Pfau, and C. Monroe. "Shadows and Mirrors: Reconstructing Quantum States of Atom Motion". In: *Physics Today* 51.4 (Apr. 1998), 22–28.

[107]  G. Lindblad. "On the generators of quantum dynamical semigroups". In: *Communications in Mathematical Physics* 48.2 (1976), p. 119.

[108]  Alexander I Lvovsky and Michael G Raymer. "Continuous-variable optical quantum-state tomography". In: *Reviews of Modern Physics* 81.1 (2009), p. 299.

[109]  Alexander I Lvovsky et al. "Quantum state reconstruction of the single-photon Fock state". In: *Physical Review Letters* 87.5 (2001), p. 050402.

[110] R. Löhner. *Applied Computational Fluid Dynamics Techniques: An Introduction based on Finite Elements Methods.* 2nd. John Wiley & Sons Ltd., 2008. ISBN: 978-0-470-51907-3.

[111] P. Marcati, P. A. Markowich, and R. Natalini, eds. *Mathematical Problems in semiconductor physics.* Pitman Research notes in methematics. Harlow, Essex: Longman, 1995.

[112] P. A. Markowich, C. A. Ringhofer, and C. Schmeiser. *Semiconductor Equations.* Wien: Springer, 1990. ISBN: 3-211-82157-0.

[113] C. B. Mendl. "Matrix-valued quantum lattice Boltzmann method". In: *International Journal of Modern Physics C* 26.10 (Feb. 2015).

[114] Mendoza M., Succi S., and Herrmann H. J. "Flow Through Randomly Curved Manifolds". In: *Sci. Rep.* 3 (2013). DOI: 10.1038/srep03106. URL: http://www.nature.com/srep/2013/131031/srep03106/abs/srep03106.html\#supplementary-information.

[115] M. Mendoza, H. J. Herrmann, and S. Succi. "Preturbulent Regimes in Graphene Flow". In: *Phys. Rev. Lett.* 106 (15 2011), p. 156601. DOI: 10.1103/PhysRevLett.106.156601. URL: https://link.aps.org/doi/10.1103/PhysRevLett.106.156601.

[116] M. Mendoza et al. "Fast Lattice Boltzmann Solver for Relativistic Hydrodynamics". In: *Phys. Rev. Lett.* 105 (1 2010), p. 014502. DOI: 10.1103/PhysRevLett.105.014502. URL: http://link.aps.org/doi/10.1103/PhysRevLett.105.014502.

[117] C. Moler and C. Van Loan. "Nineteen dubious ways to compute the exponential of a matrix, twenty-five years later ". In: *SIAM Review* 45.1 (Mar. 2003), 3–49.

[118] J. E. Moyal. "Quantum Mechanics as a statistical theory". In: *Mathematical Proceedings of the Cambridge Philosophical Society* 45.01 (Jan. 1949), 99–124.

[119] Markus Müller, Jörg Schmalian, and Lars Fritz. "Graphene: A Nearly Perfect Fluid". In: *Phys. Rev. Lett.* 103 (2 2009), p. 025301. DOI: 10.1103/PhysRevLett.103.025301. URL: https://link.aps.org/doi/10.1103/PhysRevLett.103.025301.

[120] S. Nakajima. "On quantum theory of transport phenomena". In: *Prog. Theor. Phys.* 20 (1958), 948–959.

[121] J. von Neumann. *Mathematische Grundlagen der Quantenmechanik.* Berlin: Springer, 1932.

[122] B. Niclot, P. Degond, and F. Poupaud. "Deterministic Particle Simulations of the Boltzmann Transport Equation of Semiconductors ". In: *Journal of Computational Physics* 78 (1988), 313–350.

[123] Michael A Nielsen and Isaac Chuang. *Quantum computation and quantum information.* 2002.

[124] W. Pauli. "The Connection Between Spin and Statistics". In: *Physical Review* 58 (Oct. 1940).

[125] J. P. Paz and W. H. Zurek. "Quantum Limit of Decoherence: Environment Induced Superselection of Energy Eigenstates". In: *Physical Review Letters* 82.26 (June 1999), 5181–5185.

[126] L. Pintschovius. "Electron-phonon coupling effects explored by inelastic neutron scattering". In: *Physica Status Solidi b* (Nov. 2004).

[127] Alessandro Principi et al. "Bulk and shear viscosities of the two-dimensional electron liquid in a doped graphene sheet". In: *Phys. Rev. B* 93 (12 2016), p. 125410. DOI: 10.1103/PhysRevB.93.125410. URL: https://link.aps.org/doi/10.1103/PhysRevB.93.125410.

[128] P. Pérez-Fernandez et al. "Excited-state phase transition and onset of chaos in quantum optical models". In: *Physical Review E* 83 (2011).

[129] P. Pérez-Fernandez et al. "Quantum quench influenced by an excited-state phase transition". In: *Physical Review A* 83 (2011).

[130] Manijeh Razeghi. *Fundamentals of Solid State Engineering.* 3rd. Springer Publishing Company, Incorporated, 2009. ISBN: 9780387921679.

[131] C. A. Ringhofer, D. K. Ferry, and N. Kluksdahl. "Absorbing Boundary Conditions for the Simulation of Quantum Transport Phenomena". In: *Transport Theory and Statistical Physics* 18.3 (1989), 331–346.

[132] C. Ringhofer. "A spectral method for the numerical simulation of quantum tunneling phenomena". In: *SIAM Journal of Numerical Analysis* 27.1 (Feb. 1990), 32–50.

[133] Christian Ringhofer. "Computational methods for semiclassical and quantum transport in semiconductor devices". In: *Acta Numerica* 6 (1997), 485–521.

[134] O. Rodrigues. "Des lois géometriques qui regissent les déplacements d' un systéme solide dans l' espace, et de la variation des coordonnées provenant de ces déplacement considérées indépendent des causes qui peuvent les produire". In: *J. Math. Pures Appl.* 5 (1840), 380–440.

[135] J. Rosenberg. "A selective history of the Stone-von Neumann theorem". In: Contemporary Mathematics 365 (2004). Ed. by R. S. Doran and R. V. Kadison.

[136] W. Rudin. *Analysis.* 4th. München: Oldenbourg. ISBN: 978-3-486-58730-2.

[137] J. J. Sakurai and J. Napolitano. *Modern quantum mechanics.* 2nd. Harlow: Pearson, 2014.

[138] Gernot Schaller. *Open quantum systems far from equilibrium.* Vol. 881. Springer, 2014.

[139] O. Schenk and K. Gaertner. "On fast factorization pivoting methods for symmetric indefinite systems". In: *Elec. Trans. Numer. Anal.* 23 (2006), 158–179.

[140] O. Schenk and K. Gaertner. "Solving Unsymmetric Sparse Systems of Linear Equations with PARDISO". In: *Journal of Future Generation Computer Systems* 20.3 (2004), 475–487.

[141] Wolfgang P Schleich. *Quantum optics in phase space.* John Wiley & Sons, 2011.

[142] M. Schlosshauer. *Decoherence and the Quantum-To-Classical Transition.* The Frontiers Collection. Berlin: Springer, 2007.

[143] M. Schlosshauer. "Decoherence, the measurement problem, and interpretations of quantum mechanics". In: *Reviews of Modern Physics* 76.4 (2005), 1267–1305.

[144] M. Schlosshauer and A. Fine. "On Zurek's derivation of the Born rule". In: *Found. Phys.* 35 (2005), 197–213.

[145] M. Schlosshauer, J. Kofler, and A. Zeilinger. "A snapshot of foundational attitudes toward quantum mechanics". In: *Studies in History and Philosophy of Science Part B: Studies in History and Philosophy of Modern Physics* 44.3 (2013), 222–230. ISSN: 1355-2198.

[146] E. Schrödinger. "Die gegenwärtige Situation in der Quantenmechanik". In: *Naturwissenschaften* 23.48 (1935), 807–812. ISSN: 1432-1904. DOI: 10.1007/BF01491891. URL: http://dx.doi.org/10.1007/BF01491891.

[147] E. Schrödinger. "Quantisierung als Eigenwertproblem". In: *Annalen der Physik* 80.4 (1926).

[148] Erwin Schrödinger. "Der stetige Übergang von der Mikro-zur Makromechanik". In: *Naturwissenschaften* 14.28 (1926), 664–666.

[149] Erwin Schrödinger. "The final affine field laws I". In: *Proceedings of the Royal Irish Academy. Section A: Mathematical and Physical Sciences.* Vol. 51. JSTOR. 1945, 163–171.

[150] J. W. Schumer and J. P. Holloway. "Vlasov Simulations Using Velocity-Scaled Hermite Representations". In: *Journal of Computational Physics* 144 (1998), 626–661.

[151] J. M. Sellier and I. Dimov. "A Wigner Monte Carlo approach to density functional theory". In: *Journal of Computational Physics* 270 (2014), 265–277.

[152] J. M. Sellier and I. Dimov. "On the simulation of indistinguishable fermions in the many-body Wigner formalism". In: *Journal of Computational Physics* 280 (2015), 287–294.

[153] J.M. Sellier, M. Nedjalkov, and I. Dimov. "An introduction to applied quantum mechanics in the Wigner Monte Carlo formalism". In: *Physics Reports* 577 (2015). An Introduction to Applied Quantum Mechanics in the Wigner Monte Carlo Formalism, 1–34. ISSN: 0370-1573. DOI: 10.1016/j.physrep.2015.03.001. URL: http://www.sciencedirect.com/science/article/pii/S0370157315001982.

[154]  S. Shao, T. Lu, and W. Cai. "Adaptive Conservative Cell Average Spectral Element Methods for Transient Wigner Equation in Quantum Transport". In: *Communications Computational Physics* 9.3 (Mar. 2011), 711–739.

[155]  S. Shao and Y. Xiong. "A computable branching random walk for the many-body Wigner quantum dynamics". arXiv:1603.00159 [physics.comp-ph]. 2016.

[156]  Neil G Shephard. "From characteristic function to distribution function: a simple framework for the theory". In: *Econometric theory* 7.4 (1991), 519–529.

[157]  R. B. Sidje. "EXPOKIT: A software Package for Computing Matrix Exponentials". In: *AcM-Transactions on Mathematical Software* 245.1 (1998), 130–156.

[158]  H. Smith and H. H. Jensen. *Transport Phenomena*. Oxford Science Publications. Oxford University Press, 1989. ISBN: 0198519850.

[159]  J. Snygg. *Clifford Algebra A Computational Tool for Physicists*. Oxford Univ Pr, Jan. 1997.

[160]  S. Solórzano, M. Mendoza, and H. J. Herrmann. "Second-order kinetic Kohn-Sham lattice model". In: *Physical Review A* 93 (June 2016).

[161]  J. L. Steger and R. F. Warming. "Flux Vector Splitting of the Inviscid Gasdynamic Equations with Application to Finite-Difference Methods". In: *Journal of Computational Physics* 40 (1981), 263–293.

[162]  O. Steuernagel, D. Kakofengitis, and G. Ritter. "Wigner flow reveals topological order in quantum phase space". In: *Physical Review Letters* 110.030401 (2013).

[163]  G. Strang. "On the construction and comparison of difference schemes". In: *SIAM Journal of Numerical Analysis* 5 (1968), 506–517.

[164]  N. Straumann. *General Relativity*. 2nd. Graduate Texts in Physics. Springer, Oct. 2012. ISBN: 9789400799547.

[165]  D. J. Struik. *Lectures on Classical Differential Geometry*. Dover Publications, 1988.

[166]  S. Succi. "Lattice Boltzmann schemes for quantum applications". In: *Computational Physics Communications* 146 (2002), p. 317.

[167]  S. Succi. *The Lattice Boltzmann Equation for Fluid Dynamics and Beyond*. Numerical Mathematics and Scientific Computation. New York: Oxford University Press, 2009.

[168]  S. Succi and R. Benzi. "Lattice Boltzmann equation for quantum mechanics". In: *Physica D* 69 (1993), p. 327.

[169]  Sauro Succi. "Lattice Boltzmann 2038". In: *EPL (Europhysics Letters)* 109.5 (2015), p. 50001. URL: http://stacks.iop.org/0295-5075/109/i=5/a=50001.

[170]  D Svintsov et al. "Hydrodynamic model for electron-hole plasma in graphene". In: *Journal of Applied Physics* 111.8 (2012), p. 083715.

[171]  A. R. Tackett and M. Di Ventra. "Targeting specific eigenvectors and eigenvalues of a given Hamiltonian using arbitrary selection criteria". In: *Physical Review B* 66.245104 (2002).

[172]  M. Tavis and F. W. Cummings. "Exact Solution for an N-Molecule-Radiation-Field Hamiltonian". In: *Physical Review* 170.2 (June 1968).

[173]  L. N. Trefethen and D. Bau. *Numerical Linear Algebra*. SIAM, 1997.

[174]  Matthias Troyer and Uwe-Jens Wiese. "Computational Complexity and Fundamental Limitations to Fermionic Quantum Monte Carlo Simulations". In: *Phys. Rev. Lett.* 94 (17 May 2005), p. 170201. DOI: 10.1103/PhysRevLett.94.170201. URL: https://link.aps.org/doi/10.1103/PhysRevLett.94.170201.

[175]  F. Verstraete, M. M. Wolf, and J. I. Cirac. "Quantum computation, quantum state engineering, and quantum phase transitions driven by dissipation". In: *Nature Physics* 5 (July 2009), 633–636.

[176]  R. Von Mises and H. Pollaczek-Geiringer. "Praktische Verfahren der Gleichungsauflösung". In: *Zeitschrift für Angewandte Mathematik and Mechanik* 9 (1929), 152–164.

[177] Sascha Wald and Malte Henkel. "Lindblad dynamics of a quantum spherical spin". In: *Journal of Physics A: Mathematical and Theoretical* 49.12 (2016), p. 125001.

[178] L.-W. Wang and A. Zunger. "Solving Schrödinger's equation around a desired energy: Application to silicon quantum dots". In: *The Journal of Chemical Physics* 100.3 (Feb. 1994), p. 2394.

[179] S. Weinberg. "What happens in a Measurement?" In: *Physical Review A* 93.3 (Mar. 2016).

[180] Gregor Wentzel. "Zur Quantenoptik". In: *Zeitschrift für Physik A Hadrons and Nuclei* 22.1 (1924), 193–199.

[181] Hermann Weyl. "Gravitation and electricity". In: *Sitzungsber. Preuss. Akad. Berlin* 465 (1918).

[182] Hermann Weyl. *The theory of groups and quantum mechanics*. Courier Corporation, 1950.

[183] J. A. Wheeler and W. H. Zurek. *Quantum Theory and Measurement*. Princeton Series in Physics. Princeton, NJ: Princeton University Press, 1983.

[184] S. Wiggins. *Introduction to Applied Nonlinear Dynamical Systems and Chaos*. New York: Springer, 2003.

[185] E. Wigner. "On the quantum correction for thermodynamic equilibrium". In: *Physical Review* 40 (June 1932), 749–759.

[186] Mark M Wilde. *Quantum information theory*. Cambridge University Press, 2013.

[187] C.-Y. Wong. "Explicit solution of the time evolution of the Wigner function". In: *Journal of Optics B: Quantum and Semiclassical Optics* 5 (2003), 420–428.

[188] H. J. Xiang et al. "Linear scaling calculation of band edge states and doped semiconductors". In: *The Journal of Chemical Physics* 126.24 (2007), p. 244707. DOI: 10.1063/1.2746322. eprint: http://dx.doi.org/10.1063/1.2746322. URL: http://dx.doi.org/10.1063/1.2746322.

[189] C. K. Zachos, D. B. Fairlie, and T. L. Curtright, eds. *Quantum Mechanics in Phase Space: An Overview with Selected Papers*. Vol. 34. World Scientific Series in 20th Century Physics. Singapore: World Scientific, 2005.

[190] Zurek Wojciech Hubert. "Sub-Planck structure in phase space and its relevance for quantum decoherence". In: *Nature* 412.6848 (Aug. 2001), 712–717. ISSN: 0028-0836.

[191] W. H. Zurek. "Decoherence and the transition from quantum to classical". In: *Physics Today* 44 (1991), 36–44.

[192] W. H. Zurek. "Environment-Assisted Invariance, Entanglement, and Probabilities in Quantum Physics". In: *Physical Review Letters* 90.12 (Mar. 2003).

[193] W. H. Zurek. "Quantum Darwinism, classical reality, and the randomness of quantum jumps". In: *Physics Today* 67.10 (Oct. 2014), p. 44.